The Dissertation Committee for William Harold Asquith certifies that this is the approved version of the following dissertation:

MODELING OF RUNOFF-PRODUCING RAINFALL HYETOGRAPHS IN TEXAS USING L-MOMENT STATISTICS

Committee:

_____

John M. Sharp, Supervisor

_____

Clark R. Wilson

_____

Zong-Liang Yang

_____

David R. Maidment

_____

David B. Thompson

MODELING OF RUNOFF-PRODUCING RAINFALL HYETOGRAPHS IN TEXAS USING L-MOMENT STATISTICS

by

William Harold Asquith, B.S., M.S.

Dissertation

Presented to the Faculty of the Graduate School of

the University of Texas at Austin

in Partial Fulfillment

of the Requirements

for the Degree of

Doctor of Philosophy

The University of Texas at Austin

May 2003

Dedication

This dissertation is dedicated to my parents, George and Anne, who have supported me throughout my life, encouraged me to become an author, and to become a scientist by an education through engineering and then the geosciences. This dissertation is also dedicated to my wife, D'Anne, for many wonderful years of boundless encouragement and support during times when my attention was directed on school, and for giving me Nathan and Caroline. These individuals have continuously inspired me to appreciate the complexity of the world around us all.

Acknowledgements

I would like to thank the following people/institutions for their assistance, encouragement, and friendship. I thank the dissertation committee members: Drs. John Sharp, Clark Wilson, Liang Yang, David Maidment, and David Thompson. I especially thank John Sharp for years of friendship and for assuming the role of supervisor. I thank Dr. James Famiglietti for encouraging me to return to school, sponsoring my admission to the Department of Geosciences, and for several extremely rewarding years. I thank the Geology Foundation for financial support. I thank the United States Geological Survey (USGS) for providing an academically favorable environment, for providing unlimited opportunities for research, and for periodic tuition support. I thank the Texas Department of Transportation Research Management Committee No. 3 for over ten years of research sponsorship including large portions of the effort behind this dissertation. I thank Raymond Slade, Jr. for hiring me at the USGS, for guiding me through my early career, and for being a friend. I thank the USGS technical writing and editorial staff, Peter Bush, Gail Sladek, and Judy Voigt, for greatly enhancing my technical writing skills and encouraging my pursuit of excellence in graphical and tabular presentation. I thank David Stolpa, Rudy Herrmann, and Amy Ronnfeldt and Drs. Ted Cleveland and Xing Fang for their assistance. I thank Drs. Jonathan Hosking, James Wallis, Robert Serfling, and Warren Gilchrist for reading and commenting on drafts of this dissertation. I also thank Jonathan Hosking and countless others for the beautiful world of L-moment statistics. I thank Larry Wall and the rest of the Perl community for developing a wonderfully expressive open-source programming language upon which nearly all algorithms used in this dissertation are based. And I acknowledge Tkg2, a Perl-based data-plotting software package that generated all data graphics in this dissertation and was my programming passion between 1999 and 2001.

May 2003

MODELING OF RUNOFF-PRODUCING RAINFALL HYETOGRAPHS IN TEXAS USING L-MOMENT STATISTICS

Publication No. _____

William Harold Asquith, Ph.D.
The University of Texas at Austin, 2003

Supervisor: John M. Sharp

Temporal distributions of storm rainfall are known as hyetographs. Design hyetographs are important for cost-effective risk-mitigated rainfall-runoff modeling. The hyetographs considered are known to produce or generate runoff on small watersheds (typically about 50 square kilometers) in Texas. L-moment statistics and the nonparametric median are used to summarize the dimensionless representations of over 1,600 observed hyetograph distributions. A focus is made on storm depths in excess of about 25 mm and durations of 0–12, 12–24, and 24 hours and greater. Statistical distributions are fit to the L-moments of the dimensionless hyetographs including the newly described L-gamma. L-gamma hyetograph models are anticipated to be reliable predictors of expected hyetographs. Finally, a separate permeability-related L-moment application to the popular Carman-Kozeny equation is described.

TABLE OF CONTENTS

LIST OF TABLES

LIST OF FIGURES

NOMENCLATURE

Conventions

The editorial and format style of this dissertation follows that of the U.S. Geological Survey (Hansen, 1991). One topic requiring clarification is when specific references to content in chapters, figures, tables, or pages within the works of others are made in this dissertation, the content is indicated after the year of publication. For example, "Pani and Haragan (1981, fig. 5)" refers to figure 5 of Pani and Haragan (1981) and not figure 5 of this dissertation, or "Pilgrim and Cordery (1975, p. 81)" refers to page 81 of Pilgrim and Cordery (1975) and not page 81 of this dissertation.

Conversion Factors

The inch-pound unit system (English units) used in this dissertation can be converted to International System of Units (SI) by the following conversion factors:

Multiply	By	To obtain
inch (in.)	25.40	millimeter (mm)
foot (ft)	0.3048	meter (m)
mile (mi)	1.609	kilometer (km)
square mile (mi^2)	2.590	square kilometers (km^2)
cubic foot per second (ft^3/s)	0.02832	cubic meter per second (m^3/s)

Within the body of the text both units systems are reflected for the convenience of international readers. For example in the text, 1 in. is written as 1 in. (25.4 mm). Both unit systems are shown on figures when context permits, and the head notes of each table contain unit conversion details as well. In some places in the dissertation, hyetographs are classified into categories that are label by depth, since these are proper names, a conversion to SI is not universally shown.

Lower Case Symbols and Acronyms

a **Parameter of the triangular and Beta distributions**

a_v **Ratio of internal surface to volume of solids for porous media**

$\bar{a}_v$ **Mean a_v**

b **Parameter of the triangular, L-gamma, and Beta distributions**

c **Parameter of the L-gamma distribution**

h **Second shape parameter of the Generalized Lambda and Kappa distributions**

k **Intrinsic permeability**

$\bar{k}$ **Mean intrinsic permeability**

l_1 **Sample mean**

The first sample L-moment computed from unbiased estimators.

l_2 **Sample L-scale or sample L-variation**

The second sample L-moment computed from unbiased estimators.

l_3 **Sample third L-moment**

A measure of sample skew computed from unbiased estimators, see L-skew.

l_4 **Sample fourth L-moment**

A measure of sample kurtosis computed from unbiased estimators, see L-kurtosis.

n **Sample size**

$p_{j:n}$ **Plotting position**

The plotting position for the jth ascending order observation of a random sample of size n. A common formula is $p_{j:n} = (j + \delta)/(n + \varepsilon)$ for $\delta > \varepsilon > -1$.

psd **Particle-size distribution**

t **Sample coefficient of L-variation**

The first sample L-moment ratio, l_2/l_1, computed from unbiased estimators.

t_3 **Sample L-skew**

The second sample L-moment ratio, $-1 \le t_3 \le 1$, computed from unbiased estimators.

t_4 **Sample L-kurtosis**

The third sample L-moment ratio, $\frac{1}{4}(5t_3^2 - 1) \le t_4 < 1$, computed from unbiased estimators.

$w_{j,r}$ **Unbiased weight factor**

The unbiased weight factor on a specific $x_{j:n}$ for computation of sample L-moments by unbiased estimators.

$\tilde{w}_{j,r}$ **Plotting-position weight factor**

The plotting-position weight factor on a specific $x_{j:n}$ for computation of sample L-moments by plotting-position estimators.

$\hat{w}_{j,r}$ **Prior-probability weight factor**

The prior-probability weight factor on a specific $x_{j:n}$ for computation of sample L-moments by p-PWMs.

$x_{m:n}$ **Sample order statistic**

Sample order statistics of an n sized sample are $x_{1:n} \le x_{2:n} \le \ldots \le x_{n:n}$.

Upper Case Symbols and Acronyms

C **Coefficient of variation**

CDA **Cumulative distribution analysis**

CDF **Cumulative distribution function**

CK **Carman-Kozeny equation**

D **Grain size diameter**

$\overline{D}$ **Diameter of mean grain size**

DDF **Depth-duration frequency of precipitation**

E_2 **Second noncentral product moment**

E_3 **Third noncentral product moment**

F **Nonexceedance probability, Percent of storm duration**

$0 \le F \le 1$ or in percent $0 \le F \le 100$, the cumulative probability of an observation, the compliment of the exceedance probability, recurrence interval in years equals $1/(1-F)$.

G **Gini's mean difference statistic**

IcR_r **Inter-cile range**

The intercile range of order r.

IDF **Intensity-duration frequency of precipitation**

IQR **Inter-quartile range**

One quarter of the data is within the inter-quartile range.

ITR **Inter-tercile range**

One third of the data is within the inter-tercile range, $ITR = UT - LT$.

LT **Lower tercile**

Two-thirds of the data is greater than the lower tercile.

M **Median**

Fifty percent of the data values are greater than or less than the median. The median is also the quantile for a nonexceedance probability of 0.50.

M-MLM **Modified Method of L-moments**

The median and inter-tercile range of the distribution are estimated using the mean and L-scale values. Then the parameters of the L-gamma distribution are solved to match the median and inter-tercile range. This method differs from the common Method of L-moments in which the parameters are estimated directly from the L-moments.

$M_{p,\,r,\,s}$ **The probability weighted moments, PWMs**

$M_{p,\,r,\,s} = E[x(F)^p F^r (1-F)^s]$. The PWMs are useful for defined measure of distribution expressible in inverse or quantile form.

MVUE **Minimum Variance Unbiased Estimator**

NRCS **Natural Resources Conservation Service**

PDF **Probability Density Function**

p-PWMs **Prior-Probability Weighted Moments**

PWMs **Probability Weighted Moments**

R **Rainfall in percent**

RE **Relative Efficiency**
Variance of an unbiased L-moment estimator divided by either plotting-position estimator or the p-PWM estimator variance.

SCS **Soil Conservation Service**

s_{UMVU} **Uniformly Minimum Variance Unbiased Estimate of the Standard Deviation**

TxDOT **Texas Department of Transportation**

USGS **U.S. Geological Survey**

UT **Upper tercile**
Two-thirds of the data is less than the upper tercile.

X **Random variable**

Functions

$a_v(F)$ **Quantile function of** a_v

$B(a, b)$ **Beta function**

$D(F)$ **Grain size diameter quantile function**

$k(F)$ **Intrinsic permeability quantile function**

e^x **Natural, Naperian, or hyperbolic exponent of** x
$e = 2.71828\ldots.$

$f(x)$ **Probability density function**

$\log(x)$ **Natural, Naperian, or hyperbolic logarithm of** x
The logarithm have a base of e as opposed to the Briggsian or base-10 logarithms.

$x(F)$ **Quantile function**
Quantile function definition canonical with L-moment literature.

$\binom{a}{b}$ **Combinatorial function**

The formula for the combinations of n distinct items taken r at a time is $\binom{a}{b} = {}_aC_b = \frac{a!}{b!(a-b)!}$ and by definition $\binom{a}{0} = 1$.

$E[\ ]$ **The expectation operator**

In terms of the probability density function $f(x)$ is $E[X^r] = \int_{-\infty}^{\infty} x^r f(x)dx$, and in terms of the quantile function $x(F)$ is $E[X^r] = \int_0^1 x(F)^r dF$. The first expectation of a random variable is the mean.

$Q(F)$ **Quantile function**

The quantile for nonexceedance probability F; $x(F)$ also is used to denote the quantile function for random variable X. The derivative of the quantile function, $\frac{d}{dF}Q(F)$ is the quantile density function.

$\Gamma(x)$ **Gamma function**

$\Lambda(F)$ **Quantile function of the L-gamma distribution**

Parameters are not defined but implied.

$\Lambda(b, c, F)$ **Quantile function of the L-gamma distribution**

Parameters are specifically defined.

$P^*_{r-1}(F)$ **Legendre polynomial**

The $r-1$ shifted Legendre polynomial. The polynomial is used in the derivation and definition of the L-moments.

$P(m, nx)$ **Incomplete gamma function**

Greek Symbols

α **Scale parameter of the Kappa and Linear distribution**

α_r **The alpha-series of probability weighted moments**

$\alpha_r = M_{1,0,r}$, see probability weighted moments.

β_r **The beta-series of probability weighted moments**

$\beta_r = M_{1, r, 0}$. The beta-series is preferred for L-moment derivation, see probability weighted moments.

β **Shape parameter for the Power and Govindarajulu distributions**

γ **Product moment skew**

ε **Location parameter of two-parameter Power distribution**

ξ **Location parameter of the Generalized Lambda and Kappa distributions**

ζ **Integral term for the Carman-Kozeny equation**

κ **First shape parameter of the Generalized Lambda and Kappa distributions**

λ_1 **Mean**

The first L-moment.

λ_2 **L-scale or L-variation**

The second L-moment.

λ_3 **Third L-moment**

A measure of skew, see L-skew.

λ_4 **Fourth L-moment**

A measure of kurtosis, see L-kurtosis.

σ **Standard deviation**

σ^2 **Product moment variance**

τ **Coefficient of L-variation**

The first L-moment ratio, λ_2 / λ_1.

τ_3 **L-skew**

The second L-moment ratio, $-1 \leq \tau_3 \leq 1$.

τ_4 **L-kurtosis**

The third L-moment ratio, $(1/4)(5\tau_3^2 - 1) \leq \tau_4 < 1$.

$\tilde{\lambda}_1$ **Sample mean**

The first sample L-moment computed from plotting-position estimators.

$\tilde{\lambda}_2$ **Sample L-scale or sample L-variation**

The second sample L-moment computed from plotting-position estimators.

$\tilde{\lambda}_3$ **Sample third L-moment**

A measure of sample skew computed from plotting-position estimators, see L-skew.

$\tilde{\lambda}_4$ **Sample fourth L-moment**

A measure of sample kurtosis computed from plotting-position estimators, see L-kurtosis.

$\tilde{\tau}$ **Sample coefficient of L-variation**

The first sample L-moment ratio, l_2 / l_1, computed from plotting-position estimators.

$\tilde{\tau}_3$ **Sample L-skew**

The second sample L-moment ratio, $-1 \le t_3 \le 1$, computed from plotting-position estimators.

$\tilde{\tau}_4$ **Sample L-kurtosis**

The third sample L-moment ratio, $\frac{1}{4}(5t_3^2 - 1) \le t_4 < 1$, computed from plotting-position estimators.

$\hat{\lambda}_1$ **Sample mean**

The first sample L-moment computed from prior-PWM estimators.

$\hat{\lambda}_2$ **Sample L-scale or sample L-variation**

The second sample L-moment computed from prior-PWM estimators.

$\hat{\lambda}_3$ **Sample third L-moment**

A measure of sample skew computed from prior-PWM estimators, see L-skew.

$\hat{\lambda}_4$ **Sample fourth L-moment**

A measure of sample kurtosis computed from prior-PWM estimators, see L-kurtosis.

$\hat{\tau}$ **Sample coefficient of L-variation**

The first sample L-moment ratio computed from prior-PWM estimators.

$\hat{\tau}_3$ **Sample L-skew**

The second sample L-moment ratio computed from prior-PWM estimators.

$\hat{\tau}_4$ **Sample L-kurtosis**

The third sample L-moment ratio computed from prior-PWM estimators.

Υ **Tortuosity**

CHAPTER 1
INTRODUCTION

The time history of rainfall depth on the ground for a specific location or over a specific area is described by a *hyetograph* (Schaefer, 1993, p. 18). For this dissertation, however, the term "hyetograph" specifically refers to the accumulation of rainfall depth with the duration of the storm—a cumulative hyetograph. The instantaneous time history of rainfall rate, also known as an intensity in a length scale per time, is referred to as an *instantaneous* hyetograph. The separate distinction for the instantaneous hyetograph is made so that the one-word term hyetograph is reserved for the cumulative hyetograph. A *dimensionless* hyetograph has the units of time (storm duration) and cumulative rainfall depth (storm depth) expressed in percentages of the respective totals; dimension can be removed by other techniques. The dimensionless hyetograph is convenient in many applications and comprises a substantial concept for the research presented here. An instantaneous dimensionless hyetograph also can be constructed from the first derivative of the dimensionless hyetograph.

Hyetographs are useful for computer based rainfall-runoff modeling and other applications. Because the shape and timing of the runoff hydrograph is primarily driven by the magnitude and temporal distribution of rainfall, the hyetograph is an important component of the modeling. The modeling is important for cost-effective and risk-mitigated hydrologic design of hydraulic (open-channel) structures. Discussion of hyetograph basics and relation of hyetographs to hydraulic design is found in numerous hydrologic engineering textbooks (for example, Chow and others,

1988, p. 75, 136; Haan and others, 1994, pp. 44–52). An example event-specific hyetograph that is known to produced runoff is provided on figure 1.

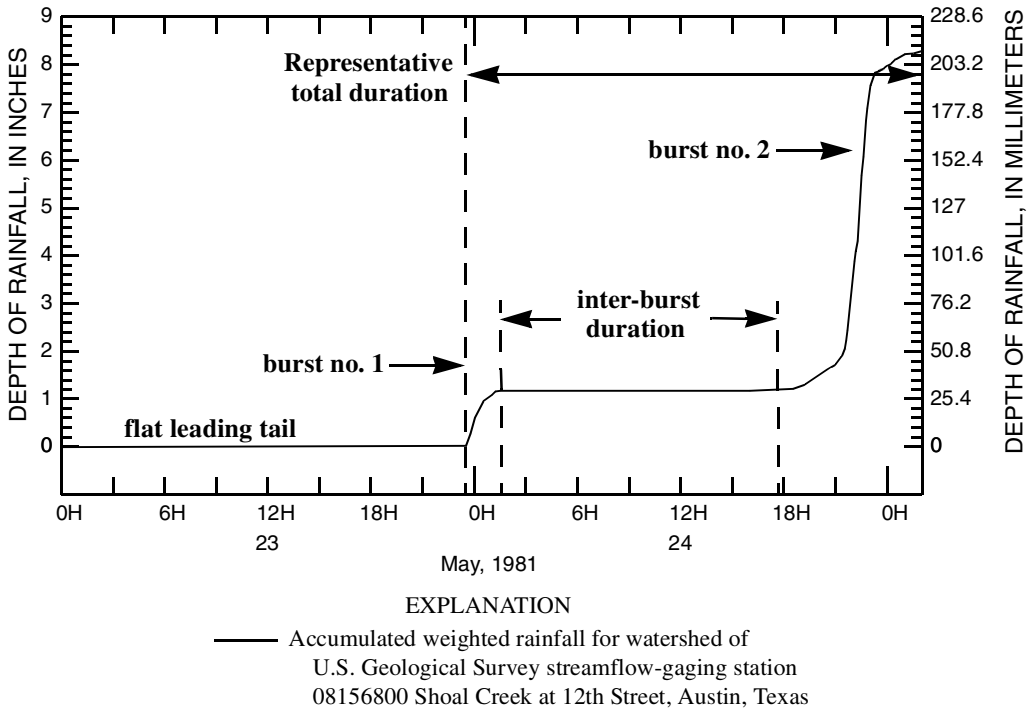

Figure 1. Example of a cumulative rainfall hyetograph

It is obvious on figure 1 that two short duration bursts or rainfall sub-events (less than a few hours each) occurred on or about May 24, 1981. There is one burst starting just before about 00:00 hours (hr) and the other burst starting at about 18:00 hr. Each burst could be considered a distinct hyetograph, but their proximity in time suggests that one storm event, likely generated by similar meteorological mechanisms, is represented. If the duration of the storm event is considered as lasting about one day, then the event is characterized as having multiple bursts—two in this case. A long unchanging leading tail of the hyetograph is present because of a zero depth data value

at 00:00 hr on May 23rd. The tail is an artifact of the method by which the original data was recorded and preserved (see *Data Sources* section). The tail leaves the *numerical impression* that the storm duration was just over two days long. Preprocessing of the underlying data to remove unchanging tails before subsequent analysis would be required to more accurately represent the duration shown in the figure by reducing the numerical duration of the data. This preprocessing is referred to as "tail trimming" and is described and used in several chapters of this dissertation.

Problem

A recurring problem in the study of hyetographs is the reproduction of the observed rainfall hyetograph with a small number of values. These values could include entries in a look-up table, parameters of empirical models, or the statistical moments of the hyetograph distribution. There is considerable interest by designers of hydraulic structures (such as culverts, inlets, roadways, water-quality "ponds") in estimating an average or *expected* hyetograph for a location based on observed data. Further, often predictions of the expected hyetograph are required at ungaged or un-monitored locations. The predictions typically are made through statistical regionalization.

Statistical regionalization is an analysis technique that abounds in the hydrologic sciences (for example, Kite, 1988, chapter 13; Stedinger and others, 1992, pp. 18.33–37; Asquith, 1998; Asquith and Slade, 1997; Hosking and Wallis, 1997). For hyetograph analysis, regionalization requires statistical transference of specific

characteristics of the hyetograph between gaged and ungaged locations by quantifiable relations between potentially influential factors such as storm duration, season of occurrence, total rainfall depth, geographic position, topography, and regional vegetation and soil types. The use of the term location reflects geographic position as well as other "coordinates" of the multidimensional parameter space represented the identified factors.

Hypotheses and Objectives

The hypotheses of this research are that expected hyetographs in Texas are definable using L-moment statistics (Hosking, 1990) and quantile distribution functions (Gilchrist, 2000). The expected hyetograph is defined in the next section. A secondary hypothesis is that reliable parameter estimates for candidate hyetograph quantile function models are possible. The term reliable in this context reflects that the model, including the parameter estimates, is statistically defendable even if a rigorous assessment of model validity is not possible.

In particular, it is hypothesized that the sample L-moments and the nonparametric sample median of hyetograph distributions will provide a basis for statistical analysis by summarizing actual storm events. The hyetographs for individual storm events are collectively referred to as observed hyetographs. The L-moments are regionalized by investigation of relations between the L-moments and several of the influential factors already identified. Not all factors can be investigated within the scope of this dissertation. The regionalized L-moments could provide a basis for interpretation of

the processes that generate rainfall time distributions, such as synoptic scale and meso scale weather systems. L-moments are useful for parameter estimation for candidate models, such as: $R = F^b e^{c(1-F)}$ where R is rainfall, F is cumulative time, and the parameters b and c require estimation.

Although the theory of L-moments and its application in hydrologic magnitude and frequency regional analyses became popular in the last decade or so (Asquith, 1998; Asquith, 2002; and references therein; and many other publications), L-moment application to the study of hyetographs appears unprecedented. The lack of previous work is attributable in part to the comparatively limited adoption of L-moments compared to the well-known classical moments for statistical analysis in general and the limited number of hyetograph investigators in particular. The analytical scope of this dissertation generally is limited to L-moment statistics.

Expected Hyetograph

The expected hyetograph is a synthetic storm that is intended to represent the typical characteristics of a storm when the analyst is given values of the potentially influential factors. Examples of these factors have already been identified in this dissertation. The expected hyetograph represents a hydrostatologic (study of water statistics) model based on the *statistical* characteristics of observed hyetographs from a data base instead of a meteorological model in which a direct coupling of fundamental components of the atmosphere and principles of physics such as

humidity, temperature, pressure, and conservation of energy or momentum are represented. As defined here, the expected hyetograph also does not represent the average of all storms that could be aggregated for either a given location or larger geographical area, but rather represents the average for storms that are known to produce runoff—an important condition in rainfall-runoff analysis. The fact that only runoff-producing storms are considered distinguishes the research here when compared to most of the works described in chapter 2.

Although the expected hyetograph as developed here is not meteorologically based, it should still be possible to make inferences—that is, statistically-based inferences—of the meteorological and physical processes that generate and influence the temporal distribution of storm events. To that end, statistical characteristics of observed hyetographs are used to measure fundamental properties of the rainfall time distribution. The nonparametric median and L-moment statistics of observed hyetographs distributions are used. These statistics measure fundamental properties of a distribution such as location on the real-number line (mean), scale or spread on the real-number line (variance), and various "so-called" higher measures of distribution shape (skew and kurtosis).

Data Sources

A data base of rainfall and concomitant runoff values for small watersheds in Texas is available from ongoing (as of 2002) collaborative rainfall-runoff characterization research projects (project nos. 0–4193 and 0–4194) funded by the

Texas Department of Transportation (TxDOT) and the U.S. Geological Survey (USGS), and performed by researchers at Texas Tech University (Lubbock), the University of Houston, Lamar University (Beaumont), and the USGS (Austin). The data base includes 1,659 storms for 91 small rural and urban watersheds of USGS streamflow-gaging stations in Texas. The locations of the stations are shown on figure 2. Each storm within the data base is represented by a single rainfall data file. The data was manually entered into an open-source computer text file versioning software system (*http://www.cvshome.org*) on a RedHat™ Linux™ server (*http://www.redhat.com*) over the course of two years by project staff scattered between the four research entities. The data was derived from over 220 historical USGS data reports that occupy approximately eight linear feet of book shelf space. A comprehensive citation list for the reports is provided in Appendix A.

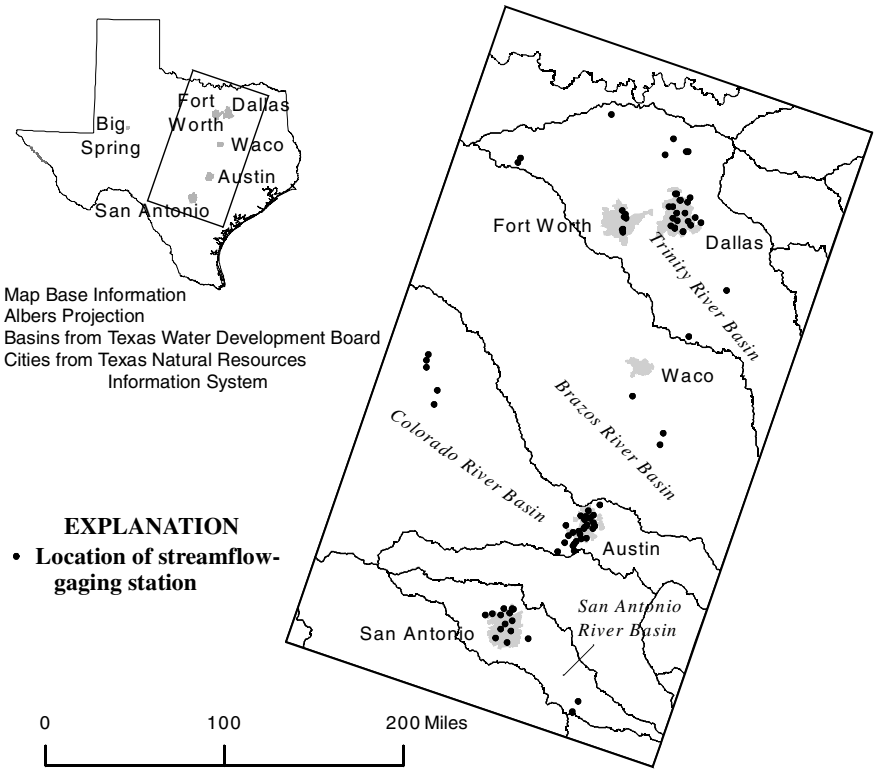

Figure 2. Map showing locations of USGS streamflow-gaging stations represented in the hyetograph data base

The composite data base is divided into five data base "modules". These modules are broken into four urban centers and are called `austin`, `dallas`, `fortworth`, and `sanantonio`, for the Austin, Dallas, Fort Worth, and San Antonio areas of Texas, respectively. The fifth module is referred to as the `smallruralsheds` data base and contains clusters of intensively monitored small rural watershed study units within the Brazos River, Colorado River, San Antonio River, and Trinity River basins of Texas. The stations for which incremental values of concomitant streamflow and rainfall for storm events are available in the data base and are listed in tables 1–5.

Table 1. U.S. Geological Survey streamflow–gaging stations within the `austin` data base module

[Approx., approximate; mi^2, square miles. SH, State highway; FM, Farm to market road; IH, Interstate highway. One mi^2 equals 2.59 square kilometers (km^2).]

Station no.	Station name	Latitude	Longitude	Drainage area (mi^2)	Approx. period of record	No. of storm events
08154700	Bull Creek at Loop 360, Austin, Texas	30°22'19"	97°47'04"	22.3	1978–1986	14
08155200	Barton Creek at SH 71, Oak Hill, Texas	30°17'46"	97°55'31"	89.7	1978–1982	6
08155300	Barton Creek at Loop 360, Austin, Texas	30°14'40"	97°48'07"	116.0	1979–1986	8
08155550	West Bouldin Creek at Riverside Drive, Austin, Texas	30°15'49"	97°45'17"	3.12	1977–1985	10
08156650	Shoal Creek at Steck Avenue, Austin, Texas	30°21'55"	97°44'11"	2.79	1975–1982	13
08156700	Shoal Creek at Northwest Park, Austin, Texas	30°20'50"	97°44'41"	7.03	1976–1983	17
08156750	Shoal Creek at White Rock Drive, Austin, Texas	30°20'21"	97°44'50"	7.56	1976–1980	14
08156800	Shoal Creek at 12th Street, Austin, Texas	30°16'35"	97°45'00"	12.3	1975–1986	24
08157000	Waller Creek at 38th Street, Austin, Texas	30°17'49"	97°43'36"	2.31	1967–1980	41
08157500	Waller Creek at 23rd Street, Austin, Texas	30°17'08"	97°44'01"	4.13	1967–1980	40
08158050	Boggy Creek at U.S. 183, Austin, Texas	30°15'47"	97°40'20"	13.1	1976–1985	10
08158100	Walnut Creek at FM 1325, Austin, Texas	30°24'35"	97°42'41"	12.6	1976–1986	15
08158200	Walnut Creek at Dessau Road, Austin, Texas	30°22'30"	97°39'37"	26.2	1976–1986	17
08158380	Little Walnut Creek at Georgian Drive Austin, Texas	30°21'15"	97°41'52"	5.22	1985–1986	2
08158400	Little Walnut Creek at IH 35, Austin, Texas	30°20'57"	97°41'34"	5.57	1976–1981	10
08158500	Little Walnut Creek at Manor Road, Austin, Texas	30°18'34"	97°40'04"	12.1	1976–1981	15
08158600	Walnut Creek at Webberville Road, Austin, Texas	30°16'59"	97°39'17"	51.3	1974–1986	21
08158700	Onion Creek near Driftwood, Texas	30°04'59"	98°00'29"	124	1980–1987	6
08158800	Onion Creek at Buda, Texas	30°05'09"	97°50'52"	166	1980–1983	2
08158810	Bear Creek below FM 1826, Driftwood, Texas	30°09'19"	97°56'23"	12.2	1980–1986	8
08158820	Bear Creek at FM 1626, Manchaca, Texas	30°08'25"	97°50'50"	24.0	1980–1983	2
08158825	Little Bear Creek at FM 1626, Manchaca, Texas	30°07'31"	97°51'43"	21.0	1980–1983	2

Station no.	Station name	Latitude	Longitude	Drainage area (mi^2)	Approx. period of record	No. of storm events
08158840	Slaughter Creek at FM 1826, Austin, Texas	30°12'32"	97°54'11"	8.24	1979–1986	11
08158860	Slaughter Creek at FM 2304, Austin, Texas	30°09'43"	97°49'55"	23.1	1981–1982	2
08158880	Boggy Creek (south) at Circle "S" Road, Austin, Texas	30°10'50"	97°46'55"	3.58	1976–1986	14
08158920	Williamson Creek at Oak Hill, Texas	30°14'06"	97°51'36"	6.3	1979–1984	14
08158930	Williamson Creek at Manchaca Road, Austin, Texas	30°13'16"	97°47'36"	19.0	1976–1984	18
08158970	Williamson Creek at Jimmy Clay Road, Austin, Texas	30°11'21"	97°43'56"	27.6	1976–1986	16
08159150	Wilbarger Creek near Pflugerville, Texas	30°27'16"	97°36'02"	4.61	1967–1977	29

Table 2. U.S. Geological Survey streamflow–gaging stations within the `dallas` data base module

[Approx., approximate; mi^2, square miles; IH, Interstate highway. One mi^2 equals 2.59 square kilometers (km^2).]

Station no.	Station name	Latitude	Longitude	Drainage area (mi^2)	Approx. period of record	No. of storm events
08055580	Joes Creek at Royal Lane, Dallas, Texas	32°53'43"	96°41'36"	1.94	1974–1979	7
08055600	Joes Creek, Dallas, Texas	32°51'41"	96°52'27"	7.51	1973–1979	10
08055700	Bachman Branch, Dallas, Texas	32°51'37"	96°50'13"	10.0	1964–1979	41
08056500	Turtle Creek, Dallas, Texas	32°48'26"	96°48'08"	7.98	1964–1979	42
08057020	Coombs Creek at Sylvan Avenue, Dallas, Texas	32°46'01"	96°50'07"	4.75	1965–1979	7
08057050	Cedar Creek at Bonnie View Road, Dallas, Texas	32°44'50"	96°47'44"	9.42	1974–1979	3
08057120	Spanky Branch at McCallum Lane, Dallas, Texas	32°57'58"	96°48'11"	6.77	1973–1978	5
08057130	Rush Branch at Arapaho Road, Dallas, Texas	32°57'45"	96°47'44"	1.22	1973–1979	7
08057140	Cottonwood Creek at Forest Lane, Dallas, Texas	32°54'33"	96°45'54"	8.5	1973–1978	6
08057160	Floyd Branch at Forest Lane, Dallas, Texas	32°54'33"	96°45'34"	4.17	1974–1979	8
08057320	Ash Creek at Highland Road, Dallas, Texas	32°48'18"	96°43'04"	6.92	1973–1978	5
08057415	Elam Creek at Seco Boulevard, Dallas, Texas	32°44'14"	96°41'36"	1.25	1973–1979	8
08057418	Fivemile Creek at Kiest Boulevard, Dallas, Texas	32°42'19"	96°51'32"	7.65	1976–1979	7

Station no.	Station name	Latitude	Longitude	Drainage area (mi^2)	Approx. period of record	No. of storm events
08057420	Fivemile Creek at U.S. 77, Dallas, Texas	32°41'15"	96°49'22"	13.2	1973–1979	10
08057425	Woody Branch at U.S. 77, Dallas, Texas	32°40'58"	96°49'22"	11.5	1973–1979	10
08057435	Newton Creek at IH 635, Dallas, Texas	32°39'19"	96°44'41"	5.91	1976–1979	4
08057440	Whites Branch at IH 635, Dallas Texas	32°39'26"	96°44'25"	2.53	1976–1979	4
08057445	Prairie Creek at U.S. 175, Dallas, Texas	32°42'17"	96°40'11"	9.03	1976–1979	8
08061620	Duck Creek at Buckingham Road, Garland, Texas	32°55'53"	96°39'55"	8.05	1973–1979	8
08061920	South Mesquite Creek at SH 352, Mesquite, Texas	32°46'09"	96°37'18"	13.4	1973–1979	9
08061950	South Mesquite Creek at Mercury Road, Mesquite, Texas	32°43'32"	96°34'12"	23.0	1969–1979	31

Table 3. U.S. Geological Survey streamflow–gaging stations within the `fortworth` data base module

[Approx., approximate; mi^2, square miles. IH, Interstate highway; W, West. One mi^2 equals 2.59 square kilometers (km^2). --, not available]

Station no.	Station name	Latitude	Longitude	Drainage area (mi^2)	Approx. period of record	No. of storm events
—	Seminary South Shopping Center and associated drainage area, Fort Worth, Texas	—	—	0.38	1970–1976	21
08048520	Sycamore Creek at IH 35–W, Fort Worth, Texas	32°39'55"	97°19'16"	17.7	1970–1977	24
08048530	Sycamore Creek tributary above Seminary South Shopping Center, Fort Worth, Texas	32°41'08"	97°19'44"	0.97	1970–1977	28
08048540	Sycamore Creek tributary at IH 35–W, Fort Worth, Texas	32°41'18"	97°19'11"	1.35	1970–1976	24
08048550	Dry Branch at Blandin Street, Fort Worth, Texas	32°47'19"	97°18'22"	1.08	1969–1976	25
08048600	Dry Branch at Fain Street, Fort Worth, Texas	32°46'34"	97°17'18"	2.15	1969–1977	27
08048820	Little Fossil Creek at IH 820, Fort Worth, Texas	32°50'22"	97°19'22"	5.64	1969–1977	20
08048850	Little Fossil Creek at Mesquite Street, Fort Worth, Texas	32°48'33"	97°17'28"	12.3	1969–1977	25

Table 4. U.S. Geological Survey streamflow–gaging stations within the sanantonio data base module

[Approx., approximate; mi^2, square miles. FM, Farm to market road. One mi^2 equals 2.59 square kilometers (km^2).]

Station no.	Station name	Latitude	Longitude	Drainage area (mi^2)	Approx. period of record	No. of storm events
08177600	Olmos Creek tributary at FM 1535, Shavano Park, Texas	29°34'35"	98°32'45"	0.33	1970–1981	14
08177700	Olmos Creek at Dresden Drive, San Antonio, Texas	29°29'56"	98°30'36"	21.2	1969–1978	23
08178300	Alazan Creek at St. Cloud Street, San Antonio, Texas	29°27'29"	98°32'59"	3.26	1969–1979	30
08178555	Harlendale Creek at West Harding Street, San Antonio, Texas	29°21'05"	98°29'32"	2.43	1977–1980	10
08178600	Panther Springs Creek at FM 2696 near San Antonio, Texas	29°37'31"	98°31'06"	9.54	1969–1975	13
08178620	Lorence Creek at Thousand Oaks Boulevard, San Antonio, Texas	29°35'24"	98°27'47"	4.05	1981–1981	3
08178640	West Elm Creek at San Antonio, Texas	29°37'23"	98°26'29"	2.45	1976–1979	8
08178645	East Elm Creek at San Antonio, Texas	29°37'04"	98°25'41"	2.33	1976–1979	6
08178690	Salado Creek tributary at Bitters Road, San Antonio, Texas	29°31'36"	98°26'25"	0.26	1969–1981	41
08178736	Salado Creek tributary at Bee Street, San Antonio, Texas	29°26'38"	98°27'13"	0.45	1972–1976	12
08181000	Leon Creek tributary at FM 1604, San Antonio, Texas	29°35'14"	98°37'40"	5.57	1970–1979	10
08181400	Helotes Creek at Helotes, Texas	29°34'42"	98°41'29"	15.0	1969–1981	15
08181450	Leon Creek tributary at Kelly Air Force Base, Texas	29°23'12"	98°36'00"	1.19	1969–1979	30

Table 5. U.S. Geological Survey streamflow-gaging stations within the smallruralsheds data base module

[Approx., approximate; mi^2, square miles; Sub., Subwatershed; The * notes that two different drainage areas have been published for this station. One mi^2 equals 2.59 square kilometers (km^2).]

Station no.	Station name	Latitude	Longitude	Drainage area (mi^2)	Approx. period of record	No. of storm events
08042650	North Creek Sub. 28A near Jermyn, Texas	33°14'52"	98°19'19"	6.82	1973–1979	14
08042700	North Creek near Jacksboro, Texas	33°16'57"	98°17'53"	21.6	1959–1979	58
08050200	Elm Fork Sub. 6 near Muenster, Texas	33°37'13"	97°24'15"	0.77	1961–1970	34

Station no.	Station name	Latitude	Longitude	Drainage area (mi^2)	Approx. period of record	No. of storm events
08052630	Little Elm Creek Sub. 10 near Gunter, Texas	33°24'33"	96°48'41"	2.10	1966–1976	29
08052700	Little Elm Creek near Aubrey, Texas	33°17'00"	96°53'33"	75.5	1959–1976	58
08057500	Honey Creek Sub. 11 near McKinney, Texas	33°18'12"	96°41'22"	2.14	1960–1970	32
08058000	Honey Creek Sub.12 near McKinney, Texas	33°18'20"	96°40'12"	1.26	1959–1970	29
08063200	Pin Oak Creek near Hubbard, Texas	31°48'01"	96°43'02"	17.6	1959–1971	33
08094000	Green Creek Sub. 1 near Dublin, Texas	32°10'00"	98°20'30"	*3.18/ 4.19	1959–1971	29
08096800	Cow Bayou Sub. 4 near Bruceville, Texas	31°19'59"	97°16'02"	*5.25/ 5.04	1959–1975	51
08098300	Little Pond Creek near Burlington, Texas	31°01'35"	96°59'17"	22.2	1964–1972	19
08108200	North Elm Creek near Cameron, Texas	30°55'52"	97°01'13"	48.6	1964–1972	21
08136900	Mukewater Creek Sub. 10A near Trickham, Texas	31°39'01"	99°13'30"	21.8	1966–1973	22
08137000	Mukewater Creek Sub. 9 near Trickham, Texas	31°41'40"	99°12'18"	4.02	1961–1973	38
08137500	Mukewater Creek at Trickham, Texas	31°35'24"	99°13'36"	70.4	1959–1961	5
08139000	Deep Creek Sub. 3 near Placid,Texas	31°17'25"	99°09'22"	3.42	1960–1971	29
08140000	Deep Creek Sub. 8 near Mercury, Texas	31°24'08"	99°07'17"	*4.32/ 5.41	1960–1971	30
08182400	Calaveras Creek Sub. 6 near Elmendorf, Texas	29°22'49"	98°17'33"	7.01	1961–1971	25
08187000	Escondido Creek Sub. 1 near Kenedy, Texas	28°46'41"	97°53'41"	3.29	1959–1971	32
08187900	Escondido Creek Sub. 11 near Kenedy, Texas	28°51'39"	97°50'39"	8.43	1962–1970	21

An example hyetograph data file from the data base is listed on figure 3. This data was used to produce the observed hyetograph on figure 1. From the figure, the three main components of the data file are visible. The header of the file is identified by the lines specified by the leading # sign. A single field line containing the label or column titles follows the header. This line is delimited by one or more spaces. Finally, the data records, which also are space delimited, make up the remainder of the file. Two

portions of the data lines have been removed for the figure because of limited space. As described for figure 1, the long flat leading tail of the hyetograph is an artifact of the data recording method. The 23.5 hr jump between zero precipitation and the first 0.02 inch (in.) (0.508 mm) is unacceptably too long for the purposes of hyetograph analysis. Algorithms are required to trim each tail of the observed hyetographs prior to subsequent analysis. Not all tails will require trimming, however.

```
# HYETOGRAPH FILE
# site=08156800 Shoal Creek at 12th Street, Austin, Texas.
# latitude=30()16'35"
# longitude=97()45'00"
# drainagearea (mi2)=12.3
# DATE_TIME=date and time in MM/DD/YYY@HH:MM
# PRECIP1=1SHL raw recorded data
# PRECIP2=2SHL raw recorded data
# ACCUM_WTD_PRECIP=accumulated weighted or single gage
# precipitation in inches
DATE_TIME    HOURS_PASSED    PRECIP1    PRECIP2    ACCUM_WTD_PRECIP
05/23/1981@00:00:00     0.0000    0.0000    0.0000    0.0000
05/23/1981@23:30:00    23.5000    0.0700    0.0000    0.0200
05/23/1981@23:45:00    23.7500    0.5700    0.1900    0.2800
05/24/1981@00:00:00    24.0000    0.7400    0.5700    0.6100
05/24/1981@00:30:00    24.5000    1.0400    0.9200    0.9500
05/24/1981@01:00:00    25.0000    1.1300    1.0700    1.0800
                  ... portions cut for brevity ...
05/25/1981@00:15:00    48.2500    8.5100    7.8800    8.0300
05/25/1981@00:30:00    48.5000    8.5700    7.9800    8.1200
05/25/1981@00:45:00    48.7500    8.6500    8.0200    8.1700
05/25/1981@01:00:00    49.0000    8.7300    8.0700    8.2300
05/25/1981@01:30:00    49.5000    8.7500    8.0800    8.2400
05/25/1981@02:00:00    50.0000    8.7900    8.1400    8.3000
```

Figure 3. Example data file `austin/ShoalCreek/sta08156800_d/hyetos/rain_sta08156800_1981_0523.dat` **from the** `austin` **data base**

Some other aspects of the data file on figure 3 that need description are the values for `PRECIP1`, `PRECIP2`, and `ACCUM_WTD_PRECIP`. The `ACCUM_WTD_PRECIP` (accumulated weighted precipitation) is the best available estimate for precipitation on the entire watershed and was derived from the `PRECIP1` and `PRECIP2` values. Two rain gages, labeled `PRECIP1` and `PRECIP2`, were operating during the May 1981 storm

event in the Shoal Creek watershed. If additional precipitation gages were available during the event, then the labeling follows the PRECIP# convention. The raw data is shown in the PRECIP# fields. Sometimes the rainfall data collected for a watershed might include one or more weighing or volumetric rain gages, which presumably provided (presumed by the previous USGS analysts in developing the data reports) more accurate data than the recording charts or tipping bucket type rain gages. Volumetric rain gage data is not reported in the file and hence is not represented in the data base. The ACCUM_WTD_PRECIP values were computed by the previous analysts by amalgamated weighting of partial areas on the watershed and corrections to the volumetric values when present.

The 1,659 hyetographs for the five data base modules are shown on figures 4–8. In each of the five figures, the values composing each hyetograph are plotted against the concomitant time values in the top graphs (graphs A). The period of record available in each module is seen in the graphs A. The separate watersheds within each data base module are not differentiated. It is evident in graphs A that the number of storms represented per year is relatively uniform for the four urban data base modules (figs. 4–7). Some minor clustering of events on a yearly basis is exhibited; this reflects concepts of "wet" and "dry" years. The smallruralsheds module (fig. 8) exhibits a marked reduction in the number of storm events per year starting about 1972 as the study units were decommissioned. The last storms available in the data base occur in 1987 for the austin module. Although the USGS and collaborating agencies continue

to intensively collect data in rural and urban areas, compilation and publication of rainfall and runoff for individual storms is no longer occurring.

It is important to note that the total number of visually distinct hyetographs in graphs A does not equal the number of events seen in the other graphs (B and C) or indicated in the figure title. This is because numerous events typically occur simultaneously because a single storm often effects many stations in the area surrounding the storm and the path along the storm track. This has the effect of causing many hyetographs to become masked in graphs A. Because many of the hyetographs occur on the same day or other intervals of time, the observed hyetographs are not each independent. Therefore, meteorological mechanisms generating each hyetograph are not random or statistically independent—the data base does not contain as much *independent information* as suggested by the total number of hyetographs.

In order to visualize seasonal differences in the magnitude and the number of events, the year was converted to a common base (on a leap year) for the middle graphs (graphs B) on figures 4–8. A strong seasonal clustering of events is seen for the `austin` module (fig. 4). One cluster occurs between the middle of April and the middle of June, and a secondary cluster occurs in October. The `dallas` module (fig. 5) also exhibits a primary event cluster between the middle of March and the middle of June. Distinct clusters are harder to visualize in the `fortworth` module (fig. 6); although a weak cluster near the end of May might exist. The `sanantonio` module

(fig. 7) exhibits a strong primary cluster between the middle of April and the middle of June. This is consistent with the Austin data base module. A secondary cluster for the `sanantonio` module is less distinct and much longer lasting than that for the `austin` module. The cluster begins at the beginning of August and gradually tapers off towards the end of the year. The `smallruralsheds` module, which has the greatest range in geographic location of the five modules and includes areas proximate to other four modules, exhibits two or three event clusters. One cluster occurs between the middle of April and the middle of June; a possible cluster near the end of July; and a final cluster between the end of August to the middle of October.

From the graphs B on figures 4–8, distinct meteorological mechanisms might be evident. The strong tendency for double clustering of events (spring and fall) in the Dallas area and in the `smallruralsheds` module (which has many watersheds in the upper half of Texas) might be attributed to the more northerly watershed locations. The northern watersheds around Dallas and Fort Worth areas are more frequently influenced by cold fronts over a longer time interval or fraction of the calendar than those for Austin. It is possible that Austin experiences more rainfall and runoff producing cold fronts in the late spring than in the fall. Although San Antonio is considered geographically proximate to Austin, a considerably longer fall event cluster is evident; this might be attributed to more proximity of the San Antonio area to the Gulf of Mexico and hence a moisture source than the Austin area.

In the bottom graphs (graphs C) on figures 4–8, each hyetograph is plotted against the HOURS_PASSED field. From this figure, it is obvious that a substantial variation in the temporal pattern of the storms exists. As a result, prediction of the expected hyetograph is not a problem with a straightforward or unique solution. Also from the figure, the presence of unacceptably long leading and trailing tails such as the leading tail exhibited on figures 1 and 3 are visible.

The hyetographs in the graphs C of figures 4–8 can be re-expressed in terms of cumulative percentage on both rainfall depth and time axes. The re-expression into percentages enables individual storms to be compared and simplifies the analysis and graphical presentation of the data. Other researchers have used this technique (for example, Huff, 1967, fig. 2).

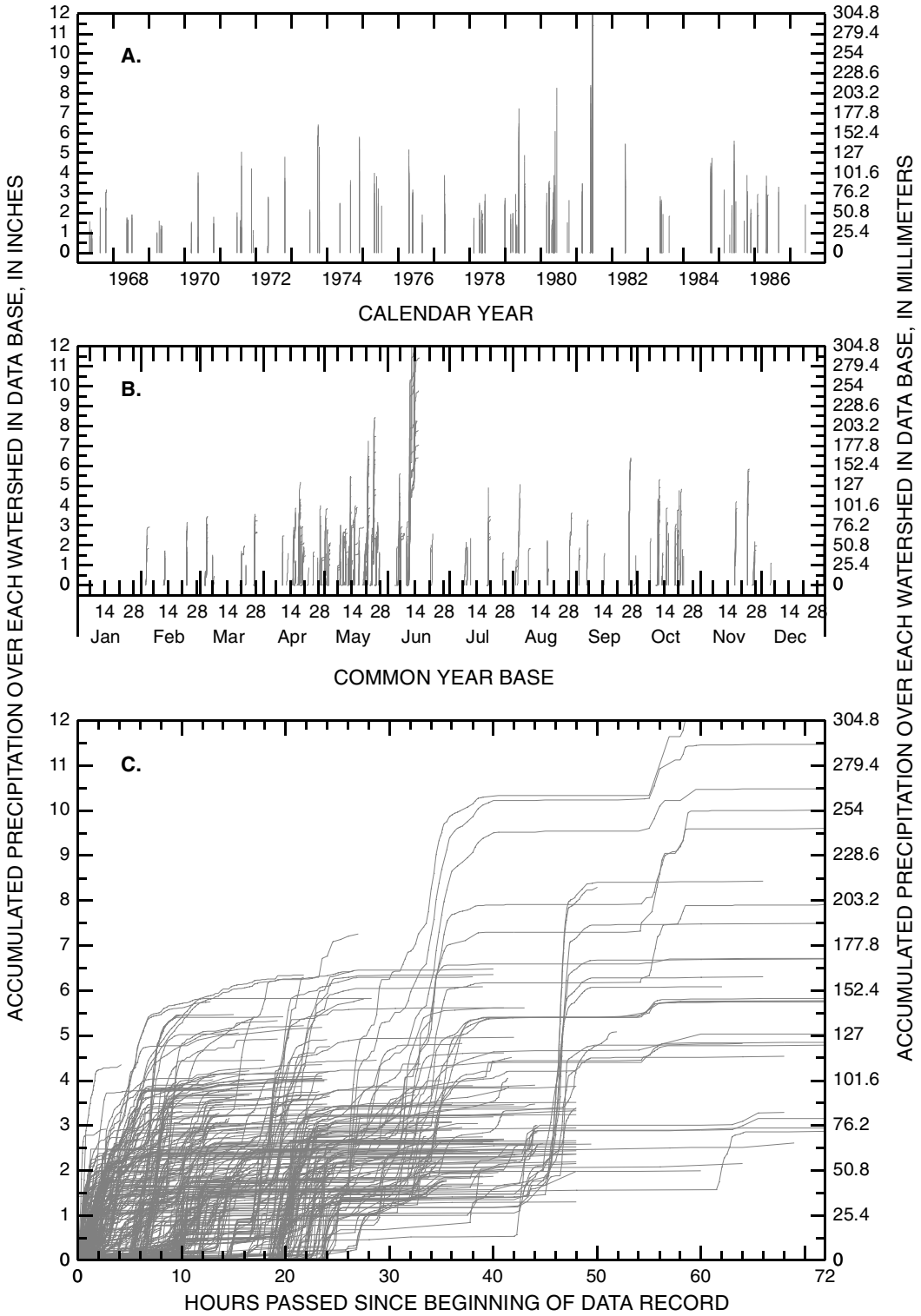

Figure 4. Hyetographs for `austin` data base module—401 storm events represented

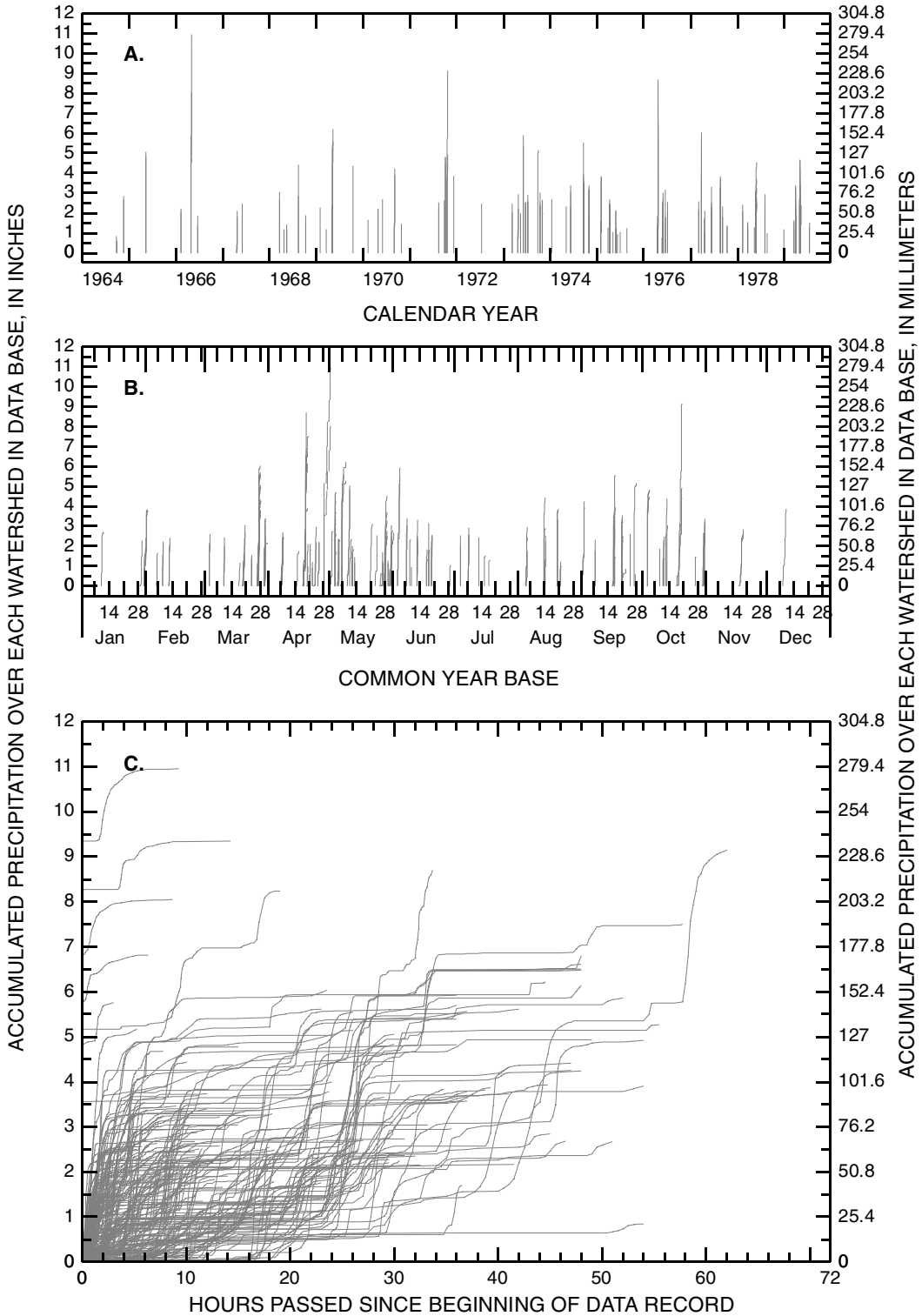

Figure 5. Hyetographs for `dallas` data base module—240 storm events represented

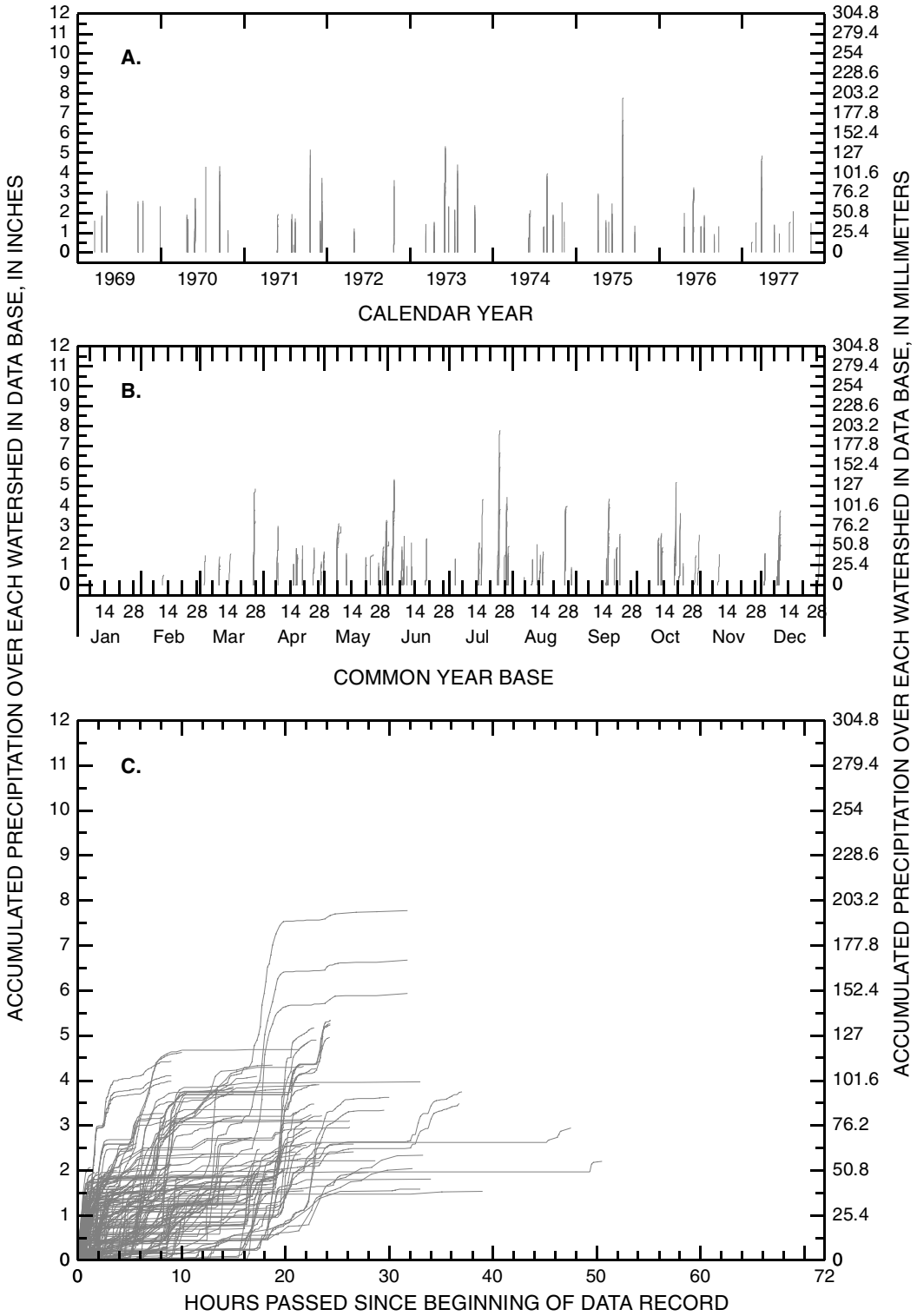

Figure 6. Hyetographs for `fortworth` data base module—194 storm events represented

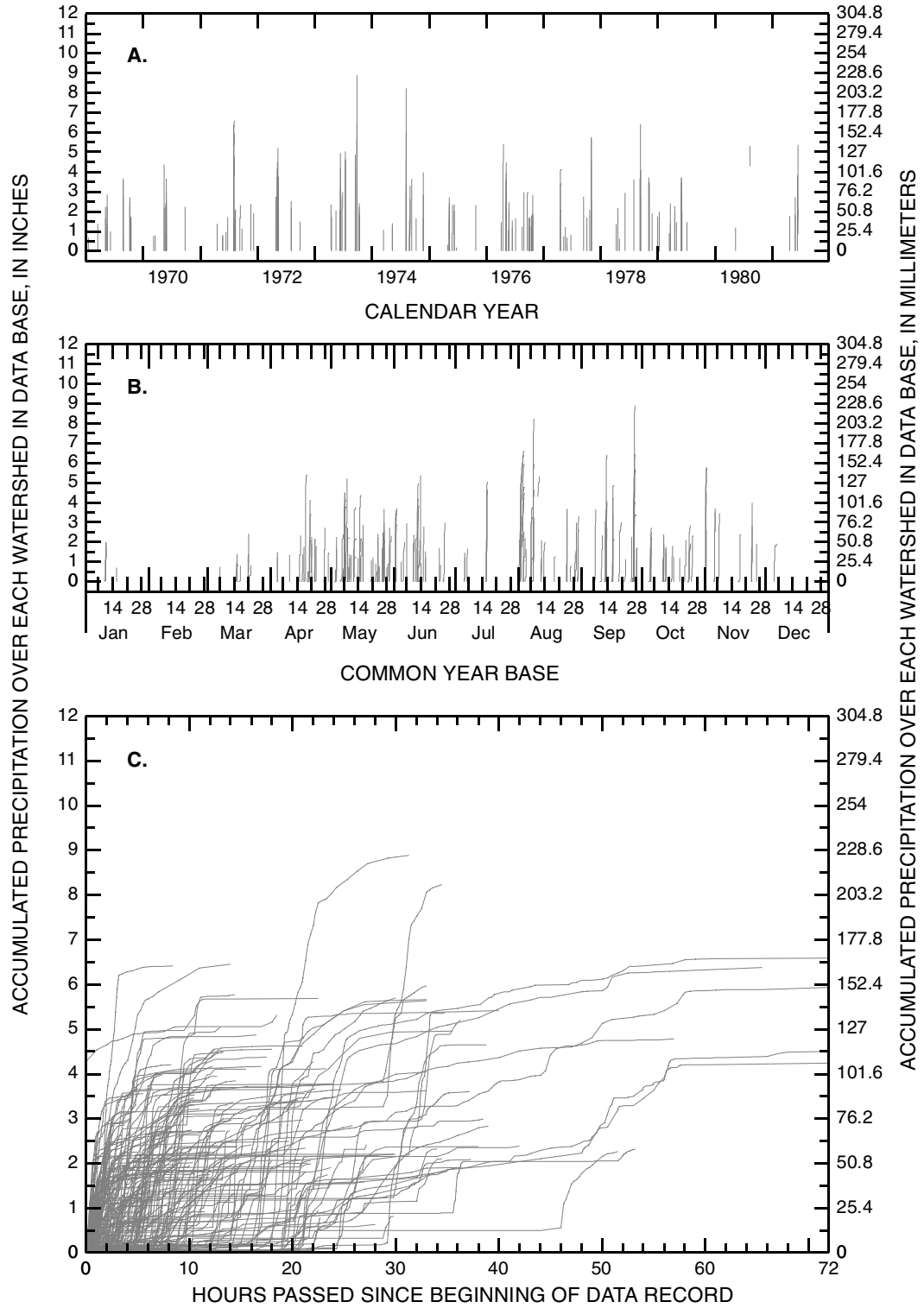

Figure 7. Hyetographs for `sanantonio` data base module—215 storm events represented

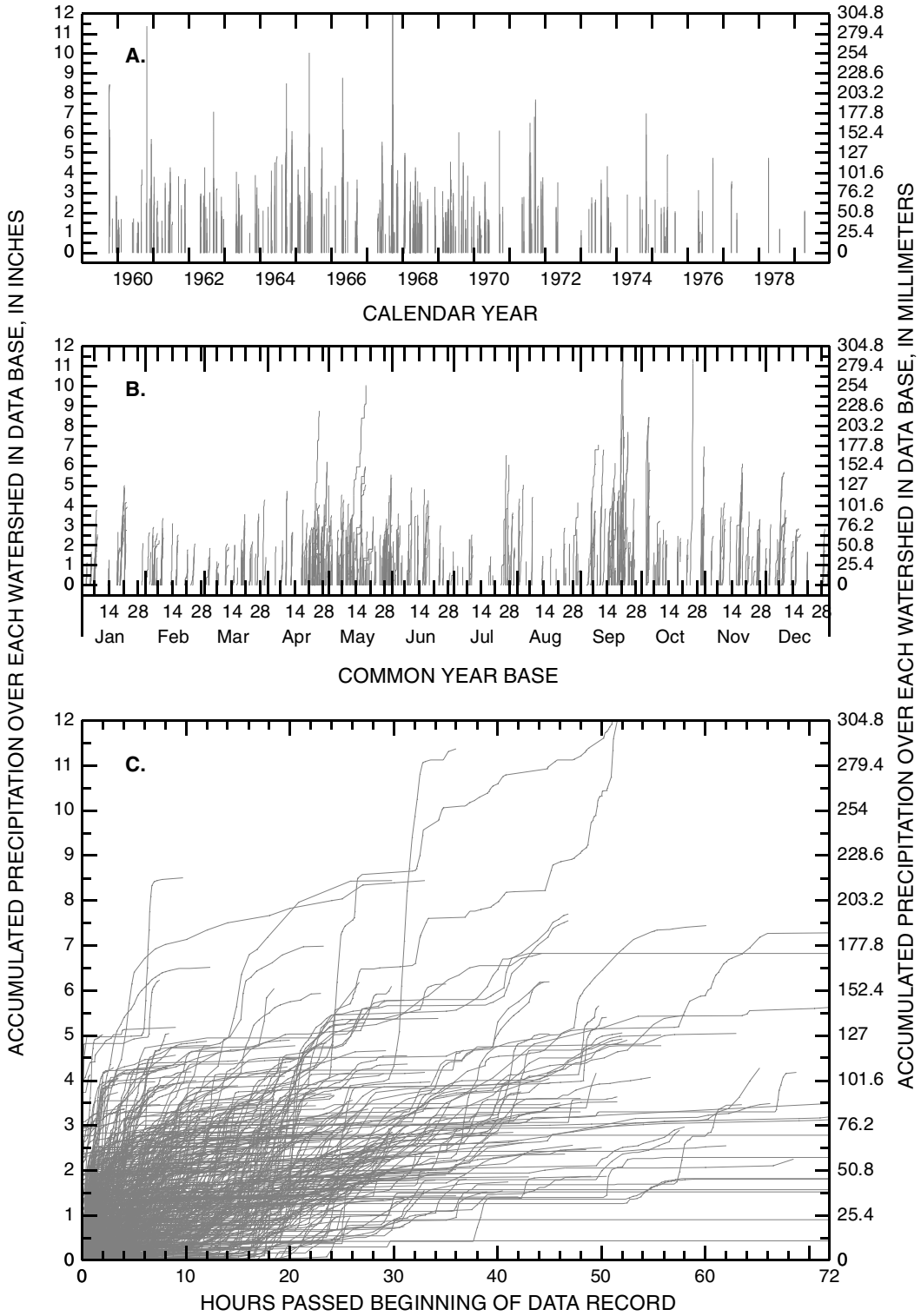

Figure 8. Hyetographs for `smallruralsheds` data base module—609 storm events represented

Dimensionless or percentile hyetographs of those on figure 6 are shown on figure 9. The hyetographs for the `fortworth` module were chosen for figure 9 because the data base had the smallest number of events, and hence, it is most attractive for display. A substantial variation in hyetograph shape is evident in the figure. From the figure, it is clear that a large number of storms have lengthy leading and trailing tail lengths compared to the general time length of the precipitation bursts. It has been observed in general that both leading and trailing tails are artificially lengthened by the data recording method. Further, the figure indicates a large number of multiple burst events; whereas for other events, the line steadily increases with duration. It is important to consider that the rainfall bursts are the predominate flood runoff producing fractions of individual hyetographs for small watersheds.

Three hypothetical expected hyetographs have been superimposed on figure 9 to illustrate the concept of the expected hyetograph. The anticipated values for the mean, median, and variability or scale statistics are indicated for each of the three expected hyetographs drawn on the figure; a complimentary figure illustrating anticipated values for the statistics is provided in figure 54 (referenced out of sequence). The primary objective of this research is to define the expected hyetograph. The expected hyetographs do not represent a fit or a conclusion of research but rather are for illustration only. It is important to note that there is a wide range in durations (few hours to days) and a wide range in precipitation magnitude (fractional inches to many inches) represented in the figure. An important component of the analysis of rainfall

hyetographs is separating the potential influences on the duration or magnitude of the event on the hyetograph. These factors are subjects of subsequent portions of this dissertation.

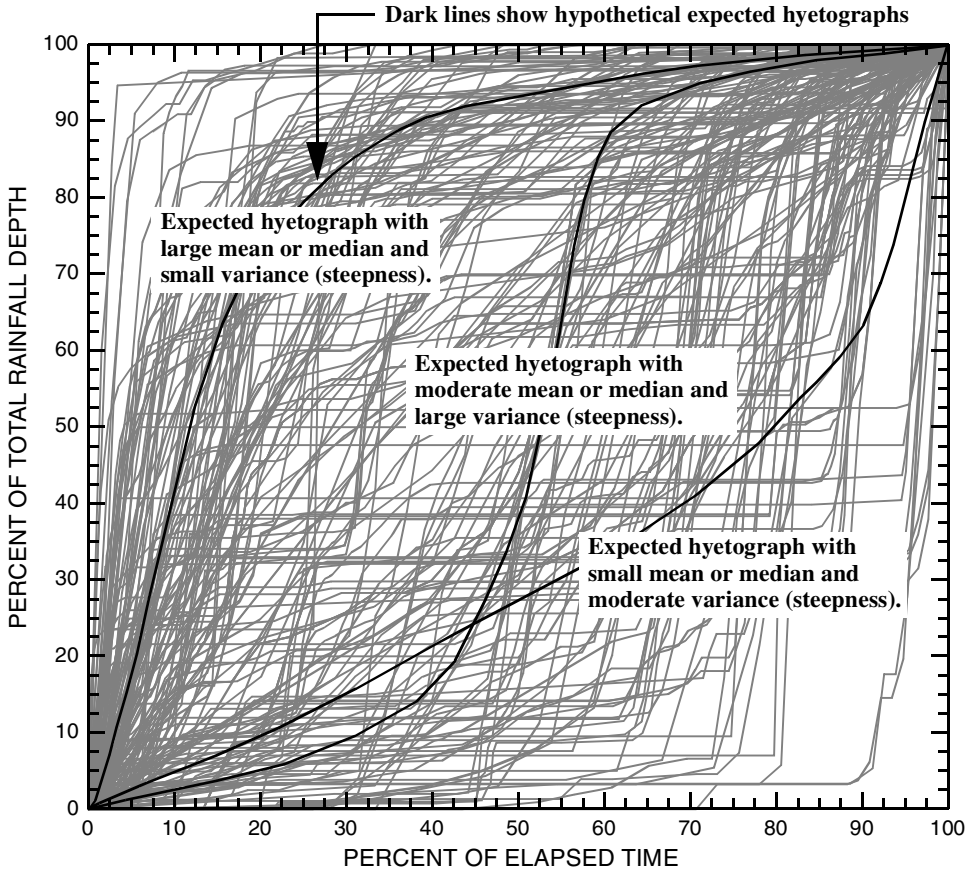

Figure 9. Dimensionless or percentile representation of the 194 hyetographs from `fortworth` data base and three hypothetical expected hyetographs

The large number of events within the entire data base provides a basis for regional analysis of hyetographs. The temporal variation of recorded storms is so great that a large data base is necessary to estimate the expected hyetograph. It is hypothesized that rainfall hyetographs in the data base can be statistically regionalized by investigation of the regional characteristics of the L-moments of hyetograph

cumulants (ordinates of the cumulative hyetograph). An extremely important consideration of the data base is that often the recorded values for each storm are *not suitable* for sample L-moment estimation techniques in current practice because there is a prior expectation that the data points within the data base are not random or evenly spaced observations of the hyetograph distribution representing individual events. Because of this expectation, a new technique for L-moment computation of a sample is required. This technique is described in chapter 4.

Model Verification and Suitability

Verification of regional statistical hydrologic models, such as hyetograph models, is an extremely difficult and perhaps an impossible task because true controlled experiments are difficult in the natural world. Heuristic arguments outlined below can be used to evaluate the suitability of the model. Thus, assessing the suitability of a hyetograph model is a more tractable goal than explicit model verification. Because expected hyetograph models are statistically based and not founded on physics, analytical thought coupled with controlled experiments can not provide a basis for verification. Proper experimental methods applicable to hyetograph analysis and prediction are difficult to envision.

Often the suitability of a hydrologic model is conducted through contrived regional statistical simulation methods on computer. Such simulations have a long and valuable history in regional hydrologic frequency analyses; numerous papers are available in journals such as *Journal of Hydrology* (such as Haktanir and Bozduman,

1995) and *Water Resources Research* (such as Fill and Stedinger, 1995). Hosking and Wallis (1993a) provide an excellent example of such simulations applicable to L-moments and frequency analysis, and the references therein are important. These schemes do not constitute a model verification technique. At the present time, it is unclear how to construct a viable hyetograph simulation framework or whether numerical weather and climate models could assist in that effort. The suitability of a hydrologic model can be assessed graphically or by statistical errors based on the fit of a model to the observed data.

Although verification in a physical sense of a statistically-based hyetograph model is difficult, the suitability of the model can be assessed by comparing features of the model to aspects of observed storms. For example, storms can be classified into three general categories of front, center, and back loaded, where the time in which the bulk of the precipitation occurs is reflected in the name of the classification. A front-loaded storm might have 70 percent of cumulative depth in the first half of time. A suitable model that is adequately fitted to a front-loaded storm should have an upper right hand tail that gradually or even asymptotically approaches the total storm depth. This implies that the second derivative is negative and decreases with increasing duration near the end of the storm, which means that rainfall rates are diminishing.

Other arguments for assessing model suitability are anecdotal accounts. Common experience and review of observed short duration (few hours or so) hyetographs suggests that runoff producing storms on small watersheds appear to be front-loaded.

Periodic observation of storms in the Austin area by public weather radar by the author indicates that many runoff producing storms on small watersheds hit hard with great intensity and then gradually diminish as time progresses; whereas occasionally other storms start gradually and then diminish.

The skewness of an observed hyetograph is a measure that reflects the loadedness of the storm: front loaded equates to positive skew, center loaded equates to near zero skew, and back loaded equates to negative skew. Very short durations (minutes to multiple hours) storms might be expected to be less front loaded than long duration (days) storms because of a limited time interval to spread the rainfall depth. Hence, skewness should be a function of duration. This is a tertiary hypothesis that is considered in chapter 5.

Dissertation Organization

The dissertation is organized so that each chapter subsequent to the *Introduction* chapter is either a stand-alone paper or nearly stand alone discussion of a specific topic pertinent to the research. Moderate overlap between chapters naturally is present, and occasionally there is a need to directly recall material from previous chapters or foreshadow material in later chapters. Some of the topics are methodological as opposed to topics provided that hyetograph specific research results. This is because some of the methods used here are new and substantial research into methodology was required.

Previous Studies. This chapter provides a comprehensive review of rainfall hyetograph studies and illustrates a classic method for estimating a hyetograph based entirely on depth-duration frequency values of annual precipitation maxima. Other chapters provide similar or supplemental information about the prior work of other researchers as context dictates.

Triangular Model of Dimensionless Rainfall Hyetographs Known to Produce Runoff in Texas. This chapter is organized as a stand-alone paper that has been submitted to the *Journal of the American Water Resources Association*. The chapter describes a triangular model for dimensionless hyetograph estimation, and the model is a simple example of a regional analysis. Such models have precedence for hyetograph approximation. The motivation for this chapter is that since the triangular model is straightforward to understand, the apply, and the fact that L-moments are not required, the expected hyetographs defined by the triangular model should provide a comparative basis for other analyses in the dissertation. This chapter precedes the much more complicated research and analysis chapters. This was done to provide the reader with a greater understanding of the remainder of the dissertation.

In the paper, the triangular model is fit to the observed hyetographs of the data base after dimension is removed. The fitted model produces an expected hyetograph. A separate model is fit to hyetographs from storms having 0–24 hr and 24 hr and greater durations. An important note about nomenclature is needed; this dissertation uses “24 hr and greater” to refer to storm durations between 24 hr up to about 3 days.

The hyetograph from each model is compared to a hyetograph from an earlier study of hyetographs conducted for Texas rainfall data. Some material from chapters 1 and 2 is repeated, and moderate amounts of salient previous work is freshly described. The repetition is required in order to make a distinct paper out of the chapter.

Sample L-moment Estimation using prior-Probability Weighted Moments. This chapter provides the description of an alternative method from established procedures for L-moment estimation. This method requires description because of the nature of the way that the observed hyetographs were recorded and preserved for the data base. The issue is that the data values defining the hyetograph are not either uniformly or truly randomly distributed (constant interval digitized) and adjustment to sample L-moment estimation techniques is needed. The new method requires explanation and demonstration by example by limited statistical simulation experiments. The experiments also show that the author's custom software is properly functioning.

L-moments of Runoff-Producing Dimensionless Rainfall Hyetographs in Texas. This chapter provides an analysis of the L-moment (and median) values of the hyetograph distributions. Because the L-moments of hyetograph distributions quantify various measures of the distributional shape, it is important that an understanding of potential influences on the numeric values of the L-moments is made. An investigation into the dependency of L-moment values on storm depth for three duration ranges is conducted. Another investigation into the seasonal and monthly behavior of the L-moments also is conducted. And finally, geographic influences on the L-moments

are investigated along with consideration of compatibility between the five hyetograph data modules. A sequence of important conclusions completes the chapter.

L-gamma Distribution. This chapter introduces a new statistical quantile function for modeling the quantile distribution of a random variable that is bounded by 0 and 1. The distribution is compatible with the theory of L-moments. This distribution is appealing for application to hyetographs because dimensionless hyetographs by their very definition when expressed in fractional percentages are also bounded by 0 and 1. Further, the L-gamma has an explicit quantile function form and simple first and second derivatives. Each of these facts contributes to the utility of the distribution.

L-gamma Model of Dimensionless Rainfall Hyetographs Known to Produce Runoff in Texas. This chapter describes an application of the L-gamma distribution for modeling the shape of the expected hyetograph for several durations. The models are based on statistics presented in chapter 5. The L-gamma hyetograph models are compared to both the triangular model and the well-known Beta distribution. The L-gamma and triangular models exhibit distinct differences that are discussed. The L-gamma and Beta distributions exhibit relatively minor differences. The suitability of the L-gamma model is assessed through an alternative hyetograph analysis technique. Finally, criticisms of the hyetograph models are made, and an application example of hyetographs for generation of streamflow hydrographs is presented.

Modification of the Carman-Kozeny Equation for Application of L-moment Statistics for Estimation of the Intrinsic Permeability of Porous Media. This chapter is

unrelated to the hyetograph theme of all other chapters in this dissertation. The chapter is included because an promising application of L-moments to the estimation of permeability is envisioned following the lead of product moment based analysis of previous researchers. The application is based on the L-moments of grain-size distributions and quantile functions modeling the distribution. The prior-Probability Weighted Moments described in chapter 4 have a natural application to sample L-moment computation for grain (particle) size data.

Conclusions. This chapter enumerates and describes the major conclusions and commentary of the research hypotheses. No new material is presented in this chapter.

Appendices. Several appendices are provided. Appendix A provides a comprehensive citation list of the USGS data reports that provided the rainfall hyetograph data. Appendix B provides a comprehensive background of L-moment statistical theory and is included for readers unfamiliar with L-moments. A manual example computation of the unbiased L-moments for a sample is shown in Appendix B to demonstrate how the L-moments are computed without the aid of computer software. Appendix C provides the results of supplemental simulations used to explore the suitability of prior-Probability Weighted Moments for sample L-moment estimation described in a separate chapter. Appendix D provides extensive tables mapping the solution space of the L-gamma distribution. Appendix E provides certain critical computer programs written as part of the research that require documentation. Appendix F provides supplemental tables for chapter 7.

CHAPTER 2
PREVIOUS STUDIES

Comparatively few papers treat expected hyetographs in general as opposed to other aspects of hydrologic design such as unit hydrographs (Thompson, personal commun., 2002). Two excellent starting points in the literature and references therein are Pilgrim and Cordery (1975) and Veneziano and Villani (1999). Pilgrim and Cordery (1975) and Veneziano and Villani (1999) categorize approaches to developing expected hyetographs. Each reference provides slightly different hyetograph categories, but despite differences these can be generalized as: 1) simple geometric shapes anchored to a single point on the rainfall intensity-duration frequency (IDF) curve, 2) use of the entire IDF curve, 3) standardized or statistical hyetograph profiles developed from rainfall records, 4) simulation using stochastic rainfall models, and 5) arbitrary temporal patterns. Another category is suggested by Haan and others (1994, p. 44); this is the adoption of an actual storm from the historical record in the vicinity of interest that has occurred and that is known to cause substantial flooding and damage. This category might be lumped into category 5.

Category 4 is not desirable from a basic hydrologic design requirement of repeatability. The stochastic simulation requires sophisticated computational resources, considerable evaluation of model suitability, and high overhead for general use. The arbitrary temporal patterns (category 5) likely are not based on actual rainfall data. The historical rainfall approach is advantageous as being conceptually simple and easy to use. Haan and others (1994) report a distinct disadvantage of the historical

rainfall approach; the approach produces (uses) a storm with an unknown frequency of occurrence.

Intensity-Duration Frequency (IDF) based Hyetograph Methods

Use of the IDF curve as a foundation for hyetograph generation (categories 1 and 2) is very common. Most hydrologic textbooks (for example, Chow and others, 1988; Haan and others, 1994) dealing with rainfall-runoff design problems contain hyetograph procedures based in some fashion on the IDF curve. Keifer and Chu (1957) estimated design hyetographs based somewhat on the IDF curves, and their method is sometimes known as the Chicago Method. This method is more formulaic than the widely used more ad hoc IDF methods detailed in this section.

The Soil Conservation Service (SCS, 1973), now the National Resources Conservation Service (NRCS), developed a hyetograph modelling approach very similar to the IDF curve method. The method provides dimensionless hyetographs classified into four types dependent upon specific regions of the United States. The Type II and III hyetographs are represented in Texas and elsewhere in the United States. The Type II hyetograph is applicable for most of Texas, is the most intense, and is in common use (Herrmann, written commun., 2002 and Stolpa, written commun., 2002). An example of the Type II hyetograph is shown on figure 16 (referenced out of sequence), and the Type III hyetograph is very similar in shape. The curves are essentially generalizations (by the author's reading of SCS (1973) of the balanced storm techniques based on the now outdated rainfall depth-duration frequency (DDF)

values, equivalently IDF values, of Hershfield (1962). Frederick and others (1977) provide DDF values for very short storm durations (5–60 minutes) and compliment the 30 minutes to 24 hr storm durations of Hershfield (1962). An updated report of DDF for Texas is provided by Asquith (1998). The durations considered in the Texas report include those of Hershfield (1962) and Frederick and others (1977).

There are several reasons for the widespread use of the IDF approach. First, it is assumed by many practitioners that frequency levels (recurrence intervals or return periods) can be assigned to synthetic hyetographs derived from IDF curves (IDF hyetographs). Second, these hyetographs are repeatable—they provide consistent (not necessarily accurate) results. Third, IDF hyetographs are known to represent reasonable (or at least so broadly accepted and used by the hydrologic and engineering community that "reasonable" is seldom questioned and the potential problems with the hyetograph are mitigated by other aspects of the design process) temporal storm patterns for a given frequency. Fourth, it is common to develop the IDF hyetograph in such a fashion so that the hyetograph produces a rainfall depth or intensity whose frequency is independent of the storm duration (Haan and others, 1994, p. 45). Because of the duration independence, it is presumed that these hyetographs are applicable across an entire range of watershed scales.

A limitation of the IDF based approaches is that a physical storm must have an incredibly small chance of occurring exactly as the IDF hyetograph suggests. It is important to note that the IDF curve is constructed by the most intense bursts of

rainfall, which are preserved in the historical record as annual maximum intensities for a given duration, that occur within large storms. The IDF hyetograph is not based in any fashion on the temporal nature of real events. The IDF curve based hyetograph is hence a worst case scenario and does not represent an "expectation" in a statistical sense.

Pilgrim and Cordery (1975, p. 81) observe that "design rainfall derived from frequency-duration data does not generally represent the rainfall in complete storms." Further, it seems to the author and observed by Pilgrim and Cordery that an implicit assumption in IDF hyetograph justification and usage is that a hyetograph of a given frequency level produces a flood peak and volume of the same frequency level. Thus, a 3-hr 25-year hyetograph produces the 25-year flood on a watershed characterized by a 3-hr time scale. Testing of this assumption is outside the scope of the dissertation.

Actual Rainfall Record based Hyetograph Methods

The standardized or statistical hyetograph developed from actual rainfall records (category 3) is the last general technique of hyetograph specification. A broad range of analytical and statistical methods can be used. This category is attractive because the hyetographs become expectations of real data and entire storm durations, and the hyetographs are not derived from abstractions of the non-whole storm based IDF curve.

Some important papers involving the analysis of actual rainfall records include: Huff (1967, 1990), Yen and Chow (1980), Chukwuma and Schwab (1983), Bonta and

Rao (1988a,b; 1989), Schaefer (1989), Parrett (1998), and references therein. The research by Huff is perhaps the most widely known and cited. Bonta and Rao (1989) and Huff (1990) cite Pani and Haragan (1981)—no other citations to Pani and Haragan are known. The Pani and Haragan paper provides dimensionless hyetographs for a small rain gage network in the southern High Plains of Texas. Because these hyetographs are based on Texas data, the hyetographs are directly comparable to the resulting hyetographs in this dissertation.

Hyetograph Research by Huff

Huff (1990), based largely on Huff (1967), presented dimensionless rainfall hyetographs as families of curves derived from storms that Huff classified as first-, second-, third-, and fourth-quartile. Huff defines a "storm" as a "rain period separated from preceding and succeeding rainfall by six hours or more" (Huff, 1967, p. 1007). Huff does not provide sensitivity analysis of the presumably arbitrarily chosen 6 hr definition. The quartile designation depends on whether the greatest percentage to total rainfall occurs in the first, second, third, or fourth quarter of the storm duration. Huff's data base includes a total of 261 storms on a 400 mi^2 (1,036 km^2) network of 49 recording rain gages in east-central Illinois sampled between 1955 and 1966. Each storm had an areal mean rainfall of at least 0.5 in. (12.7 mm), a duration between 3 and 48 hr, and at least one rain gage within the area had to record at least 1 in. (25.4 mm) of precipitation. An interesting inconsistency is that the 1955–1966 period is said by

Huff of contain both 11 years of data (Huff, 1967, p. 1007) and 12 years of data (Huff, 1990, p. 3).

The exact algorithm used by Huff for the storm classification is not provided by Huff, although a digital computer was used in the analysis. Huff (1967, p. 1008) does say that the classification depended "on whether the heaviest rainfall occurred in the first, second, third, or fourth quarter of the storm period." Huff (1967, table 1) determined that the relative frequencies of the quartiles were 30, 36, 19, and 15 percent for the first, second, third, and fourth quartile, respectively. These relative frequencies change somewhat in Huff (1990) by considering differences between precipitation at a point and over an area.

Huff concludes that short duration storms (less than 6 hr) were often associated with first-quartile storms, moderate duration storms (6–12 hr) were often associated with second-quartile storms. Third-quartile storms often had durations of 12–24 hr; whereas, fourth-quartile storms had durations greater than 24 hr.

The median (50th percentile) dimensionless hyetograph for each quartile classification based on point rainfall values—that is rainfall data specifically for the recording device—is presented on figure 10. These curves were generated for this dissertation from a summary data table provided by Huff (1990, table 3). Huff also provides curves representing other percentiles ranging from 10 to 90 percent which envelop the median curve. From the figure, it is clear that each storm classification has a considerably different shape than its neighbors. This variation is inherently related to

factors (Huff, 1967, p. 1009) such as developmental stage of the storm, size and complexity of the storm system, rainfall type, synoptic storm type, location of the sampling points with respect to the storm center, and the movement of the storm system across the sampling region.

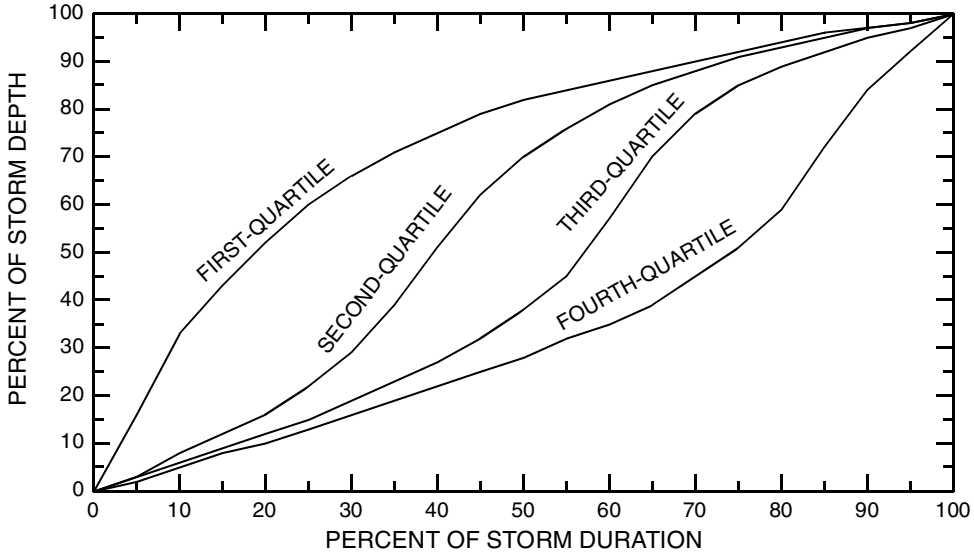

Figure 10. Median dimensionless hyetographs at a point for first, second, third, and fourth quartile heavy rainfall storms derived from Huff (1990, table 3)

The factors identified and described by Huff result in subtle differences when the dimensionless hyetographs are generated over finite areas instead of at points. Using summary data from Huff (1990, table 4), figure 11 shows the four median dimensionless hyetographs for areas ranging from 10 to 50 mi^2 (25.9 to 129 km^2). Comparison of corresponding curves on figures 10 and 11 will show that the difference between the curves generally is small. Huff concludes that the point hyetographs also are valid for areas but that the validity of the curves diminishes as area increases.

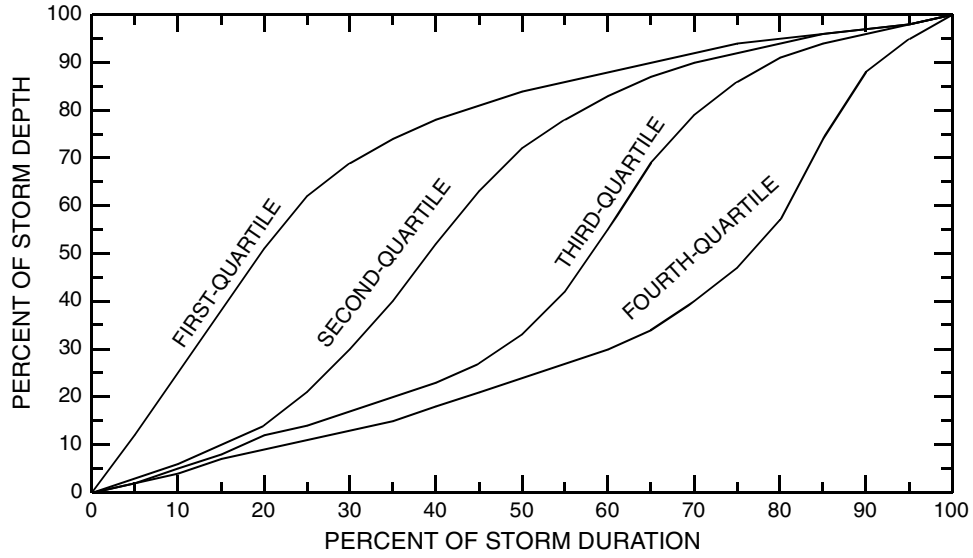

Figure 11. Median dimensionless hyetograph on areas of 10 to 50 square miles for first, second, third, and fourth quartile heavy rainfall storms derived from Huff (1990, table 4)

Huff (1967) provides considerable discussion of analysis of rainfall bursts (see figure 1 of this dissertation for a graphical description of rainfall bursts). Huff (1967) investigates the relations between rain type, storm type, and storm shape and orientation on the temporal distribution of rainfall.

Huff (1990) concludes for hydrologic design applications that first-quartile hyetographs should be used for design time scales of about 6 hr or less and second-quartile hyetographs should be used for time scales of about 6–12 hr. No direct recommendation for third- or fourth-quartile hyetographs for design applications appears to have been made.

Hyetograph Research by Pani and Haragan

The hyetograph research by Pani and Haragan (1981), although not widely known, appears to be the only hyetograph analysis done explicitly on Texas rainfall data. Their analysis followed Huff (1967), and they compare their results favorably to those of Huff. Details of the Huff approach including clarification of terminology used here are provided in the previous section.

Pani and Haragan classified storms into four quartile categories depending upon which quarter of dimensionless storm time had the greatest change in storm depth. They analyzed 117 storms that occurred between May 15 through July 31 for a 3-year period (1978–80) over the High Plains Cooperative Program (Texas HIPLEX) rain gage network (Texas Department of Water Resources, 1980). The network was located in southern High Plains of Texas near the town of Big Spring, Texas and covered about 2,600 mi^2 (6,744 km^2, reported by Pani and Haragan) The data consisted of 15-minute values. The mid May to July period was selected because the authors were interested in the hyetographs of convective-generated precipitation. The authors defined a storm as a "rain period of at least 0.75 hour duration separated by at least 1 hour" (Pani and Haragan, 1981, p. 77). Interestingly, Pani and Haragan appear to not have identified a minimum storm depth considered for analysis, but Bonta and Rao (1989, table 1) report that Pani and Haragan (1981) used about a 0.75 in. (a value of 19.3 mm was reported by Bonta and Rao) minimum depth.

Pani and Haragan (1981, table 1) determined that the relative frequencies of the quartiles were 13, 41, 32, and 14 percent for the first, second, third, and fourth quartile, respectively. These frequencies indicate that most events (73 percent) are characterized as second and third quartile. This observation differs from Huff (1967, 1990) who found that most events (66 percent) are characterized as first and second quartile. The authors used the χ^2-test (Davis, 1986, pp. 80–86) to determine whether their hyetographs are similar to Huff's. The test showed significant differences in the relative frequencies (Pani and Haragan, 1981, p. 78).

Pani and Haragan recognize the differences in relative frequencies and elaborate that the differences can be attributed to advecting storm systems moving across a network that was six times larger in areal extent than the Illinois network used by Huff. The authors conclude that "if a storm's areal extent was larger than the network, which is often the case in Illinois, the resultant temporal distribution would show more rain falling duration the early portion of the network lifetime and produce a classification in the first quartile." Hence as a network area increases, storms will increasingly be characterized as central peaking. Huff (1967) reached a similar conclusion.

The proceeding conclusion is critical because of the relevance to the research presented here. The watershed rainfall depths (the `ACCUM_WEIGHTED_PRECIP` field) for each storm contained in the data base, which were derived from one to as many as six rain gages, is assumed representative of watershed drainage areas ranging from 0.26 to

166 mi^2 (0.673 to 430 km^2) (see tables 1–5). Most watersheds are less than about 20 mi^2 (51.8 km^2), and only two or three rain gages were in operation. Hence, the "network scale" of the data base is very small relative to the scales of the network used by Pani and Haragan and the Illinois network used by Huff. Following this discussion, it is expected then that the analysis presented later in this dissertation will favor first and second quartile storm types.

Pani and Haragan (1981, figs. 3 and 4) provide median dimensionless hyetographs for only second and third quartile storms. First and fourth quartile hyetographs are not provided because of limited sample sizes (Pani and Haragan, 1981, p. 78). For this dissertation the median hyetographs were graphically extracted from the figures of Pani and Haragan and are reproduced on figure 12. Unlike Huff (1990), Pani and Haragan do not provide tables of the coordinate values for their figures. Pani and Haragan also provide the 10 and 90 percentile hyetographs to illustrate uncertainty. The authors used the χ^2-test at the 0.1 percent (0.001) significance level to test whether their hyetographs are similar to Huff's. The test showed no significant differences (Pani and Haragan, 1981, p. 79). Visually the third quartile storms have the most potential differences—compare the third quartile hyetographs on figures 11 and 12. Therefore, although the relative frequencies of quartile storm types between Illinois and Texas are statistically different, the resultant hyetographs from each apparently are not.

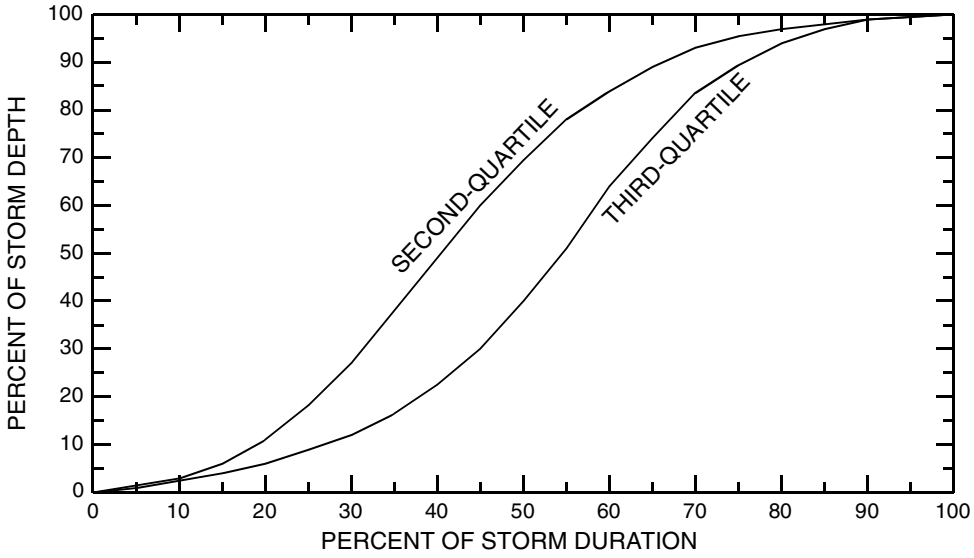

Figure 12. Median dimensionless hyetograph for second and third quartile storms for the southern High Plains of Texas derived from Pani and Haragan (1981, figs. 3 and 4)

Because the third quartile storm exhibits its greatest rate near 55 percent of the duration (see figure 12), Pani and Haragan decided that the third quartile storm was close enough to a second-quartile classification that for application purposes all second and third quartile events should be combined (Pani and Haragan, 1981, fig. 5). The median composite hyetograph along with the 10 and 90 percentile curves are shown on figure 13. The hyetograph coordinates again were graphically extracted the Pani and Haragan figure.

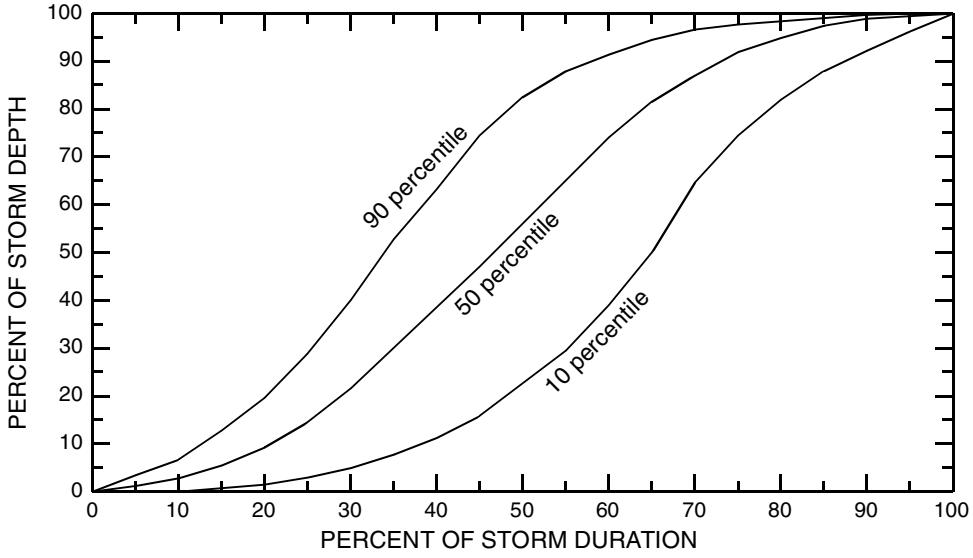

Figure 13. Median, 10-, and 90-percentile dimensionless hyetographs for the southern High Plains of Texas derived from Pani and Haragan (1981, fig. 5)

The coordinates used to generate figures 12 and 13 are shown in table 6. These are provided in facilitate the work of other researchers. The coordinates are rounded to the nearest quarter interval. As a final remark about the Pani and Haragan study is that the authors did not consider the influences of storm duration on the hyetograph. This is probably not an oversight but partly attributable limited sample sizes.

Table 6. Median, 10-, and 90-percentile dimensionless hyetograph coordinates for the southern High Plains of Texas derived from Pani and Haragan (1981)

[Note: Table entries manually extracted from figure by Pani and Haragan (1981, fig. 5) and rounded to the nearest quarter interval.]

Storm duration (percent)	10th percentile dimensionless hyetograph (percent)	Median (50th percentile) dimensionless hyetograph (percent)	90th percentile dimensionless hyetograph (percent)
0	0	0	0
5	0	1.25	3.5
10	0	2.75	6.75
15	.75	5.5	12.75
20	1.5	9.25	19.5
25	3	14.5	28.75
30	5	21.5	40
35	7.75	30	52.75
40	11.25	38.5	63.25
45	15.75	47	74.5
50	22.5	56	82.5
55	29.5	65	88
60	39	74	91.5
65	50	81.5	94.5
70	64.5	87	96.75
75	74.5	92	97.75
80	82	95	98.5
85	88	97.5	99.25
90	92.25	99	99.75
95	96.25	99.5	100
100	100	100	100

Hyetograph Research by Schaefer and Parrett

Schaefer (1989) and Parrett (1998) used similar approaches for the regional analysis of hyetographs for Washington State and Montana, respectively. Parrett (1998) largely was based on the same methodology as Schaefer. The work of Parrett is described here. Parrett analyzed 188 large storms from 87 National Weather Service (NWS) recording rain gages in and proximate to Montana. A storm was considered for

analysis if the annual exceedance probability of the total storm depth was about 0.10 or less (recurrence intervals greater than 10). The duration categories used were 2, 6, and 24 hr; the core NWS data types for each category were 5 minute, 15 minute, and 1 hr, respectively. Too few 5-minute NWS rain gages existed for analysis. A multiplier of three was used on the duration for purposes of cataloging by duration (Parrett, 1998, p. 7). For example, storms in the 2, 6, and 24 hr category could have durations as long as 6, 18, and 72 hr.

The storms were then cataloged into three-geographic generally-homogeneous regions of Montana (Regions 1, 2, and 3). Region 1 represents western mountains, region 2 represents the front range of the Rocky Mountains, and region 3 includes the eastern plains of the state. Seasonal analysis of the relative frequencies of storms on a monthly basis was performed. The "time-to-peak" intensity of each storm was measured. The graphic definition of the time-to-peak is indicated by variable "a" on figure 20 (referenced out of sequence) of this dissertation. The time-to-peak rainfall intensity influences peak discharge of the runoff process. Further, Parrett determined sequencing patterns of the three adjacent largest intensity incremental storm depths. This was an important step because the sequencing of the high-intensity portions of the event also are believed to influence peak discharge.

Following the lead of Schaefer (1989), Parrett (1998) divided each storm into equal thirds that were termed "trisectors" so that general temporal patterns of rainfall could be classified into "macro-patterns" (Parrett, 1998, fig. 3). The macro-patterns

reflect the relative total storm depth in each trisector and whether or not rainfall was continuous throughout the total storm duration. Twelve macro-patterns were considered and each of the 188 storms was assigned a pattern type. Macro-pattern 1 (a single front-loaded burst type event) was the most common pattern exhibited by the storms in all regions for the 2- and 6-hr durations for each region. Macro-pattern 3 (a multiple decreasing magnitude bursting event) was the most common for the western Mountains of Montana. The 2-hr duration storms were much more likely to have the macro-pattern 1 than either the 6- or 24-hr duration storms (Parrett, 1998, fig. 5).

Each of the 188 storms considered by Parrett (1998) was converted to dimensionless depths by division of each incremental depth by the maximum depth for the duration of interest within the event. For example, each hourly depth for a storm lasting 72 hr (the 24-hr duration category) was divided by the maximum 24-hr storm depth of that storm. Parrett does not remove dimension from the time or horizontal axis of the hyetograph; “decimal hours passed” are favored. Finally, the incremental (now dimensionless) values are cumulated into a “depth-duration curve” (Parrett’s terminology). The depth-duration curve is analogous to the “dimensionless cumulative hyetograph” considered in the dissertation. The dimension removal method by Schaefer (1989) and Parrett (1998) defers considerably from the percentile conversion favored by Huff (1967, 1990) and Pani and Haragan (1981) and used in this dissertation.

Parrett subsequently fitted the four parameter Beta distribution (Benjamin and Cornell, 1970) to the dimensionless depth data each duration within the total storm duration while maintaining the regional and storm duration categories (Regions 1, 2, and 3; and Durations 2, 6, and 24 hr). The four-parameter Beta distribution—a less well known variant of the two-parameter Beta distribution that is familiar to many statistical analysts (Ross, 1994, pp. 235; Press and others, 1992, pp. 219–221; Wilks, 1995, pp. 95–97; Evans and others, 2000, pp. 34–42; and Karian and Dudewicz, 2000, pp. 79–81)—is a flexible distribution that can take on a wide variety of shapes and is useful for describing random variables having fixed lower and upper bounds. The Method of Moments was used for parameter estimation. The Beta distribution is only expressible as a probability density function and has no explicit cumulative distribution form or quantile function form. Numerical methods are required to use the Beta distribution. To formalize a method for hyetograph estimation after the Beta distribution was fitted, Parrett continues with complex and lengthy correlation and regression analysis so that smoothed depth-duration curves can be computed for a given region, duration, and probability level. Parrett concludes with three application examples to assist the reader in estimating the instantaneous synthetic (expected) hyetograph.

Hyetograph Research by Others

Yen and Chow (1980), with a focus on small drainage system design, presented a simple triangular instantaneous hyetograph shape for runoff computations with

drainage areas less than about 10 mi^2 (25.9 km^2). They used hourly precipitation data from the National Weather Service from rain gages in Boston, MA, Urbana, IL, and Asheville, N.C. The Method of Moments was used to determine their hyetograph parameters. Their triangular hyetograph model is shown on figure 14.

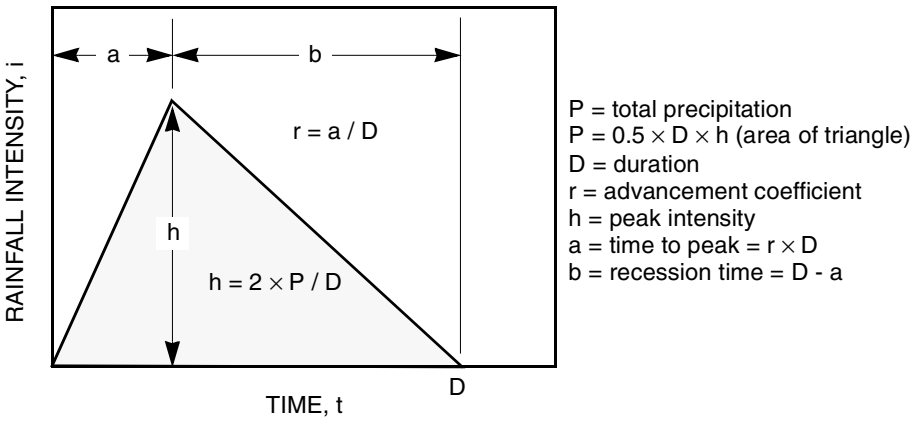

Figure 14. Definition of a triangular instantaneous hyetograph model after Yen and Chow (1980) and Chow and others (1988)

French (1983) following Yen and Chow (1980) also uses a statistical analyses using the Method of Moments to fit triangular hyetographs to the mean of the hyetograph distribution. French reports (1983, p. 6) that more complicated geometric shapes used to approximate the instantaneous hyetograph require more data and computational effort than the triangular hyetograph. French concludes that "the use of the first moment of the precipitation distribution and the assumption of a triangular shape is a reasonable compromise between accuracy and practicality."

Chukwuma and Schwab (1983) presented results from analysis of 43 years of rainfall records from the North Appalachian Experimental Watershed, Coshocton,

Ohio (NAEW). Their records comprised 454 storms of duration from 11 to nearly 24 hr that produced more than 0.5 in. (12.7 mm) of rainfall, and a break-in-time of at least 1 hr between storm periods.

Chukwuma and Schwab (1983) categorized storm events according to which third of the storm duration contained the most intense rainfall. Their general classification scheme is shown on figure 15. They subsequently performed statistical analysis on the storms within each classification to develop six type curves (not reproduced here).

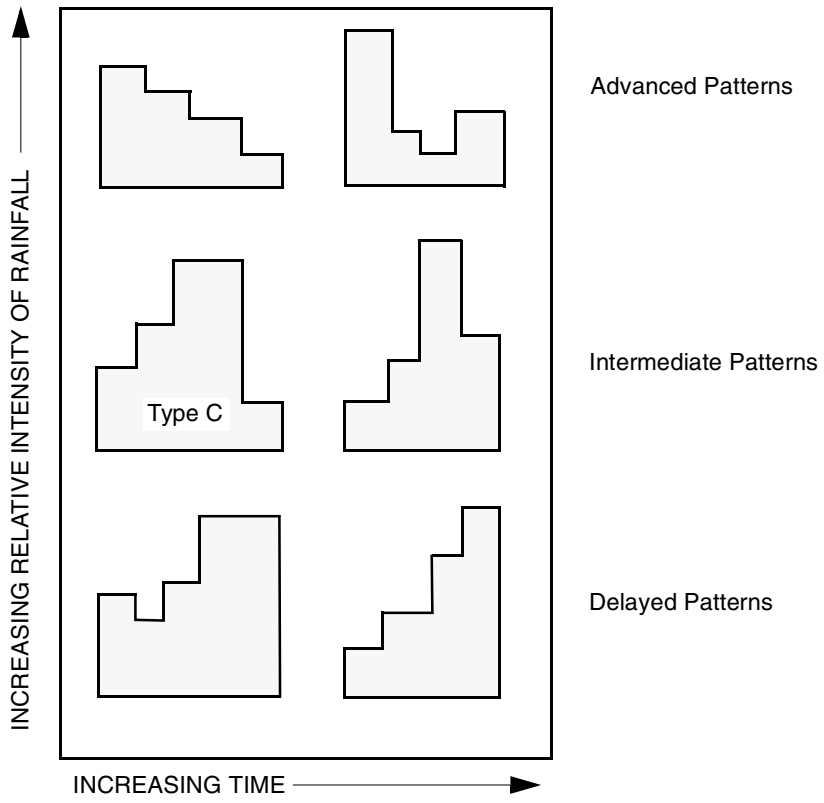

Figure 15. General instantaneous hyetograph patterns observed by Chukwama and Schwab (1983)

An important contribution of Chukwama and Schwab is that they examined the relation between sample size and the variance of the rainfall percentage within specific storm periods. They determined that a sample size of 50 storms *should be sufficient* to produce reasonable estimates of expected rainfall hyetographs. The authors also compared the SCS Type II hyetograph to their most comparable type curve (Type C). They report that the SCS Type II hyetograph has considerably more rainfall on a proportional basis in the central portion of the hyetograph and maximum 30-minute rates of rainfall for any of their six types would only amount to 40 percent or less than the maximum 30-minute rainfall rate of the SCS Type II hyetograph. This is an important observation and is consistent with the results presented in this dissertation. The peak intensities of observed hyetographs are smaller than those implied by the SCS Type II hyetograph.

Example of the Balanced Storm Hyetograph Method for Austin, Texas

The intensity-duration frequency (IDF) method for hyetograph construction, also known as the balanced storm method (Haan and others, 1994, pp. 45–46) or the alternating block method (Chow and others, 1988, p. 466), is based on the IDF curve. The method considers the IDF curve for a location such as might be derived from depth-duration frequency (DDF) values from Asquith (1998). A listing of DDF for Austin, Texas is listed in table 7. The values in the table can be converted to IDF values by dividing each depth by its corresponding duration. The IDF values are listed

in table 8. The 3-hr 25-year hyetograph can be computed from the shaded values in table 8.

Table 7. Depth-duration frequency of precipitation for Austin, Texas

[Note: Values in table derived from Asquith (1998). The location used to define the parameters of the precipitation distribution was Tom Miller Dam on the Colorado River near the center of the Austin area located at latitude 30°17'39" and longitude 97°47'12". min., minutes; in., inches. One in. equals 25.4 millimeters (mm).]

Annual non-exceedance probability	Recurrence interval	Precipitation depth for indicated duration									
		15 min.	30 min.	1 hr	2 hr	3 hr	6 hr	12 hr	1 day	2 days	3 days
(percent)	(years)	(in.)	(in.)	(in.)	(in.)	(in.)	(in.)	(in.)	(in.)	(in.)	(in.)
0.500	2	0.98	1.32	1.72	2.16	2.32	2.67	3.06	3.44	3.81	4.04
.600	2.5	1.05	1.42	1.86	2.35	2.53	2.91	3.33	3.84	4.28	4.51
.700	3.33	1.14	1.54	2.04	2.58	2.79	3.19	3.64	4.33	4.84	5.08
.800	5	1.26	1.71	2.28	2.89	3.13	3.56	4.07	4.99	5.60	5.85
.900	10	1.47	1.98	2.68	3.42	3.71	4.21	4.81	6.10	6.88	7.14
.960	25	1.76	2.36	3.28	4.20	4.55	5.14	5.90	7.64	8.63	8.91
.980	50	2.01	2.68	3.79	4.88	5.28	5.94	6.86	8.87	10.0	10.3
.990	100	2.29	3.04	4.37	5.66	6.11	6.85	7.96	10.2	11.5	11.8
.996	250	2.73	3.57	5.26	6.86	7.38	8.24	9.67	12.0	13.6	13.9
.998	500	3.11	4.02	6.06	7.94	8.51	9.47	11.2	13.5	15.2	15.6

To construct the 3-hr 25-year hyetograph in table 9, a quarter hour time interval was chosen and the intensity values were linearly interpolated to durations not available in Asquith (1998). The linearly interpolated values are represented by bracketing parentheses. Subsequently, the ranked intensity values for each duration are converted to an accumulated depth [column 1 (duration) × column 3 (intensity)]. The accumulated depth is then converted to an incremental depth by differencing column 4. The incremental depths finally were rearranged in an alternating block pattern centered on the mid point of the duration to derive the hyetograph. Dimension on the

hyetograph was removed through division by the total storm depth. The computational steps are shown in table 9. Truncation of the dimensionless values for the 2.50 and 2.75 hr durations to 1.00 was made.

Table 8. Intensity-duration frequency of precipitation for Austin, Texas
[Note: Values in table derived from Asquith (1998). The location used to define the parameters of the precipitation distribution was Tom Miller Dam on the Colorado River near the center of the Austin area located at latitude 30°17'39" and longitude 97°47'12". min., minutes; hr., hours; in./hr., inches per hour. One in. equals 25.4 millimeters (mm).]

Annual non-exceedance probability	Recurrence interval	Precipitation intensity for indicated duration									
		15 min.	30 min.	1 hr	2 hr	3 hr	6 hr	12 hr	1 day	2 days	3 days
(percent)	(years)	(in./hr.)	(in./hr.)	(in./hr.)	(in./hr.)	(in./hr.)	(in./h.r)	(in./hr.)	(in./hr.)	(in./hr.)	(in./hr.)
0.500	2	3.92	2.64	1.72	1.08	0.773	0.445	0.255	0.143	0.0794	0.0561
.600	2.5	4.20	2.84	1.86	1.18	.843	.485	.278	.160	.0892	.0626
.700	3.33	4.56	3.08	2.04	1.29	.930	.532	.303	.180	.101	.0706
.800	5	5.04	3.42	2.28	1.45	1.04	.593	.339	.208	.117	.0812
.900	10	5.88	3.96	2.68	1.71	1.24	.702	.401	.254	.143	.0992
.960	25	7.04	4.72	3.28	2.10	1.52	.857	.492	.318	.180	.124
.980	50	8.04	5.36	3.79	2.44	1.76	.990	.572	.370	.209	.143
.990	100	9.16	6.08	4.37	2.83	2.04	1.14	.663	.424	.239	.164
.996	250	10.9	7.14	5.26	3.43	2.46	1.37	.806	.501	.283	.193
.998	500	12.4	8.04	6.06	3.97	2.84	1.58	.934	.564	.318	.216

Table 9. Hyetograph for 3-hr 25-year rainfall for Austin, Texas

[Note: Rainfall intensity values in parentheses were estimated by linear interpolation. min., minutes; hr., hours, in., inches; -- dimensionless or not applicable. One in. equals 25.4 millimeters (mm).]

Duration	Percent of duration	Rainfall intensity	Accum-ulated depth	Incre-mental depth	Alter-nating depth	Hyeto-graph	Dimen-sionless hyeto-graph	Hyeto-graph based on SCS Type II	Dimen-sionless hyeto-graph based on SCS Type II
(hr)		(in./hr.)	(in.)	(in.)	(in.)	(in.)	(--)	(in.)	(--)
0.00	--	--	0.00	0.00	0.00	0.00	0.000	0.000	0.000
0.25	0.0833	7.04	1.76	1.76	.06	.06	.0132	.115	.025
.50	.167	4.72	2.36	.60	.16	.22	.0482	.122	.052
.75	.250	(4.00)	3.00	.64	.28	.50	.110	.168	.089
1.00	.333	3.28	3.28	.28	.46	.96	.211	.199	.133
1.25	.417	(2.99)	3.74	.46	.64	1.60	.351	.795	.308
1.50	.50	(2.69)	4.04	.30	1.76	3.36	.737	2.109	.771
1.75	.583	(2.40)	4.20	.16	.60	3.96	.868	.374	.854
2.00	.667	2.10	4.20	.00	.30	4.26	.934	.176	.892
2.25	.750	(1.96)	4.41	.21	.21	4.47	.980	.176	.931
2.50	.833	(1.81)	4.53	.12	.12	4.59	1.00	.107	.955
2.75	.917	(1.67)	4.59	.06	.00	4.59	1.00	.107	.978
3.00	1.00	1.52	4.56	-.03	-.03	4.56	1.00	.099	1.00
			Total	4.56	4.56			4.55	

The dimensionless hyetograph is shown on figure 16. The dimensionless hyetograph acquires the traditional nearly symmetrical S-shape of all IDF based hyetographs. The hyetograph rises slow to moderately from the origin, becomes quite steep at the midpoint of the duration, and then the ordinates flatten as the storm approaches completion. The peak intensity of the IDF hyetograph is arbitrarily shifted to the left of the storm midpoint by convention. A major facet of this research is to determine whether actual storms that are known to produce runoff would take on a shape such as this. The SCS Type II hyetograph (SCS, 1973) also was computed for Austin and is shown as the dashed line on figure 16 and the last two (right) columns of

table 9. The two curves reasonably approximate each other, but such agreement does not constitute a validation because each technique is based on the same fundamental methodology.

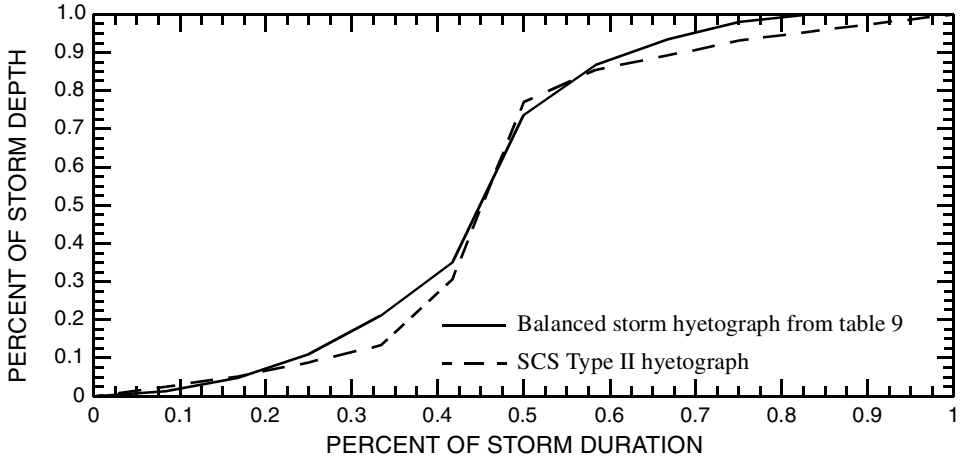

Figure 16. Dimensionless balanced storm and SCS Type II hyetographs for 3-hr 25-year rainfall for Austin, Texas derived from Asquith (1998)

CHAPTER 3
TRIANGULAR MODEL OF DIMENSIONLESS RAINFALL HYETOGRAPHS KNOWN TO PRODUCE RUNOFF IN TEXAS

Abstract

An instantaneous hyetograph (hyetograph), is the temporal distribution of rainfall occurring over a point or area during a storm. Synthetic hyetographs are estimates of the expected time distribution for a design storm and principally are used in small-watershed hydraulic-structure design. Combining a hyetograph with a unit hydrograph provides the designer with a synthetic streamflow hydrograph. A data base of more than 1,600 observed cumulative hyetographs that produced runoff from selected small watersheds in parts of Texas provided estimates of parameters of a simple triangular-shaped hyetograph model. The model provides an estimate of the average or expected hyetograph in dimensionless form for storm durations of 0–24 hr and 24 hr and greater (up to about 3 days). The modeled hyetographs are formulated, graphed, and tabulated to facilitate use in design applications. In this study, the expected dimensionless hyetographs of 0–12 hr and 12–24 hr durations were similar and were combined with minimal information loss. Also, dimensionless hyetographs are independent of the frequency level or recurrence interval of total storm depth. The frequency independence should enhance the suitability of dimensionless hyetographs for design applications.

Introduction

An instantaneous hyetograph, or simply a hyetograph, is the temporal distribution of rainfall occurring over a point or area within a storm. Other forms of the hyetograph

are common; a hyetograph integrated with time produces a cumulative hyetograph. The hyetograph in its various forms has several applications. For example, in order to time distribute the depth of a design storm, an expected or synthetic (design) hyetograph for a particular location is often used by engineers and hydrologists during the design process of hydraulic structures such as culverts or runoff detention basins in small watersheds. A design storm is characterized by the depth of rainfall having a specified duration and recurrence interval (exceedance probability) predicated by the design criteria; for example, the 12-hr 100-year storm. When a hyetograph is convoluted with a unit hydrograph, a synthetic streamflow hydrograph is produced (Chow and others, 1988, chap. 7). A convolution example is provided in chapter 7.

Purpose and Scope

The purpose of this chapter is to estimate synthetic dimensionless cumulative hyetographs for storms known to produce significant runoff in small watersheds in Texas. The synthetic hyetographs are estimated using a simple triangular model of the instantaneous hyetograph. A dimensionless cumulative hyetograph has units of percent storm duration on the horizontal axis and percent storm depth on the vertical axis. Dimension is easily restored to the hyetograph through multiplication of the storm duration and depth with the percentages of the horizontal and vertical axes respectively. The triangular model is appealing over more complicated functions or geometrical shapes because of its simplicity and ease of application.

A specialized hyetograph data base described in the next section provides the basis for the analysis. Three ranges of storm duration considered for this study were 0–12 hr, 12–24 hr, and 24 hr and greater (up to about three days). The majority of hydrologic design applications that require synthetic hyetographs for small watersheds have time scales on the order of 24 hr or less, but some might require longer durations. Hyetographs defined for these duration ranges are useful to practitioners of small watershed hydraulic design.

Data Sources

A data base of cumulative hyetographs for storm events known to produce runoff from small watersheds was compiled during the execution of multiple on-going (as of 2002) research projects that are sponsored by the Texas Department of Transportation (project nos. 0–4193 and 0–4194) and the U.S. Geological Survey (USGS). The projects are being performed by investigators at Texas Tech University, Lamar University, University of Houston, and USGS. The fact that the hyetograph data represents storms known to produce runoff is important for applications involving rainfall-runoff relations and distinguishes the analysis presented here. At this time over 1,600 events for 91 USGS streamflow-gaging stations are available. The locations of the stations are shown on figure 17; the figure is identical to figure 2.

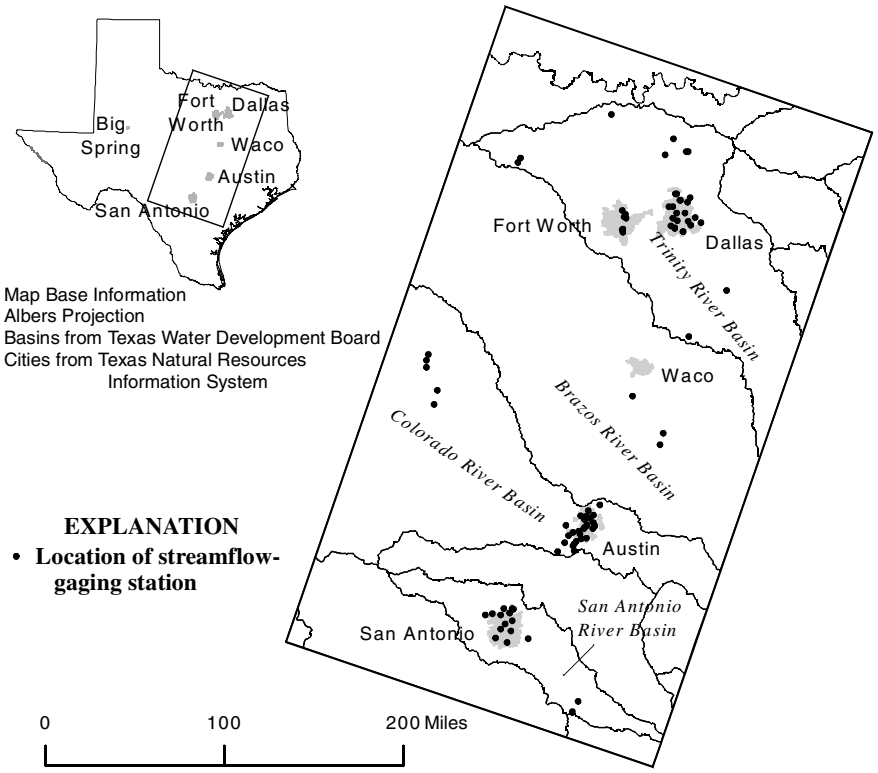

Figure 17. Map showing locations of USGS streamflow-gaging stations represented in the hyetograph data base

Each event has two data files; one file contains a rainfall hyetograph and another file contains a streamflow hydrograph. The data are recorded as either variable time spaced (break-point data) or constant time-interval. In either case, the time increments range from five minutes to several hours. The stations are now mostly discontinued and no longer in operation. The stations were located in areas around the Texas cities of Austin, Dallas, Fort Worth, and San Antonio, and special small watershed study areas in rural regions of the central to north-central portions of Texas. Because the majority of the stations were not located in the eastern and western portions of Texas,

precipitation processes in east and west Texas are likely not well represented by the data base.

The storm durations range from a few hours up to about five days and the total storm depths range from fractional inches to over 10 in. (254 mm). The rainfall data for each storm was published between the early 1960s and the middle 1980s in about 220 USGS reports. Several runoff-producing storms per year per station are documented in the reports. The reports list the incremental values (unit values) of concomitant cumulative rainfall depth and time. A citation list of the reports is listed in Appendix A.

The rainfall depths contained in the data base are assumed representative across the drainage area of the streamflow-gaging station. The drainage areas ranged from 0.26 to 166 mi^2 (0.67 to 430 km^2), and most of the watersheds had drainage areas less than about 20 mi^2 (52 km^2). The "watershed rainfall depths" were derived from as little as one to as many as six rain gages simultaneously operated in or proximal to the watershed. For events in which a single rain gage was in operation (about 25 percent of data base), the watershed depth is a point value. For about 65 percent of the events, two or three rain gages were in operation for most watersheds so the majority of hyetographs are areal values. The spatial extent is limited and the number of gages small, so it is assumed that the areal depths represent an approximate point process. Thus for the analysis here, no distinction between the areal or point values is made. The spatial scale of the data base is limited and, importantly, on the same order of areal

scale in which rainfall-runoff design using hyetographs is performed. The scale similarity is important because the hyetographs are representative of watershed sizes for which engineers and hydrologists often perform design.

Each cumulative hyetograph in the data base was expressed in a double-dimensionless fashion, which facilitates comparative analysis. The time increments were converted to percent of storm duration, and the rainfall depths were converted to percent of storm depth. The storm duration and depth generally were defined by the extent of the available data provided by the interpretation of previous analysts when the USGS reports were prepared. The converted hyetographs are dimensionless cumulative hyetographs.

Previous Studies

Pilgrim and Cordery (1975) and Veneziano and Villani (1999) categorize approaches to developing expected hyetographs. Each reference provides slightly different hyetograph categories. Despite the differences, the categories can be generalized as: 1) simple geometric shapes anchored to a single point on the rainfall intensity-duration frequency (IDF) curve, 2) use of the entire IDF curve, 3) standardized or statistical hyetograph profiles developed from rainfall records, 4) simulation using stochastic rainfall models, and 5) arbitrary temporal patterns including specific storms from the historical record (Haan and others, 1994, p. 44). Category 3 includes equation-based models (such as Yen and Chow, 1980; and French, 1983) and purely empirical definitions (such as Huff, 1967). Bonta and Rao (1988a)

compare hyetographs derived from some of the categories and are favorable to hyetographs defined by category 3 as exemplified by Huff (1967). Aron and Adl (1992) investigate the influences of hyetograph shape on runoff hydrographs; the hyetograph shapes considered were from categories 2 and 3. A rather unique hyetograph analysis modeling approach based on a so-called nonstationary Gauss-Markov model is provided by Cheng and others (2001); Cheng and others restricted their analysis to the rainfall associated with annual maximum events. An appealing aspect of the Gauss-Markov model is summarized by the last numerated benefit described by Cheng and others—the model produces irregular hyetograph shapes that resemble those of real rainfall hyetographs in contrast to regular functional shapes (such as the triangular model utilized here).

Use of intensity-duration analysis, including the IDF curve, as a foundation for synthetic hyetograph generation is common. Most hydrologic textbooks (for example, Chow and others, 1988; Haan and others, 1994) that present rainfall-runoff design problems contain hyetograph estimation procedures based in some fashion on the IDF curve. Occasionally, text books also acknowledge other methods. Preul and Papadakis (1973) define a synthetic hyetograph for an urban watershed in Ohio using intensity-duration analysis on three rain gages; their approach followed one described by Keifer and Chu (1957).

The Soil Conservation Service (SCS, 1973), now the National Resources Conservation Service, developed a hyetograph modelling approach very similar to the

IDF curve method. The method provides four types of dimensionless cumulative hyetographs. Each type is assigned to specific regions of the United States. The Type II and III hyetographs are represented in Texas. The Type II hyetograph is the most intense—predicts the greatest instantaneous rainfall rates—of the four types and is well known and in common use by engineers and hydrologists in Texas. The Type II is symmetric about the middle of the storm. The curves are generalizations of the balanced storm techniques based on the venerable rainfall depth-duration frequency (DDF) values, equivalently IDF values, of Hershfield (1962). An updated report of DDF for Texas is provided by Asquith (1998).

There are several reasons for the widespread use of the IDF approach. First, it is believed that frequency levels (recurrence intervals or return periods) can be assigned to synthetic hyetographs derived from IDF curves (IDF hyetographs). Second, IDF hyetographs are repeatable—they provide consistency. Third, IDF hyetographs are known to represent reasonable (or at least are so broadly accepted and in common use that "reasonable" is seldom questioned and the potential problems with the IDF hyetograph are mitigated by other aspects of the design process) temporal storm patterns for a given frequency. Fourth, it is common to construct the IDF hyetograph so that the hyetograph produces a rainfall depth or intensity whose frequency is independent of the storm duration (Haan and others, 1994, p. 45). Because of the duration independence it is presumed that these hyetographs are applicable across the range of watershed scales represented by the data base.

It is important to note that the IDF curve is constructed from data derived from the most intense bursts of rainfall that occur within annual maximum storms; the bursts are preserved in the historical record as annual maximum intensities for a given duration. The IDF hyetograph is not based on the temporal nature of real events. The IDF hyetograph is hence a worst case scenario and does not represent an "expectation" in a statistical sense. Pilgrim and Cordery (1975, p. 81) observe that "design rainfall derived from frequency-duration data does not generally represent the rainfall in complete storms." Pilgrim and Cordery remark that a hyetograph of a given frequency level produces a flood peak and volume of the same frequency level—this is an implicit assumption in IDF hyetograph justification and usage.

The standardized or statistical hyetograph developed from actual rainfall records (category 3) is the last general category of hyetograph specification. A broad range of analytical and statistical methods can be used. For example, various equations or functions that mimic the hyetograph shape are available to the investigator, and several parameter estimation schemes, such as least squares or the Method of Moments, can be used. This category is attractive because the hyetographs become expectations of real data and entire storm durations are considered. The hyetographs are not derived from abstractions of the non-whole storm based IDF curve. It is a critical assumption in the IDF-based approaches that the storm structure can be modeled using fractions of storms that represent the DDF curves.

Some important papers involving the analysis of actual rainfall records include: Huff (1967, 1990), Drufuca and Rogers (1978), Yen and Chow (1980), Chukwuma and Schwab (1983), Bonta and Rao (1988a, 1988b), Schaefer (1989, 1993), Parrett (1998), and references therein. The research by Huff for the analysis of Illinois data is perhaps the most widely known and cited. In Bonta and Rao (1989) and Huff (1990) a reference to Pani and Haragan (1981) is made—no other citations are known to the authors. The Pani and Haragan paper provides dimensionless hyetographs for a specialized rain gage network in the southern High Plains of Texas. The research by Pani and Haragan (1981) appears to be the only hyetograph analysis done explicitly on Texas rainfall data. Their analysis followed the empirical approach used by Huff (1967), and they compared their results to those of Huff.

Pani and Haragan classified storm hyetographs into four quartile categories depending on which quarter of dimensionless storm time had the greatest change in storm depth. They analyzed 117 storms that occurred between May 15 and July 31 for a 3-year period (1978–80) over the High Plains Cooperative Program (Texas HIPLEX) rain gage network (Texas Department of Water Resources, 1980). The network was located in the southern High Plains of Texas near the town of Big Spring, Texas and covered about 2,600 mi^2 (6,744 km^2, reported by the authors). The data consisted of 15-minute values. The convective-precipitation dominated period of mid May to July was selected because Pani and Haragan were interested in the hyetographs of convective-generated precipitation. Pani and Haragan (1981, p. 77) defined a storm as

a “rain period of at least 0.75 hour duration separated by at least 1 hour.” Pani and Haragan do not appear to have identified a minimum storm depth considered for analysis, but Bonta and Rao (1989, table 1) report that Pani and Haragan (1981) used about 0.75 in. (a value of 19.3 mm was reported by Bonta and Rao) minimum depth.

Pani and Haragan (1981) determined that the relative frequencies of the quartiles were 13, 41, 32, and 14 percent for the first, second, third, and fourth quartile, respectively. These frequencies indicate that most events (73 percent) are characterized as second and third quartile types. This observation differs from Huff (1967, 1990) who found that most events (66 percent) are characterized as first and second quartile. Pani and Haragan used the χ^2-test to determine whether their hyetographs are similar to those of Huff (1967). The test showed significant differences in the relative frequencies between Pani and Haragan (1981, p. 78) and those of Huff (1967).

Pani and Haragan (1981, p. 78) recognize the differences in relative frequencies and elaborate that the differences can be attributed to advecting storm systems of a network that was six times larger in areal extent than the Illinois network used by Huff. Pani and Haragan conclude that “if a storm’s areal extent was larger than the network, which [was] often the case in Illinois, the resultant temporal distribution would show more rain falling during the early portion of the network lifetime and produce a classification in the first quartile.” Hence storms will increasingly be characterized as central peaking—those having the largest portions of total depth near

the duration midpoint—as a network area increases relative to the typical areal extent of storms. Huff (1967) reached a similar conclusion.

The preceeding discussion is important because of the relevance to the research presented here. As reported in the description of the data used, the spatial or "network scale" of the data base is very small relative to the scales of the network used by Pani and Haragan and the Illinois network used by Huff. Following this discussion, this analysis is expected to favor first to second quartile storm types because of the limited areal extents of typical small-watershed runoff-producing storms in Texas. Asquith (1999, figs. 17 and 18), in the analysis of areal-reduction factors for the one-day design storm in Texas, shows that the areal extent of storms having large depths is limited to a spatial scale of a few hundred square miles for areas around Austin, Dallas, and Houston, Texas.

Pani and Haragan (1981, figs. 3 and 4), through empirical methods, provide median dimensionless hyetographs for only second and third quartile storms. First and fourth quartile hyetographs are not provided because of limited sample sizes (Pani and Haragan, 1981, p. 78). The ordinates of the hyetographs were graphically extracted from the figures of Pani and Haragan and are shown on figure 18. The quartiles of storm duration are emphasized by the vertical grid lines. Pani and Haragan also provide the 10th and 90th percentile hyetographs to illustrate uncertainty. Pani and Haragan used the χ^2-test to determine whether their hyetographs were similar to those of Huff. The test showed no significant differences (Pani and Haragan, 1981, p. 79).

Therefore, although the relative frequencies of quartile storm types between Illinois and Texas are statistically different, the resultant dimensionless cumulative hyetographs from each apparently are not.

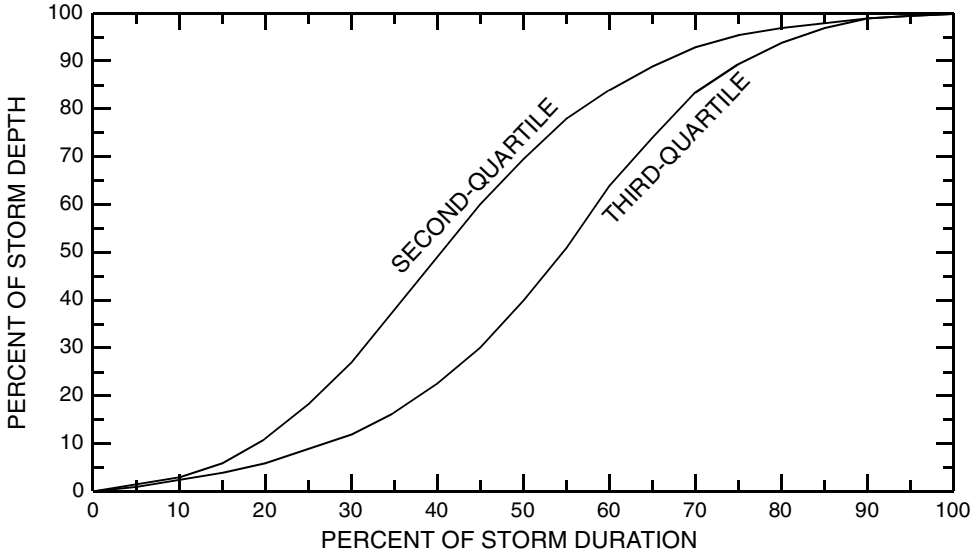

Figure 18. Median dimensionless hyetograph for second and third quartile storms for the southern High Plains of Texas derived from Pani and Haragan (1981, figs. 3 and 4)

The second quartile storm on figure 18 produces the greatest portion of depth near 40 percent; whereas the third quartile storm produces the greatest portion near 55 percent of the duration. Pani and Haragan decided that the ordinates of a third quartile storm were sufficiently close to a second-quartile classification that, for application purposes, all second and third quartile events should be "composited" (Pani and Haragan, 1981, fig. 5). The median composite hyetograph along with the 10th and 90th percentile curves are shown on figure 19. The hyetograph ordinates again were graphically extracted from the Pani and Haragan figure.

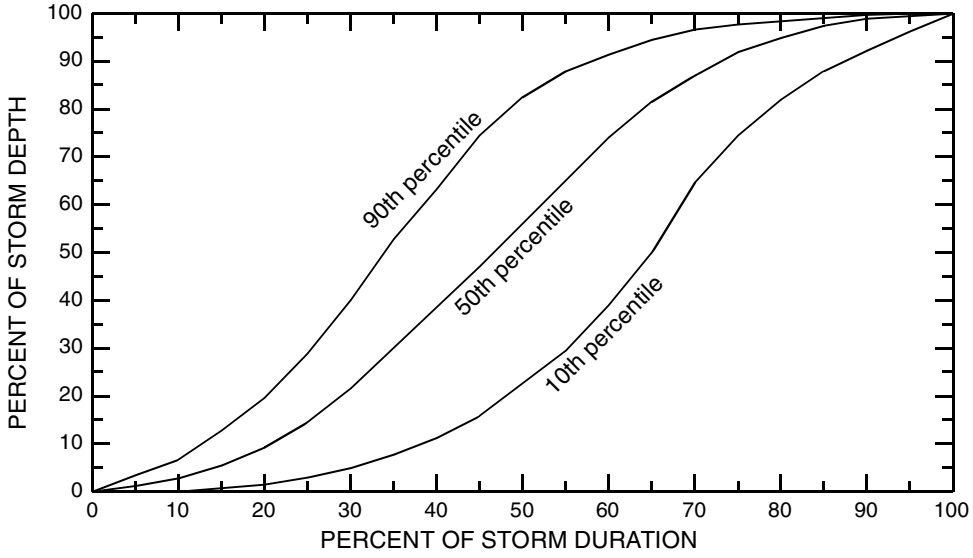

Figure 19. Median, 10-, and 90-percentile dimensionless hyetographs for the southern High Plains of Texas derived from Pani and Haragan (1981, fig. 5)

The coordinates used to generate figures 18 and 19 are shown in table 10. These are provided to facilitate later comparisons to the results of this study. The coordinates are rounded to the nearest quarter interval. A final remark about the Pani and Haragan study is that the influences of storm duration on the hyetograph were not considered. The oversight might be attributed to limited sample sizes and computational resources at the time of the Pani and Haragan study.

Table 10. Median, 10-, and 90-percentile dimensionless cumulative hyetograph coordinates for the southern High Plains of Texas derived from Pani and Haragan (1981)

[Note: Table entries manually extracted from figure by Pani and Haragan (1981, fig. 5) and rounded to the nearest quarter interval.]

Storm duration (percent)	10th percentile dimensionless hyetograph (percent)	Median (50th percentile) dimensionless hyetograph (percent)	90th percentile dimensionless hyetograph (percent)
0	0	0	0
5	0	1.25	3.5
10	0	2.75	6.75
15	.75	5.5	12.75
20	1.5	9.25	19.5
25	3	14.5	28.75
30	5	21.5	40
35	7.75	30	52.75
40	11.25	38.5	63.25
45	15.75	47	74.5
50	22.5	56	82.5
55	29.5	65	88
60	39	74	91.5
65	50	81.5	94.5
70	64.5	87	96.75
75	74.5	92	97.75
80	82	95	98.5
85	88	97.5	99.25
90	92.25	99	99.75
95	96.25	99.5	100
100	100	100	100

Yen and Chow (1980), with a focus on small drainage system design, presented a simple triangular instantaneous hyetograph shape for runoff computations with drainage areas less than 10 mi^2 (25.9 km^2). They used hourly precipitation data from the National Weather Service from rain gages in Boston, MA, Urbana, IL, and Asheville, NC. The Method of Moments was used to determine their hyetograph parameters. Their triangular hyetograph model is shown on figure 20.

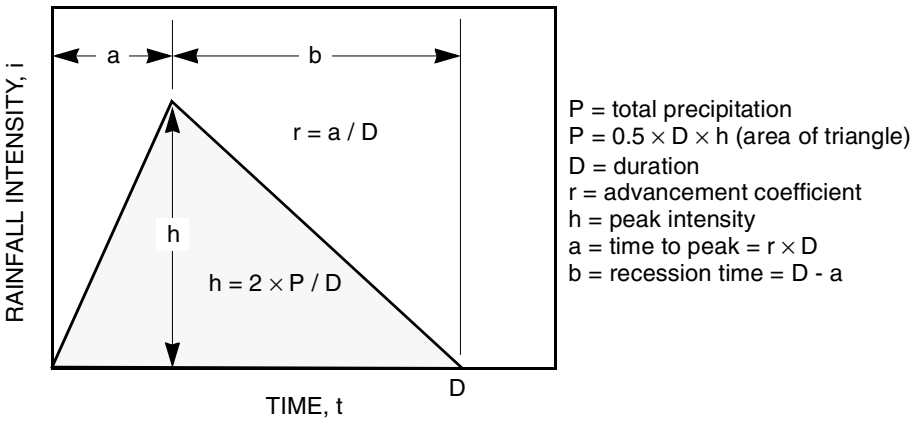

Figure 20. Definition of a triangular instantaneous hyetograph model after Yen and Chow (1980) and Chow and others (1988)

French (1983) also used a triangular based hyetograph model. Following Yen and Chow (1980), French used the Method of Moments to fit triangular hyetographs to the mean of the hyetograph distribution. In the Method of Moments, the theoretical moments of a distribution (such as the mean) are set equal to the moments of the data (such as the sample mean), and the parameters are solved to maintain the equality. The triangular hyetograph is a one parameter model and only the mean statistic is used for parameter estimation. French (1983, p. 6) reports that more complicated geometric shapes used to approximate the instantaneous hyetograph require more data and computational effort than the triangular hyetograph. French concludes (p. 6) that "the use of the first moment of the precipitation distribution and the assumption of a triangular shape is a reasonable compromise between accuracy and practicality."

Triangular Dimensionless Hyetograph Definition

Similar to the geometry of the preceding triangular model, a triangular model based on the rainfall intensity (a quantile density) and fractional percent of elapsed time is shown on figure 21, and the Method of Moments can be used for parameter estimation. The fractional percent time can be interpreted as a nonexceedance probability for purposes of model derivation and subsequent parameter estimation. The model on figure 21 clearly is related to the model on figure 20.

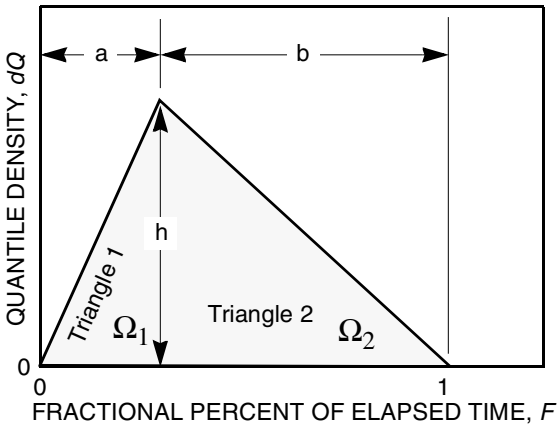

Figure 21. Definition of a triangular instantaneous hyetograph model in terms of quantile density

The following definitions for the triangular quantile density on figure 21 apply. The distances a and b provide

$$a + b = 1 \text{, thus} \tag{1}$$

$$b = 1 - a . \tag{2}$$

The area of the entire triangle is the total precipitation, which is unity for a dimensionless cumulative hyetograph, and is computed as the sum of the areas of two right triangles (Ω_1 and Ω_2).

$$\Omega_1 + \Omega_2 = \frac{1}{2}ha + \frac{1}{2}hb = 1. \tag{3}$$

It follows from eq. 3 that $h = 2$.

The quantile function $Q(F)$ and fractional duration F for the triangular instantaneous hyetograph can be computed by integration from left to right of the two right triangles. The first triangle provides a quantile function

$$Q_1(0 \le F \le a) = \int_0^F \frac{h}{a} F dF = \frac{1}{2}\frac{h}{a}F^2. \tag{4}$$

The second triangle represents a more complex geometry of the quantile function and an integration limit shift is required. The triangle provides a quantile function of

$$Q_2(a < F \le 1) = Q_1(a) + \tilde{Q}_2(0 < \tilde{F} \le b), \tag{5}$$

where $\tilde{F} = F - a$ and $\tilde{Q}_2$ is a triangular integration. It follows that

$$Q_2(a < F \le 1) = Q_1(a) + \int_0^{\tilde{F}} \left(h - \frac{h}{b}\tilde{F}\right) d\tilde{F}, \text{ so} \tag{6}$$

$$Q_2(a < F \le 1) = \frac{1}{2}ha + h\tilde{F} - \frac{1}{2}\frac{h}{b}\tilde{F}^2. \tag{7}$$

The mean μ of a quantile function is defined as

$$\mu = \int_0^1 Q(F)dF, \tag{8}$$

which for the triangular quantile function becomes

$$\mu = \int_0^a Q_1(F)dF + \int_0^b Q_2(\tilde{F})d\tilde{F}, \tag{9}$$

$$\mu = \int_0^a \frac{1}{2}\frac{h}{a}F^2 dF + \int_0^b \frac{1}{2}ha d\tilde{F} + \int_0^b h\tilde{F}d\tilde{F} - \int_0^b \frac{1}{2}\frac{h}{b}\tilde{F}^2 d\tilde{F}, \text{ and} \tag{10}$$

$$\mu = \frac{1}{2}\frac{h}{a}\frac{1}{3}a^3 + \frac{1}{2}hab + \frac{1}{2}hb^2 - \frac{1}{2}\frac{h}{b}\frac{1}{3}b^3. \tag{11}$$

Substitution of $h = 2$ into eq. 11 yields

$$\mu = \frac{a^2}{3} + ab + b^2 - \frac{b^2}{3}. \tag{12}$$

Then substitution of $b = 1 - a$ into eq. 12 yields

$$\mu = \frac{2 - a}{3}, \tag{13}$$

$$a = 2 - 3\mu, \text{ and} \tag{14}$$

$$b = 3\mu - 1. \tag{15}$$

Using eqs. 14 and 15, the parameters of a triangular model can be estimated when a value of the mean dimensionless hyetograph is available. (16)

Estimation of Triangular Hyetograph Parameters

Estimates of the triangular hyetograph parameters a and b are provided in this section. Analysis of the mean ordinate of the dimensionless hyetographs is needed. The analysis considers whether the mean ordinate is a function of the storm duration and the total storm depth for a given duration range. In other words, the question is whether a dependency between the temporal characteristics of the storm and the total storm depth exists for small watersheds.

To examine this question, three duration ranges of 0–12 hr, 12–24 hr, and 24 hr and greater are considered and within each duration range storms having a sequence of depth intervals are analyzed. For example, storms having a depth range of 1.5–2.5 in. (38.1–63.5 mm), those with 2.5–3.5 in. (63.5–88.9 mm), and so on. For each depth interval, the average of the mean of the dimensionless cumulative hyetograph for each storm therefore is computed. For example, 290 storms had durations less than 12 hr and a depth range of 0.5–1.5 in. (12.7–38.1 mm), 290 values for the mean of the dimensionless cumulative hyetograph are computed, and the average of the 290 mean values is 0.579. For purposes of tabulation, the 0.5–1.5 in. range is cataloged as 1 in. (25.4 mm), 1.5–2.5 in. range is cataloged as 2 in. (50.8 mm), and so on. The results of the analysis are provided in table 11. The coefficients of variation and sample sizes (no. of storms) also are listed in the table.

Table 11. Statistical summary of dimensionless hyetograph averages for 0–12 hr and 12–24 hr storm durations

[hr, hour; CV, coefficient of variation: standard deviation divided by mean; in., inches; na, not available; --, empty cell. One in. equals 25.4 millimeters (mm).]

Storm depth category	Range of depth represented by category	0 to 12 hr durations			12 to 24 hr durations		
		Average of the mean for the dimensionless hyetograph	CV of the mean for the dimensionless hyetograph	No. of storms (sample size)	Average of the mean for the dimensionless hyetograph	CV of the mean for the dimensionless hyetograph	No. of storms (sample size)
(in.)	(in.)	(percent)	( )	( )	(percent)	( )	( )
1	0.5–1.5	57.9	0.340	290	56.4	0.444	68
2	1.5–2.5	61.0	.302	253	57.8	.386	180
3	2.5–3.5	58.5	.309	108	58.0	.316	119
4	3.5–4.5	58.8	.279	41	61.2	.292	80
5	4.5–5.5	58.4	.248	11	59.3	.302	30
6	5.5–6.5	49.6	.411	3	70.7	.158	10
7	6.5–7.5	74.0	na	1	57.0	.362	2
8	7.5–8.5	79.8	na	1	38.2	na	1
9	8.5–9.5	22.9	na	1	48.3	na	1
10	9.5–10.5	na	na	0	na	na	na
Rounded weighted average and sample total		59	.317	709	59	.352	491
Parameter *a* of hyetograph		.23	--	--	.23	--	--
Parameter *b* of hyetograph		.77	--	--	.77	--	--

From the results listed in table 11 for the 0–12 hr duration storm, it is clear that no functional relation between storm depth and the average of the dimensionless cumulative hyetograph exists. Therefore, a bulk or weighted average of 59 percent is considered the most representative for the 0–12 hr duration.

For the 12–24 hr storm duration, it is possible that there is a weak relation between storm depth and the average of the mean values. The averages monotonically increase from 56.4 for a 1 in. (25.4 mm) depth to 61.2 for a 4 in. (101.6 mm) depth; however, given the large coefficients of variation and fact that the average for greater than 4 in.

(101.6 mm) depth decreases and then increases, it is concluded that a weighted average of 59 percent also is most representative for 12–24 hr storm durations.

Because the two weighted averages, when rounded to the nearest two-significant digits, are the same, the averages for these two duration ranges can be combined into a single 0–24 hr value. The approximate equality in the weighted averages was unexpected. The weighted average of 59 percent produces a and b parameters of 0.23 and 0.77 respectively. The parameters also are listed in table 11.

A similar analysis was performed for storm durations of 24 hr and greater. The results are listed in table 12. Based on the average of the mean (column 3 on table 3), the mean of the hyetograph distribution diminishes with increasing storm depth. This trend might be expected because the duration range is unbounded (duration can increase indefinitely). It is possible that longer duration storms (multiple days) are more likely to produce larger depths and have multiple bursts, which would increase the potential for significant rainfall to occur in later portions of the duration. The variation is large and the sample size is relatively small for the 0.5–1.5 in. and greater than 5 in. ranges. Therefore, it is concluded that, for purposes of design applications, a single weighted average should be used to represent the 24 hr or greater dimensionless cumulative hyetograph. The weighted average of 55 is preferred and produces a and b parameters of 0.35 and 0.65 respectively. The parameters also are listed in the table.

Table 12. Statistical summary of dimensionless hyetograph averages for 24 hr and greater storm duration

[hr, hour; CV, coefficient of variation: standard deviation divided by mean; in., inches (1 in. = 25.4 mm); --, empty cell. One in. equals 25.4 millimeters (mm).]

Storm depth category	Range of depth represented by category	24 hr and greater durations		
		Average of the mean for the dimensionless hyetograph	CV of the mean for the dimensionless hyetograph	No. of storms (sample size)
(in.)	(in.)	(percent)	( )	( )
1	0.5–1.5	65.0	0.369	23
2	1.5–2.5	56.8	.364	123
3	2.5–3.5	55.7	.380	131
4	3.5–4.5	55.8	.296	72
5	4.5–5.5	53.7	.355	43
6	5.5–6.5	50.6	.317	41
7	6.5–7.5	51.6	.362	12
8	7.5–8.5	50.2	.422	11
9	8.5–9.5	42.2	.527	4
10	9.5–10.5	57.0	.0368	2
Rounded average and total sample size		55	.355	462
Parameter *a* of hyetograph		.35	--	--
Parameter *b* of hyetograph		.65	--	--

The ordinates of both the 0–24 hr and the 24 hr and greater duration dimensionless cumulative hyetographs are listed in table 13. The hyetographs in the table were computed by the triangular hyetograph models. This table facilitates application of the hyetographs. The equation pairs used to calculate each hyetograph are listed below. The pairs are derived by parameter substitution into eqs. 4 and 7.

Storm durations between 0 and 24 hr

$$Q_1(0 \le F \le 0.23) = 4.35F^2, \text{ and} \tag{17}$$

$$Q_2(0.23 < F \le 1) = -1.30F^2 + 2.60F - 0.299 \tag{18}$$

Storm durations of 24 hr and greater

$$Q_1(0 \le F \le 0.35) = 2.86F^2, \text{ and} \tag{19}$$

$$Q_2(0.35 < F \le 1) = -1.54F^2 + 3.08F - 0.538 \tag{20}$$

Table 13. Dimensionless runoff-producing cumulative hyetographs for 0–24 hr and 24 hr and greater storm durations computed by triangular hyetograph model

[hr, hour]

Storm duration (percent)	Dimensionless hyetograph for 0–24 hr storm duration (percent)	Dimensionless hyetograph for 24 hr and greater storm duration (percent)
0	0.00	0.00
5	1.09	.71
10	4.35	2.86
15	9.78	6.43
20	17.4	11.4
25	27.0	17.9
30	36.4	25.7
35	45.1	35.0
40	53.3	44.6
45	60.7	53.5
50	67.5	61.5
55	73.7	68.9
60	79.2	75.4
65	84.1	81.2
70	88.3	86.2
75	91.9	90.4
80	94.8	93.9
85	97.1	96.5
90	98.7	98.5
95	99.7	99.6
100	100	100

The dimensionless cumulative hyetographs for the 0–24 hr (heavy line) and 24 hr and greater (thin line) storm durations are illustrated on figure 22. The composite hyetograph by Pani and Haragan (1981) (dashed line) is shown for comparison. By inspection of figure 22, it is clear that the triangular model produces dimensionless cumulative hyetographs that are consistent in shape and satisfactorily close to the

empirically determined ordinate of the Pani and Haragan hyetograph. However, the 0–24 hr and 24 hr and greater hyetographs peak earlier and are more front-loaded than the Pani and Haragan hyetograph, and each is a second-quartile storm.

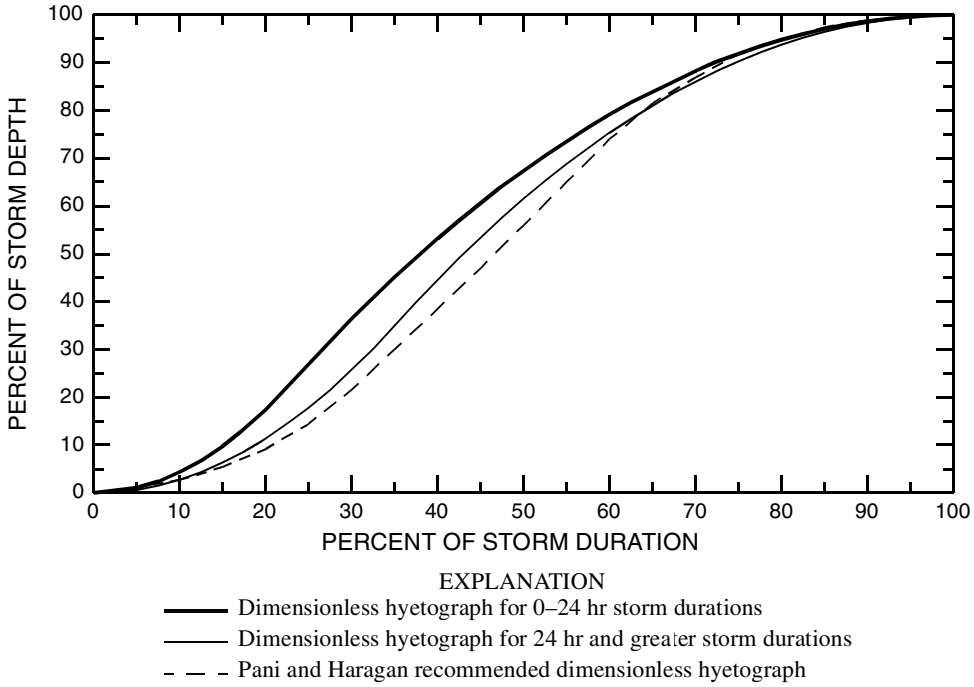

Figure 22. Dimensionless runoff-producing cumulative rainfall hyetograph for 0–24 hr and 24 hr and greater storm durations computed by triangular hyetograph models for Texas and composite hyetograph by Pani and Haragan (1981)

Example Application

The following is a brief example of the application of the 0–24 hr dimensionless cumulative hyetograph, which is shown on figure 22. Asquith (1998) provides depth-duration frequency values of precipitation in Texas. For a location coincident with Tom Miller Dam in Austin, Texas (latitude 30°17’39” and longitude 97°47’12”), the 50-year 12-hr design storm using procedures outlined by Asquith (1998) has a depth of about 6.9 in. (175.3 mm). Using the suggested 0–24 hr hyetograph, at 6 hr into the

design event (50 percent of storm duration), the dimensionless hyetograph has an ordinate of about 67.5 percent, which provides a cumulative rainfall depth of (6.9×0.675)=4.66 in. (118.4 mm). The derivative of the quantile function at $F = 0.5$ is the rainfall rate. The derivative dQ at the point $F = 0.5$ is located along the slope of the second right triangle on figure 16, so $dQ = h - (h/b)\tilde{F} = h - (h/b)(F - a)$ equals 2-(2/0.77)(0.5-0.23) = 1.30 percent of storm depth per storm duration percent. So the rainfall rate is 0.748 in./hr (1.30 × 6.9 in. / 12 hr) or 19.0 mm/hr at 50 percent of the storm duration.

Chapter Conclusions

Triangular hyetograph models were fit to the mean values for the dimensionless cumulative hyetographs from over 1,600 storms known to produce runoff on small watersheds in Texas. Although three storm durations of 0–12 hr, 12–24 hr, and 24 hr and greater originally were considered, the two sub-daily durations were combined into a single 0–24 hr duration classification. It is suggested that the two dimensionless cumulative hyetographs be considered in hydraulic design applications for small watersheds in Texas having drainage areas less than about 20 mi^2 (about 52 km^2).

For each duration classification, the mean values for each of several categories of total depth of the event are analyzed (tables 11 and 12). It is concluded from available data for each duration range that there is no substantial relation between the mean and total depth. Hence, a single average of the dimensionless hyetograph distribution for

the two duration ranges is suggested. Because no relation is observed between the mean of the hyetograph distribution and the storm magnitude as measured by the total storm depth and since storm depth is a function of the frequency level (recurrence interval or return period), a logical conclusion is that the hyetographs suggested here are independent of the frequency level. The frequency independence should enhance the suitability of the dimensionless hyetographs for design applications.

Parameters of a triangular hyetograph model are estimated from the two averages and the resulting dimensionless hyetographs are provided (eqs. 17–20, fig. 22, table 13). The triangular model is mathematically straightforward and is believed to provide a practical means for estimating the design hyetograph.

A comparison to a Texas-based dimensionless cumulative hyetograph from Pani and Haragan (1981) is shown on figure 22. The triangular model produces dimensionless cumulative hyetographs that are consistent in general shape to the Pani and Haragan hyetograph. However, the 0–24 and 24 hr and greater dimensionless hyetographs peak earlier and are more front-loaded than the Pani and Haragan hyetograph. The inconsistencies could be attributed to a large difference in the spatial scale of the rainfall data network, to meteorological differences between study areas, to limitations of the one-parameter triangular model, and other unidentified factors.

CHAPTER 4
SAMPLE L-MOMENT ESTIMATION USING PRIOR-PROBABILITY WEIGHTED MOMENTS

Preface

L-moment statistics (Hosking, 1990) are universally used, unless otherwise noted, in this dissertation in lieu of the well-known product or central moment statistics. In that light, several sections of this chapter provide the analytical and historical context of L-moments. The purpose of this chapter is to describe what modifications to the computational method for the L-moments of a sample are needed so that the L-moments of the observed hyetographs or dimensionless hyetographs are more accurately computed. This chapter also serves as verification that the custom computer program, `lmoments.pl` (Appendix E, referenced out of sequence), functioned properly.

Introduction

An alternative type of sample L-moment estimator based on what the author calls prior-Probability Weighted Moments (p-PWMs) is described and evaluated in this chapter. This estimator is relevant to the hyetograph research in the dissertation as it provides a method to estimate the L-moments. The p-PWMs are similar to the usual PWMs (Greenwood and others, 1979) except that the p-PWMs are capable of utilizing additional information provided by estimates of the cumulative probability of a given observation. The p-PWMs are only applicable to data satisfying two conditions.

The first condition is that, in addition to the observations themselves, an estimate of the cumulative probability (nonexceedance probability) or equivalently the percentile of each observation is available as part of the data collection or processing procedure. Computation of empirical cumulative probabilities after the data were collected, for example by plotting-position formula, is explicitly excluded in the first condition.

The second and more restrictive condition is that the distribution of the nonexceedance probabilities also are known to be non-randomly distributed. The second condition is the principal motivation for the p-PWMs. Examples of data sets that can satisfy both conditions are data such as grain-size distributions (Mahler, personal commun., 2002), rainfall hyetographs in the TxDOT research data base (Thompson, personal commun., 2001), and streamflow hydrographs also in the TxDOT research data base (Thompson, personal commun., 2001).

For comparison, the sample L-moments are computed in this chapter for some example data by unbiased, plotting-position, and p-PWM estimators. Limited simulation experiments presented in this chapter and in Appendix C (referenced out of sequence) suggest that the p-PWMs are unbiased and have smaller sampling variance than unbiased and plotting-position estimators for moderate to large samples when the simulation uses a uniform distribution of cumulative probability. When the simulation used a nonuniform distribution of cumulative probability, the p-PWMs substantially outperform the usual unbiased L-moment and plotting-position L-moment estimators

for most sample sizes. The simulations suggest that the p-PWMs might not perform as well for very small samples. Regardless, p-PWMs are an attractive means to extend L-moment application to previously incompatible data sets such as the rainfall hyetographs considered here. The simulations also show that custom computational software written by the author performs properly.

Background

Cumulative distribution analysis (CDA) is an important tool for an extensive range of scientific endeavors because it provides a framework to investigate distributional characteristics from finite samples. CDA commonly establishes a basis for subsequent exploratory data analysis (EDA). In some contexts CDA and EDA are synonymous terms. CDA generally is initiated by the statistical characterization of sample data sets. The characterization might include statistics such as the mean, the median, and others. Some of the other statistics, such as the inter-quartile range, are commonly used and others are not. Additional components of CDA might include tasks such as evaluating and selecting suitable parametric probability distributions, including the well-known Normal or Log-normal distributions, for distribution modeling, estimating distribution parameters, and statistical regionalization. Regionalization is a broad term but typical usage is summarized as the process of statistically transferring information about distributions of random variables from locations of data collection to locations lacking data. The ability to transfer the information is based on systematic distributional changes because of influences from location specific variables.

Within the past two decades two new branches of statistics for CDA have been developed as alternatives to the well known central or product moments and the widely used Method of Moments. These two new branches are the theories of Probability Weighted Moments (PWMs) and linear moments or L-moments. The theories principally were developed and utilized by the hydrologic research community specializing in extreme value or magnitude and frequency analysis (mainly flood and precipitation frequency applications). PWMs subsequently were followed by and provided a foundation for the theory of L-moments.

L-moment statistics have remarkably changed, invigorated, and spawned much basic and applied research and study of probability distributions, extreme value analysis, and regional analysis of data from the environmental, physical, hydrologic, and other sciences. The theory of PWMs is comprehensively described by Hosking (1986); although PWMs were already being utilized (Greenwood and others, 1979; Landwehr and others, 1979a,b; Hosking and others, 1985; among others). The theory of L-moments is described in the unifying work of Hosking (1990) and followed in book form that focused on regional extreme value analysis by Hosking and Wallis (1997). Other books or chapters therein that contain L-moment and PWM description are Stedinger and others (1992), Hosking (1995), Gilchrist (2000), and Dingman (2002)

L-moment statistics remain popular today among an established and growing cadre of investigators. PWM statistics generally are used as a means to facilitate

application of the L-moments. However, research into the PWM continues. Hosking (1995), Wang (1996a), and Zafirakou-Koulouris and others (1998) describe the so called "partial PWMs" for extension of L-moment theory to left and right censored data. Appendix B provides a substantial introduction to L-moment theory for readers who are unfamiliar with L-moments.

In typical circumstances of CDA, data samples comprise ensembles of observations generated from the distribution $x(F)$ of a real-valued random variable X having cumulative probability F. The cumulative probability is the random component, ranges from 0 to 1 by definition, and is uniformly distributed. The uniform distribution implies that each sampling of F is equally likely as any other. This has considerable ramifications on the execution of CDA. A familiar case is the computation of the arithmetic mean, otherwise known as the sample expectation of X, in which a n^{-1} weight factor on each observation is used. Hence, without additional information than the data values themselves, the incremental probability between the observations are assumed identical, and each observation is given a uniform weight equal of n^{-1}. The constant incremental probability assumption and usage in computation of the expectation conflicts with the second condition provided of the hyetograph data are considered in this dissertation.

Finite sample estimators for L-moments and PWMs are well established but require an uniform distribution of F assumption for their computation. These

estimators might not be applicable for data satisfying both of the conditions described. Fortunately, with minor modifications, the theory of PWMs is compatible with prior knowledge of F and a non-random distribution of F in a sample. A candidate PWM sample estimator is introduced here that will use the prior knowledge of F. The new estimator is referred to as the prior-Probability-Weighted Moment (p-PWM) estimator. A new class of L-moment sample estimator also is presented based on the p-PWMs.

Moments of a Distribution

Distribution description is an important component of CDA and is conducted by the statistical summarization of sample observations of a random variable X. Traditionally, the data are statistically summarized by the product moments of the data (arithmetic mean, standard deviation or variance, skew, and kurtosis). The mathematical definitions and the sampling properties of the product moments are widely known. The reader is referred to section "Moments of a Distribution" in Appendix B for a more detailed description of the moments, specifically, the product moments. The definitions provided are for reference in subsequent discussions in this chapter.

The theoretical product moments of random variable X are

$$\mu = E[X], \tag{21.1}$$

$$\sigma^2 = E[(X-\mu)^2], \tag{21.2}$$

$$\mu_3 = E[(X-\mu)^3], \text{ and} \tag{21.3}$$

$$\mu_4 = E[(X-\mu)^4] \tag{21.4}$$

where μ, σ^2, μ_3, and μ_4 denote the theoretical mean, variance, third moment, and fourth moment, respectively. In general, the higher moments $r \geq 2$ are

$$\mu_r = E[(X-\mu)^r] . \tag{22}$$

The $E[.]$ is the expectation operator and in terms of the probability density function $f(x)$ is

$$E[X^r] = \int_{-\infty}^{\infty} x^r f(x) dx , \tag{23}$$

and in terms of the quantile function $x(F)$ is

$$E[X^r] = \int_0^1 x(F)^r dF . \tag{24}$$

Note that the dF term in eq. 24 is analogous to the incremental probability previously described for finite samples. A special treatment of the dF term plays a central role in the p-PWMs.

The product moments also are defined for finite samples. The first sample product moment is the mean and is

$$m = \frac{1}{n} \sum_{j=1}^{n} x_j . \tag{25}$$

The quantity m is a minimum variance unbiased estimator (MVUE) of the theoretical mean μ. The higher product moments $r \geq 2$ are

$$\overline{m}_r = \frac{1}{n} \sum_{j=1}^{n} (x - m)^r . \tag{26}$$

$\overline{m}_r$ are not unbiased because for $r \geq 2$ less independent information (information content proportional to sample size) is available to compute a given statistic because the mean m also required estimation from the sample. The bias is inversely proportional to sample size. Unbiased product moment estimators are presented in Appendix B. The important concept here is that each data value is given a weight of n^{-1}. This weight is another representation of the dF term in eq. 24.

L-moments and Probability Weighted Moments of a Distribution

The product moments are not satisfactory for many types of data sets, particularly those with large ranges, non-normal distributions, and a tendency to contain outliers (unexpectedly large or small values) because the biases and sampling variances are often so large as to render the statistics unattractive (Kirby, 1974; Wallis and others, 1974). Many data sets in the hydrologic sciences including floods, droughts, and extreme precipitation exhibit the above characteristics. Barnett and Lewis (1995) provide an excellent presentation and review of outliers in statistical data. The product moments are incompatible with distributions that can only be expressed in quantile

form. Most of the common distributions (Normal, Beta) are expressible in at least a PDF form and sometimes a CDF form, and frequently no explicit quantile form exists. The quantiles of distributions that do not have explicit quantile expressions have to be solved by numerical integration.

The L-moments provide an attractive theoretical framework because of some statistical considerations and their applicability to quantile functions. The L-moments have many well documented statistical advantages over the product moments. Specifically, L-moments are less sensitive to the presence of outliers in the data, exhibit less bias, are more accurate in small samples, and do not require logarithmic or other power transformations of the data. Transformations are traditionally used to reduce the skewness of the data and compensate for the shortcomings of the product moments by reducing the influence of large data values. Transformations, particularly logarithmic, are not always possible with data possessing zero or negative values. Furthermore, logarithmic transformations generally inflate the influence of small values, especially positive values considerably less than one. The L-moments also provide more secure inferences of distributional form than do the product moments. The L-moments specify a distribution even if some of the product moments do not exist (Hosking, 1990, p. 108), and Hosking also reports that an L-moment specification of a distribution is unique, which is not true of a product moment specification.

Some of the more important references (some repeated from earlier citation for list completeness) on L-moment theory and related statistics include: Greenwood and others (1979), David (1981), Hosking (1986, 1990, 1992, 1996), Hosking and Wallis (1993a,b), Hosking and Wallis (1995), Landwehr and others (1979a,b), Vogel and Fennessey (1993), Wang (1996a,b), and Zafirakou-Koulouris and others (1998). Only a limited number of books or chapters therein are available with descriptions of L-moments: Stedinger and others (1992), Hosking (1995), Hosking and Wallis (1997), Gilchrist (2000), and Dingman (2002).

A comprehensive review of L-moments is provided in Appendix B. Some portions of Appendix B are repeated in this chapter in order to properly set the context of the p-PWMs. The primary concept is that the L-moments are exact analogs to the product moments in that features of a distribution such as the mean, variance, skew, kurtosis, and higher measures. The L-moment analogs have similar interpretations but do not acquire similar numerical values as the product moments.

As in the product moment case, consider a real-valued random variable X with a cumulative distribution function $F(x)$ and a quantile function $x(F)$. As before, F is a cumulative probability or nonexceedance probability and $0 \le F \le 1$. If a random sample of size n is drawn from the distribution of X, and the sample is *arranged in ascending order*, the values $X_{1:n} \le X_{2:n} \le \ldots \le X_{n:n}$ become the *order statistics* of X.

The expectation of an order statistic can be expressed as

$$E[X_{j:r}] = \frac{r!}{(j-1)!(r-j)!}\int_0^1 x(F)F^{j-1}(1-F)^{r-j}dF\,. \tag{27}$$

The order statistics for X are theoretical random observations—no ties occur. In practice, real samples can contain ties. Hosking (written commun., 2002) reports that the presence of ties should not influence the accuracy of the order statistics and hence the L-moments when defined in terms of order statistic expectations. When the integral definitions of the L-moments of quantile functions (continuous functions, no ties are possible) are considered the situation changes in the presence of ties, but the topic has not been researched.

The L-moments are the expectations of specific linear combinations of the order statistic expectations. In general, the L-moments are defined by

$$\lambda_r \equiv \frac{1}{r}\sum_{k=0}^{r-1} -1^k \binom{r-1}{k} E[X_{r-k:r}]\,. \tag{28}$$

The first four L-moments derived from eq. 28 are

$$\lambda_1 = E[X_{1:1}]\,, \tag{29.1}$$

$$\lambda_2 = \frac{1}{2}E[X_{2:2} - X_{1:2}]\,, \tag{29.2}$$

$$\lambda_3 = \frac{1}{3}E[X_{3:3} - 2X_{2:3} + X_{1:3}]\,, \text{ and} \tag{29.3}$$

$$\lambda_4 = \frac{1}{4}E[X_{4:4} - 3X_{3:4} + 3X_{2:4} - X_{1:4}] \ . \tag{29.4}$$

The first L-moment λ_1 is the mean (μ). The mean is the expected value of a single observation of X. The second L-moment λ_2 is a measure of the dispersion or spread of X much like the usual standard deviation. The value λ_2 is read as one half the expected difference between the two order statistics of a sample of size $n = 2$, and is referred to as L-scale or L-variation. The value $\tau = \lambda_2/\lambda_1$ is known as the coefficient of L-variation. The values of λ_3, λ_4, and λ_5 when divided by λ_2 become the L-moment ratios and measure skew (τ_3 or L-skew), kurtosis (τ_4 or L-kurtosis), and higher measures of shape (τ_5 or Tau5). Before further development, a segue into PWMs will be useful.

The PWMs defined by Greenwood and others (1979) for quantile function $x(F)$ and cumulative probability F are

$$M_{p,\,r,\,s} = E[x(F)^p F^r (1 - F)^s] \ . \tag{30}$$

The PWM $M_{1,\,0,\,0} = E[x(F)]$ is the mean. The higher PWMs $r > 0$ and $s > 0$ are not easily interpreted. However, the L-moments and PWMs can be expressed as linear combinations of each other. Because of linearity, procedures based on L-moments or the PWMs are equivalent. The PWMs actually predate the L-moments, but the L-moments usually are far more convenient and directly interpretable as measures of

distributions. The PWMs thus are generally considered in recent times as a means to compute the L-moments.

Particularly useful PWMs for L-moment theory are $\alpha_r = M_{1,0,r}$ and $\beta_r = M_{1,r,0}$. The author, following convention by other researchers, focuses here on β_r, and remarks that α_r and β_r can be shown as linear combinations of each other

$$\alpha_r = \int_0^1 x(F)(1-F)^r dF \text{ and} \tag{31.1}$$

$$\beta_r = \int_0^1 x(F)F^r dF . \tag{31.2}$$

Contrast β_r with the usual product moment definition (eq. 24), which is repeated below

$$E[X^r] = \int_0^1 x(F)^r dF . \tag{32}$$

The L-moments defined in linear terms of the PWMs are the quantities

$$\lambda_{r+1} = \sum_{k=0}^{r} p^*_{r,k}\beta_k \text{ for } r = 0, 1, \ldots, n-1 , \tag{33}$$

where

$$p^*_{r,k} = -1^{r-k}\binom{r}{k}\binom{r+k}{k} = \frac{-1^{r-k}(r+k)!}{(k!)^2(r-k)!} . \tag{34}$$

The first four L-moments are

$$\lambda_1 = \beta_0, \tag{35.1}$$

$$\lambda_2 = 2\beta_1 - \beta_0, \tag{35.2}$$

$$\lambda_3 = 6\beta_2 - 6\beta_1 + \beta_0, \text{ and} \tag{35.3}$$

$$\lambda_4 = 20\beta_3 - 30\beta_2 + 12\beta_1 - \beta_0, \tag{35.4}$$

or equivalently in terms of the quantile function as

$$\lambda_1 = \int_0^1 x(F)dF, \tag{36.1}$$

$$\lambda_2 = \int_0^1 x(F)(2F-1)dF, \tag{36.2}$$

$$\lambda_3 = \int_0^1 x(F)(6F^2 - 6F + 1)dF, \text{ and} \tag{36.3}$$

$$\lambda_4 = \int_0^1 x(F)(20F^3 - 30F^2 + 12F - 1)dF. \tag{36.4}$$

Sample L-moments and Probability Weighted Moments

L-moments and PWMs are defined for the quantile distribution function $x(F)$, but in general are estimated for finite samples of size n by arranging the sample in ascending order $x_{1:n} \le x_{2:n} \le \ldots \le x_{n:n}$ to acquire the *sample order statistics* of random variable X. Presently there are two classes of L-moment estimators for finite samples, the unbiased estimators and the plotting-position estimators. An additional class of estimator based on p-PWMs is proposed in a later section of this chapter.

Unbiased Estimators

Unbiased estimates of β_r, hence λ_r, can be made by

$$b_r = \frac{1}{n}\binom{n-1}{r}^{-1} \sum_{j=r+1}^{n} \binom{j-1}{r} x_{j:n} \quad \text{for } r = 0, 1, \ldots, n-1 . \tag{37}$$

The "unbiased" weight factor on a specific $x_{j:n}$ is $w_{j,r}$ and is given by

$$w_{j,r} = \frac{\binom{j-1}{r}}{n\binom{n-1}{r}} . \tag{38}$$

The multiplication to the left of the summation has been included in the unbiased weight factor to facilitate later analysis.

The first four unbiased PWM estimators are

$$b_0 = \frac{1}{n} \sum_{j=1}^{n} x_{j:n}, \tag{39.1}$$

$$b_1 = \frac{1}{n} \sum_{j=1}^{n} \frac{j-1}{n-1} x_{j:n}, \tag{39.2}$$

$$b_2 = \frac{1}{n} \sum_{j=1}^{n} \left(\frac{j-1}{n-1}\right)\left(\frac{j-2}{n-2}\right) x_{j:n}, \text{ and} \tag{39.3}$$

$$b_3 = \frac{1}{n} \sum_{j=1}^{n} \left(\frac{j-1}{n-1}\right)\left(\frac{j-2}{n-2}\right)\left(\frac{j-3}{n-2}\right) x_{j:n} . \tag{39.4}$$

Unbiased estimates of the first four L-moments in terms of the unbiased PWM estimates are

$$l_1 = b_0 , \tag{40.1}$$

$$l_2 = 2b_1 - b_0 , \tag{40.2}$$

$$l_3 = 6b_2 - 6b_1 + b_0 , \text{ and} \tag{40.3}$$

$$l_4 = 20b_3 - 30b_2 + 12b_1 - b_0 . \tag{40.4}$$

Hence, in general the unbiased L-moment and L-moment ratios are estimated as

$$l_{r+1} = \sum_{k=0}^{r} p^*_{r,k} b_k \text{ for } r = 0, 1, \ldots, n-1 , \tag{41}$$

$$t = l_2 / l_1 , \text{ and} \tag{41.1}$$

$$t_r = l_r / l_2 \text{ for } r \geq 3 . \tag{41.2}$$

A manual example computation of the unbiased L-moments for a sample is shown in Appendix B to demonstrate how the L-moments are computed without the aid of computer software.

Plotting-Position Estimators

Estimates of β_r and λ_r also can be made with a second class of estimator called plotting-position estimators. A plotting position is a distribution free or nonparametric estimator of cumulative probability $F(x_{j:n})$. Historically, plotting positions commonly have been used for graphical display of random samples of X (Stedinger and others,

1992, pp. 18.23–18.27), but they also can be used for parameter estimation (Gilchrist, 2000, chapter 9; Karian and Dudewicz, 2000, chapter 4). Often recognized reasonable choices include $p_{j:n} = (j + \delta)/(n + \varepsilon)$ for $\delta > \varepsilon > -1$, where $p_{j:n}$ is the plotting position for the jth ascending order observation of a random sample of size n. Hence, the PWMs are estimated as

$$\tilde{\beta}_r = \frac{1}{n} \sum_{i=1}^{n} (p_{j:n})^r x_{j:n}. \tag{42}$$

The plotting-position weight factor on a specific $x_{j:n}$ is $\tilde{w}_{j,r}$ and is given by

$$\tilde{w}_{j,r} = \frac{(p_{j:n})^r}{n}. \tag{43}$$

The constant n^{-1} is included in the plotting-position weight factor to facilitate later comparisons.

The plotting-position L-moments and L-moment ratios are estimated as

$$\tilde{\lambda}_{r+1} = \sum_{k=0}^{n} p^*_{r,k} \tilde{\beta}_r, \tag{44.1}$$

$$\tilde{\tau} = \tilde{\lambda}_2 / \tilde{\lambda}_1, \text{ and} \tag{44.2}$$

$$\tilde{\tau}_r = \tilde{\lambda}_r / \tilde{\lambda}_2 \text{ for } r \geq 3. \tag{44.3}$$

The unbiased L-moments generally are preferred over plotting-position estimators (Hosking and Wallis, 1997, pp. 31–34). In rare cases, plotting-position estimators can produce L-moments with theoretically impossible values such as $\lambda_2 < 0$ or $\tau_3 > 1$; such occurrences are not possible with unbiased estimators. This is a very important consideration for algorithm development involving plotting-position PWM estimation and has ramifications of the p-PWM method described next. Confirmation that the bounds of the L-moments are satisfied is absolutely required.

Prior-Probability Weighted Moments (p-PWMs)

Thus far the PWMs and hence the L-moments for finite samples are computed only through weight factors ($w_{j,r}$ or $\tilde{w}_{j,r}$) applied to an ordered sample. The ordered sample is derived from a random sample of X. Because the sample is random, the weight factors are chosen because no prior or no additional information about specific observations of X is known. This ignores the observation by the author that selection of a correct plotting-position formula arguably implies some sort of prior knowledge of the distribution generating the data. An interesting question to ask is how might the sample estimators of PWMs be effected by *a priori* knowledge of the cumulative probability of each ordered observation of X in a sample? A follow up question is how are sample PWMs computed in situations in which this additional information is available? These questions are explored and a suitable method is developed in this section. The term "prior-Probability Weighted Moments" (p-PWMs) is used to

describe how the method stresses that the cumulative probability F of the sample observations is utilized in the computational process.

It is useful to repeat the definition of the theoretical PWMs (eq. 31.2).

$$\beta_r = \int_0^1 x(F)F^r dF . \tag{45}$$

How could β_r be estimated for a sample in the situation in which the cumulative probabilities F are available? If the values for F were available, it is possible to evaluate dF with a finite difference approximation. Extension of the above integral to a sample results in

$$\hat{\beta}_r = \sum_{j=1}^{n} x_{j:n}(F_j)^r dF_j^* \tag{46}$$

where dF_j^* is a finite difference estimator of the incremental cumulative probability for the jth ascending ordered observation. The operator dF_j^* has a natural estimator of

$$dF_j^* = \begin{cases} \frac{F_{j+1} - F_j}{2} + F_j - 0 & j = 1 \\ \frac{F_{j+1} - F_j}{2} + \frac{F_j - F_{j-1}}{2} & 1 < j < n \\ 1 - F_j + \frac{F_j - F_{j-1}}{2} & j = n \end{cases} \tag{47}$$

or

$$dF_j^* = \begin{cases} \dfrac{F_{j+1} + F_j}{2} & j = 1 \\ \dfrac{F_{j+1} - F_{j-1}}{2} & 1 < j < n \\ 1 - \dfrac{F_j + F_{j-1}}{2} & j = n \end{cases} . \tag{48}$$

Finally, the dF_j^* estimator must satisfy the condition of

$$\sum_{j=1}^{n} dF_j^* = 1 . \tag{49}$$

Equations 46 and 48 were first considered by the author in October 2001 stemming from communication with Thompson (personal commun., 2001). It should be pointed out that eq. 48 is similar to equations in Shen and Julien (1993, eqs. 12.1.3, 12.1.4) and an equation in Haan and others (1994, eq. 7.24). Although, Shen and Julien and Haan and others only describe a procedure for estimating the mean grain size of a sediment sample and not the higher product moments and not the L-moments.

A late note (Dec. 2002) regarding the p-PWM moment estimator shown in eq. 48 is needed. According to communication with Hosking (2002) an alternative estimator can be developed. This estimator adjusts the data and not the probability of the data. Hosking suggests

$$\tilde{x}(F) = x_j + \frac{F - F_j}{F_{j+1} - F_j}(x_{j+1} - x_j)$$

for $F_j < F < F_{j+1}$ and $j = 0, \ldots, n$, and then define the sample estimator

$$\tilde{B}_r = \int_0^1 \tilde{x}(F) F^r dF .$$

Hosking also states "L-moments obtained by this procedure are the population L-moments of an actual probability distribution (the distribution whose quantile function is $\tilde{x}(F)$), 'theoretically impossible' values of the L-moments can not occur." Further, Hosking reports that the idea of estimating PWMs by constructing an empirical distribution is due to Jones (1985) in an internal report. Finally, the alternative estimator was not utilized for the research presented in this dissertation. Since theoretically impossible L-moments were not used and the simulations in this chapter indicate that the author's implementation of the eq. 48 estimator, the research results are statistically defensible.

The "prior probability" weight factor on a specific $x_{j:n}$ is $\hat{w}_{j,r}$ and is given by

$$\hat{w}_{j,r} = (F_j)^r dF_j^* . \tag{50}$$

Contrast this weight factor with the plotting-position weight factor. The n^{-1} term in the plotting-position weight factor is a constant approximation to the dF term of the PWM integral (eq. 45) that is based solely on the sample size. Each data point in the plotting-position weight factor represents a uniform fraction of the $F[0, 1]$ probability range. Whereas dF_j^* is not uniform in magnitude across the $[0, 1]$ interval. It is difficult to compare the constant term $\left[n\binom{n-1}{r}\right]^{-1}$ of the unbiased weight factor (eq. 38) to the dF term of the PWM integral.

The prior probability L-moments and L-moment ratios therefore are estimated as

$$\hat{\lambda}_{r+1} = \sum_{k=0}^{n} p_{r,k}^* \hat{\beta}_r , \tag{51.1}$$

$$\hat{\tau} = \hat{\lambda}_2 / \hat{\lambda}_1 \text{, and} \tag{51.2}$$

$$\hat{\tau}_r = \hat{\lambda}_r / \hat{\lambda}_2 \text{ for } r \geq 3 . \tag{51.3}$$

An intuitive argument of the suitability of $\hat{\beta}_r$ as an estimator of β_r can be made. Because an arbitrary sample possessing pair-wise x and F values can have F assuming arbitrary probability, so must the dF term. Furthermore, the plotting-position formula is an arbitrary estimator of F, so the dF term is derivable from plotting-positions as well. Hence, the $\hat{\beta}_r$ most surely measure the same characteristics of the distribution as $\tilde{\beta}_r$ and should take on an approximately equivalent value for sufficiently large n. It follows by $\tilde{\beta}_r$ and b_r equivalence that b_r, $\tilde{\beta}_r$, and $\hat{\beta}_r$ should all be approximately equal.

To test without loss of generality the argument that b_r, $\tilde{\beta}_r$, and $\hat{\beta}_r$ are approximately equal by computing each for order $r = 0$ and 1 for a sample of size $n = 3$ and F computed by the plotting position formula $p_{j:n} = (j - 0.35)/n$. This plotting-position formula was selected because it has precedence for some studies utilizing L-moments. To illustrate, the plotting position probability is assumed equal to the prior probability and is used in p-PWM computation. In practice, this is not the intent of p-PWM usage. A short example of PWM and L-moment computation by

estimator class for a sample of size $n = 3$ is listed in table 14. The weight factors of each estimator class for each order on each observation are provided in the table.

Table 14. Probability Weighted Moment and L-moment weight factors by estimator class for first short example

j	$F = p_{j:n}$	$x_{j:n}$	w_0	$\tilde{w}_0$	$\hat{w}_0$	w_1	$\tilde{w}_1$	$\hat{w}_1$
1	0.217	1	0.333	0.333	0.384	--	0.0723	0.0832
2	.550	3	.333	.333	.333	0.167	.183	.183
3	.883	4	.333	.333	.284	.333	.294	.250

The PWMs for each estimator class for $r = 0$ are computed as follows

$$b_0 = \frac{1}{3}(1 + 3 + 4) = 2.67,$$

$$\tilde{\beta}_0 = \frac{1}{3}(1 + 3 + 4) = 2.67, \text{ and}$$

$$\hat{\beta}_0 = (0.384 \cdot 1 \cdot 1) + (0.333 \cdot 3 \cdot 1) + (0.284 \cdot 4 \cdot 1) = 2.52.$$

The PWMs for $r = 1$ are computed as follows

$$b_1 = (0.167 \cdot 3 + 0.333 \cdot 4) = 1.83,$$

$$\tilde{\beta}_1 = \frac{1}{3}(1 \cdot 0.217 + 3 \cdot 0.550 + 4 \cdot 0.883) = 1.80, \text{ and}$$

$$\hat{\beta}_1 = (1 \cdot 0.217 \cdot 0.384) + (3 \cdot 0.550 \cdot 0.333) + (4 \cdot 0.883 \cdot 0.284) = 1.64.$$

These PWMs produce the following first L-moments

$l_1 = b_0 = 2.67$,

$\tilde{\lambda}_1 = \tilde{\beta}_0 = 2.67$, and

$\hat{\lambda}_1 = \hat{\beta}_0 = 2.52$;

and the following second L-moments

$l_2 = 2b_1 - b_0 = 1$,

$\tilde{\lambda}_2 = 2\tilde{\beta}_1 - \tilde{\beta}_0 = 0.93$, and

$\hat{\lambda}_2 = 2\hat{\beta}_1 - \hat{\beta}_0 = 0.76$.

Thus for the example in table 14, the first two PWMs and L-moments are similar to each though they are not necessarily equal.

Some readers will note with possible concern that there are two different estimates of β_0, which is just the mean. First, note that the unbiased property for the $\hat{\beta}_0$ estimate still remains intact as the sum of the $\hat{w}_0$ weight factors is equal to unity along with the sums of the weight factors w_0 and $\tilde{w}_0$. Second, note that the $\tilde{w}_0$ weights give more leverage to the first value and less to the third. The "prior probability mean" has a value of 2.52 which accordingly is less than the usual mean (2.67). The $\hat{\lambda}_1 < l_1$, $\hat{\lambda}_1 < \tilde{\lambda}_1$, $\tilde{\lambda}_1 = l_1$ relations are expected if and only if the F were already known. By

intuition, the prior-probability mean should be less than arithmetic mean because the first data point is less far into the left tail of the distribution than the third data point is from the right tail ($0.217 - 0 > 1 - 0.883$). Necessarily a different choice in the plotting position estimator would yield different differences in $\tilde{\beta}_r$ and $\hat{\beta}_r$ as would a different estimator of the dF term.

To illustrate p-PWMs further, consider the following data set in table 15 containing the median, 10th percentile, and 90th percentile observations. The unbiased and plotting position estimators do not utilize this (median, 10th percentile, and 90th percentile). The $r = 0, 1, 2$ weight factors have been computed. The PWMs and L-moments of the distribution that generated this data are summarized in table 16. The third PWM and the third L-moment ratio (L-skew) have been included.

Table 15. Probability Weighted Moment and L-moment weight factors by estimator class for second short example

j	$F = p_{j:n}$	$x_{j:n}$	w_0	$\tilde{w}_0$	$\hat{w}_0$	w_1	$\tilde{w}_1$	$\hat{w}_1$	w_2	$\tilde{w}_2$	$\hat{w}_2$
1	0.100	1	0.333	0.333	0.3	--	0.0333	0.03	--	0.00333	0.003
2	.500	3	.333	.333	.4	0.167	.167	.2	--	.0833	.100
3	.900	4	.333	.333	.3	.333	.30	.27	0.333	.27	.243

From the PWM and L-moment estimates in table 16 it is clear that the p-PWMs produce comparable mean and L-scale values. The L-skew values do not appear comparable although the $r = 2$ PWMs appear comparable. The unbiased L-skew is negative, which indicates that the smallest observation is further away from the second observation than the second is from the third observation.

Table 16. Probability Weighted Moments and L-moments by estimator class for second short example

	Unbiased estimates	Plotting-position estimates	Prior probability estimates
Probability Weighted Moments			
β_0	2.67	2.67	2.70
β_1	1.83	1.73	1.71
β_2	1.33	1.33	1.28
L-moments			
λ_1	2.67	2.67	2.70
λ_2	1.00	.80	.72
λ_3	-.33	.27	.12
τ	.37	.30	.27
τ_3	-.33	.34	.125

p-PWM Suitable Data and Real-World Examples

A basic question is what types of data sets are characterized by the availability of cumulative probabilities? Some data sets would be those in which the percentiles of X are known through the sampling procedure. If a sampling procedure reports percentiles of each data point, these can be considered as estimates of cumulative probabilities. A grain-size distribution in which the percentages of total sample mass retained by sieves of a specific diameter or the cumulative depth of storm runoff from a watershed as a percentage of elapsed time could be considered as data having prior probability. For the grain size data, the probabilities are really the random variable as the sieve size is almost always established by the sampling procedure. For the storm rainfall (runoff) data, the rainfall (runoff) depth and percentage of elapsed time are

determined by their concomitant association. Regardless, in either example, neither plotting-position or unbiased L-moment or PWM estimators appear applicable.

A limitation of the p-PWMs estimators is that, depending upon the distribution of the prior probabilities, theoretically impossible L-moments values can be computed. Impossible L-moment values usually occur for small samples or wildly non-uniform probabilities. Theoretically impossible L-moment values are also possible from the plotting-position L-moment estimators. The weight factors for the two estimators (eq. 42 and 46) are similar. However, theoretically impossible L-moments are more likely with p-PWMs than with plotting positions because the probabilities used in the weight factors on the data values can attain an unrestricted range of values; whereas, the plotting position weight factors are constrained by the nature of the plotting-position formula.

Comparison between sample moment computation type is made by considering the rainfall for the May 23, 1981 storm for 08156800 Shoal Creek at 12th Street, Austin, Texas. Both unbiased and p-PWM computations for the trimmed and untrimmed data are listed in table 17. This storm was considered in the first chapter. The dimensionless hyetograph for the storm is shown on figure 23.

From the figure, the recorded points defining the hyetograph typically are not well distributed. If they were, there would be the expectation that the points would appear uniformly distributed along the horizontal axis. This is clearly not the case. This situation exists because the points were chosen by previous analysts in such a fashion

as to accurately represent the steeper portions of the hyetograph. Although not applicable to the hyetograph on figure 23, throughout the data base, steeper portions of the hyetograph commonly occur in the first half of the time period, and are typically defined by more points than straighter or more gradually changing portions. The straighter portions typically are on the trailing or recession end of the hydrograph. Further complicating matters is that this particular hyetograph has two distinct bursts.

A prudent double-tail one-percent trimming of the hyetograph prior to expression in a percentage basis was performed to reduce the length of the leading and trailing tail. Specifically, the event is considered to start once one percent of more of the total depth occurred and to stop once 99 percent of the depth occurred. After the trimming was performed, the percentages of duration and total depth were recomputed.

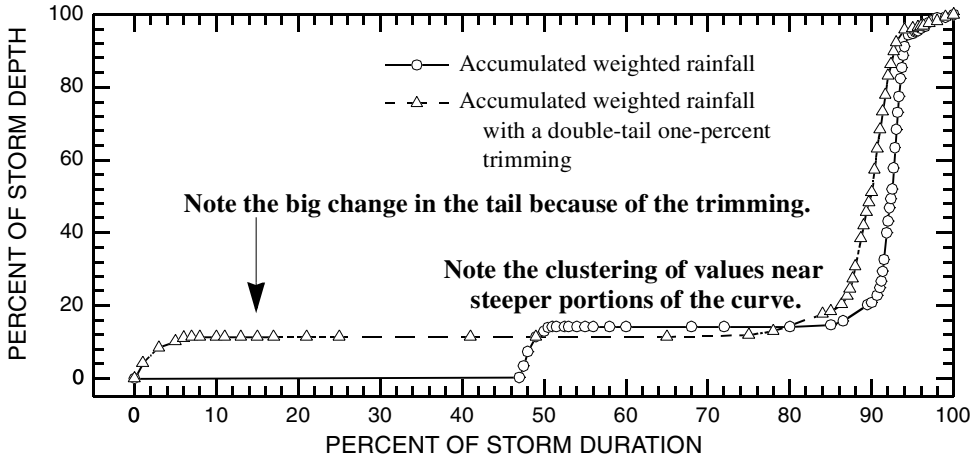

Figure 23. Two dimensionless hyetograph representations of May 23, 1981 storm for watershed of station 08156800 Shoal Creek at 12th Street, Austin, Texas

For purposes of clarity, only comparisons between the moment estimation types for the trimmed data (triangles in fig. 23) will be made with an observation that the original (untrimmed) data (circles in fig. 23) yields similar conclusions. The symmetrical one-percent trimming of the data shortens the leading tail for this particular hyetograph of the hyetograph considerably (see arrow in fig. 23), and therefore, the trimmed data is more representative of the distribution of the hyetograph. Furthermore, the comparison will focus only on the L-moments as the linearity between PWMs and L-moment makes additional comparison of the PWMs unnecessary.

Table 17. Application of prior-Probability Weighted Moments on an observed hyetograph expressed in percent duration and percent depth for May 23, 1981 storm for watershed of station 08156800 Shoal Creek at 12th Street, Austin, Texas

[The moment type symbology is defined in the text. The trimmed data represents a double one-percent tail trimming of the values from the hyetograph prior to expression as a cumulative percent.]

Moment type	Untrimmed data		Trimmed data	
	Unbiased estimators	Prior probability estimators	Unbiased estimators	Prior probability estimators
β_0	46.40	13.91	43.94	20.35
β_1	33.29	11.71	31.92	14.35
β_2	26.02	10.20	25.23	11.98
β_3	21.27	9.122	20.78	10.59
β_4	17.90	8.308	17.58	9.61
λ_1	46.50	13.91	43.94	20.35
λ_2	20.09	9.513	19.90	8.350
τ	.4320	.6840	.4529	.4103
τ_3	.1439	.5119	.1906	.7349
τ_4	-.1146	.3081	-.1101	.5061
τ_5	-.1057	.2715	-.1041	.2069

The mean for the unbiased estimator having a value of 43.94 is considerably greater than the mean for the p-PWM estimator of 20.35. This is because only the p-PWMs "see" the long flat inter-burst portion of the curve. This flat portion represents approximately 70 percent of the nonexceedance probability range. The ordinate of the flat portion is approximately 12 percent. Since the data continues to increase from 12 percent to 100 percent of storm depth between the 80 and 100 percent of the storm duration, the fact that the mean is somewhat greater than 12 is acceptable. The unbiased mean estimate is entirely out of line with careful inspection of figure 23.

The inherent variation in the data as represented by the τ values appears similar between the estimation methods. It is hard to visualize in the figure. Distribution skewness is easier to visualize in the figure. The skewness of the data as represented by τ_3 is quite different between the estimation methods (0.1906 compared to 0.7349). The L-skew for the p-PWMs is much larger which indicates that the hyetograph as measured by p-PWMs is far more left tailed. This occurs because the second burst is so much bigger than the first burst and occurs relatively late in the event. The higher measures of distribution shape τ_4 (L-kurtosis) and τ_5 actually have opposite signs. It is very difficult to visualize these higher measures on figure 23.

p-PWM Sampling Properties

By intuition and by example, the p-PWM estimators of the sample L-moments produce reasonable values. Intuitive reasoning and examples are necessary but not sufficient to justify p-PWM usage on qualifying data sets. Investigation of the sampling properties of p-PWM estimators such as bias and their relative efficiency compared to the unbiased estimators is required. An exhaustive investigation is difficult to perform. The statistical experiments described here were performed in Fall of 2001 on a streamflow hydrograph that was arbitrarily selected. The dimensionless hydrograph is for the May 11, 1965 storm on 08178000 Escondido Creek subwatershed #1 near Kenedy, Texas. This hydrograph is shown on figure 24.

It likely is somewhat confusing to many readers why a hydrograph and not a hyetograph is considered and why the simulations reported on in this section used data for a hydrograph instead of data for a hyetograph. On an historical note, when application for the p-PWMs was first considered for this dissertation, application to streamflow hydrographs was chosen. The change in application was made because of a change in research interests by the author. Although the focus of the simulations is on runoff data and not specifically rainfall data, the generalization to hyetographs is should be self evident.

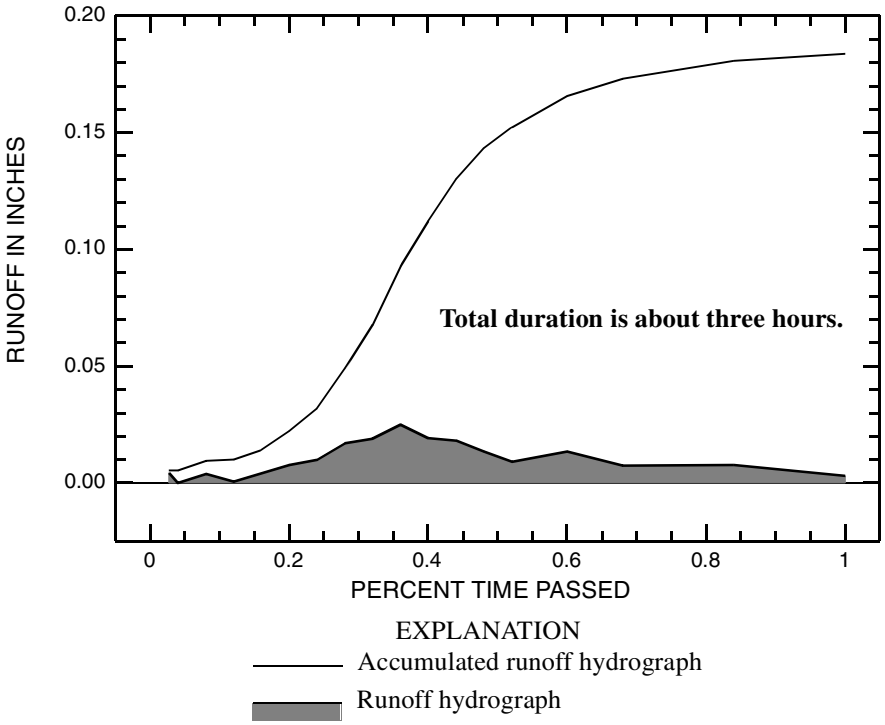

Figure 24. Dimensionless streamflow hydrograph for May 11, 1965 storm for station 08187000 Escondido Creek subwatershed #1 near Kenedy, Texas

In order to assess the sampling properties of a statistical estimator, such as PWM or L-moment estimators, statistical experimentation or simulation can be used. Statistical simulation (also known as the Monte-Carlo method) is based on random number generators.

Because of the desire to compute L-moment estimates, only results for the L-moment estimators previously described and not for the PWMs are reported. In simulation a parent distribution and parameters are chosen and various sample sizes are drawn from the distribution. The L-moments are computed for each simulated sample of a specific sample size. The differences between the simulated L-moments

and the specified or true L-moments of the distribution also are computed. When a sufficient number of simulation runs are performed, the mean difference is determined. This mean is referred to as bias and is defined here as the simulated mean statistic minus the true value. An unbiased estimator will have a mean difference of zero.

The variance of the differences commonly also is computed. This variance is known as the sampling variance. Relative efficiency (RE) between estimators is defined as the ratio of the sampling variances. RE is computed here as the variance of the unbiased estimator divided by either the plotting-position estimator or the p-PWM estimator. Values of RE greater than one indicate that the candidate estimator outperforms the unbiased L-moment estimator.

The Kappa distribution (Hosking, 1994) was selected for simulation using the inverse transformation method (Ross, 1994, p. 445). This method is convenient with the Kappa distribution because the distribution is expressed as a quantile function. The Kappa distribution is described in the next section.

Kappa Distribution

The Kappa distribution is a four parameter distribution that is commonly used in L-moment studies requiring simulated or artificial data to assess the accuracy of statistical methods. Because it has four parameters, the distribution is capable of assuming a wide range of scales and shape combinations not possible with more common two or three parameter distributions such as the Normal or the Generalized

Extreme Value (GEV). The Kappa distribution quantile function has the following form

$$x(F) = \xi + \frac{\alpha}{\kappa}\left\{1 - \left(\frac{1 - F^h}{h}\right)^{\kappa}\right\} . \tag{52}$$

The four parameters are ξ (location), α (scale), κ (shape 1), and h (shape 2). There is no simple expression for the cumulative distribution function (CDF) $F(x)$ or the probability density function (PDF) $f(x)$ for the distribution. The quantile is subject to the following restrictions. For the upper bound of x the restriction is

$$x \le \xi + \alpha/\kappa \quad \text{if } \kappa > 0 \text{ and} \tag{53.1}$$

$$x = \infty \qquad \text{if } \kappa \le 0 . \tag{53.2}$$

For the lower bound of x the restriction is

$$x \ge \xi + \alpha(1 - h^{-\kappa})/\kappa \quad \text{if } h > 0 , \tag{54.1}$$

$$x \ge \xi + \alpha/\kappa \qquad \text{if } h \le 0 \text{ and } \kappa < 0 , \text{ and} \tag{54.2}$$

$$x \ge -\infty \qquad \text{if } h \le 0 \text{ and } \kappa \ge 0 . \tag{54.3}$$

The L-moments of the Kappa distribution are defined if $h \ge 0$ and $\kappa > -1$, or if $h < 0$ and $-1 < \kappa < -1/h$ and are

$$\lambda_1 = \xi + \alpha(1 - g_1)/\kappa , \tag{55.1}$$

$$\lambda_2 = \alpha(g_1 - g_2)/\kappa , \tag{55.2}$$

$$\tau_3 = (-g_1 + 3g_2 - 2g_3)/(g_1 - g_2) , \text{ and} \tag{55.3}$$

$$\tau_4 = (-g_1 + 6g_2 - 10g_3 + 5g_4)/(g_1 - g_2) \tag{55.4}$$

where

$$g_r = \begin{cases} \dfrac{r\Gamma(1+\kappa)\Gamma(r/h)}{h^{1+\kappa}\Gamma(1+\kappa+r/h)} & \text{for } h > 0 \\ \dfrac{r\Gamma(1+\kappa)\Gamma(-\kappa-r/h)}{(-h)^{1+\kappa}\Gamma(1-r/h)} & \text{for } h < 0 \end{cases} \tag{56}$$

and

$$\Gamma(k) = \int_0^\infty u^{k-1} e^{-u} du \tag{57}$$

is the Gamma function.

The Kappa parameters in terms of the L-moments have no simple expressions. Equations 55.3 and 55.4 can be solved for κ and h by Newton-Raphson iteration. Hosking (1996) describes a suitable algorithm.

Kappa based Simulation Results

Uniform Distribution of Nonexceedance Probability

A logical starting point in the experimentation is to assess the p-PWM estimator using a uniform distribution of F. A uniform distribution of F is normally done in statistical simulation. The p-PWM L-moment estimates of 0.114, 0.333, -0.148, and 0.0476 for λ_1, τ, τ_3, and τ_4, respectively were used for experimentation. These

L-moment values were derived from a representative cumulative streamflow hydrograph (fig. 24) for Escondido Creek.

The L-moments above correspond to Kappa parameters of $\xi = 0.0699$, $\alpha = 0.1439$, $\kappa = 1.022$, and $h = 0.5045$. Eight sample sizes, which ranged from 5 to 1,000, were chosen for experimentation. The number of simulations per estimator was 50,000. Hence, the number of simulation runs for $n = 5$ was 10,000 and the number of simulation runs for $n = 1{,}000$ was 50.

The biases for the mean, L-scale, L-CV, L-skew, and L-kurtosis are listed in table 18. The bias in the mean is relatively small for all three estimators, but the p-PWM estimator has substantially larger bias for small sample sizes ($n \leq 20$). As sample size increases, the p-PWM estimator shows the least bias. A similar observation is made about the bias for L-scale. The p-PWM estimator again shows the largest bias for small samples sizes. For larger sample sizes, the biases of the three estimators are approximately equal, but the p-PWM estimator consistently has the least bias for $n \geq 200$. For all three estimators, the bias of L-CV decreases in absolute magnitude as sample size increases. The p-PWM estimator consistently has the least bias for $n \geq 100$. For L-skew, it appears that the unbiased and p-PWM estimators have similar bias with the edge going to the unbiased estimator. The plotting-position estimators possess considerably larger bias for $n < 500$, and exhibit very large bias for small

sample sizes. Finally, for L-kurtosis, it is apparent that the p-PWM estimator is very biased for $n = 5$, but the bias diminishes rapidly as sample size increases.

Table 18. Comparison of sample biases for a simulated Kappa distribution using a uniform distribution of probability

[The Kappa distribution had specified L-moments of 0.114, 0.0378, -0.148, and 0.0476 for the mean, L-scale, L-skew, and L-kurtosis, respectively. These L-moments correspond to estimated Kappa parameters of 0.0669, 0.1439, 1.022, and 0.5045 for the location, scale, shape 1, and shape 2 parameters, respectively. Bias is defined as the simulated mean statistic minus the true value. UB, unbiased; PP, plotting position based probability weighted moments; XF, prior-probability weighted moments. Number of simulations per estimator was 50,000.]

Sample size	Estimator type	Mean bias	L-scale bias	L-CV bias	L-skew bias	L-kurtosis bias
n=5	UB	-0.0002	-0.0001	0.0451	0.0127	0.0209
	PP	.0001	-.0008	.0524	.1769	.0424
	XF	.0021	-.0032	-.0359	-.0023	.1947
n=10	UB	.0001	-.0002	.0179	.0052	.0100
	PP	-.0001	-.0004	.0165	.1161	.0350
	XF	.0011	-.0029	-.0278	-.0524	.0585
n=20	UB	.0002	.0001	.0101	-.0021	.0035
	PP	.0002	-.0001	.0072	.0610	.0213
	XF	.0005	-.0012	-.0112	-.0287	-.0075
n=50	UB	.0002	.0	.0031	-.0030	.0012
	PP	.0003	-.0001	.0017	.0227	.0100
	XF	.0002	-.0003	-.0030	-.0019	-.0162
n=100	UB	-.0006	.0003	.0063	-.0002	.0001
	PP	-.0002	.0001	.0036	.0109	.0044
	XF	.0001	-.0001	-.0010	-.0005	-.0051
n=200	UB	.0003	-.0001	-.0008	-.0012	.0022
	PP	-.0001	.0	.0010	.0084	.0028
	XF	.0	.0	-.0003	-.002	-.0022
n=500	UB	.0003	-.0002	-.0019	.0003	-.0001
	PP	-.0004	.0001	.0029	.0038	.0020
	XF	.0	.0	-.0001	.0001	-.0001
n=1,000	UB	.0002	-.0001	-.0013	-.0016	.0024
	PP	-.0004	.0002	.0030	-.0001	.0012
	XF	.0	.0	.0	.0	.0

From the simulation experiments, it is apparent that all three L-moment estimators are unbiased at sufficiently large sample sizes. Most importantly for the objectives of

this dissertation, p-PWM estimators appear to be competitive against the unbiased estimators and the plotting-position estimators for sample sizes greater than 10. For very large sample sizes it appears as though the p-PWM estimators have the least bias.

Although an estimator might be unbiased, unbiasedness alone should not justify its use, as the sampling variability of the estimator could be so large as to render it unusable against other more biased estimators possessing minimal variance. Often it is possible to remove the bias from an estimator if sufficient understanding of its sampling distribution is known. Hence, the sampling variability requires analysis. The sampling standard deviations for the simulation runs in table 18 are listed in table 19. It is cumbersome to directly compare standard deviations, so corresponding relative efficiencies to the unbiased estimator are listed in table 20.

Table 19. Comparison of sample standard deviations for a simulated Kappa distribution using a uniform distribution of probability

[The Kappa distribution had specified L-moments of 0.114, 0.0378, -0.148, and 0.0476 for the mean, L-scale, L-skew, and L-kurtosis, respectively. These L-moments correspond to estimated Kappa parameters of 0.0669, 0.1439, 1.022, and 0.5045 for the location, scale, shape 1, and shape 2 parameters, respectively. The sample standard deviation (SD) is defined as the square root of the sampling variance of the estimator. UB, unbiased; PP, plotting position based probability weighted moments; XF, prior-probability weighted moments. Number of simulations per estimator was 50,000.]

Sample size	Estimator type	SD for Mean	SD for L-scale	SD for L-CV	SD for L-skew	SD for L-kurtosis
n=5	UB	0.0299	0.0126	0.2640	0.2934	0.3681
	PP	.0303	.0093	3.036	.1477	.1305
	XF	.0135	.0134	.1185	.3977	.2843
n=10	UB	.0210	.0082	.1276	.1590	.1408
	PP	.0215	.0070	.1185	.1165	.0905
	XF	.0057	.0068	.0627	.2497	.1897
n=20	UB	.0151	.0056	.0851	.0994	.0760
	PP	.0146	.0051	.0786	.0836	.0649
	XF	.0022	.0029	.0274	.1370	.0979

Sample size	Estimator type	SD for Mean	SD for L-scale	SD for L-CV	SD for L-skew	SD for L-kurtosis
n=50	UB	.0095	.0034	.0521	.0554	.0418
	PP	.0093	.0032	.0485	.0549	.0469
	XF	.0006	.0007	.0075	.0330	.0438
n=100	UB	.0065	.0024	.0359	.0358	.0275
	PP	.0069	.0024	.0370	.0383	.0399
	XF	.0002	.0002	.0026	.0087	.0234
n=200	UB	.0049	.0015	.0248	.0305	.0195
	PP	.0049	.0016	.0254	.0286	.0316
	XF	.0001	.0001	.0009	.0035	.0114
n=500	UB	.0030	.0011	.0161	.0195	.0148
	PP	.0029	.0010	.0154	.0164	.0322
	XF	<.0001	<.0001	.0003	.0005	.0006
n=1,000	UB	.0021	.0008	.0118	.0122	.0086
	PP	.0018	.0006	.0087	.0129	.0340
	XF	<.0001	<.0001	<.0001	<.0001	<.0001

Table 20. Comparison of relative efficiencies for a simulated Kappa distribution using a uniform distribution of probability

[The Kappa distribution had specified L-moments of 0.114, 0.0378, -0.148, and 0.0476 for the mean, L-scale, L-skew, and L-kurtosis, respectively. These L-moments correspond to estimated Kappa parameters of 0.0669, 0.1439, 1.022, and 0.5045 for the location, scale, shape 1, and shape 2 parameters, respectively. Relative efficiency (RE) is defined as the variance of the unbiased estimator to the variance of the plotting position or prior-probability weighted moment estimator. UB, unbiased; PP, plotting position based probability weighted moments; XF, prior-probability weighted moments. Number of simulations per estimator was 50,000.]

Sample size	Estimator type	RE for Mean	RE for L-scale	RE for L-CV	RE for L-skew	RE for L-kurtosis
n=5	UB	1	1	1	1	1
	PP	.974	1.84	.0076	3.95	7.96
	XF	4.91	.884	4.96	.544	1.68
n=10	UB	1	1	1	1	1
	PP	.954	1.37	1.16	3.47	2.42
	XF	13.6	1.45	4.14	.405	.551
n=20	UB	1	1	1	1	1
	PP	1.07	1.21	1.17	1.41	1.37
	XF	47.1	3.73	9.65	.526	.603
n=50	UB	1	1	1	1	1
	PP	1.04	1.13	1.15	1.02	.794
	XF	250	23.6	48.3	2.82	.911
n=100	UB	1	1	1	1	1
	PP	.89	1	.94	1.01	.475
	XF	1060	144	191	19.6	1.38

Sample size	Estimator type	RE for Mean	RE for L-scale	RE for L-CV	RE for L-skew	RE for L-kurtosis
n=200	UB	1	1	1	1	1
	PP	1	.879	.953	114	.381
	XF	2400	225	759	7590	2.93
n=500	UB	1	1	1	1	1
	PP	1.07	1.21	1.09	1.41	.211
	XF	>2400	>225	2880	1521	608
n=1,000	UB	1	1	1	1	1
	PP	1.36	1.77	1.84	.894	.064
	XF	>2400	>225	>2880	>1521	>608

The p-PWM estimators of the mean, L-scale, and L-CV are more efficient than the unbiased estimators and the plotting-position estimators by the fact that the REs are often very much greater than one. However, for small sample sizes, plotting-position estimators have greater efficiency for L-skew and L-kurtosis. By $n = 50$ or so, the p-PWM estimators are more efficient for these two statistics as well. In general the p-PWM estimator appears to be more efficient than the other two estimator types. The greater efficiency for the p-PWM estimator is attributed to its incorporation of more information of the simulated variable by using the cumulative probability. Obviously, the uniform simulations reported here represent a single distribution form and parametric specification. So it is uncertain how the bias and RE of the p-PWM L-moment estimator would change in different experiments.

Nonuniform Distribution of Nonexceedance Probability

The p-PWMs are suggested for application on qualifying data sets. As a reminder, a qualifying data set has both the cumulative probabilities of the observations known and knowledge or reasonable expectation that the distribution of the cumulative

probabilities is not uniform. Simulation experiments were conducted with a nonuniform distribution of F. There is an infinite variety of nonuniform distributions that could be constructed but as a starting experiment it was decided to redraw a value for F if the initially generated was $F > 0.5$. As a result, three-quarters of the time $F \leq 0.5$ and only one quarter of the time is $F > 0.5$ in the generation of a single realization from the Kappa distribution. This provides a similar non-uniformity that might be seen in streamflow or runoff hydrographs or rainfall hyetographs in which more observations are reported early in cumulative time than later because the hydrograph is steeper and requiring greater resolution for accurate representation of shape.

The same Kappa distribution and parameters, sample sizes, and simulation count used in the simulations reported in tables 18, 19, and 20 were used with the nonuniform distribution just described. The biases for the mean, L-scale, L-CV, L-skew, and L-kurtosis are listed in table 21. From the table it is apparent that only the p-PWM estimator continues to be an unbiased estimator of all the L-moments for sufficiently large samples. The bias of the unbiased estimator—the unbiased estimator is biased under the circumstances of nonuniform probability that are considered here—and the plotting-position estimators rapidly approaches a constant for each L-moment or L-moment ratio as sample size increases. This is not particularly surprising given than a significant fraction of the parent distribution is not sampled as often as it would be under random conditions. The p-PWM estimator does have

considerably larger bias for L-kurtosis for samples sizes less than about 50. The sampling standard deviations for the nonuniform simulations are listed in table 22 and followed by the relative efficiencies in table 23.

Table 21. Comparison of sample biases for a simulated Kappa distribution using a non-uniform distribution of probability by redrawing F if initial F was greater than 0.5

[The Kappa distribution had specified L-moments of 0.114, 0.0378, -0.148, and 0.0476 for the mean, L-scale, L-skew, and L-kurtosis, respectively. These L-moments correspond to estimated Kappa parameters of 0.0669, 0.1439, 1.022, and 0.5045 for the location, scale, shape 1, and shape 2 parameters, respectively. Bias is defined as the simulated mean statistic minus the true value. UB, unbiased; PP, plotting position based probability weighted moments; XF, prior-probability weighted moments. Number of simulations per estimator was 50,000.]

Sample size	Estimator type	Mean bias	L-scale bias	L-CV bias	L-skew bias	L-kurtosis bias
n=5	UB	-0.0276	-0.0012	0.2173	0.1322	0.0669
	PP	-.0276	-.0030	.1226	.2504	.0244
	XF	-.0087	-.0070	-.0595	.0918	.2620
n=10	UB	-.0281	-.001	.1252	.1280	.0546
	PP	-.0281	-.0021	.1120	.2074	.0464
	XF	-.0036	-.0063	-.0530	.0044	.1716
n=20	UB	-.0278	-.0010	.1074	.1277	.0487
	PP	-.0277	-.0016	.1001	.1739	.0500
	XF	-.0011	-.0031	-.0257	-.0420	.0844
n=50	UB	-.0276	-.0010	.0984	.1272	.0445
	PP	-.0273	-.0012	.0943	.1452	.0434
	XF	-.0001	-.0006	-.0046	-.0219	.0025
n=100	UB	-.0285	-.001	.0997	.1286	.0411
	PP	-.0280	-.0011	.0970	.1365	.0434
	XF	.0	-.0002	-.0013	-.0034	-.0067
n=200	UB	-.0269	-.0009	.0927	.1307	.0400
	PP	-.0272	-.0010	.0927	.1314	.0423
	XF	.0	-.0001	-.0004	-.0025	-.0048
n=500	UB	-.0277	-.0010	.0946	.1274	.0415
	PP	-.0277	-.0010	.0945	.1280	.0426
	XF	.0	.0	.0	-.0003	.0
n=1,000	UB	-.0273	-.0009	.0933	.1279	.0394
	PP	-.0278	-.0009	.0966	.1295	.0386
	XF	.0	.0	.0	.0	.0

The p-PWM estimators of the mean, L-scale, and L-CV are more efficient than the unbiased estimators and the plotting-position estimators by the fact that the REs are

often very much greater than one. The p-PWM estimators are not as efficient for small sample sizes as they were for the uniform simulations reported in the previous section. The p-PWM seem to perform poorly in terms of efficiency for L-skew and L-kurtosis for sample sizes of 200 or less. The p-PWM estimator for L-skew and L-kurtosis had the least bias for sample sizes greater than about 50. It appears as though the p-PWM estimators can have trouble making reliable estimates of L-skew and likely all higher L-moment ratios for small to moderately small samples. p-PWM estimators perform well for the mean, L-scale, and L-CV for all sample sizes.

Table 22. Comparison of sample standard deviations for a simulated Kappa distribution using a non-uniform distribution of probability by redrawing F if initial F was greater than 0.5

[The Kappa distribution had specified L-moments of 0.114, 0.0378, -0.148, and 0.0476 for the mean, L-scale, L-skew, and L-kurtosis, respectively. These L-moments correspond to estimated Kappa parameters of 0.0669, 0.1439, 1.022, and 0.5045 for the location, scale, shape 1, and shape 2 parameters, respectively. The sample standard deviation (SD) is defined as the square root of the sampling variance of the estimator. UB, unbiased; PP, plotting position based probability weighted moments; XF, prior-probability weighted moments. Number of simulations per estimator was 50,000.]

Sample size	Estimator type	SD of Mean	SD of L-scale	SD of L-CV	SD of L-skew	SD of L-kurtosis
n=5	UB	0.0283	0.0121	4.5813	0.2939	0.3627
	PP	.0285	.0097	.7668	.1479	.1218
	XF	.0151	.0141	.1269	.4576	.3200
n=10	UB	.0201	.0078	.1667	.1514	.1417
	PP	.0206	.0071	.1647	.1126	.0886
	XF	.0077	.0105	.0908	.3472	.2662
n=20	UB	.0139	.0053	.1025	.0880	.0773
	PP	.0144	.0050	.1011	.0794	.0687
	XF	.0030	.0064	.0539	.2400	.1876
n=50	UB	.0090	.0031	.0611	.0519	.0398
	PP	.0089	.0032	.0607	.0471	.0487
	XF	.0005	.0014	.0113	.0933	.0763
n=100	UB	.0064	.0024	.0434	.0353	.0288
	PP	.0064	.0024	.0450	.0329	.0418
	XF	.0001	.0003	.0026	.0213	.0410
n=200	UB	.0048	.0015	.0318	.0246	.0197
	PP	.0048	.0016	.0313	.0232	.0389
	XF	<.0001	.0001	.0012	.0089	.0220

Sample size	Estimator type	SD of Mean	SD of L-scale	SD of L-CV	SD of L-skew	SD of L-kurtosis
n=500	UB	.0029	.0010	.0180	.0154	.0118
	PP	.0029	.0010	.0193	.0161	.0370
	XF	<.0001	<.0001	.0001	.0022	.0065
n=1,000	UB	.0020	.0008	.0140	.0110	.0091
	PP	.0023	.0008	.0155	.0135	.0356
	XF	<.0001	<.0001	<.0001	<.0001	<.0001

Table 23. Comparison of relative efficiencies for a simulated Kappa distribution using a non-uniform distribution of probability by redrawing F if initial F was greater than 0.5

[The Kappa distribution had specified L-moments of 0.114, 0.0378, -0.148, and 0.0476 for the mean, L-scale, L-skew, and L-kurtosis, respectively. These L-moments correspond to estimated Kappa parameters of 0.0669, 0.1439, 1.022, and 0.5045 for the location, scale, shape 1, and shape 2 parameters, respectively. Relative efficiency (RE) is defined as the variance of the unbiased estimator to the variance of the plotting position or prior-probability weighted moment estimator. UB, unbiased; PP, plotting position based probability weighted moments; XF, prior-probability weighted moments. Number of simulations per estimator was 50,000.]

Sample size	Estimator type	RE of Mean	RE of L-scale	RE of L-CV	RE of L-skew	RE of L-kurtosis
n=5	UB	1	1	1	1	1
	PP	.986	1.56	3570	3.95	8.87
	XF	3.51	.736	1300	.413	1.28
n=10	UB	1	1	1	1	1
	PP	.952	1.21	1.02	1.81	2.56
	XF	6.81	.552	3.37	.190	.283
n=20	UB	1	1	1	1	1
	PP	.932	1.12	1.03	1.23	1.27
	XF	21.5	.686	3.62	.134	.170
n=50	UB	1	1	1	1	1
	PP	1.02	.938	1.01	1.21	.668
	XF	3.24	4.90	29.2	.309	.272
n=100	UB	1	1	1	1	1
	PP	1	1	.930	1.15	.475
	XF	4100	64	279	2.75	.493
n=200	UB	1	1	1	1	1
	PP	1	.879	1.03	1.12	.256
	XF	>4100	225	702	7.64	.802
n=500	UB	1	1	1	1	1
	PP	1	1	.870	.915	.102
	XF	>4100	>225	32400	49	330
n=1,000	UB	1	1	1	1	1
	PP	.756	1	.816	.664	.0653
	XF	>4100	>225	>32400	>49	>330

Supplemental simulations showing the bias using a variety of non-uniform distribution of F constructions are provided in Appendix C. Similar conclusions concerning p-PWMs can be made from the tables in Appendix C.

Chapter Conclusions

Intuitive argument, example computations, and limited simulation experiments strongly indicate that prior-Probability Weighted Moments (p-PWMs) and a proposed estimator (eq. 46) are attractive for L-moment estimation on previously incompatible data sets. These data sets have two properties that make traditional L-moment computation unsuitable. The first property is that the cumulative probability of each observation of the distribution is known (estimated), and the second property is that there exists prior knowledge or reasonable expectation that the distribution of the probabilities is not uniformly distributed or equally likely. In the uniform simulations, the p-PWMs estimators might have substantial bias and sampling variance in very small samples $n < 10$, but as sample size increases, the p-PWMs rapidly become unbiased and exhibit minimal sampling variance. For nonuniform simulation, the p-PWMs outperform in terms of bias and outperform in terms of efficiency both of unbiased and plotting-position L-moment estimators. For small samples under nonuniform simulation, the p-PWM can exhibit particularly large sampling variance, but the variance drops and the efficiency rapidly increases with sample size. Caution with p-PWM estimators in small samples is advised.

Two obvious candidate data sets for p-PWM application are rainfall hyetographs and streamflow hydrographs, and examples of each were provided in the chapter. The rainfall hyetograph or streamflow hydrograph data can possess cumulative percent time passed and the cumulative runoff; cumulative percent time is naturally considered as a probability. Finally, a particularly intriguing application would be p-PWM based L-moment estimation of distributions shown in historical reports in which portions, such as the middle third, of the distribution is missing because of media degradation or reproduction induced fading. The p-PWMs thus can be applied to data sets containing missing portions of the distribution. Some types of missing data can be thought of as censored data. Comparison (if one could be made) of the p-PWMs to Partial-PWMs, which are used for censored data applications (Wang, 1996a), is beyond the scope of this dissertation.

For the remainder of this dissertation, the p-PWMs will be used without notification for L-moment computation of rainfall hyetographs; chapter 3 is included. Unbiased L-moment estimators will be used in all other circumstances.

CHAPTER 5
L-MOMENTS OF DIMENSIONLESS RAINFALL HYETOGRAPHS KNOWN TO PRODUCE RUNOFF IN TEXAS

Introduction

Using a variety of perspectives this chapter documents research into L-moments of runoff-producing dimensionless rainfall hyetographs in Texas. The L-moments include the mean, L-scale, L-skew, and L-kurtosis, and τ_5 statistics; the nonparametric median also is included. If the L-moments of the hyetograph distribution are predictable using information such as the total depth of the storm, the time of year that the storm occurred, and geographic location, then progress towards reliable estimation of the hyetograph is achieved. Three principle research components in this chapter are:

1. An investigation of potential dependency or graphical correlations between storm depth and the mean, median, L-scale, L-skew, and L-kurtosis, and τ_5 of dimensionless hyetographs. The double one-percent hyetograph tail trimming preprocessing method is investigated as well as a no-tail-trimming method.

2. An investigation of the influence of month or season of storm occurrence on the hyetograph mean, median, L-scale, and L-CV statistics. The investigation focuses on the monthly mean values of these four statistics.

3. An investigation of the relation L-scale to the mean and median of dimensionless hyetographs for each of the five hyetograph data base modules (`austin`, `dallas`, `fortworth`, and `sanantonio` and the `smallruralsheds` modules). Both hyetograph tail trimming methods are considered. Because the

urban hyetograph data bases are spatially limited and geographically distinct, the comparison also considers the influence of geographic location on the dimensionless hyetograph. A subcomponent is a modal analysis of the mean, median, and L-scale statistics; the objective of the modal analysis is to estimate the most likely value for each statistic.

The sample L-moment statistics presented here are computed by prior-Probability Weighted Moments, which are described in the previous chapter. The median of the hyetograph is computed by linear interpolation between the samples bracketing the mean. The mean summary statistics of the hyetograph L-moments computed by p-PWMs or the median are not computed using p-PWMs but by the common arithmetic average.

Relations between Storm Depth and Hyetograph Statistics

For the storm depth dependency or correlation investigation (component no. 1), if the L-moments and the nonparametric median are independent of—that is not a substantial function of—the storm magnitude as measured by depth, the logical conclusion is that the shape of L-moment-fitted expected hyetographs are independent of the frequency level (nonexceedance probability) or recurrence interval of the storm. The frequency independence would greatly simplify the use of expected hyetographs for design applications because a separate hyetograph for each level of risk (nonexceedance probability) is not needed. A conclusion drawn within the earlier triangular model chapter (chapter 3) for a given duration is that a substantial relation

does not exist between the mean and the storm depth; therefore, a frequency independence assumption is possible.

The dependency investigation centers on the same three durations originally considered in the triangular hyetograph model chapter. Specifically, the 0–12 hr, 12–24 hr, and 24 hr and greater (up to about 3 days) storm durations are considered. Separate, but parallel, analysis for each duration is provided in three sections. Within each analysis, box plots (Helsel and Hirsch, 1992, pp. 24–26) of the distributions for a given statistic (such as L-skew) for each storm depth category (1 in. through 10 in. by 1 in. (25.4 mm) increments) are drawn. These same categories were used in the triangular hyetograph chapter. From graphs of the box plots it is possible to make visual inferences about whether one or more aspects of the distribution of the statistic are dependent on storm depth.

Detailed explanations of the box plots shown on figures 26–46 (introduced shortly) are shown on figure 25. Multiple explanations are necessary for the figures because rendering of box plots for small sample sizes is not feasible. If the sample size is greater than four, then a traditional box plot showing the mean, median, quartiles, and range of the data is drawn. If the sample size is equal to three, then the mean, median, and the upper and lower data values are drawn; the remaining data point corresponds to the median so it is not plotted. If the sample size is equal to two, then the mean and the two data points are drawn; the median corresponds to the mean in this case. If the sample size is equal to one, then the mean is drawn; the median and the

single data point each correspond to the mean. If no data were available for a depth category, then “no data” is indicated in the figures.

A few general comments about the interpretation of box plots in this section are required before their introduction. Regarding the stems that indicate the data range by extending to the maximum and minimum values of the data from the upper and lower quartiles, respectively, it is natural for the range of identically distributed data to increase with increasing sample size. Regarding the quartiles, the quartiles were computed according to USGS policy regarding box plot construction (Dennis Helsel, written commun., 1989). This policy advocates linear interpolation between data points bracketing the quartiles; each quartile estimate is prorated. Regarding distribution skewness, if the median plots above the mean, the distribution is said to be negatively skewed; whereas, if the median plots below the mean, the distribution is said to be positively skewed. Helsel and Hirsch (1992, p. 9–10, fig. 1.1) provide an excellent description of distribution skewness.

A final introductory note concerning figures 26, 27, 33, 34, 40, and 41 is that the loadedness of the storm is annotated on the ordinate (vertical) axis to assist readers in visualization the influence of the mean or median statistic on the general shape of the hyetograph. A storm with a large mean or median is front-loaded, and a storm with a small mean or median is back-loaded. This concept is illustrated on figures 9 and 54.

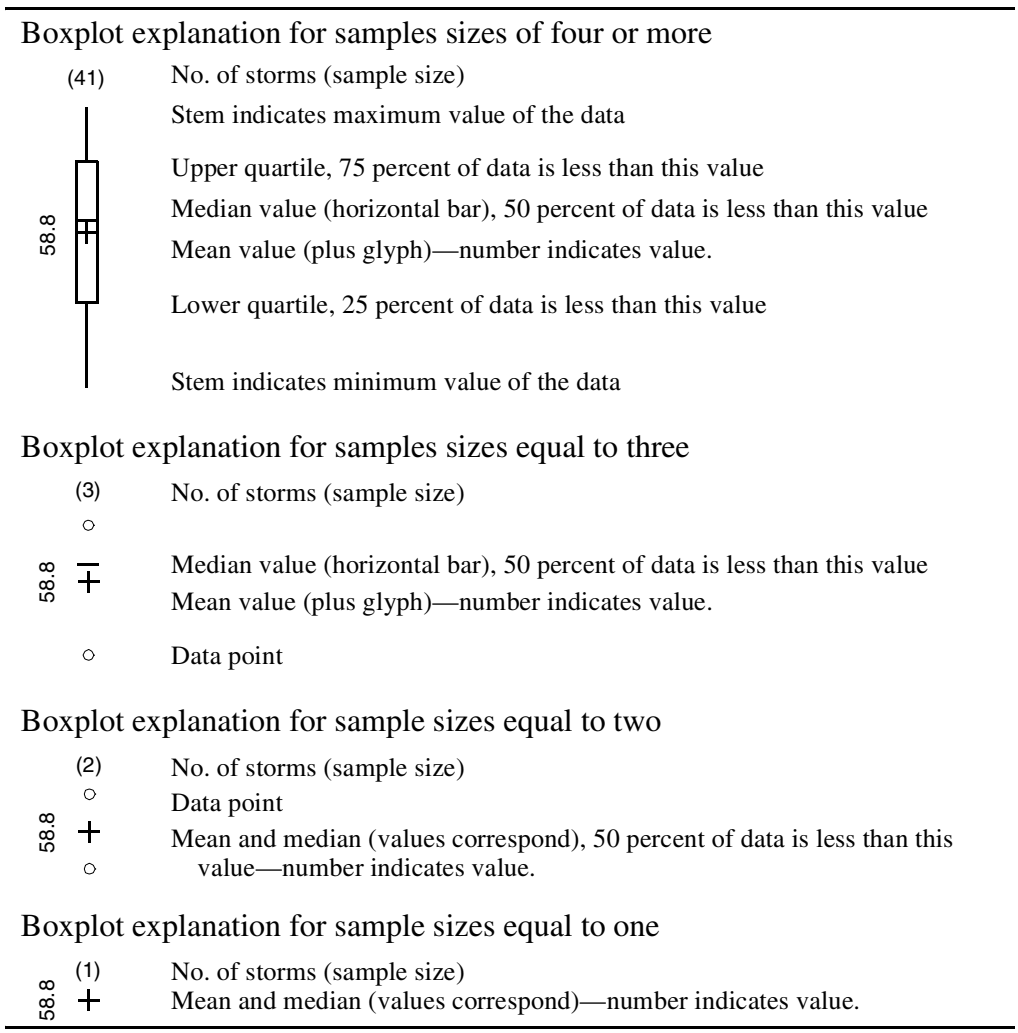

Figure 25. Explanation of box plots and ancillary glyphs shown on figures 26–46

Storm Durations of 0 to 12 Hours

A graph of box plots summarizing the distribution of the mean statistics of the 0–12 hr hyetographs for each depth category is shown on figure 26. The overall mean (plus glyph) of each category and sample size values match the averages and sample sizes listed in columns 3 and 5 of table 11. Neither the category means or medians show substantial dependency on the storm depth. A similar observation using the same

data was made in the triangular hyetograph chapter. Furthermore, the inter-quartile range and the quartile values themselves also do not appear dependent on the storm depth. The 0–12 hr hyetograph mean and its distribution are not substantially dependent on storm depth.

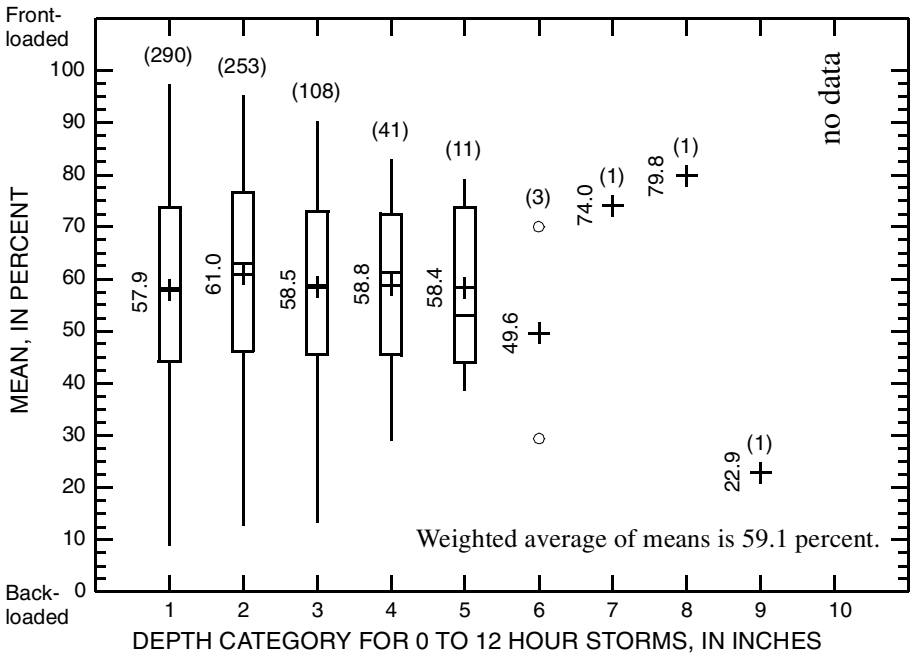

Figure 26. Box plots showing distribution of hyetograph mean for 0–12 hr storm durations for integer storm depth categories

A graph of box plots summarizing the distribution of the median statistics of the 0–12 hr hyetographs for each depth category is shown on figure 27. The sample sizes match those on figure 26. Neither the category means or medians show substantial dependency on the storm depth. Furthermore, the inter-quartile range and the quartile values themselves also do not appear dependent on the storm depth. The 0–12 hr hyetograph median and its distribution are not substantially dependent on storm depth.

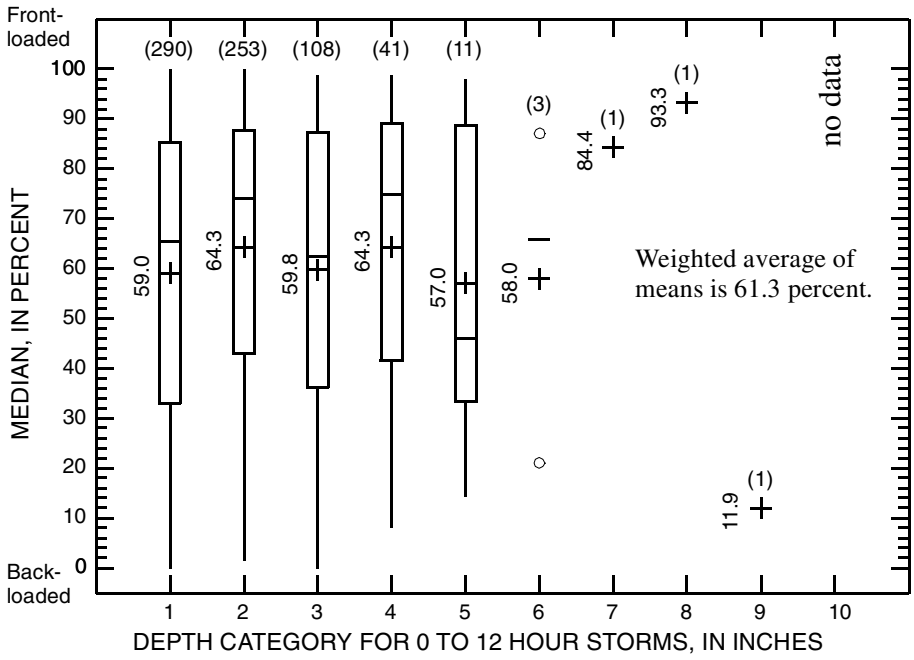

Figure 27. Box plots showing distribution of hyetograph median for 0–12 hr storm durations for integer storm depth categories

A graph of box plots summarizing the distribution of the L-scale statistics of the 0–12 hr hyetographs for each depth category is shown on figure 28. The sample sizes match those on figures 26 and 27. The sample size values are slightly different for the 1 in. and 2 in. categories owing to four poorly digitized hyetographs from which no L-scale could be determined—a hyetograph defined by a single data point. Neither the category means or medians show substantial dependency on the storm depth. Furthermore, the inter-quartile range and the quartile values themselves also do not appear dependent on the storm depth. The maximum values of L-scale for the 1 in. and 3 in. depth categories are dissimilar from the maximum values for the other categories;

this is attributed to just three spurious events (two for the 1 in. category). The 0–12 hr hyetograph L-scale and its distribution are not substantially dependent on storm depth.

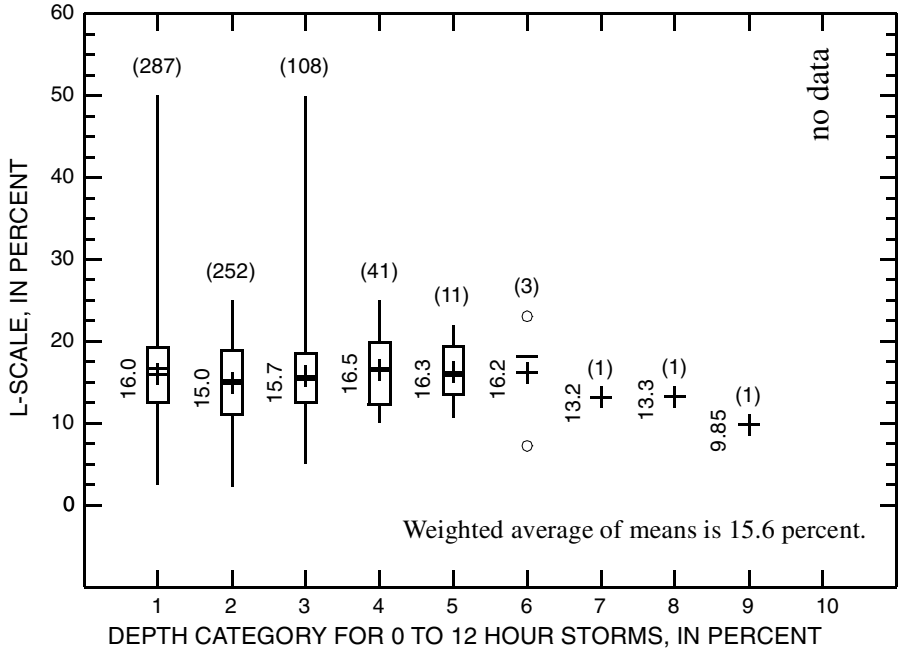

Figure 28. Box plots showing distribution of hyetograph L-scale for 0–12 hr storm durations for integer storm depth categories

A graph of box plots summarizing the distribution of the coefficient of L-variation (L-CV) statistics of the 0–12 hr hyetographs for each depth category is shown on figure 29. The sample sizes for the 1 in. and 2 in. depth categories are different than those seen on figures 26 and 27; this is attributable to four spurious events with zero values L-scale. Neither the category means or medians show substantial dependency on the storm depth. This necessarily is consistent with the discussion of figures 26 and 28 because L-CV is a ratio of the L-scale to the mean (λ_2/λ_1).

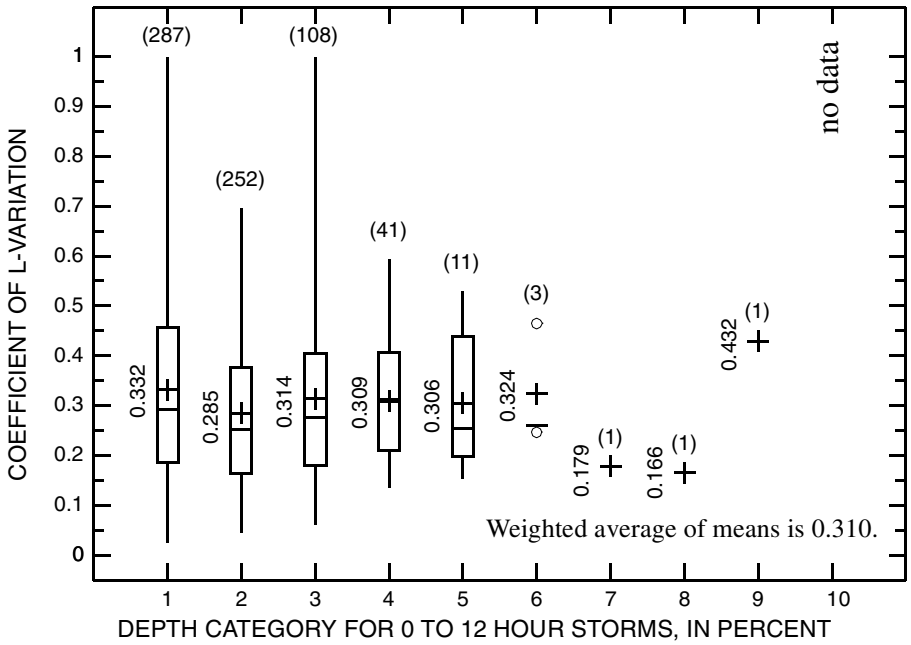

Figure 29. Box plots showing distribution of hyetograph coefficient of L-variation for 0–12 hr storm durations for integer storm depth categories

A graph of box plots summarizing the distribution of the L-skew statistics of the 0–12 hr hyetographs for each depth category is shown on figure 30. The sample sizes are slightly different than those seen on figures 26 and 27 because theoretically impossible values occurred; this is due to poor sampling of the hyetograph ordinates (see chapter on p-PWMs and comments concerning p-PWM sample L-moment estimators producing theoretically impossible values). Both the category means or medians seem to decrease with increasing storm depth. The quartile values also seem to decrease with increasing storm depth. However, the inter-quartile range appears independent of storm depth. The maximum value of L-skew for the 1 in. and 2 in. depth category are dissimilar from the maximum values for the other categories. This is attributed to the substantially larger sample size for these depth categories and a few

spurious events. The L-skew of the 0–12 hr hyetograph is substantially dependent on storm depth. Hence the skewness of the hyetograph is influenced by the storm depth. The hyetograph becomes slightly negatively skewed with large storm depths.

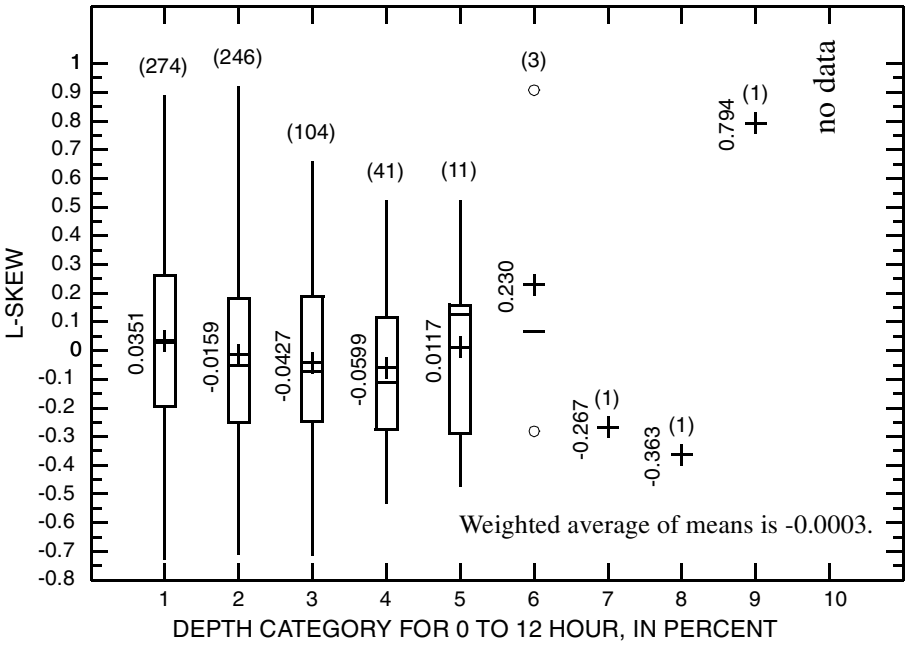

Figure 30. Box plots showing distribution of hyetograph L-skew for 0–12 hr storm durations for integer storm depth categories

A graph of box plots summarizing the distribution of the L-kurtosis statistics of the 0–12 hr hyetographs for each depth category is shown on figure 31. The sample sizes compared to L-skew (figure 30) are decreased further because even more theoretically impossible values occurred; again this is due to poor sampling of the hyetograph ordinates. Both the category means or medians seem to decrease with increasing storm depth. The quartile values also seem to decrease with increasing storm depth. However, the inter-quartile range appears independent of storm depth. The maximum

value of L-kurtosis for the 1 in. and 2 in. depth categories are dissimilar from the maximum values for the other categories. This is attributed to the substantially larger sample sizes for these depth categories and a few spurious events. The L-kurtosis of the 0–12 hr hyetograph is substantially dependent on storm depth. Hence the kurtosis of the hyetograph is influenced by the storm depth. The hyetograph becomes less kurtotic with large storm depths.

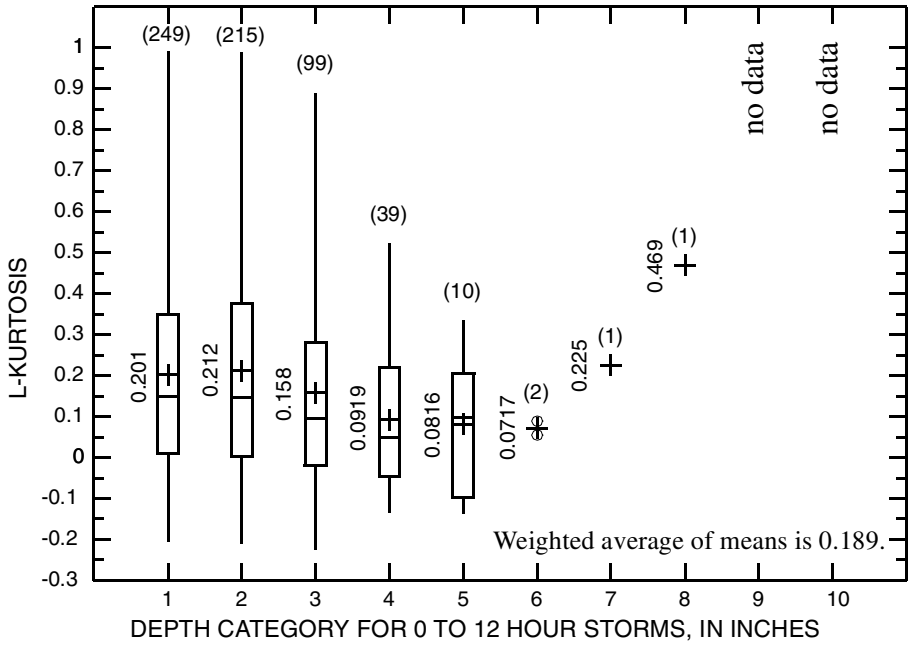

Figure 31. Box plots showing distribution of hyetograph L-kurtosis for 0–12 hr storm durations for integer storm depth categories

A graph of box plots summarizing the distribution of the τ_5 L-moment statistics of the 0–12 hr hyetographs for each depth category is shown on figure 32. The sample sizes compared to L-kurtosis (figure 31) are decreased further because even more theoretically impossible values occurred; again this is due to poor sampling of the

hyetograph ordinates. Both the category means or medians seem to decrease with increasing storm depth. The quartile values also seem to decrease with increasing storm depth. However, the inter-quartile range appears independent of storm depth. The maximum value of τ_5 for the 1 in. through 3 in. depth categories are dissimilar from the maximum values for the other categories. This is attributed to the substantially larger sample size for these depth categories and a few spurious events. The τ_5 of the 0–12 hr hyetograph is substantially dependent on storm depth. Hence the τ_5 of the hyetograph is influenced by the storm depth. Whether the influence is substantial is difficult to assess.

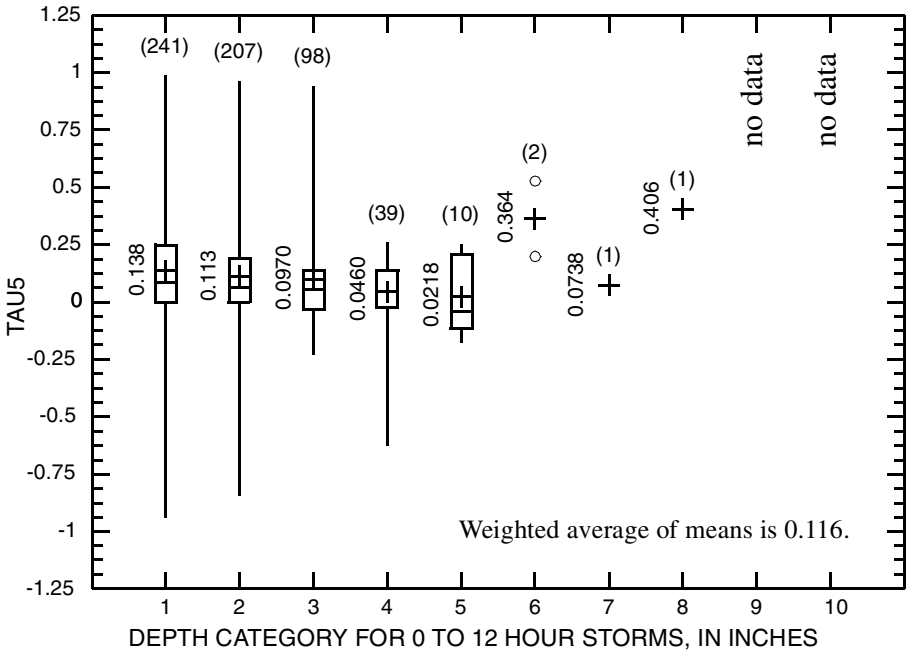

Figure 32. Box plots showing distribution of hyetograph Tau5 for 0–12 hr storm durations for integer storm depth categories

Storm Durations of 12 to 24 Hours

A graph of box plots summarizing the distribution of the mean statistics of the 12–24 hr hyetographs for each depth category is shown on figure 33. The overall mean (plus glyph) of each category and sample size values match the averages and sample sizes listed in columns 6 and 8 of table 11. A slight increase in both the category mean and median with increasing storm depth is seen, but the increase is considered unsubstantial. A similar observation was made (using the same data) in the triangular hyetograph chapter. The inter-quartile range seems to contract with increasing storm depth. The contraction is due to the increasing lower quartile; the upper quartile remains essentially constant. The 12–24 hr hyetograph mean and its distribution are not substantially dependent on storm depth.

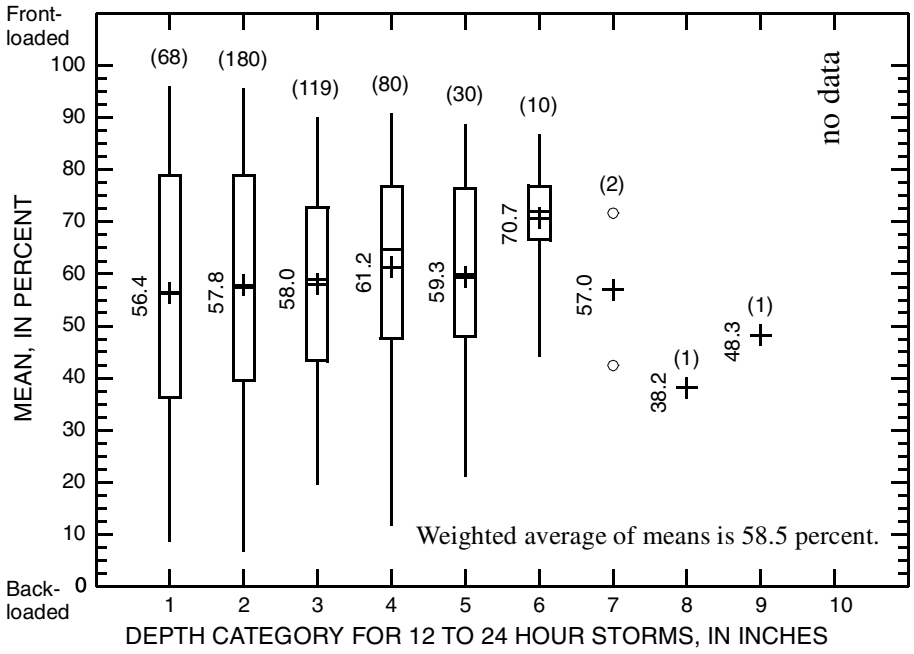

Figure 33. Box plots showing distribution of hyetograph mean for 12–24 hr storm durations for integer storm depth categories

A graph of box plots summarizing the distribution of the median statistics of the 12–24 hr hyetographs for each depth category is shown on figure 34. The sample sizes match those on figure 33. An increase in both the category mean and median with increasing storm depth is seen, but the increase could be considered unsubstantial. The inter-quartile range seems to contract abruptly between the 1 in. and 2 in. depth categories; this might be attributable to sample size or other factors. The 12–24 hr hyetograph median and its distribution are not substantially dependent on storm depth.

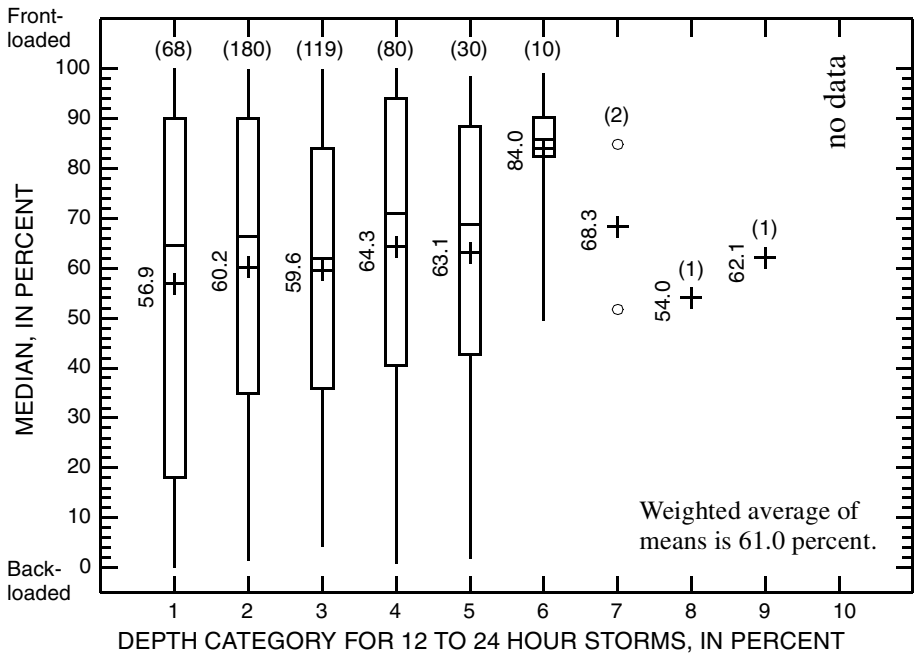

Figure 34. Box plots showing distribution of hyetograph median for 12–24 hr storm durations for integer storm depth categories

A graph of box plots summarizing the distribution of the L-scale statistics of the 12–24 hr hyetographs for each depth category is shown on figure 35. The sample sizes match those on figures 33 and 34. Neither the category means or medians show

substantial dependency on the storm depth. Furthermore, the inter-quartile range and the quartile values themselves also do not appear dependent on the storm depth. The 12–24 hr hyetograph L-scale and its distribution are not substantially dependent on storm depth.

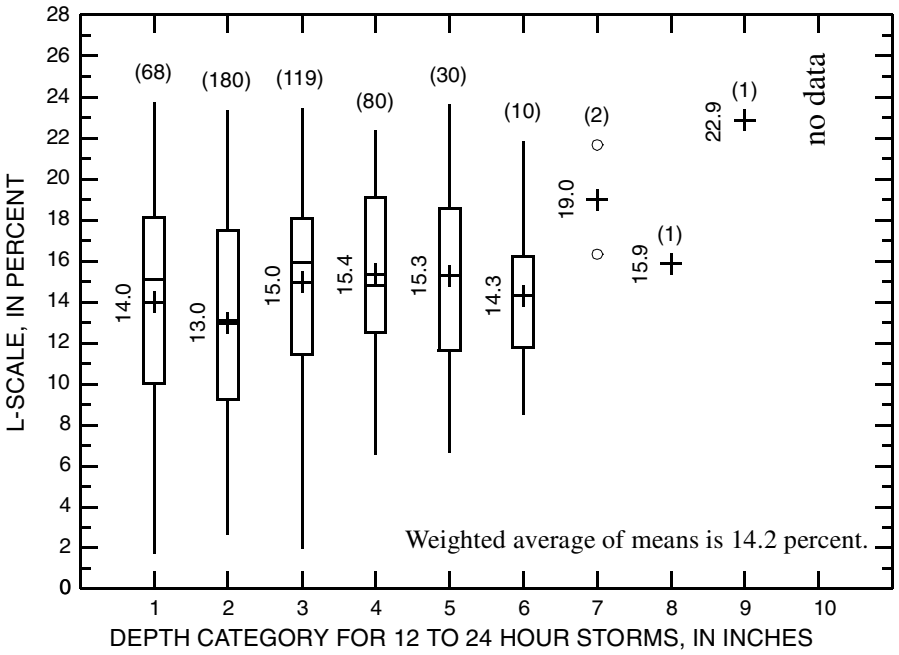

Figure 35. Box plots showing distribution of hyetograph L-scale for 12–24 hr storm durations for integer storm depth categories

A graph of box plots summarizing the distribution of the coefficient of L-variation (L-CV) statistics of the 12–24 hr hyetographs for each depth category is shown on figure 36. Neither the category means or medians show substantial dependency on the storm depth. This necessarily is consistent with the discussion of figures 33–35 because L-CV is a ratio of the L-scale to the mean (λ_2/λ_1).

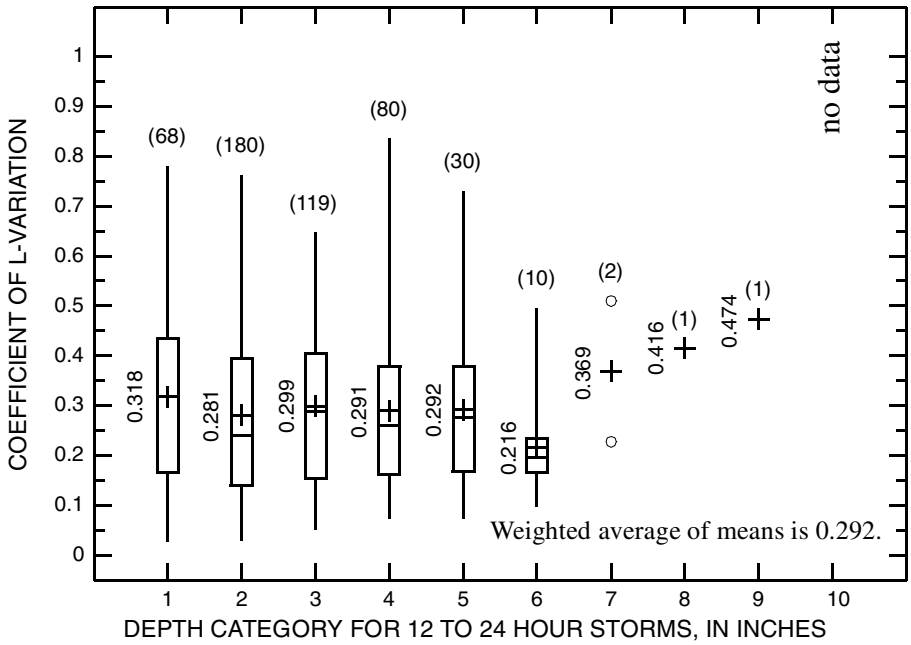

Figure 36. Box plots showing distribution of hyetograph coefficient of L-variation for 12–24 hr storm durations for integer storm depth categories

A graph of box plots summarizing the distribution of the L-skew statistics of the 12–24 hr hyetographs for each depth category is shown on figure 37. The sample sizes are different than those seen on figures 33–36 because theoretically impossible values occurred. Both the category means or medians seem to decrease with increasing storm depth—using the large sampled 1 in. through 4 in. categories. Visual inferences on the inter-quartile range and quartile values themselves is difficult. The L-skew of the 12–24 hr hyetograph is weakly dependent on storm depth. Hence the skewness of the hyetograph is influenced by the storm depth. The hyetograph becomes slightly negatively skewed with large storm depths.

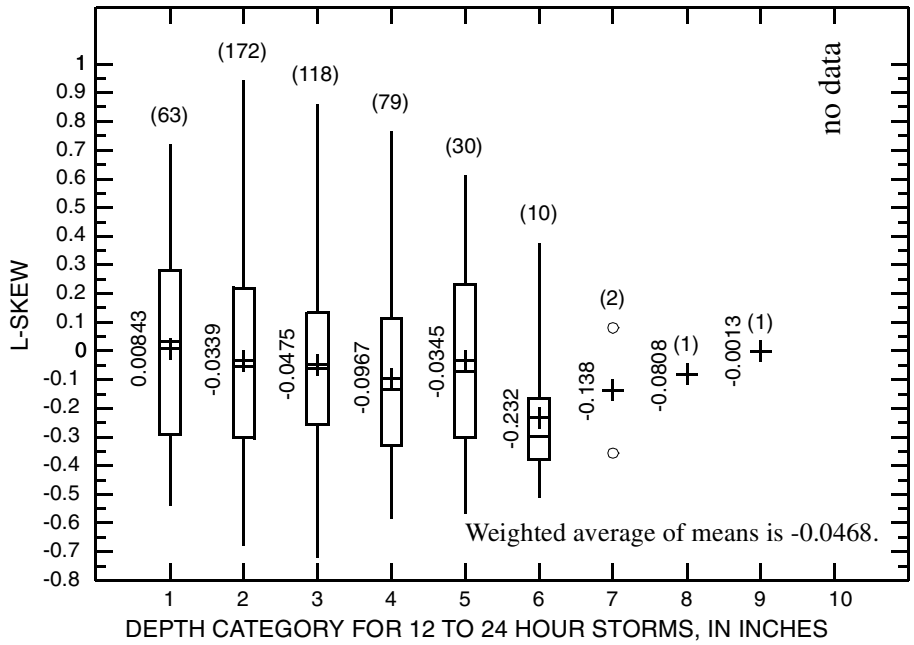

Figure 37. Box plots showing distribution of hyetograph L-skew for 12–24 hr storm durations for integer storm depth categories

A graph of box plots summarizing the distribution of the L-kurtosis statistics of the 12–24 hr hyetographs for each depth category is shown on figure 38. The sample sizes compared to L-skew (figure 37) are further decreased from those seen on figures 33–36 because theoretically impossible values occurred; again this is due to poor sampling of the hyetograph ordinates. Both the category means or medians show decrease with increasing storm depth for the 2 in. and greater categories. Furthermore, the inter-quartile range and the quartile values themselves also appear slightly dependent on the storm depth. The L-kurtosis of the 12–24 hr hyetograph is substantially dependent on storm depth. Storms become less kurtotic with increasing storm depth, but the L-kurtosis remains positive (greater than zero).

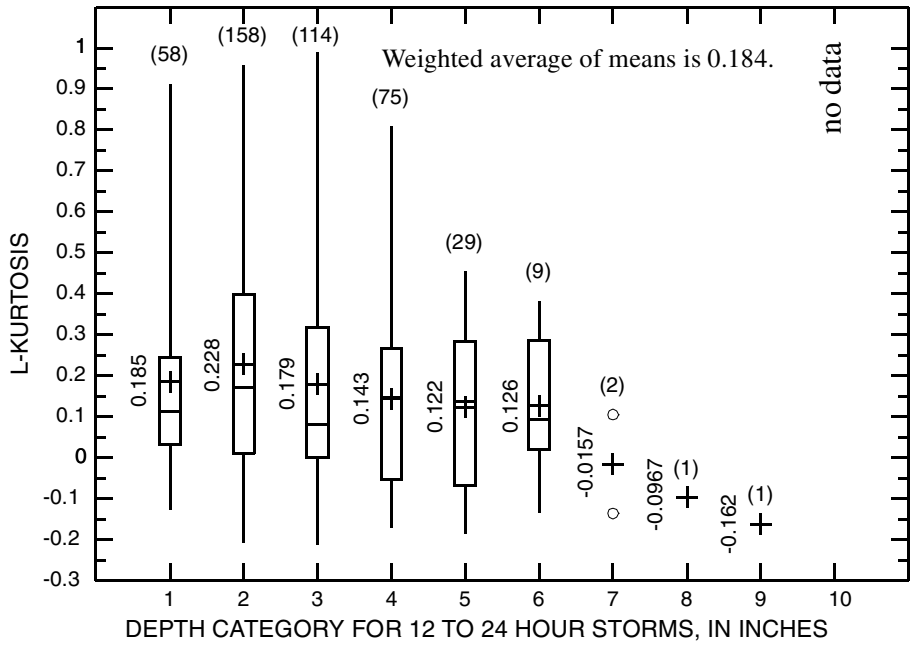

Figure 38. Box plots showing distribution of hyetograph L-kurtosis for 12–24 hr storm durations for integer storm depth categories

A graph of box plots summarizing the distribution of the τ_5 statistics of the 12–24 hr hyetographs for each depth category is shown on figure 39. The sample sizes are further decreased, compared to L-kurtosis (figure 38), from those seen on figures 32–35 because theoretically impossible values occurred; again this is due to poor sampling of the hyetograph ordinates. Neither the category means or medians show substantial dependency on the storm depth. Furthermore, the inter-quartile range and the quartile values themselves also do not appear dependent on the storm depth. The τ_5 of the 12–24 hr hyetograph is not substantially dependent on storm depth.

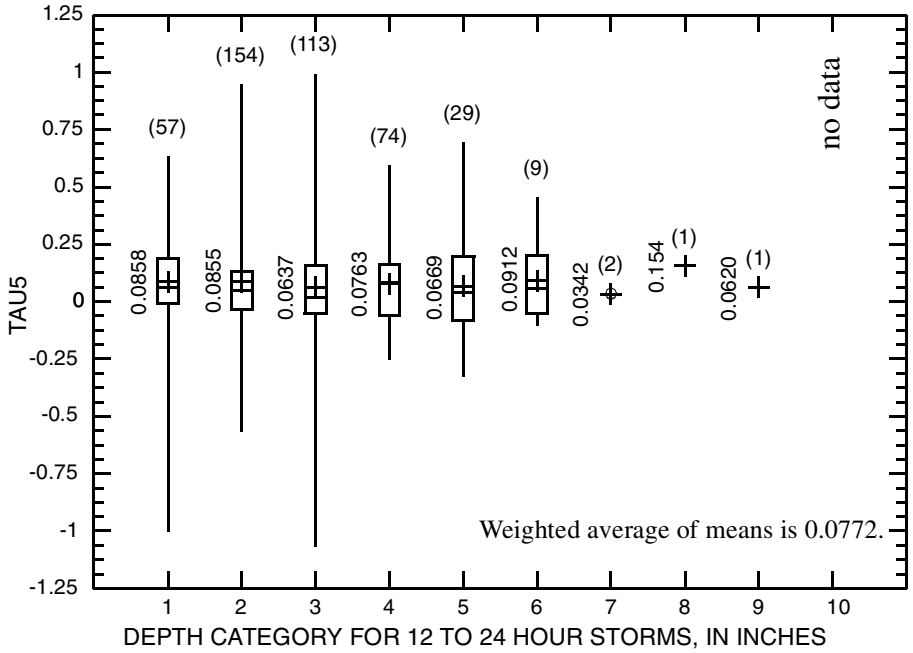

Figure 39. Box plots showing distribution of hyetograph Tau5 for 12–24 hr storm durations for integer storm depth categories

Storm Durations of 24 Hours and Greater

A graph of box plots summarizing the distribution of the mean statistics of the 24 hr and greater hyetographs for each depth category is shown on figure 40. The overall mean (plus glyph) of each category and sample size values match the averages and sample sizes listed in columns 3 and 5 of table 12. Both the category means or medians show a decrease with increasing storm depth; a decrease of about 10 percentage points. A similar observation is made (using the same data) in the triangular hyetograph chapter. The inter-quartile range does not appreciably change with storm depth, but the quartile values themselves appear to be weakly dependent on the storm depth by decreasing with increasing storm depth. The 24 hr and greater hyetograph mean and its distribution are dependent on storm depth.

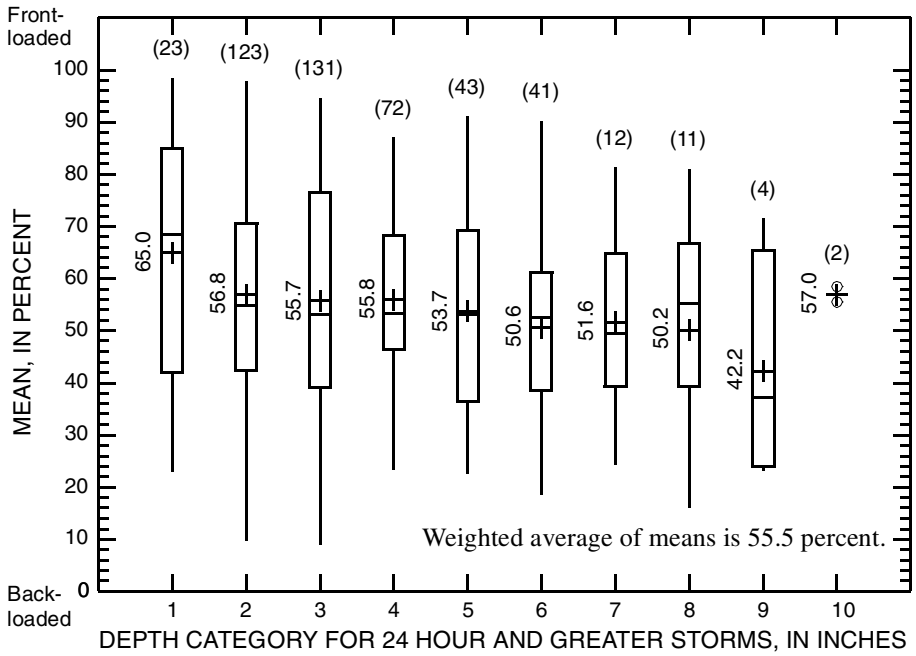

Figure 40. Box plots showing distribution of hyetograph mean for 24 hr and greater storm durations for integer storm depth categories

A graph of box plots summarizing the distribution of the median statistics of the 24 hr and greater hyetographs for each depth category is shown on figure 41. The sample sizes match those on figure 40. A substantial decrease (about 25 percentage points) in both the category mean and median with increasing storm depth is seen. The inter-quartile range is large and appears to increase slightly with increasing storm depth. The quartile change accordingly. The decrease in the median and mean (figure 39) might be attributable to a tendency for the larger depth storms to simply last longer—that is to have longer periods of substantial rainfall—than the smaller depth storms. Thus distribution location measures such as the median or mean would be smaller. The 24 hr and greater hyetograph median is substantially dependent on storm depth.

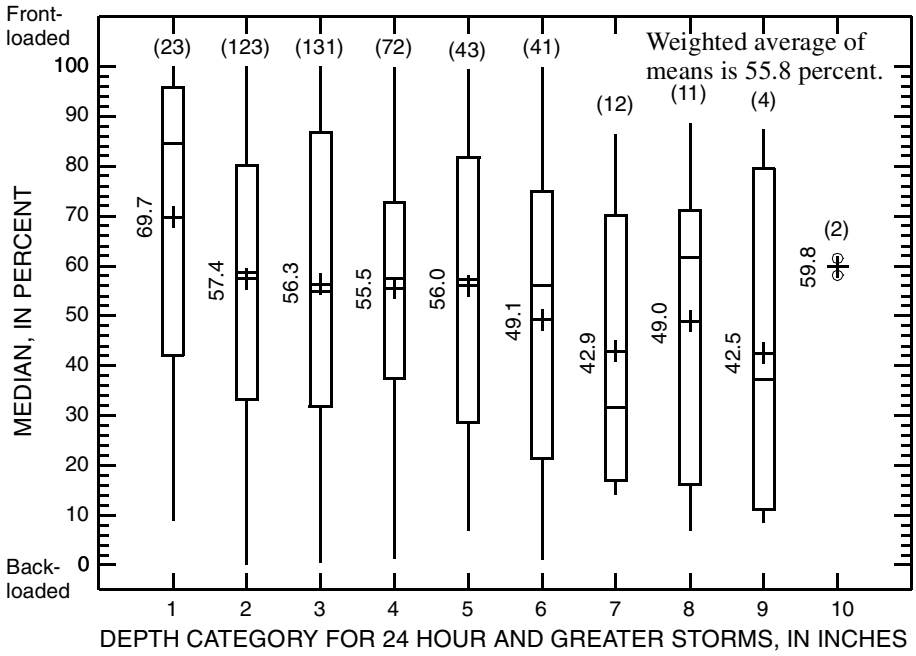

Figure 41. Box plots showing distribution of hyetograph median for 24 hr and greater storm durations for integer storm depth categories

A graph of box plots summarizing the distribution of the L-scale statistics of the 24 hr and greater hyetographs for each depth category is shown on figure 42. The sample sizes match those on figures 40 and 41. Both the category means or medians show a slight increase with increasing storm depth. Furthermore, the inter-quartile range and the quartile values themselves also do not appear dependent on the storm depth. The maximum value of L-scale for the 2 in. depth category is dissimilar from the maximum values for the other categories; this is attributed to just one spurious event. The 24 hr and greater hyetograph L-scale and its distribution is substantially dependent on storm depth.

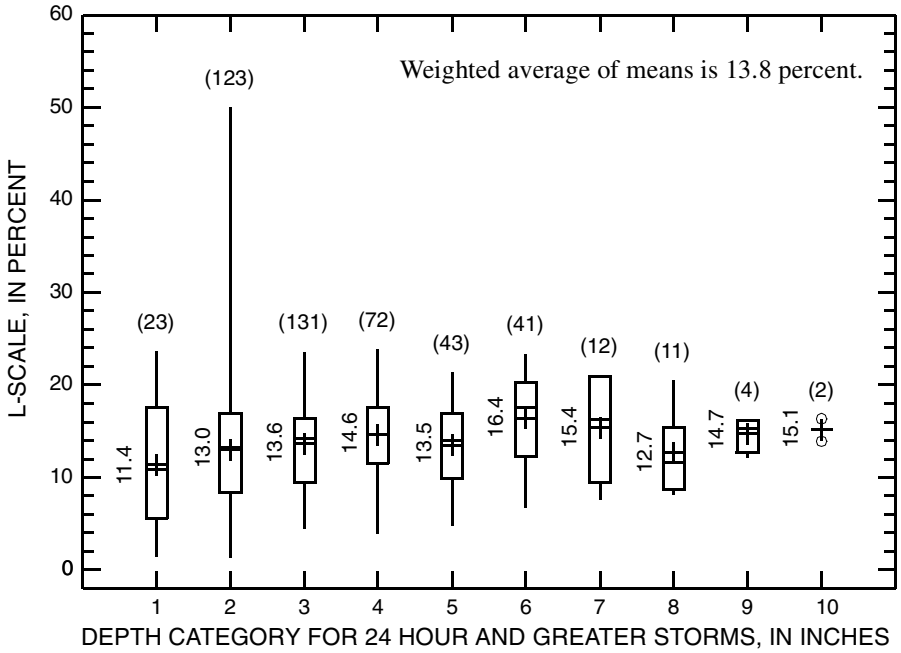

Figure 42. Box plots showing distribution of hyetograph L-scale for 24 hr and greater storm durations for integer storm depth categories

A graph of box plots summarizing the distribution of the coefficient of L-variation (L-CV) statistics of the 24 hr and hyetographs for each depth category is shown on figure 43. Both the category means or medians show substantial dependency on the storm depth. This necessarily is consistent with the discussion of figures 40–42 because L-CV is a ratio of the L-scale to the mean. As the mean decreases (figure 40), the L-CV must increase.

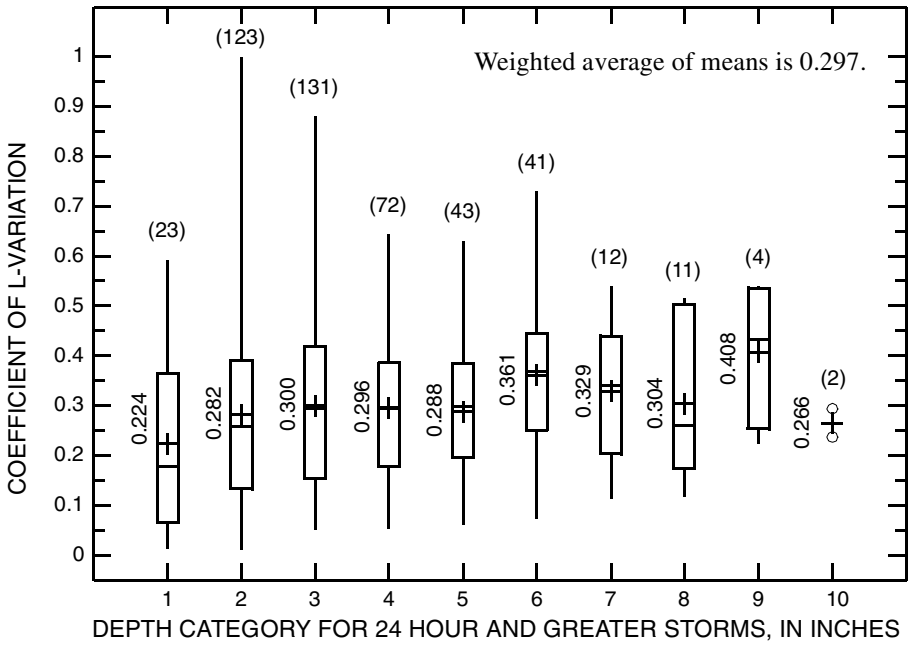

Figure 43. Box plots showing distribution of hyetograph coefficient of L-variation for 24 hr and greater storm durations for integer storm depth categories

A graph of box plots summarizing the distribution of the L-skew statistics of the 24 hr and greater hyetographs for each depth category is shown on figure 44. The sample sizes are different than those seen on figures 40–43 because theoretically impossible values occurred; this is due to poor sampling of the hyetograph ordinates. Both the category means or medians increase with increasing storm depth. This is opposite of the observation made on the 12–24 hr duration L-skew on figure 37. Visual inferences on the inter-quartile range and quartile values themselves is difficult. The L-skew of the 24 hr and greater hyetograph is substantially dependent on storm depth. Hence the skewness of the hyetograph is influenced by the storm depth. The hyetograph becomes slightly positively skewed with large storm depths.

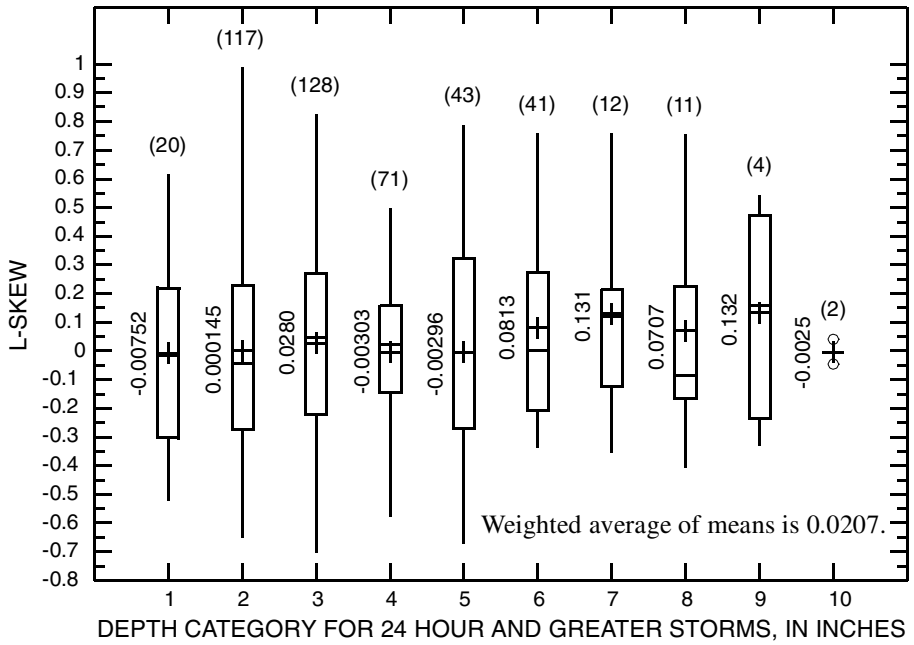

Figure 44. Box plots showing distribution of hyetograph L-skew for 24 hr and greater storm durations for integer storm depth categories

A graph of box plots summarizing the distribution of the L-kurtosis statistics of the 24 hr and greater hyetographs for each depth category is shown on figure 45. The sample sizes compared to L-skew (figure 43) are further decreased from those seen on figures 40–42 because theoretically impossible values occurred; again this is due to poor sampling of the hyetograph ordinates. Neither the category means or medians show substantial dependency on the storm depth. Furthermore, the inter-quartile range and the quartile values themselves also do not appear dependent on the storm depth. The possible contraction of the inter-quartile range for the depth categories 4–6 in. is curious; a possible reason for the contraction are unknown. The L-kurtosis of the 24 hr and greater hyetograph is independent of storm depth.

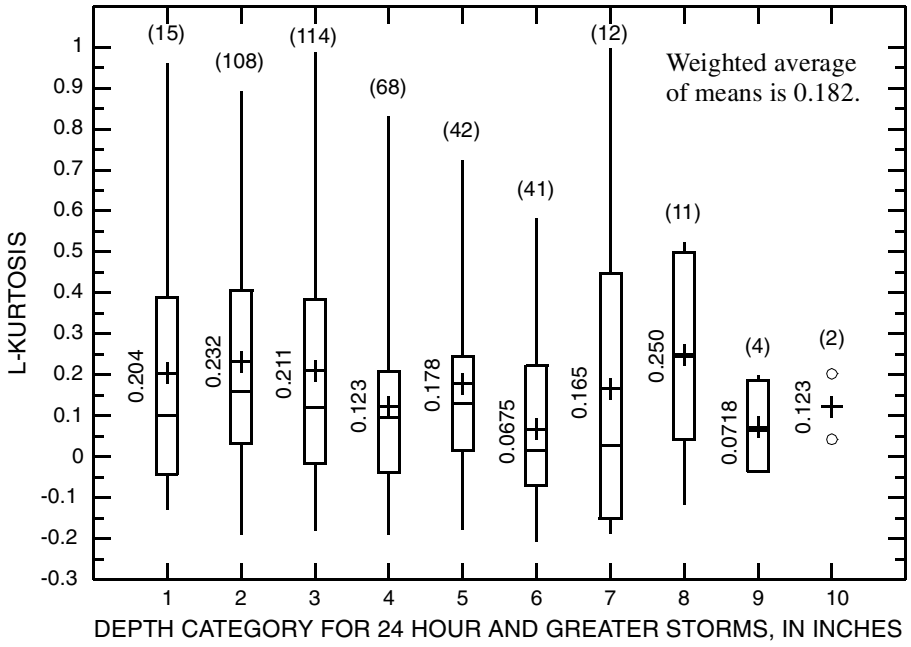

Figure 45. Box plots showing distribution of hyetograph L-kurtosis for 24 hr and greater storm durations for integer storm depth categories

A graph of box plots summarizing the distribution of the τ_5 statistics of the 24 hr and greater hyetographs for each depth category is shown on figure 46. The sample sizes are further decreased, compared to L-kurtosis (figure 45), from those seen on figures 40–42 because theoretically impossible values occurred; again this is due to poor sampling of the hyetograph ordinates. Neither the category means or medians show substantial dependency on the storm depth. Furthermore, the inter-quartile range and the quartile values themselves also do not appear dependent on the storm depth. The τ_5 of the 24 hr and greater hyetograph is not substantially dependent on storm depth.

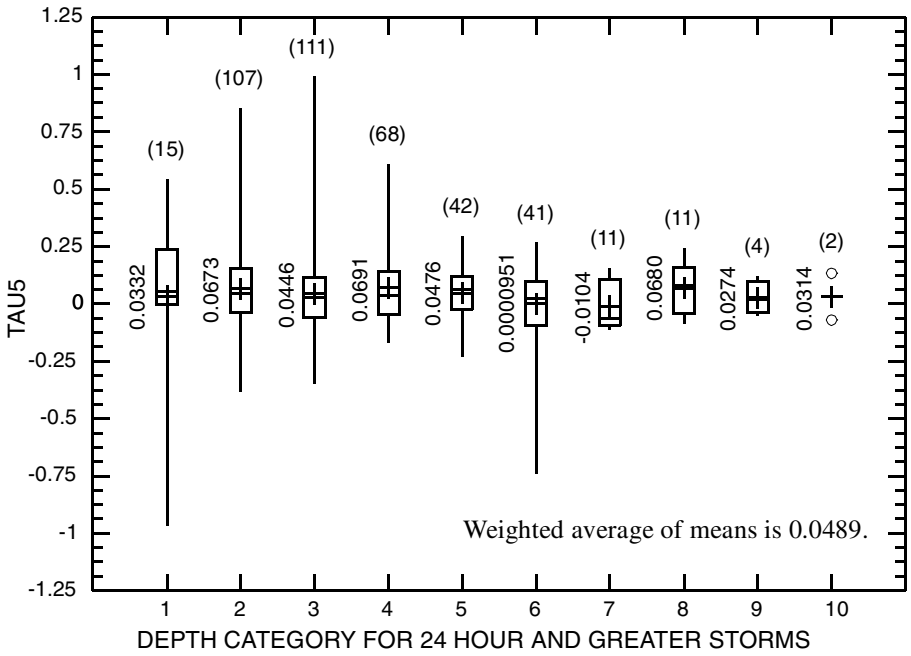

Figure 46. Box plots showing distribution of hyetograph Tau5 for 24 hr and greater storm durations for integer storm depth categories

Section Conclusions

A summary of the dependency observations made for figures 26–46 is shown in table 24. The mean, median, and L-scale statistics and influences on their values are most critical for defining the expected hyetograph because the lowest order moments contain the greatest degree of information about the hyetograph distribution. In a loose interpretation, it appears for the 0–12 hr and 12–24 hr duration that only the high L-moments (L-skew, L-kurtosis, and τ_5) are substantially dependent on the storm depth. For the 24 hr and greater storm duration, the lower order statistics (mean, median, L-scale, L-CV, L-skew) appear influenced by storm depth. L-kurtosis and τ_5 do not. A factor that could contribute to these statistics changing with depth is that the storms lumped into the 24 hr and greater duration—some durations might be many

days—are more heterogeneous than those having shorter durations. Even the 12–24 hr duration might have excessive heterogeneity expressed because of the slight to moderate upward trend in the mean and the median.

The weighted average values for the category means for each statistic for each duration also are listed in table 24. All of the weighted averages, except perhaps τ_5, for the 0–12 hr and 12–24 hr durations are close in value, which suggests that these durations can be combined. It is therefore concluded that the distribution of the sub-daily hyetographs (0–24 hr) might be combinable. This affirms a similar conclusion using just the mean statistic in the triangular hyetograph chapter. The remainder of this dissertation however continues to consider the 0–12 hr and 12–24 hr durations distinct.

The weighted average values for the category means for each statistic for the 24 hr and greater duration are similar in value to those for the two other durations. However, the mean, median, L-scale, and L-CV values appear different enough from those for the other two durations that the 24 hr and greater duration should be considered separate. The values for L-skew and L-kurtosis appear comparable to the corresponding values for the other two durations. The values for τ_5 appear less comparable between the three durations, but each is greater than zero.

Table 24. Summary of observations made and weighted average values for statistics from the box plot graphs on figures 26–46

[hr, hour; --, no dependency between statistic and storm depth observed; up, an increasing statistic value with increasing storm depth observed; down, a decreasing statistic value with increasing storm depth observed; na, not available]

Statistic name	Statistic symbol	0–12 hr duration	12–24 hr duration	24 hr and greater duration
Storm dependency summary				
Mean	λ_1	--	up (not sub-stantial)	down
Median	M	--	up (not sub-stantial)	down
L-scale	λ_2	--	--	up
L-CV	τ	--	--	up
L-skew	τ_3	down	down	up
L-kurtosis	τ_4	down	down	--
Tau5	τ_5	down	--	--
Weighted average values of statistics				
Mean	λ_1	59.1	58.5	55.5
Median	M	61.3	61.0	55.8
L-scale	λ_2	15.6	14.2	13.8
L-CV	τ	.310	.292	.297
L-skew	τ_3	-.0003	-.0468	.0207
L-kurtosis	τ_4	.189	.184	.182
Tau5	τ_5	.116	.0772	.0489

The three L-skew means appear nearly equal to zero; hence a near symmetry in the expected hyetograph distribution is implied. Hosking (1990, p. 112) reports that the L-skew of the Normal distribution (a symmetrical distribution) and the Logistic distribution [$Q(F) = a + b \times \ln(F/(1-F))$] (also a symmetrical distribution) is $\tau_3 = 0$. The near symmetry in the expected hyetograph distribution is unexpected by

the author considering visual inspection of individual hyetographs seen on figures such as figure 9.

The three L-kurtosis means appear nearly equal to a value of about 0.18. Visualization of the L-kurtosis on individual hyetographs seen on figures such as figure 9 is difficult. Hosking (1990, p. 112) also reports that L-kurtosis for the Normal distribution is $\tau_4 = 30\pi^{-1}\operatorname{atan}(\sqrt{2})-9 = 0.1226$. Also reported by Hosking is that the Logistic distribution has an L-kurtosis of $\tau_4 = 6^{-1} = 0.1667$. The L-kurtosis of the hyetographs is greater than the Normal distribution or the Logistic distribution. The L-kurtosis of the Kappa distribution described in the previous chapter can not acquire a value greater than 0.1667 for an L-skew value of zero. The hyetographs are more peaked as reflected by the L-kurtosis than well documented distributions.

Monthly and Seasonal Influences on Hyetograph Statistics

Analysis of monthly and seasonal differences of the hyetograph statistics (component no. 2) contributes to documentation of the influence of time of year on dimensionless hyetographs. Specifically, the statistics considered are the mean, median, L-scale, and L-CV of the hyetograph distributions. As used in previous analyses, the same 0–12 hr, 12–24 hr, and 24 hr and greater storm durations are considered. All storms having a depth equal to or greater than 1 in. (25.4 mm) within a given duration category were combined for the analysis. Note that for the 1 in. depth category considered in the previous section depths as small as 0.5 in. (12.7 mm) were

included; depths as small as this are not considered in this section. For each duration, the mean of each statistic (a monthly mean) for each of the twelve months of the year was computed. Monthly mean values of the mean, median, L-scale, and L-CV of the dimensionless hyetographs are shown on figure 47.

Graph A of the figure compares the monthly means of the hyetograph means to the month of the year; graph A also shows the sample size for the mean. From the graph, it is evident that substantial month to month variation exists for a given duration as well as substantial variation between the durations. However, some possible subtle trends are interpreted. From inspection of graph A it appears that the hyetograph mean increases from an annual low in January to a maximum between May and July. By about August through the end of the year, the hyetograph mean appears unrelated to the month. A larger mean is indicative—albeit not as strongly as the median—of a dimensionless hyetograph that peaks earlier and is steeper than those having smaller values for the mean (see figure 54, referenced out of sequence). The 24 hr and greater duration shows the smoothest trend or with suppressed variation. The sample sizes for each of the three durations indicates that most events occur in May, and April has the second largest number of occurrences.

Graph B of the figure compares the monthly means of the hyetograph median to the month of the year. From the graph, it is evident that substantial month to month variation exists for a given duration as well as substantial variation between the durations. More variation in the medians than in the means exists as evidenced by a

comparison of graph A and graph B; each graph is plotted on the same scale to facilitate the comparison. The median is known to have a larger sampling variation than the mean, so the greater variation in graph B than in graph A is anticipated. The dashed line representing the 24 hr and greater duration shows the smoothest patterning on the graph. The dashed line also indicates that the two minimums in the hyetograph median are seen about February and again about September, and two maximums are seen between April to June and between October and November. The month intervals for the maximums are coincident with the most frontal activity. The storms during the "frontal seasons" (April, May, and June and then September(?), October, and November) might exhibit faster advection rates and hence are more front-loaded (higher median values)—see discussion in *Previous Studies* chapter for more discussion of storm advection on hyetograph shape. It is possible that similar behavior is exhibited in the 0–12 hr and 12–24 hr duration lines, but the results are vague and likely inconclusive.

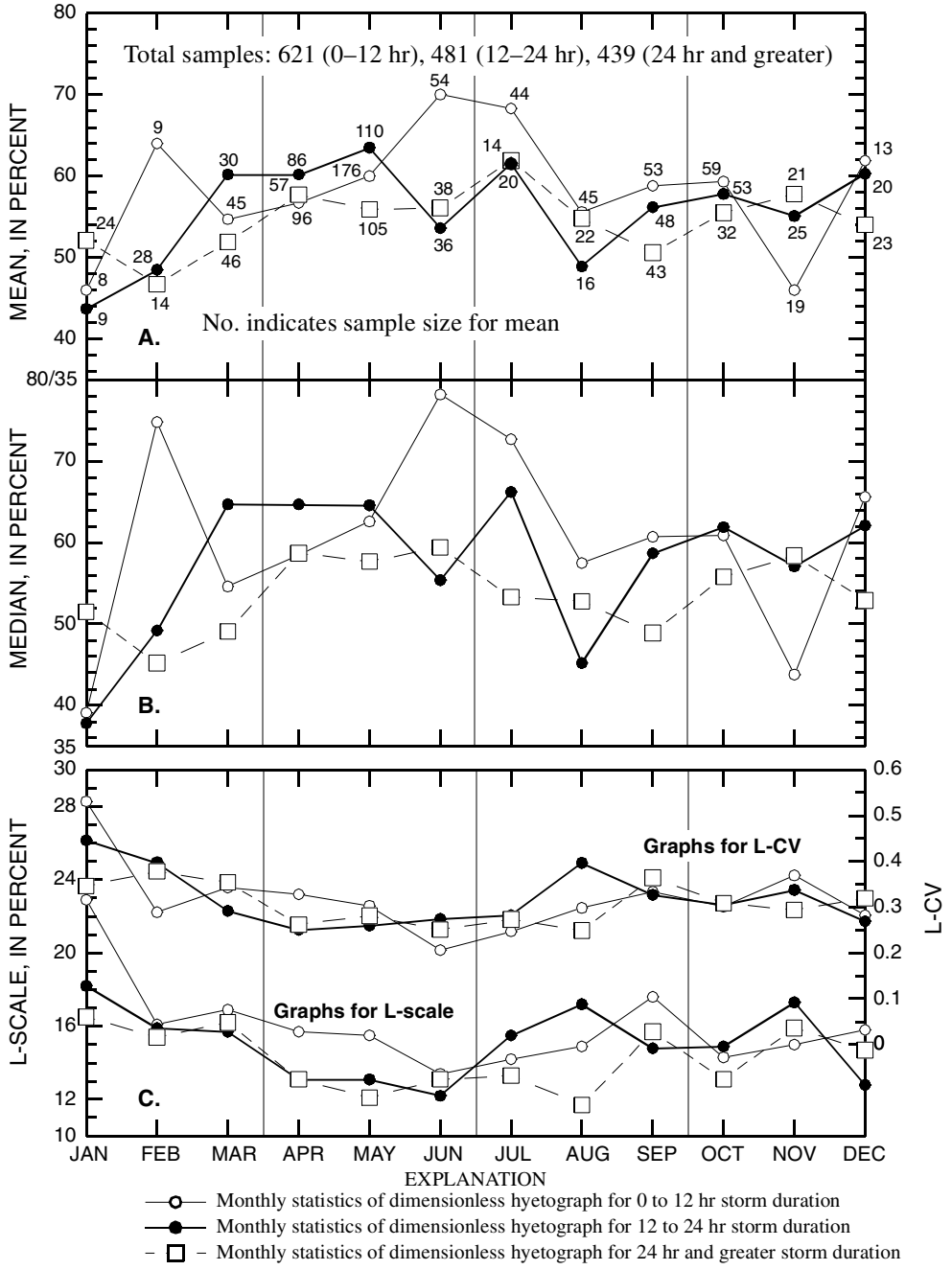

Figure 47. Comparison of monthly mean values for the mean, median, L-scale, and L-CV of dimensionless hyetographs for 0–12 hr, 12–24 hr, and 24 hr and greater storm durations for storms having greater than one inch of precipitation

Graph C of the figure compares both the monthly means of the hyetograph L-scale and the monthly means of L-CV values to the month of the year. By inspecting the

graph it is evident that L-scale diminishes from January through about June and then gradually increases to December. The coefficient of L-variation (L-CV) as expected exhibits similar behavior. Interpretation of the L-scale and L-CV is difficult owing to its coupling with the mean or median. Highly front-loaded or alternatively back-loaded storms leave little room within the bounds of the dimensionless hyetograph space for large distribution spread. Therefore, the minimums in distribution spread coincide with the maximums in the hyetograph mean and median values. The geometry of this reasoning is illustrated on figure 54 (again referenced out of sequence).

Geographic Influences and Data Base Differences on Hyetograph Statistics

Analysis of the potential influences of geographic location on the dimensionless hyetograph mean, median, and L-scale statistics (component no. 3) contributes to the statistical understanding of the hyetograph. If limited geographic patterning is evident or if geographic patterning is absent in the hyetograph statistics, then a logical conclusion is that the five data bases can be combined. Resulting expected hyetographs from the combination hence will have broad geographic applicability in Texas. A further benefit of the analysis is that potential systematic differences between the data bases as expressed in the dimensionless hyetograph statistics can be evaluated. In the first subsection, the analysis is for the dimensionless hyetographs generated from a *double one-percent trimming* of the hyetograph tails. In the second subsection, the analysis is for the dimensionless hyetographs with *no trimming* of the

hyetograph tails. Readers are reminded that the double one-percent trimming is performed in all statistical processing of hyetographs in this dissertation unless otherwise stated or when two different trimming methods are juxtaposed as in this section. As with the previous section for all analysis in this section, only hyetographs with precipitation depths equal to or greater than 1 in. (25.4 mm) were used.

Double One-Percent Trimming of Hyetograph Tails

The relation between values for the mean and median of 0–12 hr dimensionless hyetographs computed with double one-percent tail trimming and values for L-scale are shown on figure 48. Summary statistics for the this figure are listed in table 25. These statistics reflect the aggregation of each of the five data bases. For example, the arithmetic mean of the hyetograph means (graph A), medians (graph B), and L-scale values (graphs A and B) are 59.6 percent, 62.0 percent, and 15.5 percent, respectively. The medians of the hyetograph means, medians, and L-scale values are 61.0 percent, 71.0 percent, and 16.0 percent, respectively. The table also list other statistics for other durations indicated on figures in this subsection and the next subsection.

Table 25. Summary mean and median statistics for the mean, median, and L-scale values of dimensionless hyetographs for 0–12 hr, 12–24 hr, and 24 hr and greater storm durations and both tail trimming methods for one inch and greater storm depths

[hr, hour; Number in parenthesis beside the entries in the two columns for the 24 hr and greater duration does not include the Dallas hyetograph data base.]

Summary statistic	Dimensionless hyetograph statistic type	Double one-percent tail trimming			No tail trimming		
		0–12 hr duration (percent)	12–24 hr duration (percent)	24 hr and greater duration (percent)	0–12 hr duration (percent)	12–24 hr duration (percent)	24 hr and greater duration (percent)
Mean of values for the values of the hyetograph statistics							
	Mean	59.6	58.2	54.8 (56.0)	62.0	61.8	58.2 (59.4)
	Median	62.0	60.6	54.7 (56.3)	64.4	67.0	59.4 (61.4)
	L-scale	15.5	14.3	13.8 (13.6)	16.0	15.0	15.4 (15.2)
Median of values for the values of the hyetograph statistics							
	Mean	61.0	59.5	53.2 (54.8)	64.1	65.1	55.7 (58.6)
	Median	71.0	66.5	57.3 (59.0)	79.0	77.6	62.4 (66.4)
	L-scale	16.0	14.7	14.1 (13.9)	16.6	15.4	15.8 (15.7)
Graphically estimated modes for the values of the hyetograph statistics							
	Mean	67	66	54. (54)	78	74	54. (54)
	Median			indeterminate			
	L-scale	17	15	14. (14)	19	17	19. (17)

From graph A on the figure it is evident that a large variation in the mean exists—the mean appears capable of acquiring almost any value between about 10 and about 95 percent. However, a pronounced joint clustering of mean and L-scale between mean values of about 55 percent to about 90 percent is evident. The clustering is indicated in the figure by the light grey region labeled “cluster”.

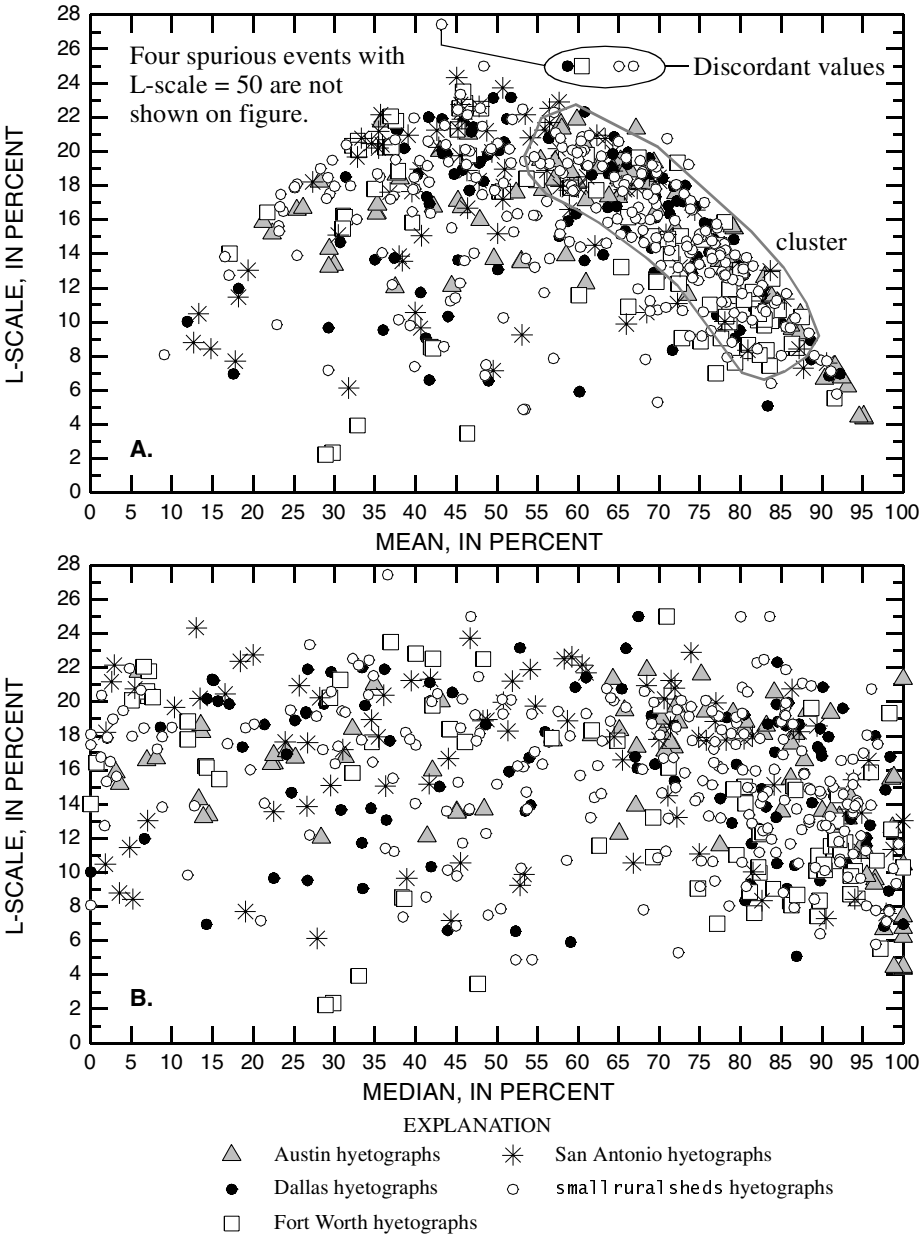

Figure 48. Relation between hyetograph mean or median and L-scale for 0–12 hr storm durations and depths greater than or equal to one inch for each of the five hyetograph data base modules when double one-percent trimming of the hyetograph tails is performed

L-scale also exhibits much variation, but unlike the mean, L-scale seems to approach a limiting value for a given mean. The limiting characteristic is seen in the inverted "U" shape of graph A. This behavior between the mean and L-scale on figure

48 is repeatedly seen in pending figures 49–53. An unpublished theoretical or mathematical proof of a limiting L-scale value has been made by Hosking (written commun., 2002). The limits are $0 \leq \lambda_2 \leq \lambda_1(1 - \lambda_1)$. A reason by partial description is that as the mean of the dimensionless hyetograph gets large (or small), there is little "room" in the 0 to 100 percent range for large hyetograph slope (large L-scale) near the middle regions of the duration. A graphic further representing a geometric description of this reasoning is shown on figure 54.

From graph B on figure 48, it also is evident that the median exhibits much variation and appears to acquire almost any value between 0 and 100 percent. This range is slightly larger than that for the mean. In contrast with the mean (graphs A) the L-scale values do not appear influenced by the median and distinct limiting values for a given median are not evident. Although moderate joint clustering of median and L-scale values at median values between about 65 percent to 100 percent is seen, the cluster is not nearly as pronounced as it was for the mean.

From both graphs on figure 48, little visual difference between the four urban data bases is apparent. However, neither the Austin or `smallruralsheds` (accounting for its much larger sample size) data bases have L-scale values as low as those computed in the remaining three urban data bases. All data bases exhibit similar ranges for both the mean and the median. The appearance of a few very small mean and L-scale values could be attributable to sampling biases, poor digitizing of the data, an artifact (desirable or not) of the double one-percent trimming or other unidentified factors. It is

concluded that for the 0–12 hr duration that all five data bases can be aggregated for purposes of estimation of the mean, median, and L-scale statistics.

Similar behavior as seen for the 0–12 hr duration with the mean, median, and L-scale values is apparent on figures 49 and 50 for the 12–24 hr and 24 hr and greater durations, respectively. Similar conclusions as those for the 0–12 hr duration thus are made including a conclusion that the five data bases are compatible for the 12–24 hr duration. For the 24 hr and greater duration, the Dallas data points are unexpectedly few for mean values between about 60 and 80 percent and for median values between about 65 and 95 percent. There appears a bias towards smaller values of both the mean and median. The result is that the summary mean or median statistics (table 25) are smaller when the Dallas data is included. Alternative statistics without the Dallas data also are listed in table 25. It is unknown whether or not the Dallas data for the 24 hr and greater duration should be used. Reasons for the discrepancy of this particular group of Dallas data are not apparent and inspection of figure 5 provides no insight.

A couple of other notable observations of figures 49 and 50 are made. First, for the 12–24 hr duration (fig. 49), less pronounced clustering is evident than that identified for the 0–12 hr duration (fig. 48). No identified clustering is seen for the 24 hr and greater duration (fig. 50). Second, for the 24 hr and greater duration (fig. 50), the values for L-scale do not appear to approach the limiting value as frequently as seen in graphs A of figures 48 and 49.

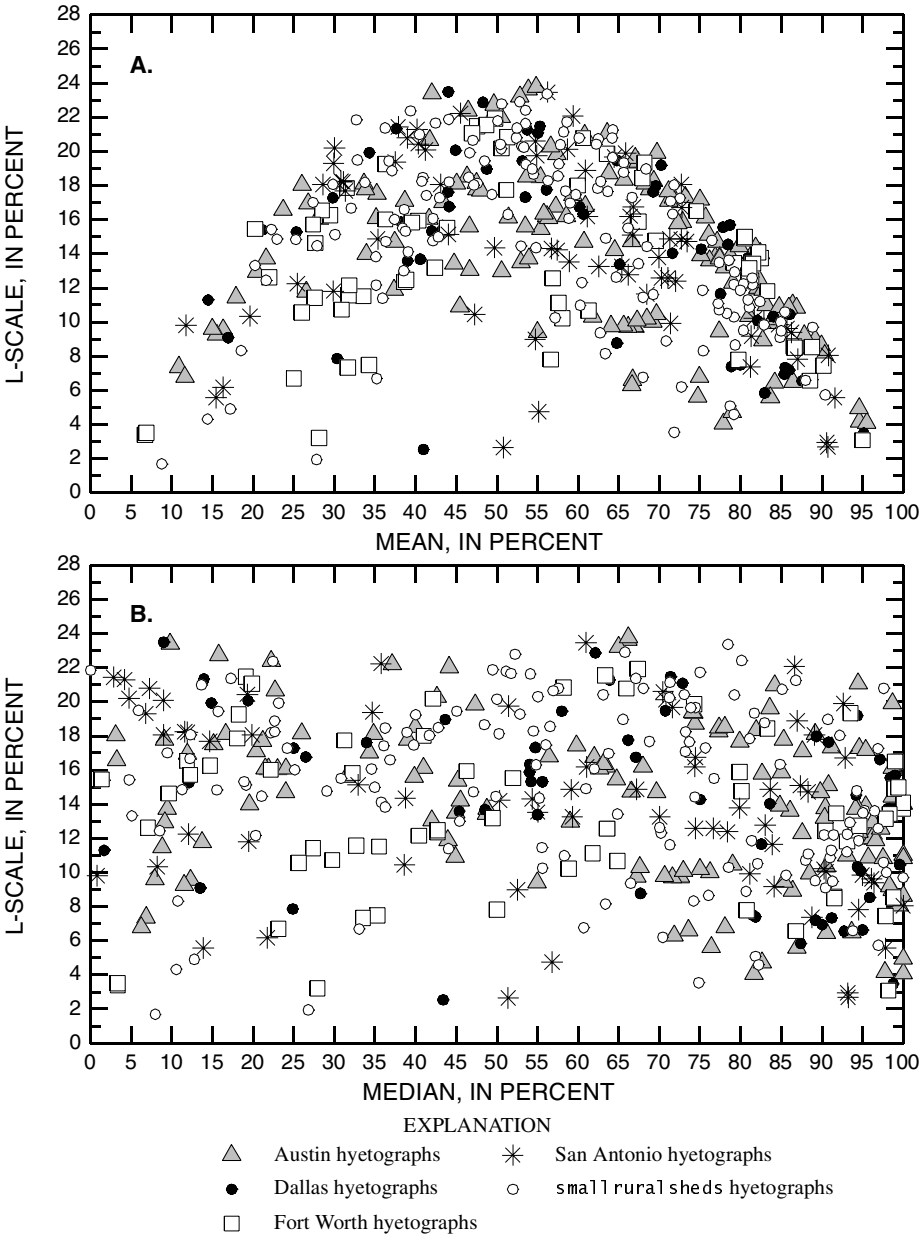

Figure 49. Relation between hyetograph mean or median and L-scale for 12–24 hr storm durations and depths greater than or equal to one inch for each of the five hyetograph data base modules when double one-percent trimming of the hyetograph tails is performed

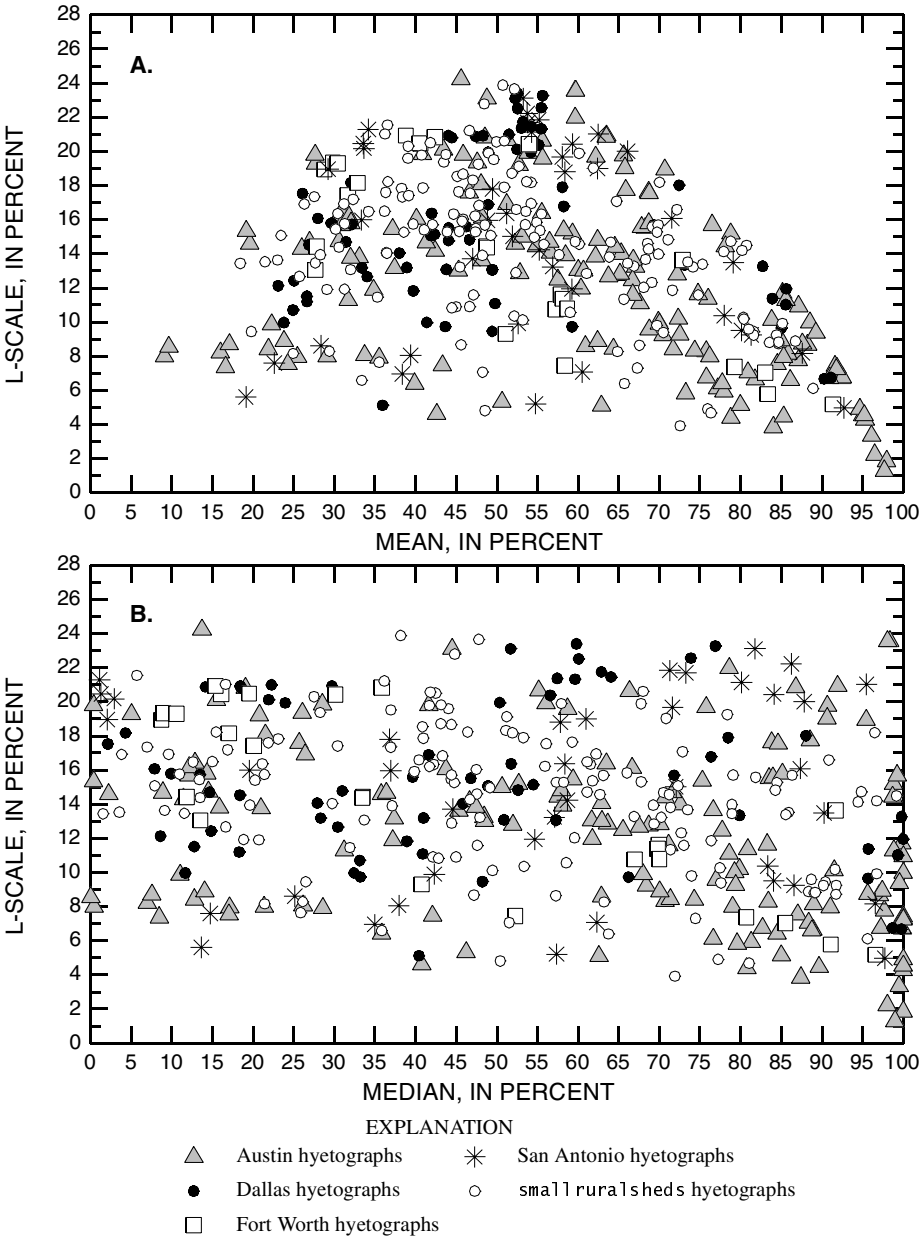

Figure 50. Relation between hyetograph mean or median and L-scale for 24 hr and greater storm durations and depths greater than or equal to one inch for each of the five hyetograph data base modules when double one-percent trimming of the hyetograph tails is performed

No Trimming of Hyetograph Tails

The relation between values for the mean and median of 0–12 hr dimensionless hyetographs computed with no tail trimming and values for L-scale are shown on figure 51. The relation between mean, median, and L-scale for the 12–24 hr and 24 hr and greater duration are shown on figures 52 and 53, respectively. Summary statistics for each of these figures are listed in table 25. For example, the arithmetic mean of the 0–12 hr dimensionless hyetograph means (graph A), medians (graph B), and L-scale values (graphs A and B) are 62.0 percent, 66.4 percent, and 16.0 percent, respectively, and the medians of the hyetograph means, medians, and L-scale values are 64.1 percent, 79 percent, and 16.6 percent, respectively.

Similar discussion of the characteristics of figures 48–50 can be made for figures 51–53. The 0–12 hr duration graphs (fig. 51) show similar pronounced clustering of the mean and medians. The 12–24 hr duration graphs (fig. 52) also show pronounced clustering—more than that visible on figure 49. The L-scale values for the untrimmed hyetographs visible to more tightly approach a limiting value for a given mean than seen on figures 48–50. This is attributable to the lack of trimming for the figures 51–53. It is unknown which tail trimming method is preferable when judged by the degree of approach to the limiting L-scale values.

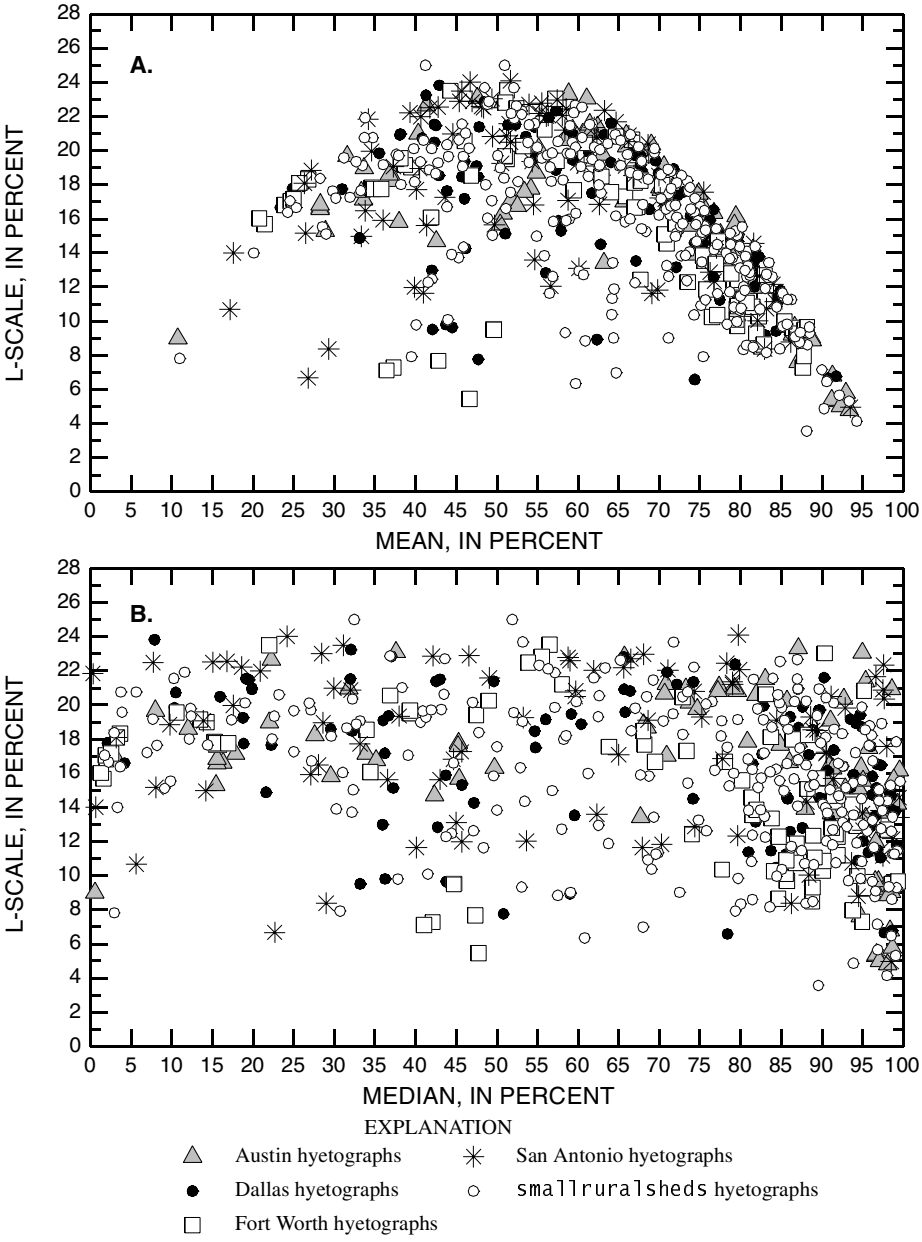

Figure 51. Relation between hyetograph mean or median and L-scale for 0–12 hr storm durations and depths greater than or equal to one inch for each of the five hyetograph data base modules when no trimming of the hyetograph tails is performed

An inspection of table 25 shows that the mean and median summary statistics increase slightly when no trimming is used. However, numerically the statistics are generally comparable. Finally, it is concluded that few visual differences between the

data bases can be seen; hence, the five data bases should be combined if no tail trimming method is used.

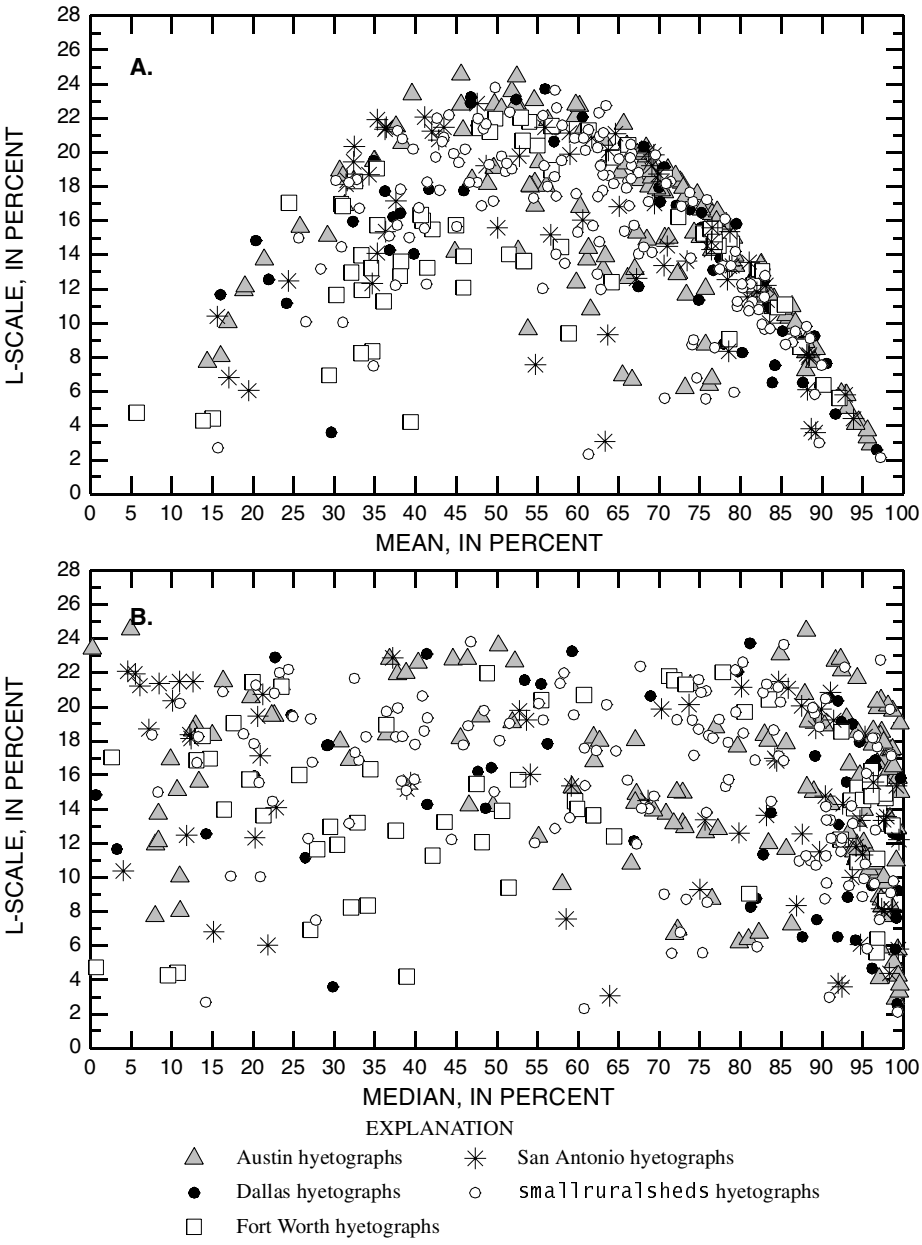

Figure 52. Relation between hyetograph mean or median and L-scale for 12–24 hr storm durations and depths greater than or equal to one inch for each of the five hyetograph data base modules when no trimming of the hyetograph tails is performed

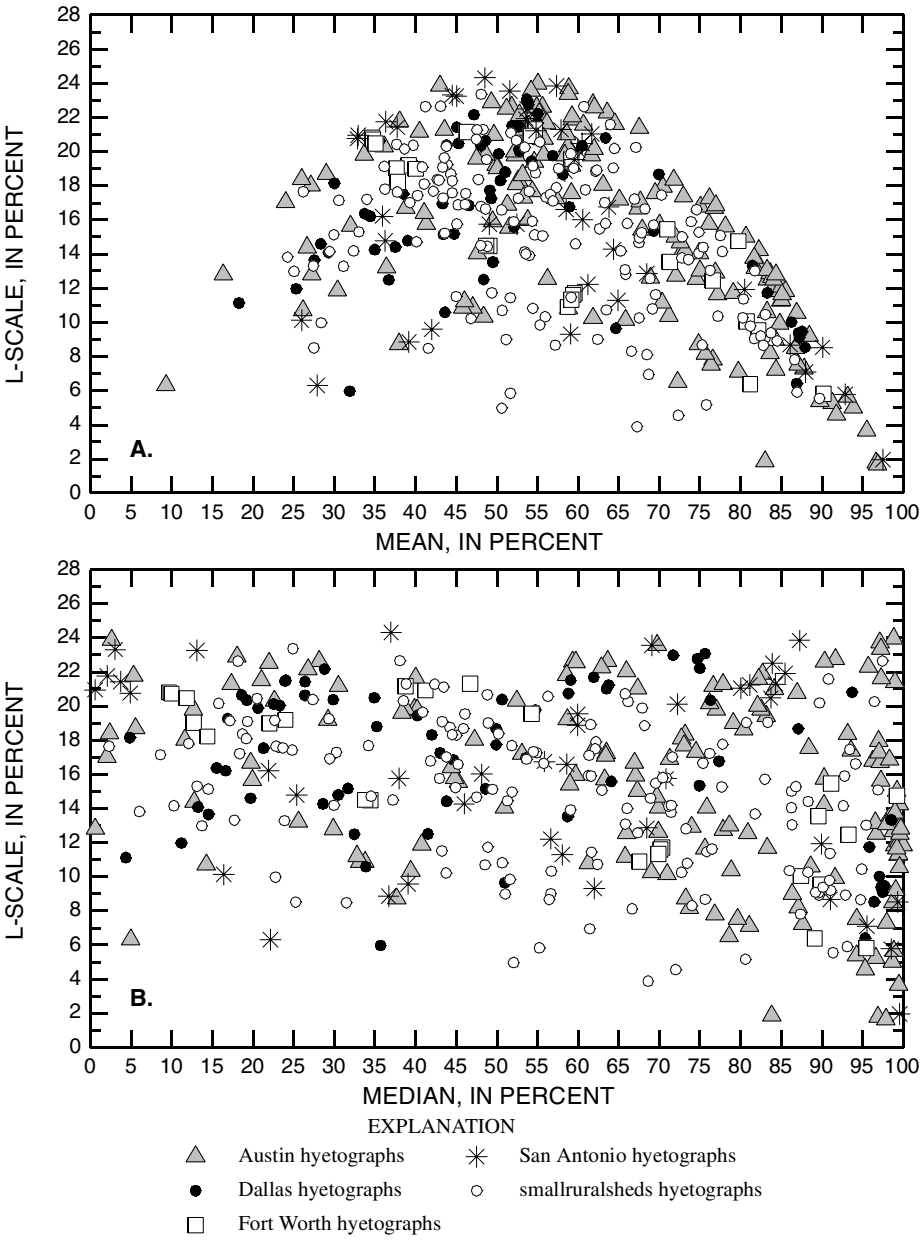

Figure 53. Relation between hyetograph mean or median and L-scale for 24 hr and greater storm durations and depths greater than or equal to one inch for each of the five hyetograph data base modules when no trimming of the hyetograph tails is performed

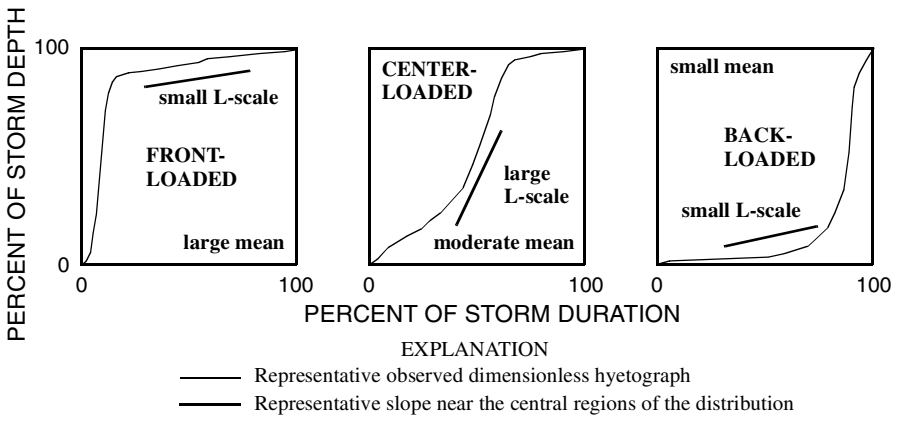

Shallow central slopes are consistent with little spread in the data and hence small L-scale values.
Steep central slopes are consistent with large spread in the data and hence large L-scale values.

Figure 54. Illustration of geometric reasoning behind the limiting of L-scale values with the hyetograph mean as seen in graphs A of figures 48–53

Modal Analysis of Hyetograph Statistics

The relation between the mean or median and L-scale of dimensionless hyetographs for storm depths greater than or equal to 1 in. (25.4 mm) was documented on figures 48–53 of the previous section. The expected hyetograph could be defined by the summary statistics (table 25) of the figures. For example, an expected hyetograph for the 0–12 hr duration could be defined as a distribution having a mean of 59.6 and L-scale of 15.5 (see fig. 48 and row 1, column 1 and row 3, column 1 of table 25). However, the coordinate (59.6, 15.5) when plotted on graph A of figure 48 would lay just outside of the generalized cluster indicated on the figure. In the author's opinion, however, the most "likely" hyetograph—the expected hyetograph—should be defined somewhere within the cluster. There is a strong tendency for the joint values of mean and L-scale of a random hyetograph to occur within the approximate space of the cluster. Pronounced clusters also were visible on figures 51 and 52. Less

pronounced clusters are visible on figure 49. No obvious clustering is visible on figures 50 and 53. In the opinion of the author, it is possible that not all of the summary statistics in table 25 reliably represent the joint distribution of the mean and L-scale values. The author concludes that when joint clustering of the values is visible that the mode or "most likely values" of the mean and L-scale might be preferable to define the expected hyetograph. The graphical modal analysis of the data on figures 48–53 is presented in this subsection.

The modal analysis for the three durations considered (0–12 hr, 12–24 hr, and 24 hr and greater) is shown on figures 55–60. The double one-percent tail trimming method is represented on figures 55–57, and the no-tail-trimming method is represented on figures 58–60. Because the mean, median, and L-scale statistics are not integers but are real numbers, aggregation of the values within intervals is required to define the general distributional of the data and hence the mode. For the mean and median 4-percent wide interval was used and a 2-percent wide interval was used for the L-scale values.

Within each interval the number or count of values was determined. For purposes of illustration the count is plotted on the right-hand side of each interval—an offset of half the interval width to the left is needed to more accurately compute the mode. The symbol plotted for statistics of zero (far left of the figures) is for a zero-width interval. The interval widths and the right-hand side plotting styles prudently are indicated on figures 55–60.

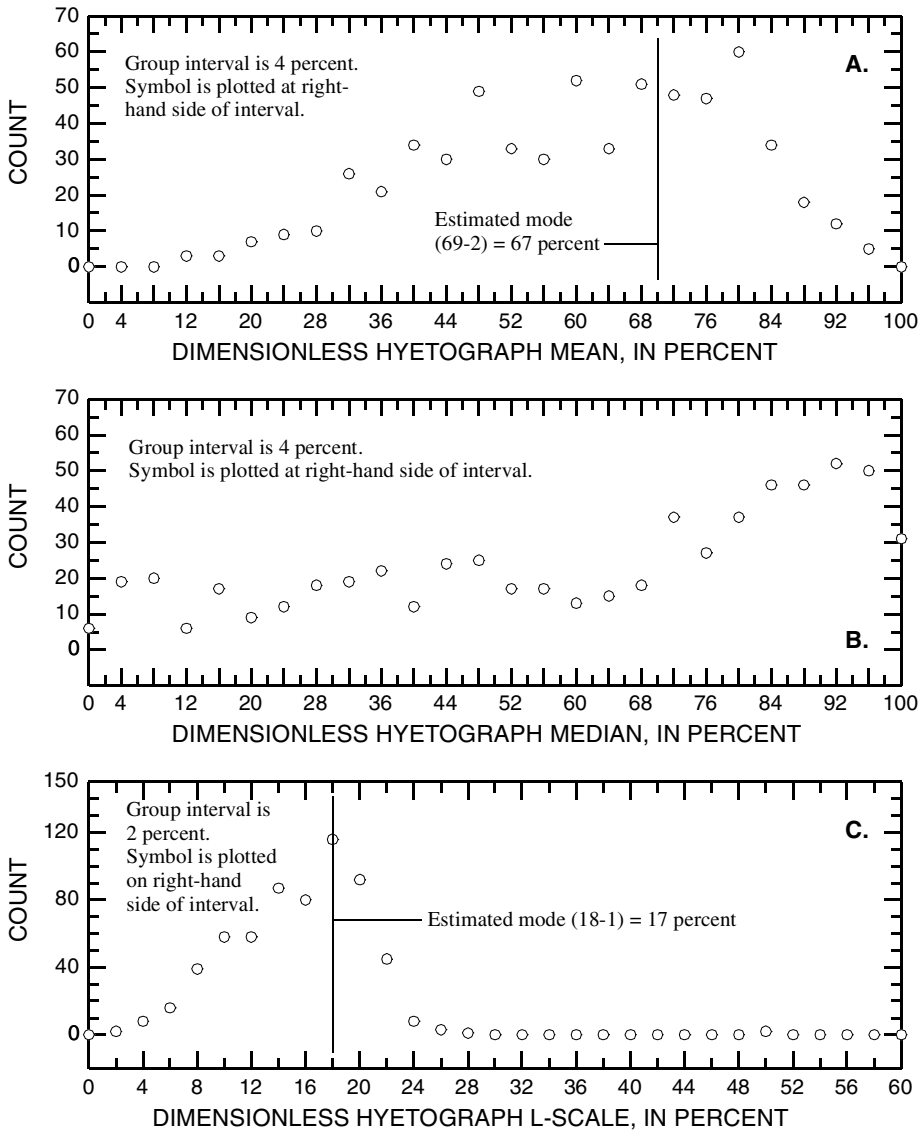

Figure 55. Modal analysis of mean, median, and L-scale statistics of double one-percent trimmed dimensionless hyetographs having storm durations of 0–12 hr and depths equal to or greater than one inch

The most likely value for the hyetograph means (graphs A on figures 55–60) and the L-scale values (graphs C) is indicated by the labeled thin vertical line. The modes for the medians (graphs B) explicitly are not identified because the counts generally

are similar across nearly all intervals. It is noted that the mode of the medians are generally greater than about 88 percent.

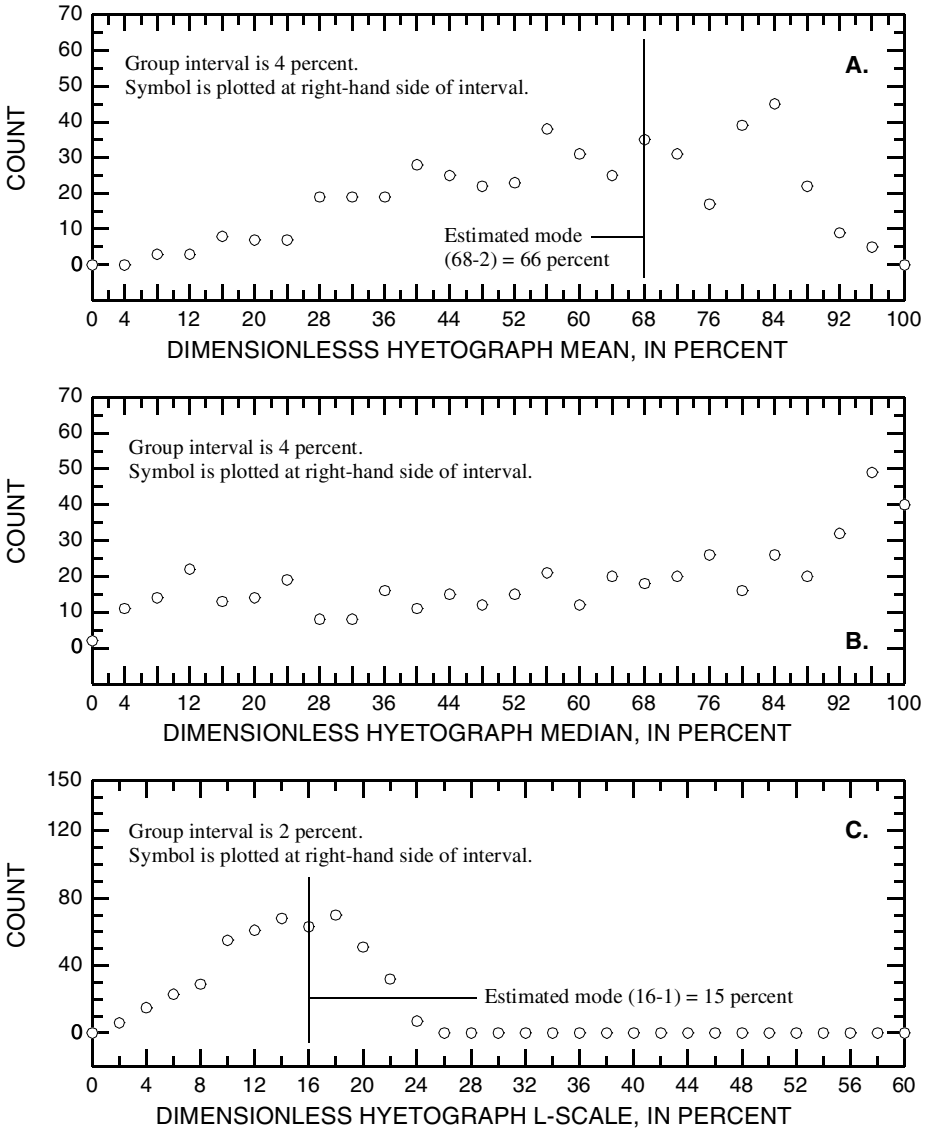

Figure 56. Modal analysis of mean, median, and L-scale statistics of double one-percent trimmed dimensionless hyetographs having storm durations of 12–24 hr and depths equal to or greater than one inch

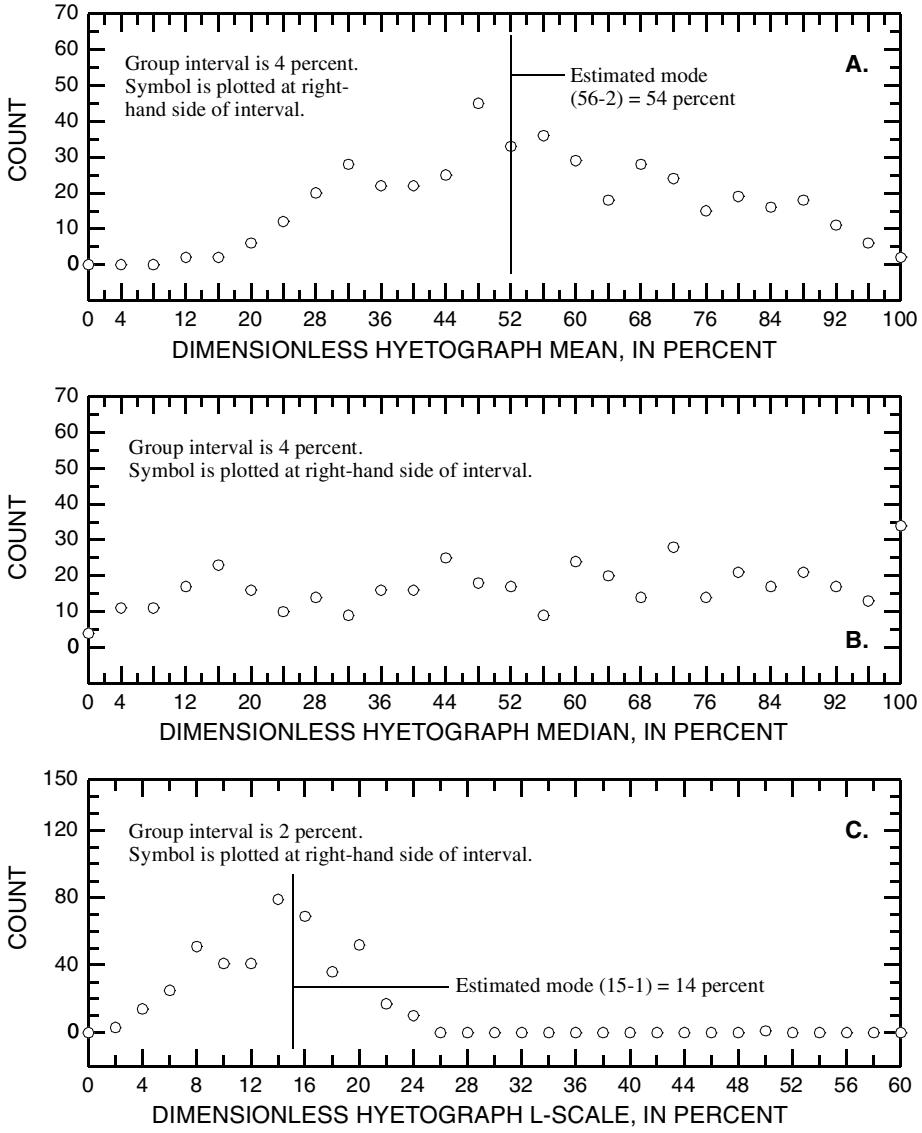

Figure 57. Modal analysis of mean, median, and L-scale statistics of double one-percent trimmed dimensionless hyetographs having storm durations of 24 hr and greater and depths equal to or greater than one inch

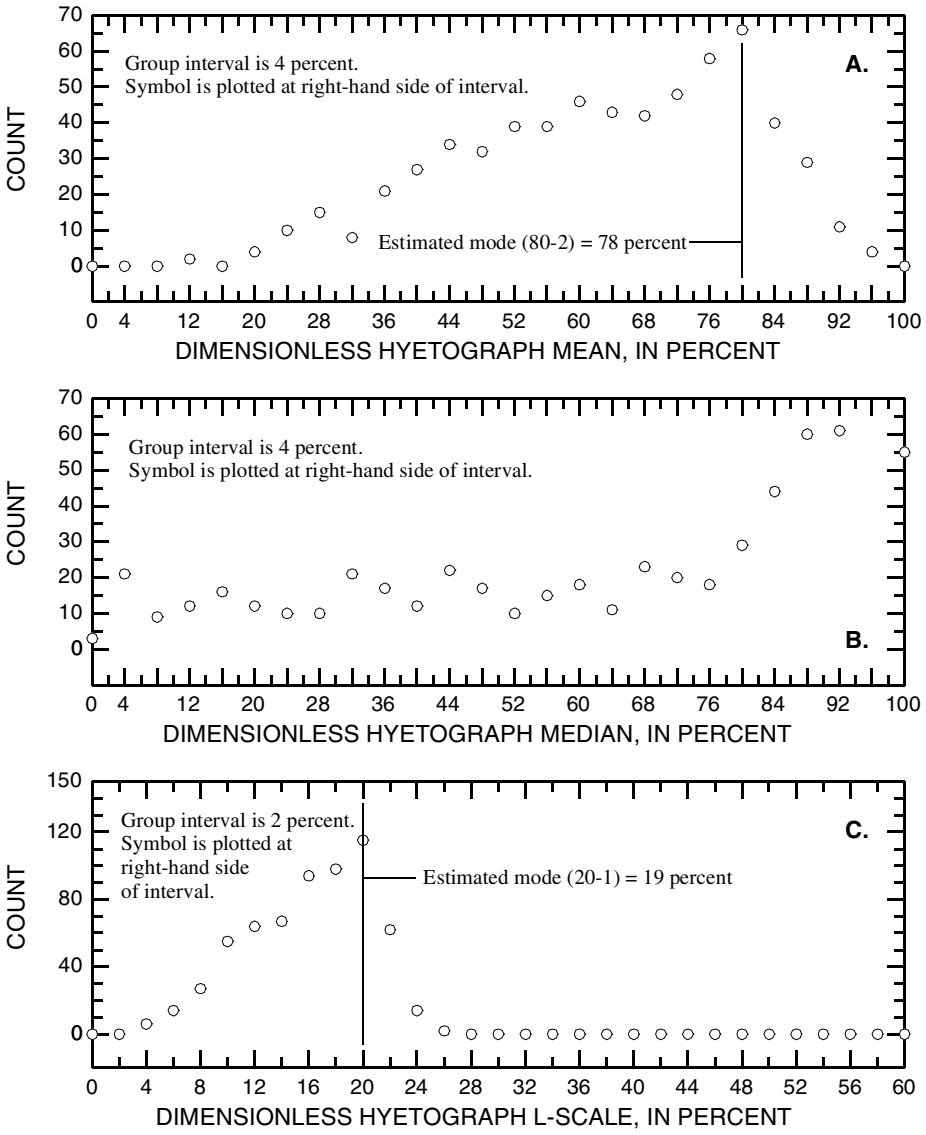

Figure 58. Modal analysis of mean, median, and L-scale statistics of untrimmed dimensionless hyetographs having storm durations of 0–12 hr and depths equal to or greater than one inch

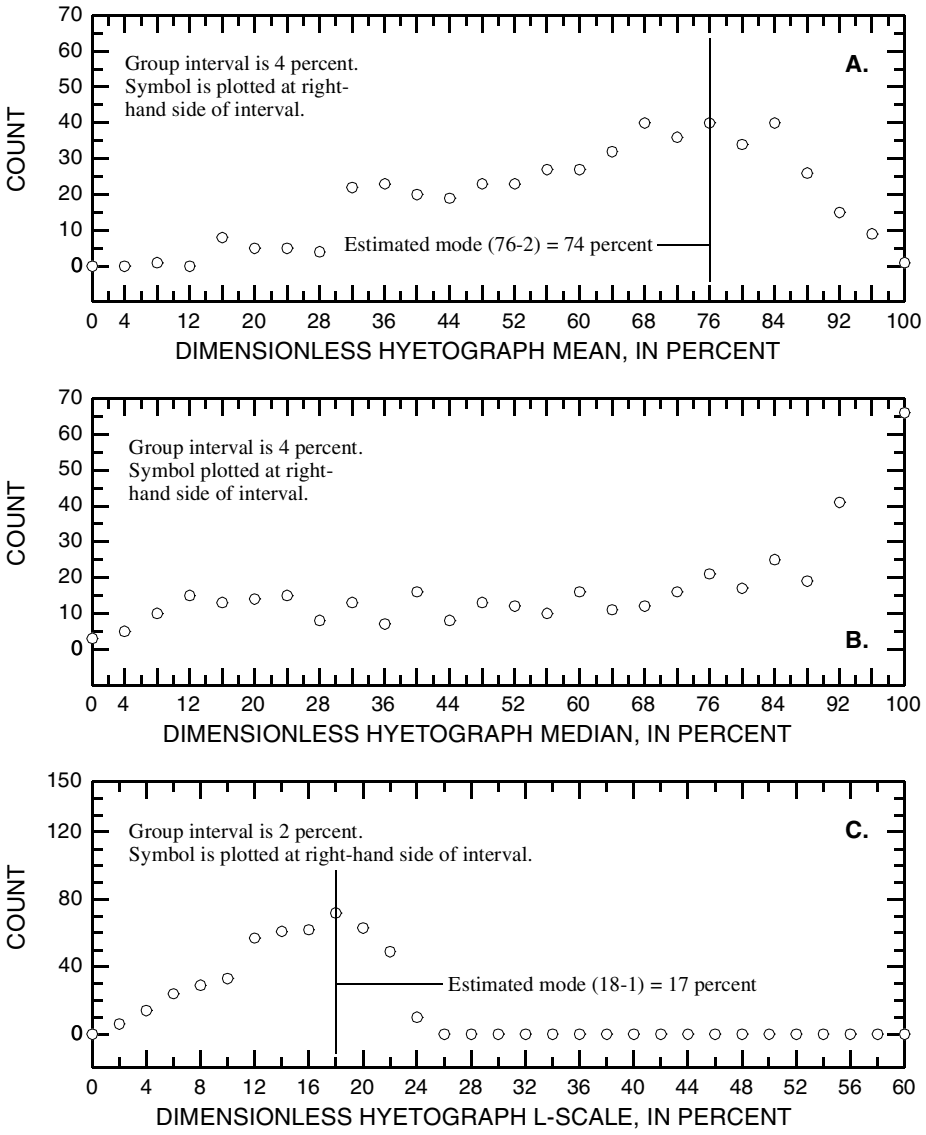

Figure 59. Modal analysis of mean, median, and L-scale statistics of untrimmed dimensionless hyetographs having storm durations of 12–24 hr and depths equal to or greater than one inch

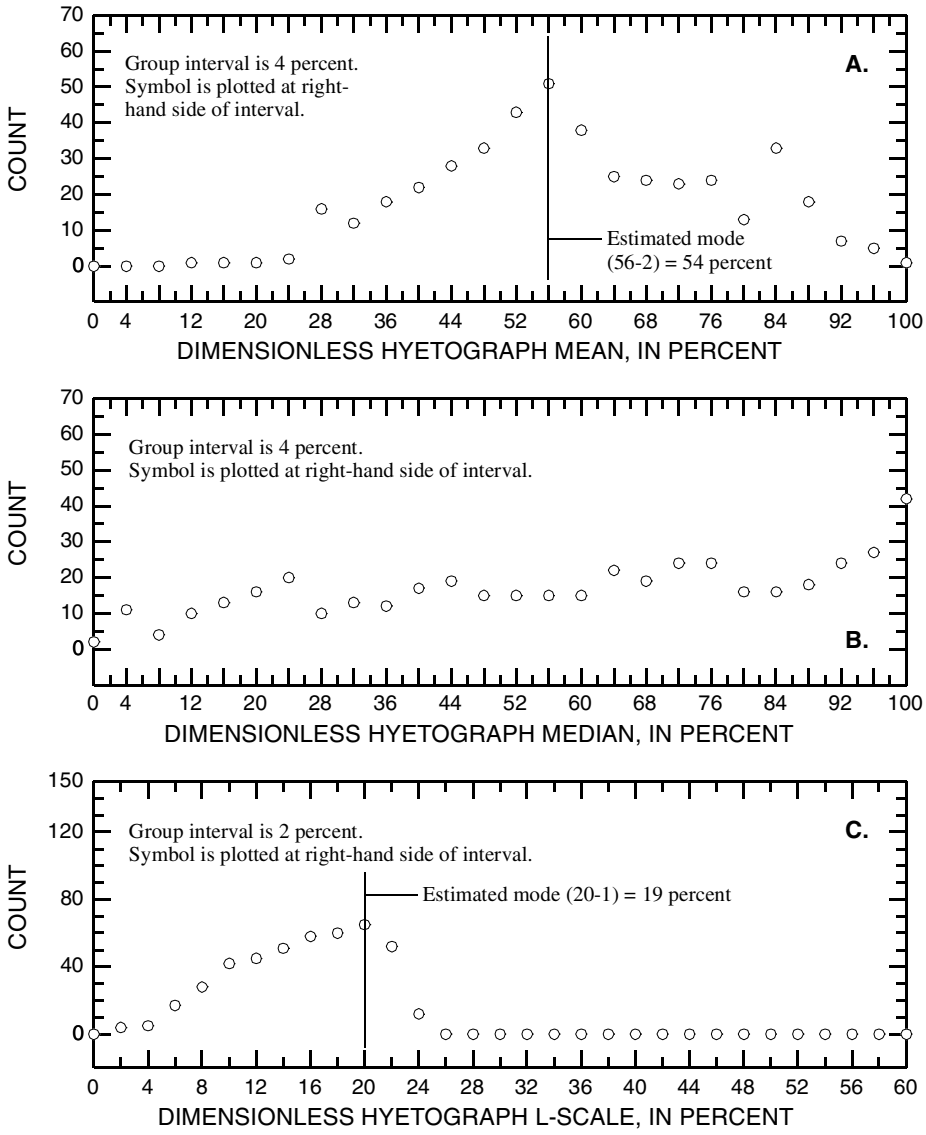

Figure 60. Modal analysis of mean, median, and L-scale statistics of untrimmed dimensionless hyetographs having storm durations of 24 hr and greater and depths equal to or greater than one inch

The graphically estimated mode indicated on the figures is an *interpretation of the peak of the overall distributional shape* of the plotted points and is *not* always coincident with the point with the largest count. Further, the half-interval offset to the left of the vertical line on the graphs is indicated on the figures for clarity. The author

explicitly acknowledges that the graphically estimated mode is contrary to the strict interpretation of an empirical or sample mode. The author concludes that it is necessary and prudent to visually consider the trends in the plotted points when judging and hence estimating the most likely value for the mean and L-scale statistics. The author also acknowledges that other analysts might determine alternative values. Finally, graphical modes of the statistics for the 24 hr and greater storm duration without the Dallas data were separately determined (graphs not presented here), and the modal values also reported in table 25.

Chapter Conclusions

The follow conclusions drawn from the analysis in this chapter include:

1. The 0–12 hr and 12–24 hr durations dimensionless hyetographs appear compatible. When overall means and medians are compared, these statistics for each duration are very similar. These two durations will continue to remain separate for the remainder of this dissertation.

2. The 24 hr and greater duration dimensionless hyetographs have statistics that appear dissimilar from the other two durations. Further, consultation of storm depth dependency of the hyetograph median and L-moments suggests that the 24 hr and greater duration is more heterogeneous than the shorter durations.

3. The dimensionless hyetographs for the 0–12 hr duration appears independent of storm depth—hence storm frequency—by the independence of the mean, median, and L-scale statistics on the storm depth. The hyetographs for the

12–24 hr duration are slightly dependent but it is assumed independent for subsequent analysis in this dissertation.

4. The dimensionless hyetograph distribution as a whole have near zero values for L-skew, which suggests that the distributions are nearly symmetrical.

5. The L-kurtosis of the dimensionless hyetographs as a whole have L-kurtosis values larger than existing L-moment compatible distributions, such as the Normal or the Logistic. Albeit, these distributions are not similarly bounded as the hyetograph distributions are.

6. The dimensionless hyetographs appear affected by the month or season of occurrence. Although the relations between the monthly mean of the mean, median, and L-scale statistics and the month of the calendar are vague, it seems that storms occurring in April through June and again in October and November are more front-loaded than at other times of the year. For purposes of application, it is concluded that annual patterns of the hyetograph distribution are minor and the season or month of storm occurrence is not a critical factor in expected hyetograph estimation.

7. Little geographic differences are seen through graphical analysis of the mean, median, and L-scale statistics. Further, each of the data base modules appears compatible with the other four modules. The lone exception appears to be storms have 24 hr and greater durations for the Dallas data. Separate statistics without consideration of the Dallas data are reported.

8. The modal analysis suggests that mean and L-scale values for the 0–12 hr and 12–24 hr durations are different. The analysis also suggests that the graphically estimated modes might be more reliable predicators of most likely mean and L-scale of the dimensionless hyetographs than either the mean or median statistics.

CHAPTER 6
L-GAMMA DISTRIBUTION

Introduction

A promising two-parameter distribution for modeling dimensionless hyetographs is referred to by the author as the L-gamma distribution. The distribution does not appear to have prior description. Written communications to other researchers with interests in quantile functions or L-moments has provided no prior reference (Gilchrist, 2002; Hosking, 2002; Kroll, 2002; Serfling, 2002; Vogel, 2002; Wallis, 2002). It is important to stress that the L-gamma distribution as applied here provides a functional form of the hyetograph and is not intended to represent a random variable whose distribution has a quantile function represented by the hyetograph. The linkage between a quantile function and the hyetograph is useful in the context of the hyetograph modeling objective here but is artificial in a statistical sense. This linkage has precedence in the hydrologic sciences and applications similar to dimensionless hyetograph modeling (Yue and others, 2002, and references therein).

The quantile function, $Q(F)$, of the L-gamma distribution is

$$Q(F) = \Lambda(b, c, F) = F^b e^{c(1-F)} = e^c F^b e^{-cF}, \tag{58}$$

where $\Lambda(b, c, F)$ is the quantile for a nonexceedance probability F and $0 \le F \le 1$. The variables b and c are shape parameters that require estimation. The e^c is shown separately on the right-hand side of the equation to facilitate subsequent derivations.

The range of the function is $0 \le Q(F) \le 1$ for $0 \le F \le 1$. The curves on figure 61 provide examples of shapes for the L-gamma distribution.

The motivation for the L-gamma distribution is that it has an explicit quantile function form, an algebraic first derivative, and is compatible with the theory of L-moments. Further, the L-gamma distribution is attractive for dimensionless hyetograph modeling because the quantiles are bounded by 0 and 1 regardless of the values of the parameters. The boundedness of the distribution is critical in this modeling because, by definition, the dimensionless hyetograph has 0 and 1 lower and upper bounds, respectively. The presence of the quantile function form facilitates practical application of the distribution in hyetograph computations because the distribution is compact and algebraically simple. A simple first derivative permits direct computation of rainfall rates. Finally, the compatibility with the theory of L-moments is needed for this dissertation.

It is interesting to note that the L-gamma, with minor adjustments, normally is considered the probability density function (PDF) of the Gamma distribution (Evans and others, 2000, p. 98). The "L-gamma" name given to eq. 58 reflects the Gamma distribution heritage and the "L-" is added to reflect the applicability to L-moment statistical theory.

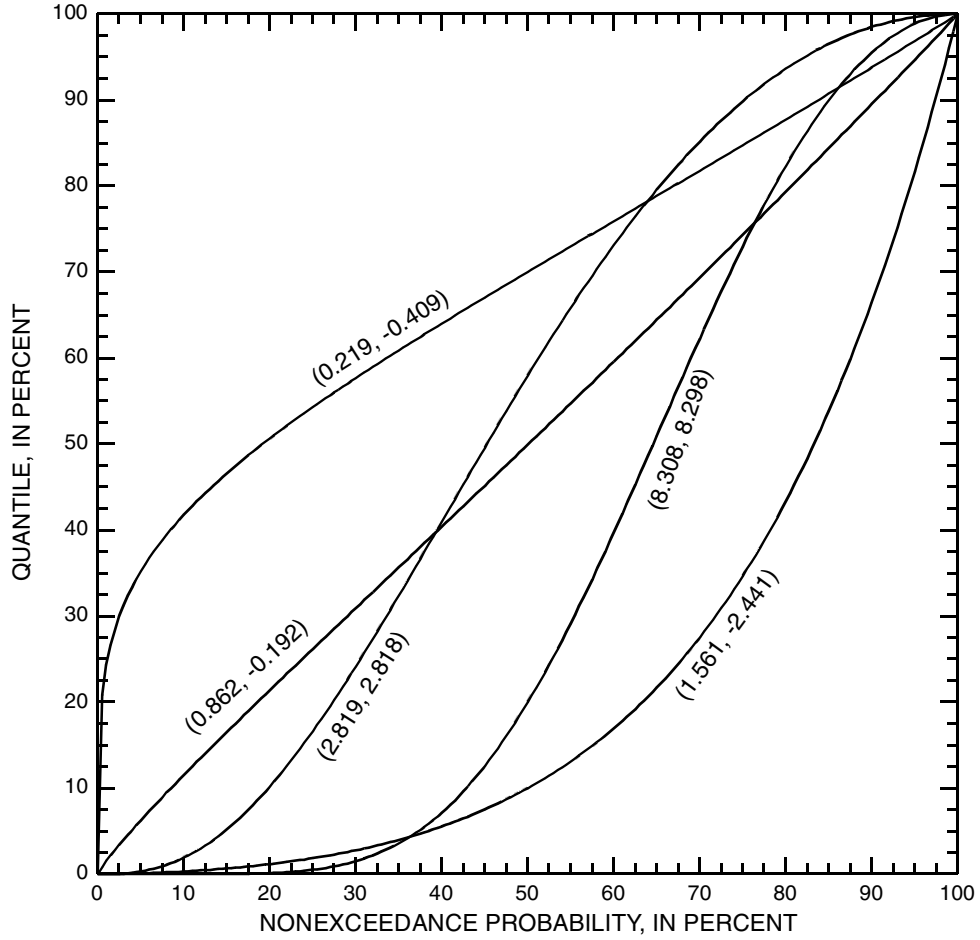

Figure 61. Example shapes of L-gamma distribution with selected pairs of (b, c) parameters

The Gamma has a prominent place in statistics and hydrology (Cunnane, 1989, table 3.1; Stedinger and others, 1992, pp. 18.19–20; Ross, 1994, p. 231–232; Wilks, 1995, pp. 86–93; Hald, 1998; Karian and Dudewicz, 2000, pp. 75–76) and it has historical use in modeling of streamflow hydrographs (Nash, 1959; Croley, 1980; Jin, 1992; and Haan and others, 1994, and references therein). A Log-gamma distribution, which is explicitly based on the Gamma distribution, is described in the literature (Prentice, 1974; Lawless, 1980; and Balakrishnan and Chan, 1995a,b).

The L-gamma distribution contains two shape parameters and, therefore, is more flexible. The distribution and can better fit the hyetograph data than single parameter distributions. The greater flexibility is the principal motivation for using the L-gamma distribution in this dissertation. Other quantile functions, which obtain similar bounds, are the one-parameter Power (Evans and others, 2000, chap. 3; Gilchrist, 2000, p. 120–121).

$$Q(F) = F^{\beta} \tag{59}$$

and the Govindarajulu (Gilchrist, 2000, p. 139)

$$Q(F) = (\beta + 1)F^{\beta} - \beta F^{(\beta + 1)} \tag{60}$$

functions. The β parameter controls the shape of both distributions. Besides noting that the L-gamma is the product of the Power distribution and $e^{c(1-F)}$ (the cumulative distribution function of the Log distribution). The Log distribution (Serfling, written commun., 2002) is attributable to Tocher (1954), Pinkham (1961), and references therein, and Serfling reports that the Log distribution in practice is quite uncommon. The author was not familiar with the Log distribution at the time that the L-gamma was formulated. The noncontinuous triangular distribution used in a previous chapter is another example of a one-parameter distribution.

Various parameterization styles of the four (eq. 95, referenced out of sequence) and five parameter Generalized Lambda distributions have quantile functions that are

bounded by 0 and 1. Parameter estimation for these distributions is complex (Karian and Dudewicz, 2000; Gilchrist 2000). The so-called symmetric Lambda or Tukey-Lambda distribution (Gilchrist, 2000, p. 157–159), in which parameter estimation is slightly more tractable, is not suitable for hyetograph modeling because an asymmetry of the hyetograph distribution is anticipated.

Parameter Constraints

The first and second derivatives of the L-gamma distribution are

$$\frac{d}{dF}\Lambda(F) = \Lambda' = e^{c(1-F)}[bF^{b-1} - cF^{b}] \tag{61.1}$$

$$\frac{d}{dF}\Lambda' = \Lambda'' = e^{c(1-F)}[b(b-1)F^{b-2} - 2bcF^{b-1} + c^{2}F^{b}] \tag{61.2}$$

If the parameters b and c of eq. 58 meet two restrictions then the function is monotonically increasing on $0 \le F \le 1$, and therefore a valid quantile function (Gilchrist, 2000, chap. 1). To meet the monotonic condition, the first derivative, a quantile density function, must be greater than zero. Hence, for a monotonic increase on $0 \le F \le 1$, then $\Lambda' \ge 0$

$$0 \le e^{c(1-F)}[bF^{b-1} - cF^{b}] \text{ and} \tag{62.1}$$

$$0 \le bF^{b-1} - cF^{b}. \tag{62.2}$$

For $F = 0$, $\Lambda' = 0$ is a degenerate case, but for $F = 1$, $0 \le b - c$, which in order to have $\Lambda' \ge 0$, implies that $b \ge c$ and that $b \ge 0$. Therefore, eq. 58 is a quantile function if and only if both $b \ge c$ and $b \ge 0$.

L-moments of the Distribution

To fit the L-gamma to a sample, the parameters b and c require estimation. A natural estimation procedure is the Method of L-moments (MLM) (Hosking, 1990, p. 119). The method equates the sample L-moments and expressions for the theoretical L-moments of a distribution; the parameter values then are solved. The expressions for the theoretical L-moments of the L-gamma distribution are derived in this section.

The first L-moment is the familiar mean and is the quantity

$$\lambda_1 = \int_0^1 \Lambda(F)dF = \int_0^1 e^c F^b e^{-cF} dF . \tag{63}$$

Evaluation of the right hand side of eq. 63 requires the Incomplete Gamma function (P)

$$n^{-m} P(m,nx) = \frac{n\gamma(m, nx)}{\Gamma(m)} = \frac{1}{\Gamma(m)} \int_0^x F^{m-1} e^{-nF} dF . \tag{64}$$

The complete Gamma function is $\Gamma(x)$ (eq. 57). It is useful to multiply eq. 64 by e^c and solve for the integral

$$\int_0^1 e^c F^{m-1} e^{-nF} dF = e^c n^{-m} \Gamma(m) P(m, n) . \tag{65}$$

A useful property of the Gamma function is

$$\frac{\Gamma(m+2)}{\Gamma(m+1)} = m + 1 . \tag{66}$$

The definitions, identities, and properties of the Gamma and related functions are described in Abramowitz and Stegun (1964). Continuation of the first L-moment definition in eq. 63 coupled with the Incomplete Gamma function in which $m = b + 1$ and $n = c$ provides

$$\lambda_1 = \frac{e^c}{c^{b+1}}\Gamma(b+1)P(b+1, c)\,. \tag{67}$$

The second L-moment, L-scale, measures the spread of a distribution and is

$$\lambda_2 = \int_0^1 \Lambda(F)(2F-1)dF \text{ and} \tag{68.1}$$

$$\lambda_2 = \int_0^1 2e^c F^{b+1} e^{-cF} dF - \int_0^1 e^c F^b e^{-cF} dF\,. \tag{68.2}$$

The standard deviation is related to L-scale by $\sigma = \lambda_2\sqrt{\pi}$ (Hosking, 1990, p. 120). Applying the Incomplete Gamma function to eq. 68.2 with $m = b + 2$ and $n = c$ results in

$$\lambda_2 = \frac{2e^c}{c^{b+2}}\Gamma(b+2)P(b+2, c) - \lambda_1\,. \tag{69}$$

A useful identity from eq. 69 is

$$\frac{\lambda_2 + \lambda_1}{2} = \int_0^1 e^c F^{b+1} e^{-cF} dF\,. \tag{70}$$

The coefficient of L-variation, L-CV, is

$$\tau_2 = \lambda_2/\lambda_1 . \tag{71}$$

It follows that

$$\tau_2 = \frac{2e^c c^{-b-2}\Gamma(b+2)P(b+2,c) - e^c c^{-b-1}\Gamma(b+1)P(b+1,c)}{e^c c^{-b-1}\Gamma(b+1)P(b+1,c)} . \tag{72}$$

Which upon simplification, eq. 72 yields

$$\tau_2 = \frac{2}{c}(b+1)\frac{P(b+2,c)}{P(b+1,c)} - 1 . \tag{73}$$

The third L-moment measures the skew of a distribution and is

$$\lambda_3 = \int_0^1 \Lambda(F)(6F^2 - 6F + 1)dF , \tag{74.1}$$

$$\lambda_3 = \int_0^1 e^c F^b e^{-cF}(6F^2 - 6F + 1)dF , \text{ and} \tag{74.2}$$

$$\lambda_3 = 6\int_0^1 e^c F^{b+2} e^{-cF} dF - 6\int_0^1 e^c F^{b+1} e^{-cF} dF + \int_0^1 e^c F^b e^{-cF} dF . \tag{74.3}$$

Substituting the first and second L-moments and applying the Incomplete Gamma function with $m = b + 3$ and $n = c$ as the first integral results in

$$\lambda_3 = \frac{6e^c}{c^{b+3}}\Gamma(b+3)P(b+3, c) - 6\left(\frac{\lambda_2 + \lambda_1}{2}\right) + \lambda_1 \text{ and} \tag{75.1}$$

$$\lambda_3 = \frac{6e^c}{c^{b+3}}\Gamma(b+3)P(b+3, c) - 3\lambda_2 - 2\lambda_1 \tag{75.2}$$

A useful identity from eq. 75.2 is

$$\frac{\lambda_3 + 3\lambda_2 + 2\lambda_1}{6} = \int_0^1 e^c F^{b+2} e^{-cF} dF. \tag{76}$$

A more conventional expression of skew is L-skew and is

$$\tau_3 = \lambda_3 / \lambda_2. \tag{77}$$

The most convenient means to compute L-skew is through eq. 77 rather than through an algebraic expansion of eq. 75.2 divided by eq. 70.

The fourth L-moment measures the kurtosis of a distribution and is

$$\lambda_4 = \int_0^1 \Lambda(F)(20F^3 - 30F^2 + 12F - 1) dF \text{ and} \tag{78.1}$$

$$\lambda_4 = 20\int_0^1 e^c F^{b+3} e^{-cF} dF - 30\int_0^1 e^c F^{b+2} e^{-cF} dF + \quad \ldots \tag{78.2}$$

$$+ 12\int_0^1 e^c F^{b+1} e^{-cF} dF - \int_0^1 e^c F^b e^{-cF} dF. \tag{78.3}$$

Substituting the first, second, and third L-moments and applying the Incomplete Gamma function with $m = b + 4$ and $n = c$ for the first integral in eq. 78.2 results in

$$\lambda_4 = \frac{20e^c}{c^{b+4}} \Gamma(b+4) P(b+4, c) - 30\left(\frac{\lambda_3 + 3\lambda_2 + 2\lambda_1}{6}\right) + \quad \ldots \tag{79.1}$$

$$+ 12\left(\frac{\lambda_2 + \lambda_1}{2}\right) - \lambda_1. \tag{79.2}$$

Expanding and collecting the L-moment terms results in

$$\lambda_4 = \frac{20e^c}{c^{b+4}}\Gamma(b+4)P(b+4,c) - 5\lambda_3 - 9\lambda_2 - 5\lambda_1 . \quad (80)$$

A more conventional expression of L-moment kurtosis (τ_4) is the quantity

$$\tau_4 = \lambda_4/\lambda_2 . \quad (81)$$

The most convenient means to compute L-kurtosis is through eq. 81 rather than through an algebraic expansion of eq. 80 divided by eq. 70.

Equations were derived for each of the first four L-moments and L-CV in terms of the parameters b and c. Any two equations can be used to estimate b and c. Convention is to fit a distribution to the lowest order moments as the higher moments increasingly reflect less information about the population.

Parameter estimation by MLM using eqs. 64 and 70 is difficult because there are no explicit solutions for the parameters in terms of the L-moments. Evaluation of the Gamma and Incomplete Gamma functions require numerical techniques. Although computer algorithms for the Gamma and Incomplete Gamma functions are described by Press and others (1992, pp. 206–213) and root solution schemes seem possible, it was decided to implement an alternative method.

Another reason to pursue an alternative method is that the parameter space of the L-gamma distribution based on λ_1 and λ_2 is restricted. From the Incomplete Gamma function integral definition and numerical recipes (Press and others, 1993), the

Incomplete Gamma function is difficult to solve for $c < 0$ (complex numbers are involved); the theoretical L-moments of the L-gamma therefore are difficult to formulate for $c < 0$. The L-gamma, however, remains a valid quantile function for $c < 0$. For example, three of the five quantile curves on figure 25 have $c < 0$. The alternative method avoids this impediment.

A late note (Dec. 2002) regarding solution of the Incomplete Gamma function for $c < 0$ is needed. According to communication with Hosking (2002), the recipes by Press and others (1993) are incomplete. Hosking reports that the Incomplete Gamma function P(b,c) for $c < 0$ is

$$P(\alpha, x) = \frac{x^{\alpha}}{\alpha}\Phi(\alpha, \alpha + 1, -x), \text{ where}$$

$$\Phi(a, b, x) = \sum_{k=0}^{n} \frac{(a)_k}{(b)_k} \times \frac{x^k}{k!} \text{ and}$$

$$(x)_k = \frac{\Gamma(x + k)}{\Gamma(x)}.$$

The function Φ is the confluent hypergeometric function (Abramowitz, p. 504), and Pochhammer Symbols are described in Abramowitz and Stegun (1964, p. 256). These equations were not used to define solution space of the L-gamma for $c < 0$.

Parameter Estimation

The alternative parameter estimation method, called the modified Method of L-moments (M-MLM), is based on the median (M), inter-tercile range (ITR), the mean (λ_1), and L-scale (λ_2) and is described in this section. Not only is the method straightforward to implement but also is applicable for $c < 0$. The theoretical median of a distribution is the quantile value for which $F = 0.5$. The sample median can be computed from the sample order statistics $x_{1:n} \le x_{2:n} \le \ldots \le x_{n:n}$ of the sample by the

following (Hollander and Wolfe, 1973, p. 453; David, 1981, p. 5): if n is even ($n = 2k$, for some integer k) then $M = (x_{k:n} + x_{k+1:n})/2$ and if n is odd ($n = 2k+1$ for some integer k) then $M = x_{k+1:n}$. Alternatively, if estimates of the cumulative probabilities of each data value are not regularly spaced then the median can be estimated using linear interpolation.

Following the definition of the theoretical median, the median of the L-gamma quantile function is

$$M = \Lambda(0.5) = (0.5)^{b} e^{c(1-0.5)}. \tag{82}$$

The parameters b or c can be directly solved for, using the natural logarithm ($\ln$), as

$$b = \frac{\ln(M) - 0.5c}{\ln(0.5)} \text{ or} \tag{83.1}$$

$$c = 2\frac{\ln(M)}{b \times \ln(0.5)}. \tag{83.2}$$

The ability to explicitly express either b or c on the left-hand side of the equations is important. A comparison and contrast of eqs. 64 and 70 with eqs. 82 and 83 indicates that the later equations are considerably easier to use.

To continue with the M-MLM development, the definition of the inter-tercile range ITR is used. The ITR is defined as the difference between the upper tercile UT and the lower tercile LT. The ITR can be expressed in terms of the expectations of order statistics and the quantile function

$$ITR = UT - LT = \Lambda\left(\frac{2}{3}\right) - \Lambda\left(\frac{1}{3}\right). \tag{84}$$

Expansion of the $\Lambda(F)$ in eq. 84, followed by algebraic manipulation results in

$$ITR = \frac{1}{3^b} e^{\frac{2}{3}c}\left(2^b e^{-\frac{1}{3}c} - 1\right). \tag{85}$$

Substitution of eq. 83.2 for c expresses the ITR as a function of b only.

$$ITR = \frac{1}{3^b} e^{\frac{4 \times \ln(M)}{3b \times \ln(0.5)}}\left(2^b e^{\frac{-2 \times \ln(M)}{3b \times \ln(0.5)}} - 1\right). \tag{86}$$

Thus eqs. 82 and 86 can be used to estimate b and c in terms of the median and ITR. Numerical methods are still required to solve for b in eq. 86, but such root solutions are reasonably straightforward.

Other "inter-cile ranges" such as the inter-quartile range (IQR) can be defined in a similar fashion. The inter-cile range of order r is denoted by IcR_r. The IQR for example has $r = 4$ and the previously shown ITR has $r = 3$.

$$IcR_r = upper - lower \tag{87.1}$$

$$IcR_r = Q\left(\frac{r-1}{r}\right) - Q\left(\frac{1}{r}\right) \tag{87.2}$$

$$IcR_r = e^c\left(\frac{r-1}{r}\right)^b e^{-\frac{r-1}{r}c} - e^c\left(\frac{1}{r}\right)^b e^{-\frac{1}{r}c} \tag{87.3}$$

Root solution by numerical methods is needed to convert the median and ITR into the parameters b and c of the L-gamma distribution. Once this is performed, then it is possible to convert the parameters into the mean and L-scale of the distribution. If lookup tables mapping all of these six variables with one another are available, then the M-MLM comprises the following steps.

1. Using the value for L-scale, consult a table to determine a range of median and ITR values of the L-gamma that approximate the L-scale value. L-scale varies closely with ITR so more attention to the ITR and L-scale is suggested in this step. L-scale values generally identify which table group to use.

2. Using the range of suitable median and ITR values from step 1, determine the most suitable pairing of these values that simultaneously most approximate both the mean and L-scale values of the data.

3. Using the most approximate median and ITR values from step 2, perform a table lookup of the b and c parameters of the L-gamma distribution.

In general, the M-MLM determines the pairing of the median and ITR that produce an L-gamma distribution, which has a mean and L-scale best approximating those of the data. Then the "best" median and ITR values are converted to the b and c parameters of the L-gamma distribution. Therefore, in order to provide simple and portable framework for parameter estimation, conversion maps (tables) of the solution space of the distribution were created (Appendix D).

Appendix D contains a series of six table groups. A table group is composed of four tables. Each table has columns for constant values of ITR and rows for constant values of the median. Tables with cells containing the b parameter are enumerated by D#.1; the c parameter tables are enumerated by D#.2; the mean tables are enumerated by D#.3; and the L-scale tables are enumerated by D#.4. The tables were generated by a Perl (*http://www.perl.org*) computer program called `solutionspaceLGamma.pl` and is listed in Appendix E. In order for the program to operate, it was necessary to develop a Perl module to support a port of FORTRAN Gamma functions of Press and others (1992) and another module specifically for the L-gamma distribution. These modules are `GammaFunctions.pm` and `LGammaDistribution.pm` and also are listed in Appendix E. The mean and L-scale of the L-gamma distribution can not be solved for using the Incomplete Gamma function for $c < 0$; for the entries corresponding to a $c < 0$, direct simulation of the L-gamma distribution and subsequent computation of the L-moments was performed. The simulated values in tables D#.3 and D#.4 are denoted by a leading "s" on the table entries. Comparison of the entries with the simulated values to neighboring non-simulated cells suggests a smooth and anticipated transition from one cell to another. The performance of the simulation appears acceptable.

Parameter Estimation Example

To illustrate the use of the parameter space tables, consider the solution for a data set with a median of $M = 0.54$ and inter-tercile range of $ITR = 0.48$. From table D5.1, b is equal to 2.504 and from table D5.2, c is equal to 2.239. The L-gamma distribution corresponding to these parameter values is shown on figure 62. The mean and L-scale values of a $\Lambda(2.504, 2.239)$ are available in tables D5.3 and D5.4, respectively. From table D5.3 and the entry for $M = 0.54$ and $ITR = 0.48$, the mean is 0.513. From table D5.4 and the entry for $M = 0.54$ and $ITR = 0.48$, the L-scale is 0.199. Finally, the value for the upper tercile is

$$UT = Q(2/3) = (2/3)^{2.504} e^{2.239(1-2/3)} = 0.764,$$

and the value for the lower tercile is

$$LT = Q(1/3) = (1/3)^{2.504} e^{2.239(1-1/3)} = 0.284.$$

Dashed vertical lines along the median and the terciles have been included in the figure for clarity and intersecting horizontal dashed lines correspond to the values for the median and the upper and lower terciles. Experiments (not presented here) suggest that the Govindarajulu distribution often mimics the shape of the L-gamma distribution when b and c are greater than one and similar in value. The Power distribution is considerably different from either of the other two distributions shown in the figure.

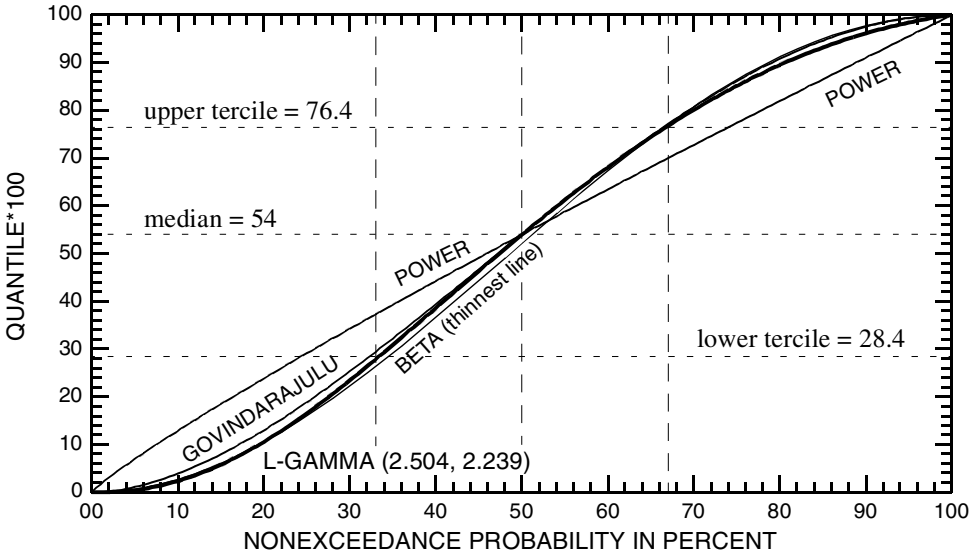

Figure 62. Comparison between the L-gamma distribution fit to a median of 0.54 and L-scale of 0.24 and Govindarajulu and Power distributions fit to the same median and the Beta distribution fit to L-scale and the mean of the L-gamma distribution

Although, it does not have a quantile function form, the Beta distribution (Ross, 1994, pp. 235–236; Evans and others, 2000, pp. 34–42) is numerically integrated quantile bounds of 0 and 1. Because the Beta distribution is well known it also is shown on figure 62. The probability density function of the Beta distribution is

$$f(x) = \frac{1}{B(a, b)} x^{a-1}(1-x)^{b-1} \text{ for } 0 < x < 1 \tag{88}$$

where

$$B(a, b) = \int_0^1 x^{a-1}(1-x)^{b-1} dx \tag{89}$$

and a and b are shape parameters. Parameter estimation for the Beta distribution is straightforward using the product moments (mean and variance) in terms of the parameters as follows.

$$E[X] = \mu = \lambda_1 = \frac{a}{a+b}, \text{ and} \tag{90}$$

$$Var[X] = E[X^2] = \sigma^2 = (\lambda_2\sqrt{\pi})^2 = \frac{ab}{(a+b)^2(a+b+1)}. \tag{91}$$

The parameters in terms of the "moments" (Evans and others, 2000, p. 40) are

$$a = \lambda_1\left(\frac{\lambda_1(1-\lambda_1)}{(\lambda_2\sqrt{\pi})^2} - 1\right), \text{ and} \tag{92}$$

$$b = (1-\lambda_1)\left(\frac{\lambda_1(1-\lambda_1)}{(\lambda_2\sqrt{\pi})^2} - 1\right). \tag{93}$$

The product moment variance (σ^2) can be estimated using L-scale as ($(\lambda_2\sqrt{\pi})^2$) according to the preference of the "true devotee of L-moments" (Hosking, 1990, p. 117). Using a mean and L-scale of 0.513 and 0.199, respectively, Beta parameter estimates are 0.517 and 0.491 for a and b, respectively. The quantiles for this function also are shown on figure 62. The Beta distribution is used for comparisons to the L-gamma in the next chapter.

The steepest portion of the L-gamma distribution on figure 62 exists where the second derivative of the function is zero. Using eq. 61.2 and substituting $b = 2.504$

and $c = 2.239$, setting the equation to zero, and solving for F, a value of $F = 0.412$ is determined. Thus the L-gamma distribution is steepest at this nonexceedance probability; this is confirmed by inspection of figure 62 confirms. The rate of change is computed using the first derivative (eq. 61.1), substituting the values for b, c, and F, the first derivative is 1.55 percent per percent.

A second and more involved parameter estimation example is needed to fully illustrate the M-MLM. Suppose a data set has a mean of 66 percent (0.66) and an L-scale of 17 percent (0.17). After browsing the tables D#.3 and D#.4, it is determined that tables D4.3 and D4.4 contain cells with matching column and row locations that contain entries whose values approximate the mean and L-scale of the data. Specifically, the entries of 0.659 (table D4.3) and 0.168 (table D4.4) for mean and L-scale, respectively, are located on for the median row of 0.75 and ITR column of 0.33 and are closest to the 0.66 (mean) and 0.17 (L-scale) values of the data. Hence, it is estimated the an L-gamma distribution with a mean of 0.66 and L-scale of 0.17 has a median of 0.75 and ITR of 0.33. It follows from table D4.1 that the b parameter is 1.195 and from table D4.2 that the c parameter is 1.081.

Verification of Theoretical L-moments

Validation of the derivations of the L-moments for the L-gamma distribution is needed. Example computations presented in this section verify eqs. 63–81. Consider an L-gamma distribution having parameter values of 3 and 1 for b and c, respectively.

The sample L-moment statistics of the $\Lambda(3, 1)$ L-gamma computed from unbiased estimators for the distribution are listed in table 26. The sample comprised 200 quantile values computed between $0 \leq F \leq 1$ at 0.05 nonexceedance probability spacing intervals. The computer program `useLgammaDistribution.pl` was used to compute the quantiles. The program is available in Appendix E.

In order to evaluate the theoretical L-moments of the L-gamma, values for the Gamma and Incomplete gamma functions are required. A computer program, `useGammaFunctions.pl` was written based on algorithms provided by Press and others (1992) to compute the values. The program is available in Appendix E. The output of the program for $b = 3$ and various values of $b + i$ in which i is an integer are shown on figure 63. The values for each function seen in the figure are used in the following computations.

Table 26. Comparison of theoretical L-moment and sample L-moment statistics for L-gamma distribution chosen for the verification example

[L-CV, coefficient of L-variation. Percent difference is computed by theoretical value minus sample estimate divided by theoretical value. The L-gamma distribution has values for *b* and *c* of 3 and 1, respectively. Supporting computation are described in the text.]

Moment type	Moment symbol	Sample estimates	Theoretical values	Percent difference
Mean	λ_1	31.1	31.0	-0.32
L-scale	λ_2	17.0	16.8	-1.2
L-CV	τ	.546	.542	-.74
L-skew	τ_3	.242	.238	-1.7
L-kurtosis	τ_4	-.0047	-.0046	2.2

The theoretical mean is computed by eq. 67, and the computation steps are

$$\lambda_1 = \frac{e^c}{c^{b+1}}\Gamma(b+1)P(b+1, c),$$

$$\lambda_1 = \frac{e^1}{1^4}\Gamma(4)P(4, 1), \text{ and}$$

$$\lambda_1 = 2.7182818 \times 6 \times 0.018988157 = 0.30969097.$$

```
[asquith@linuxhost] useGammaFunctions.pl
a and x for Gamma function, G(a) and
 Incomplete Gamma function, P(a,x) are required on command line
[asquith@red1ast]$ useGammaFunctions.pl 3 1
# Arguments are: a=3 and x=1
#   G(a):G(3)=1.99999999999998
# P(a,x):P(3,1)=0.0803013962397842
# G(a)*P(a,x) = 0.160602792479567

[asquith@linuxhost] useGammaFunctions.pl 4 1
# Arguments are: a=4 and x=1
#   G(a):G(4)=5.99999999999994
# P(a,x):P(4,1)=0.0189881568125562
# G(a)*P(a,x) = 0.113928940875336

[asquith@linuxhost] useGammaFunctions.pl 5 1
# Arguments are: a=5 and x=1
#   G(a):G(5)=23.9999999999997
# P(a,x):P(5,1)=0.00365984676374598
# G(a)*P(a,x) = 0.0878363223299026

[asquith@linuxhost] useGammaFunctions.pl 6 1
# Arguments are: a=6 and x=1
#   G(a):G(6)=119.999999999998
# P(a,x):P(6,1)=0.000594184813061848
# G(a)*P(a,x) = 0.0713021775674208

[asquith@linuxhost] useGammaFunctions.pl 7 1
# Arguments are: a=7 and x=1
#   G(a):G(7)=720.000000000005
# P(a,x):P(7,1)=8.32411489880215e-05
# G(a)*P(a,x) = 0.0599336272713759
```

Figure 63. Gamma and Incomplete Gamma function computation results for theoretical L-moments of L-gamma distribution verification example—G(a) is the Gamma function and P(a,x) is the Incomplete Gamma function

The theoretical L-scale of the distribution is computed by eq. 69. Steps of the computation are shown below.

$$\lambda_2 = \frac{2e^c}{c^{b+2}}\Gamma(b+2)P(b+2, c) - \lambda_1 ,$$

$$\lambda_2 = \frac{2e^1}{1^5}\Gamma(5)P(5, 1) - 0.3097 , \text{ and}$$

$$\lambda_2 = 5.4365637 \times 24 \times 0.0036598468 - 0.30969097 = 0.16783680 .$$

It follows that L-CV from eq. 71 is

$$\tau = \lambda_2 / \lambda_1 = 0.16783680 / 0.30969097 = 0.54194929 .$$

The theoretical third L-moment of the distribution is computed by eq. 75.2. Steps of the computation are shown below.

$$\lambda_3 = \frac{6e^c}{c^{b+3}}\Gamma(b+3)P(b+3, c) - 3\lambda_2 - 2\lambda_1 ,$$

$$\lambda_3 = \frac{6e^1}{1^6}\Gamma(6)P(6, 1) - 3(0.16783680) - 2(0.30969097) ,$$

$$\lambda_3 = 16.309691 \times 120 \times 0.00059418481 - 1.1228923 , \text{ and}$$

$$\lambda_3 = 0.040024136 .$$

It follows that L-skew from eq. 77 is

$$\tau_3 = \lambda_3 / \lambda_2 = 0.040024136 / 0.16783680 = 0.23847056 .$$

The theoretical fourth L-moment of the distribution is computed by eq. 80. Steps of the computation are shown below.

$$\lambda_4 = \frac{20e^c}{c^{b+4}}\Gamma(b+4)P(b+4,c) - 5\lambda_3 - 9\lambda_2 - 5\lambda_1 ,$$

$$\lambda_4 = \frac{20e^1}{1^7}\Gamma(7)P(7,1) - 5(0.040024136) - 9(0.16783680) - 5(0.30969097) ,$$

$$\lambda_4 = 54.365637 \times 720 \times 0.000083241149 - 3.2591067 , \text{ and}$$

$$\lambda_4 = -0.00077690102 .$$

It follows that L-kurtosis from eq. 81 is

$$\tau_4 = \lambda_4/\lambda_2 = -0.00077690102/0.16783680 = -0.0046289075 .$$

The theoretical values for the mean, L-scale, L-CV, L-skew, and L-kurtosis also are listed in table 26. In general, there is agreement between the sample estimates and the theoretical values. The percent differences are all small. Therefore, it is concluded that the derivations shown in eqs. 63–81 are correct. It is important to note that careful track of a substantial number of decimal places in the above computations is required. Eight significant figures were propagated through all of the above computations. Fewer significant figures rapidly cause divergence in the sample estimates and the theoretical values.

Chapter Conclusions

The two-parameter L-gamma distribution is expressible in an algebraically simple quantile function. The distribution has bounds of zero and one. The bounds of the distribution are attractive from the standpoint of modeling data sets expressed in percentage such as dimensionless hyetographs. The distribution is symbolically related to the probability density function of the well-known Gamma distribution. When restrictions on parameter values are made, the function is monotonically increasing with nonexceedance probability, which is a requirement of a quantile distribution function.

The L-moments of the L-gamma can be defined, but parameter estimation by the Method of L-moments using the L-moments alone is difficult; complex numerical techniques are required. A modified Method of L-moments for parameter estimation was presented instead. The modified Method of L-moments is suggested and is based on the median and inter-tercile range. Although numerical techniques are still required with the modified method, the problem of parameter estimation is considerably more tractable. Using the modified method fortuitously increases the usable parameter space of the distribution into a $c < 0$ region.

The parameter space of the L-gamma distribution in terms of the median and inter-tercile range was mapped and lookup tables for parameter estimation are provided in Appendix D. Examples of table usage are provided. Illustrative computations of the

theoretical L-moments of a specified L-gamma distribution agree with sample estimates—the derivations are verified.

Finally, a generalized L-gamma distribution can be formulated

$$\Lambda(A, B, b, c) = A + B \times F^{b} e^{c(1-F)}, \tag{94}$$

where A and B are location and scale parameters, respectively, and b and c remain shape parameters.

CHAPTER 7
L-GAMMA MODEL OF DIMENSIONLESS RAINFALL HYETOGRAPHS KNOWN TO PRODUCE RUNOFF IN TEXAS

Introduction

In this chapter, the L-gamma distribution is used to model dimensionless runoff-producing hyetographs in Texas. Much of the analysis is an extension of chapters 3 and 5 and application of chapter 6. L-gamma distribution hyetograph models are fit in this chapter to the estimates of the mean and L-scale values of the hyetograph distributions. Statistics from the chapter 5 provide the basis for fitting the model. The L-gamma models are compared to those from chapter 3. The comparison is enhanced by inclusion of Beta distribution modeled hyetographs. The Beta distribution has been used to model dimensionless streamflow hydrographs in an analogous fashion to the hyetograph analysis here (Yue and others, 2002). The suitability of the L-gamma hyetograph model also is considered, and an alternative hyetograph analysis technique is used in the suitability assessment.

L-gamma Model

Each pair of mean and L-scale statistics (a statistic set) in table 25 can be used to estimate the expected hyetograph. The L-gamma distribution can be fit to a statistic set and the expected hyetograph defined. However, some of the statistics in table 25 are more favorable than others. The estimated parameters of the L-gamma distribution for the corresponding favorable statistic sets and duration are listed in table 27. The Dallas data was not used for the 24 hr and greater (up to about 3 days) storm duration; the mean and L-scale values listed within the parenthesis in table 25 were used. The tables

of the L-gamma distribution solution space in Appendix D were used as a first approximation of the parameters. Subsequently, modified versions of the `solutionspaceLGamma.pl` program with restricted but higher resolution iterations were used to improve the parameter estimates to four significant figures. The parameters were then verified by computation of sample L-moments directly from the distribution.

Table 27. L-gamma distribution parameter estimates for modeling dimensionless hyetographs for 0–12 hr, 12–24 hr, and 24 hr and greater storm durations and one inch and greater storm depths

[The statistics without the Dallas hyetographs were used for the 24 hr and greater duration.]

Parameter of L-gamma distribution, $\Lambda(b, c)$	Double one-percent tail trimming		
	0–12 hr duration (percent)	12–24 hr duration (percent)	24 hr and greater duration (percent)
Parameter estimates from mean of values for the values of the hyetograph statistics			
b	0.7679	0.4775	0.2945
c	.1436	-.3866	-.7907
Parameter estimates from median of values for the values of the hyetograph statistics			
b	.9105	.5879	.3277
c	.4297	-.1475	-.7929
Parameter estimates from graphically estimated modes for the values of the hyetograph statistics			
b	1.262	.7830	.3388
c	1.227	.4368	-.8152

Not all of the mean and L-scale statistics in table 25 are favorable and used for parameter estimates reported in tables 27 and 28 for reasons now described. The author strongly believes that the double one-percent tail trimming method produces more reliable statistics of the hyetograph than the absence of a tail trimming method. Figure 23 and the supporting discussion of the figure provides firm justification that

some tail trimming is required. The right-most columns in table 25 thus explicitly are not considered here. Since the no-tail-trimmed statistics are prudently reported in table 25, other researchers could fit the L-gamma or Beta distributions to the data. The author has concluded that the modal analysis (see subsection *Modal Analysis of Hyetograph Statistics* in chapter 5) produces the most favorable mean and L-scale statistics for the 0–12 hr and 12–24 hr storm durations. And finally, the author considers reliable estimation of the 24 hr and greater duration hyetograph is problematic because of the perceived greater heterogeneity of the long-duration hyetographs. However, fitted distribution models for all of the statistic sets, including the 24 hr and greater duration and not just the graphical mode statistic sets, are presented in this chapter for completeness and for the benefit of other researchers.

The expected hyetographs defined by the L-gamma distribution fit to each parameter pair in table 27 are shown on figures 64 and 65. Each graph on figure 64 shows a comparison between the three statistic estimation methods for a specific duration. Each graph on figure 65 shows a comparison between durations for each of the three statistic estimation methods. Figures 64 and 65 compliment each other.

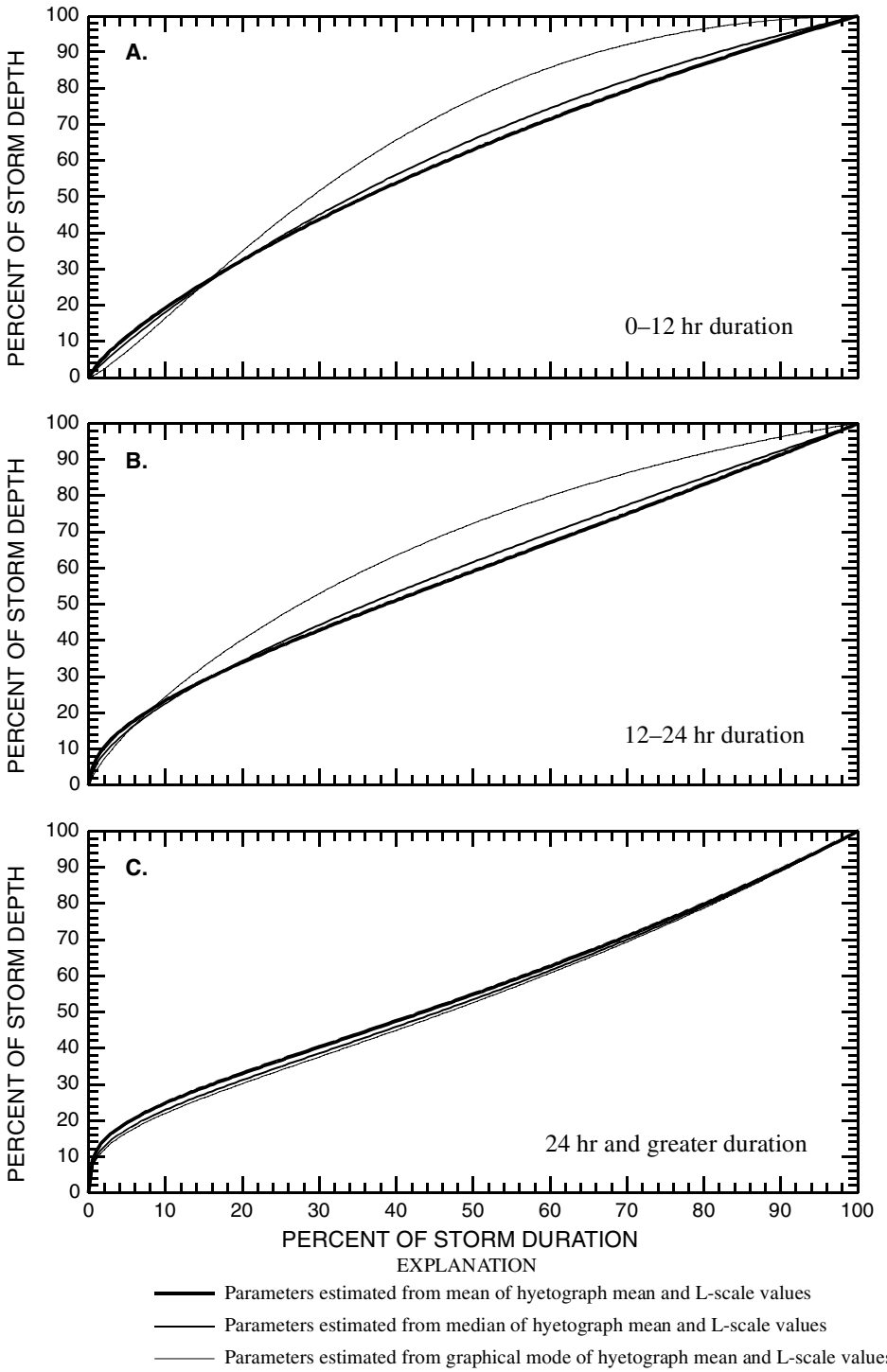

Figure 64. Comparison between statistic estimation method for L-gamma distribution hyetograph models for 0–12 hr, 12–24 hr, and 24 hr and greater storm durations and one inch and greater storm depths

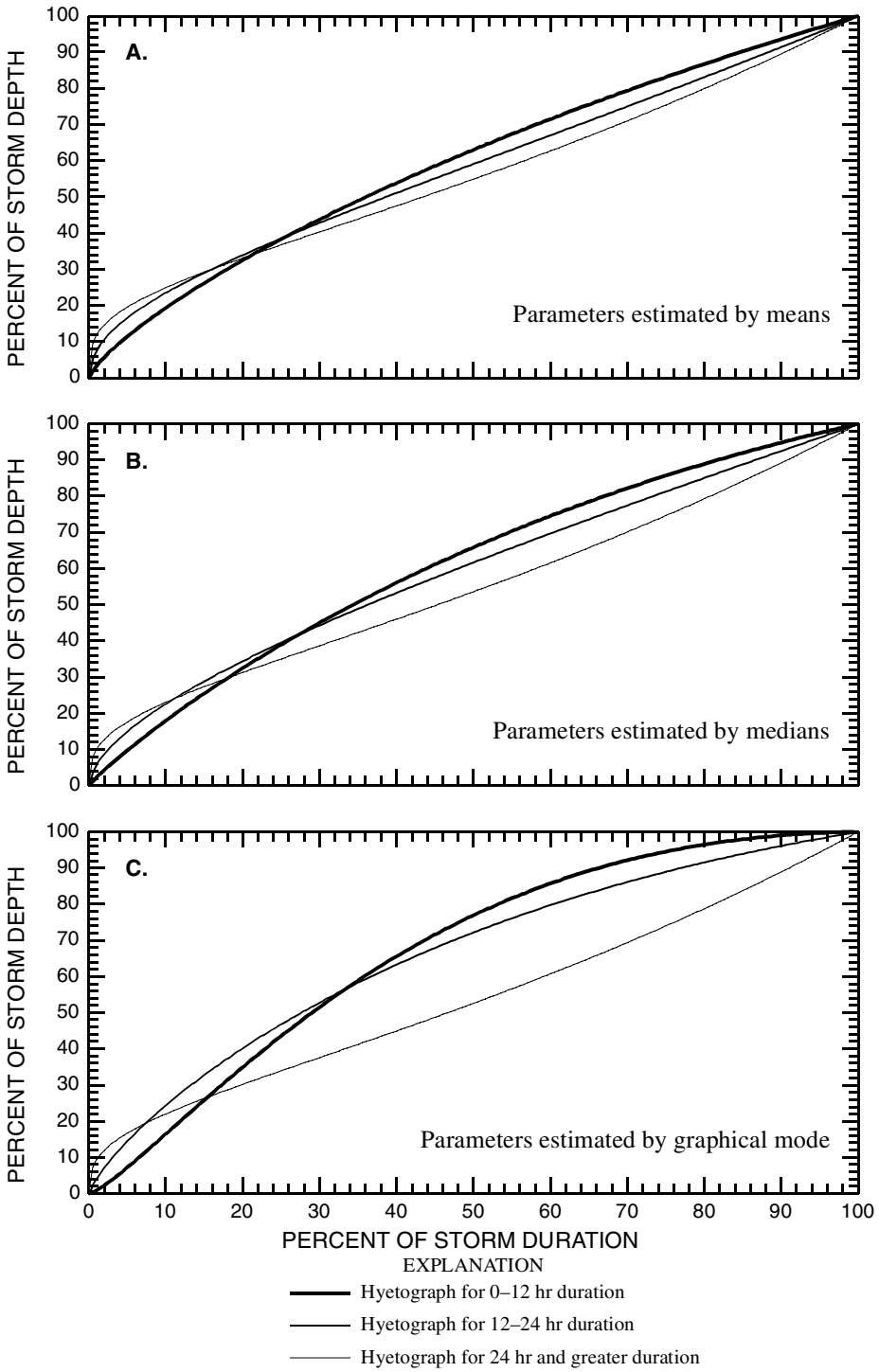

Figure 65. Comparison between L-gamma distribution hyetograph models for 0–12 hr, 12–24 hr, and 24 hr and greater storm durations and one inch and greater storm depths for each statistic estimation method

In general the curves for each statistic estimation procedure (fig. 64) are similar. The modal curves (thinnest lines) for the 0–12 hr and 12–24 hr duration are the most distinct from the other two curves. The largest differences are exhibited by the 0–12 hr modal curve. For the other durations the method of statistic estimation has limited influence on the defined expected hyetograph. Alternative curve groups are presented on figure 65 because the relative differences between the expected hyetograph for the three durations are easily visualized within each graph. For each statistic estimation method from figure 65, it is obvious that the 0–12 hr expected hyetograph has the smallest rainfall rates (as measured in percent and not absolute magnitude) early in the duration, but throughout the bulk of the storm duration larger rates are exhibited. Both the expected hyetographs for the 12–24 hr and 24 hr and greater durations have relatively large percentage rainfall rates at the storm beginning, which is followed by a period of reduced rates until the end of the storm. The L-gamma model suggests that the 24 hr and greater expected hyetograph exhibits a second period of increased rainfall rates near the end of the storm. This behavior is evidenced by the 24 hr and greater curve bending up as the end of the storm is approached. Finally, both the expected hyetographs for 12–24 hr and 24 hr and greater durations have large rainfall rates at very small duration percentages; a method to estimate more reasonable rainfall rates is described later.

Beta Model

Each pair of mean and L-scale statistics (a statistic set) in table 25 can be used to estimate the expected hyetograph using the Beta distribution. The Beta distribution can be fit to a favorable statistic set (see previous section for discussion of favorable statistics). The estimated parameters of the Beta distribution are listed in table 28. The Dallas data was not used for the 24 hr and greater duration; the mean and L-scale values listed within the parenthesis in table 25 were used. Equations 92 and 93 were used to estimate the parameters. The Beta distributions corresponding to each parameter in table 28 are shown on figures 66 and 67.

Table 28. Beta distribution parameter estimates for modeling dimensionless hyetographs for 0–12 hr, 12–24 hr, and 24 hr and greater storm durations and one inch and greater storm depths

[The statistics without the Dallas hyetographs were used for the 24 hr and greater duration.]

Parameter of Beta distribution	Double one-percent tail trimming		
	0–12 hr duration	12–24 hr duration	24 hr and greater duration
	(percent)	(percent)	(percent)
Parameter estimates from mean of values for the values of the hyetograph statistics			
a	1.305	1.622	1.815
b	.8848	1.165	1.426
Parameter estimates from median of values for the values of the hyetograph statistics			
a	1.194	1.517	1.688
b	.7636	1.033	1.392
Parameter estimates from graphically estimated modes for the values of the hyetograph statistics			
a	.9616	1.435	1.638
b	.4736	.7394	1.396

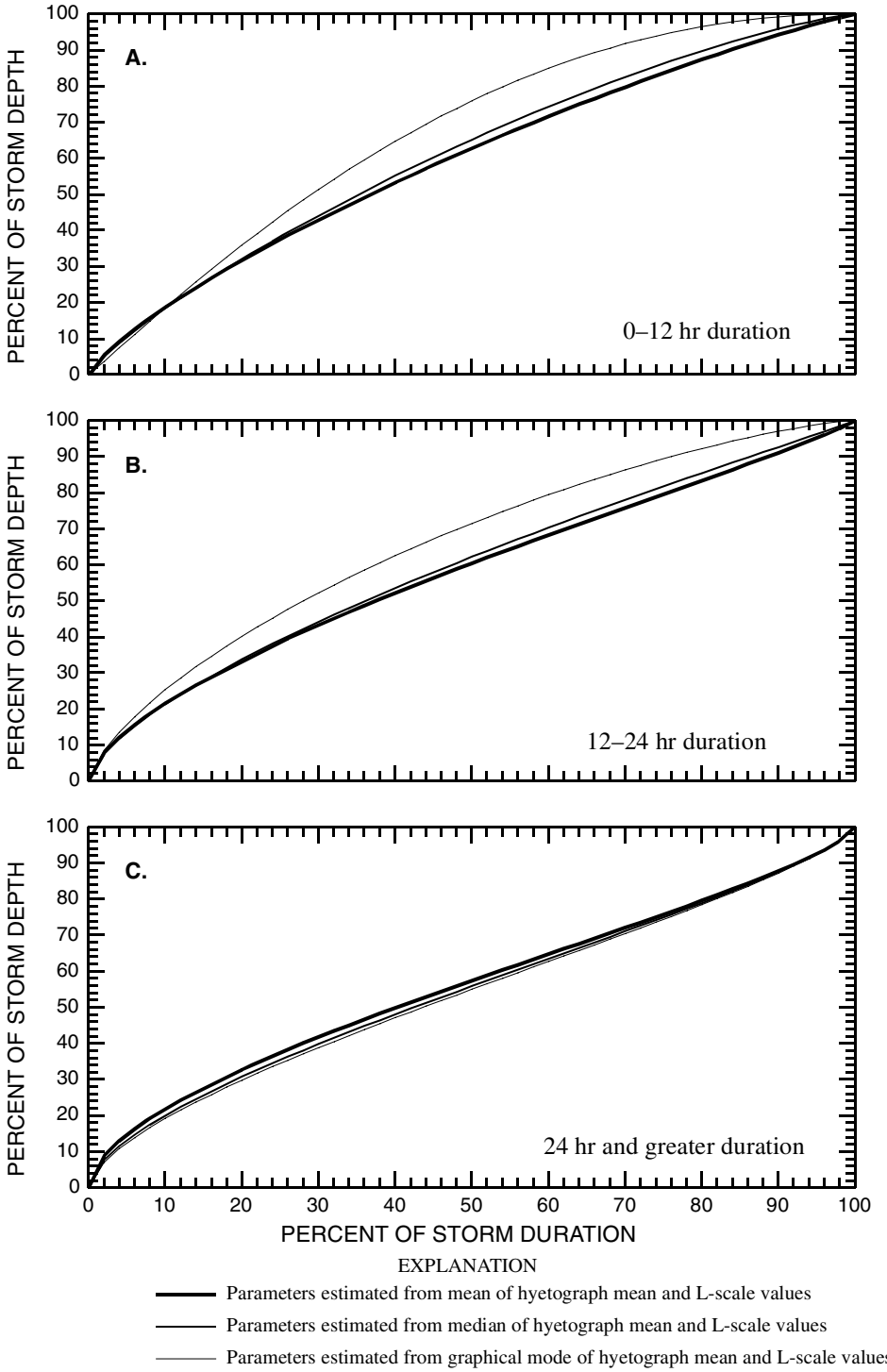

Figure 66. Comparison between statistic estimation method for Beta distribution hyetograph models for 0–12 hr, 12–24 hr, and 24 hr and greater storm durations and one inch and greater storm depths

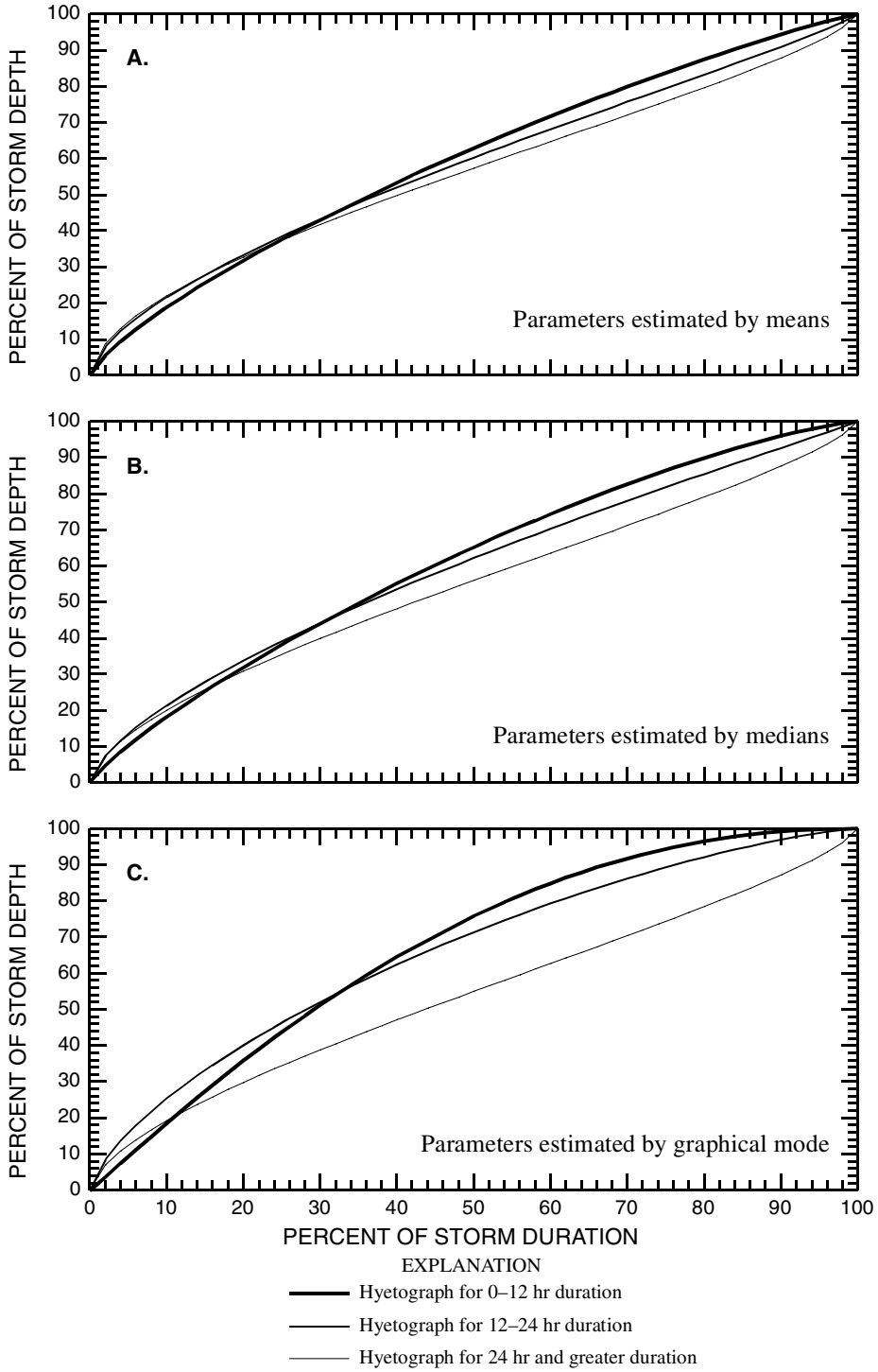

Figure 67. Comparison between Beta distribution hyetograph models for 0–12 hr, 12–24 hr, and 24 hr and greater storm durations and one inch and greater storm depths for each statistic estimation method

The BETAINV function of the well known Excel™ spreadsheet software package by Microsoft™ (*http://www.microsoft.com*) was used to compute the ordinates. Each graph on figure 66 shows a comparison between the three statistic estimation methods (mean, median, graphical mode) for a specific duration. Each graph on figure 67 shows a comparison between durations for each of the three statistic estimation methods. Figures 66 and 67 compliment each other.

Similar observations as made for the expected hyetographs using the L-gamma distribution in the previous subsection (figs. 64 and 65) are made for the expected hyetographs modeled using the Beta distribution. Some notable differences are described in the next section.

Model Comparison

The L-gamma distribution models of the expected hyetograph for the three durations based on the graphical modes of the mean and L-scale statistics are presented on figure 68. The author has judged that the graphical modes of the mean and L-scale provide the most reliable values for the expected hyetographs. Therefore, only these modal-based expected hyetographs are considered on the figure. The other statistics were prudently presented so that other researchers could fit the L-gamma or Beta distributions.

The triangular models (see chapter 3) of the hyetograph also are shown on figure 68. It is apparent that the L-gamma models are distinctively different in shape than those of the triangular models. The shape differences are due to differing functional

forms and the number of parameters. Since the L-gamma distribution was fit to both the mean and L-scale instead of solely the mean as is done for the triangular model, the L-gamma distribution is statistically preferable as it better mimics observed hyetographs. The peak rainfall rates for the triangular model occur at about 30 to 40 percent of the duration. All three L-gamma hyetographs exhibit their peak rainfall rates either at the beginning of the storm (12–24 hr and 24 hr and greater duration) or at about 12 percent (0–12 hr duration). In general, the L-gamma models predict more uniform rainfall rates than the triangular models do. This is evidenced by the more constant shape of the L-gamma curves.

The Beta distribution also is a two-parameter distribution and therefore would arguably mimic the data in a fashion equivalent to the L-gamma because both distributions are fit to the same statistics. Because the distributions are not fit to high-order L-moments such as L-skew and L-kurtosis, differences in the model tails or specifically near the beginning and ending of the storm are expected. Comparisons showing differences between the Beta and the L-gamma hyetograph models for each duration for each statistic estimation method (mean, median, or mode) are shown on figures 69–71. The mean statistic estimation method is represented on figure 69 (derived from graphs A on figures 65 and 67), the median method on figure 70 (derived from graphs B on figures 65 and 67), and the graphical mode method on figure 71 (derived from graphs C on figures 65 and 67).

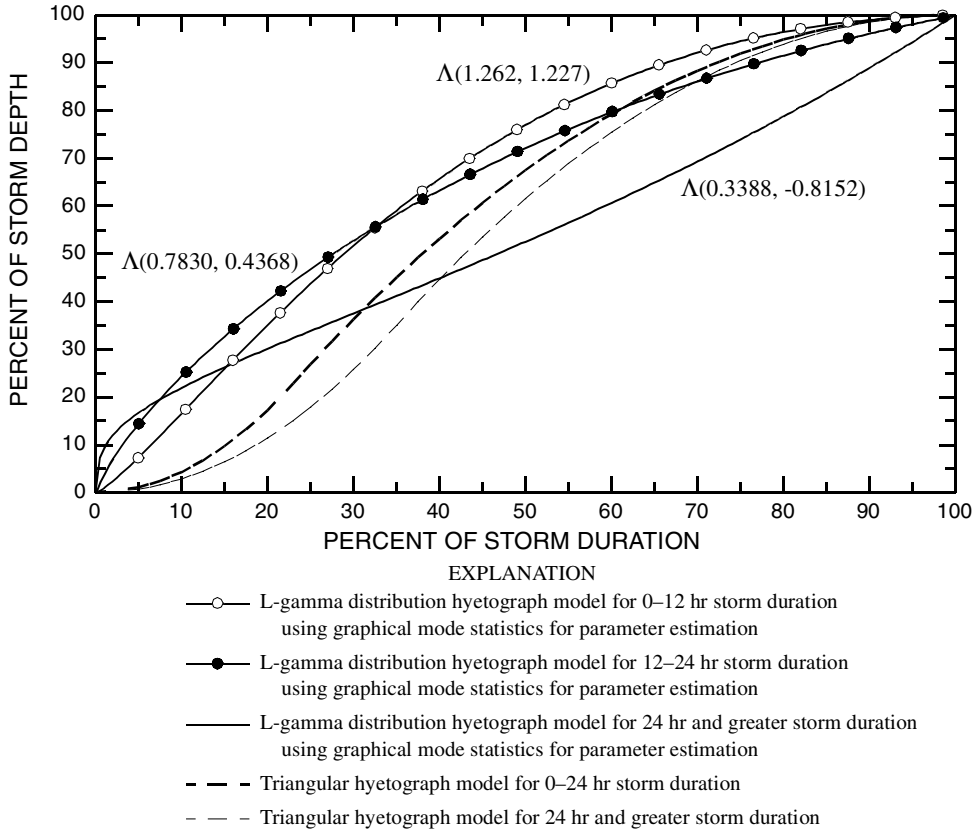

Figure 68. Comparison of L-gamma distribution and triangular hyetograph models for 0–12 hr, 12–24 hr, and 24 hr and greater storm durations and one inch and greater storm depths

Inspection of the figures suggests the Beta distribution mimics the L-gamma or alternatively the L-gamma distribution mimics the Beta. One notable difference between the curves is that expected hyetographs for the 12–24 hr and 24 hr and greater durations do not have as high rainfall rates as the corresponding curves for the L-gamma distribution.

Although the two distributions provide very similar fits, the L-gamma distribution model is preferable because it is expressed in a quantile function form. This makes the model simple to use and construction of the hyetograph straightforward as the analyst

is not encumbered with numerical integration and inversion necessary to use the Beta distribution. Furthermore, the first and second derivatives of the L-gamma are simple and permit direct computation of percentage rainfall rates. Example computation of rainfall rates are now presented.

Computation of the maximum or incremental rainfall rates of expected hyetographs as measured by percent of storm depth can be important in practice. The maximum *instantaneous* rate for the 0–12 hr duration is straightforward. The second derivative (eq. 61.2) with $b = 1.262$ and $c = 1.227$ is used to solve for the percent of storm duration with the largest rate; the largest rate is at $F = 11.3$ percent. The first derivative (eq. 61.1) with $b = 1.262$, $c = 1.227$, and $F = 0.113$ then provides a maximum rate of 1.88 percent storm depth per percent storm duration. Suppose that an application requires a 12 hr duration and a rainfall depth of 6.9 in. (175.3 mm). The duration and depth values match those in the *Example Application* section in chapter 3. The largest rainfall rate using the 0–12 hr expected hyetograph thus is 1.08 in./hr (1.88×6.9 in. / 12 hr) or 27.5 mm/hr. The 1.08 in./hr rate is considerably larger than the 0.748 in./hr (19.0 mm/hr) rate predicted by the 0–24 hr triangular hyetograph (see the previously referenced *Example Application* section).

The maximum rainfall rates for the 12–24 hr and 24 hr and greater durations are more problematic because the first derivative (eq. 61.1) is very large for very small values of F. Therefore, it is suggested that the maximum rainfall rate be defined at the

first increment of the hyetograph. Discrete hyetographs are often used in practice. For example, suppose an application requires a hyetograph duration of 48 hr and 15-minute time steps for the hyetograph are to be defined. Fifteen minutes (min) represents about 0.521 percent of the duration [100 × 15 min / (48 hr × 60 min)]. The first derivative at $F = 0.00521$ is

$$e^{-0.8152(1-0.00521)}[0.3388(0.00521)^{0.3388-1} - -0.8152(0.00521)^{0.3388}] \text{ or}$$

about 4.93 percent storm depth per percent storm duration. If the 48 hr rainfall depth for the application is 10 in. (254 mm), then the rainfall rate at the first 15-minute increment is 1.03 in./hr (4.93 × 10 in. / 48 hr) or 26.1 mm/hr. For comparison, the rainfall rate at the second 15-minute increment ($F = 0.0104$) is 3.17 percent of storm depth per percent storm duration or 0.661 in./hr (16.8 mm/hr).

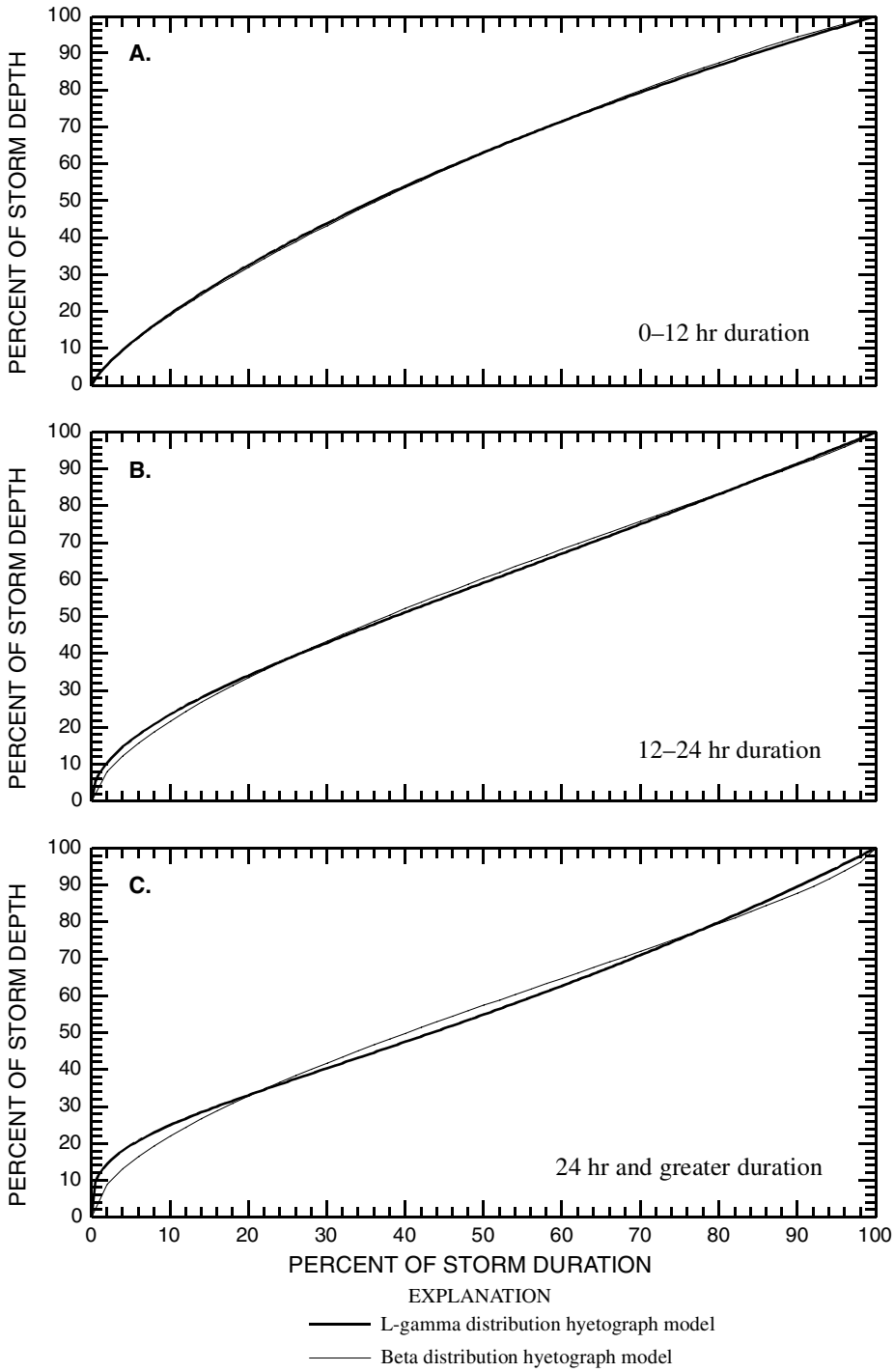

Figure 69. Comparison between L-gamma and Beta distribution hyetograph models for 0–12 hr, 12–24 hr, and 24 hr and greater storm durations and one inch and greater storm depths using the mean statistics for parameter estimation

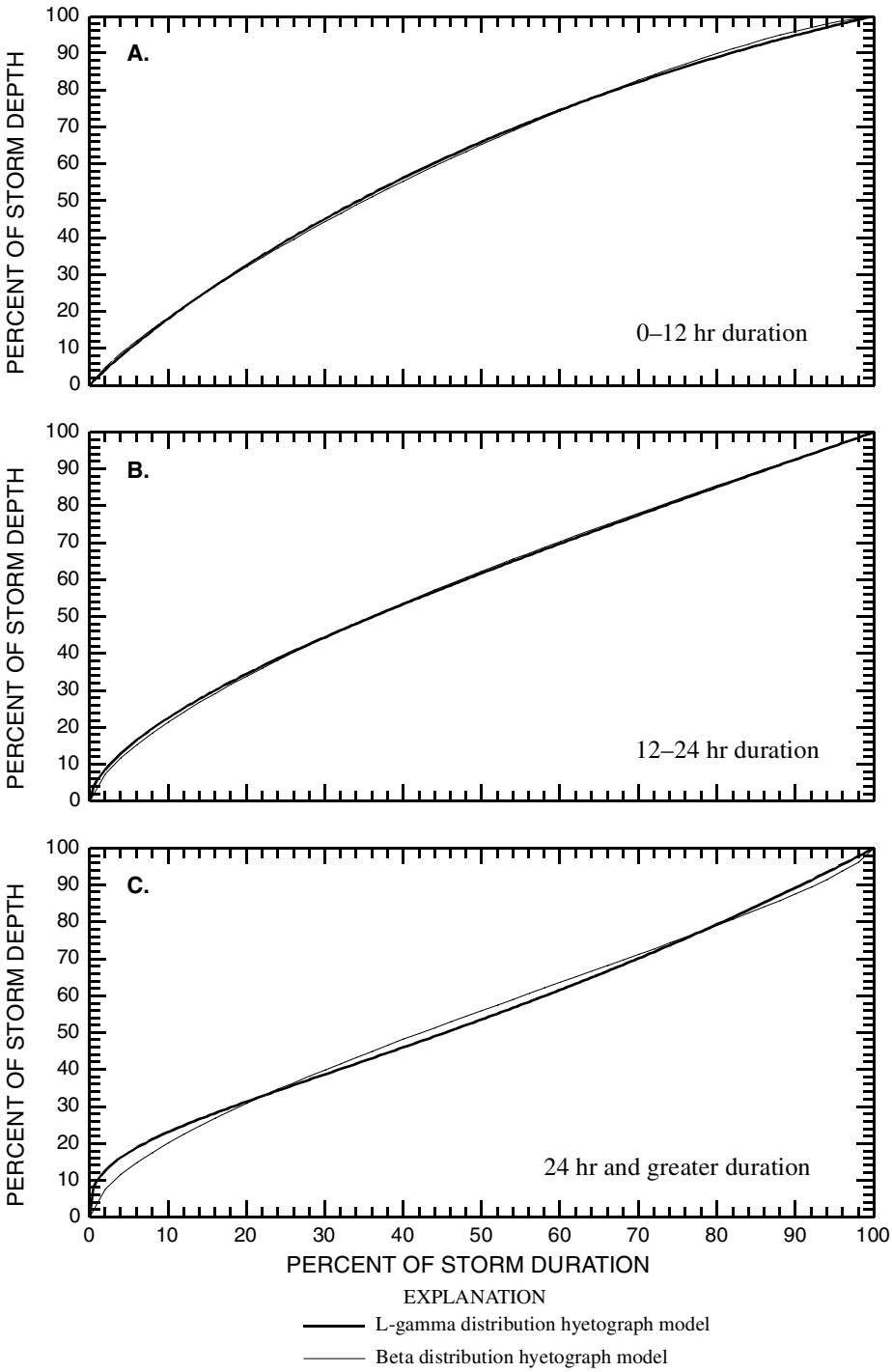

Figure 70. Comparison between L-gamma and Beta distribution hyetograph models for 0–12 hr, 12–24 hr, and 24 hr and greater storm durations and one inch and greater storm depths using the median statistics for parameter estimation

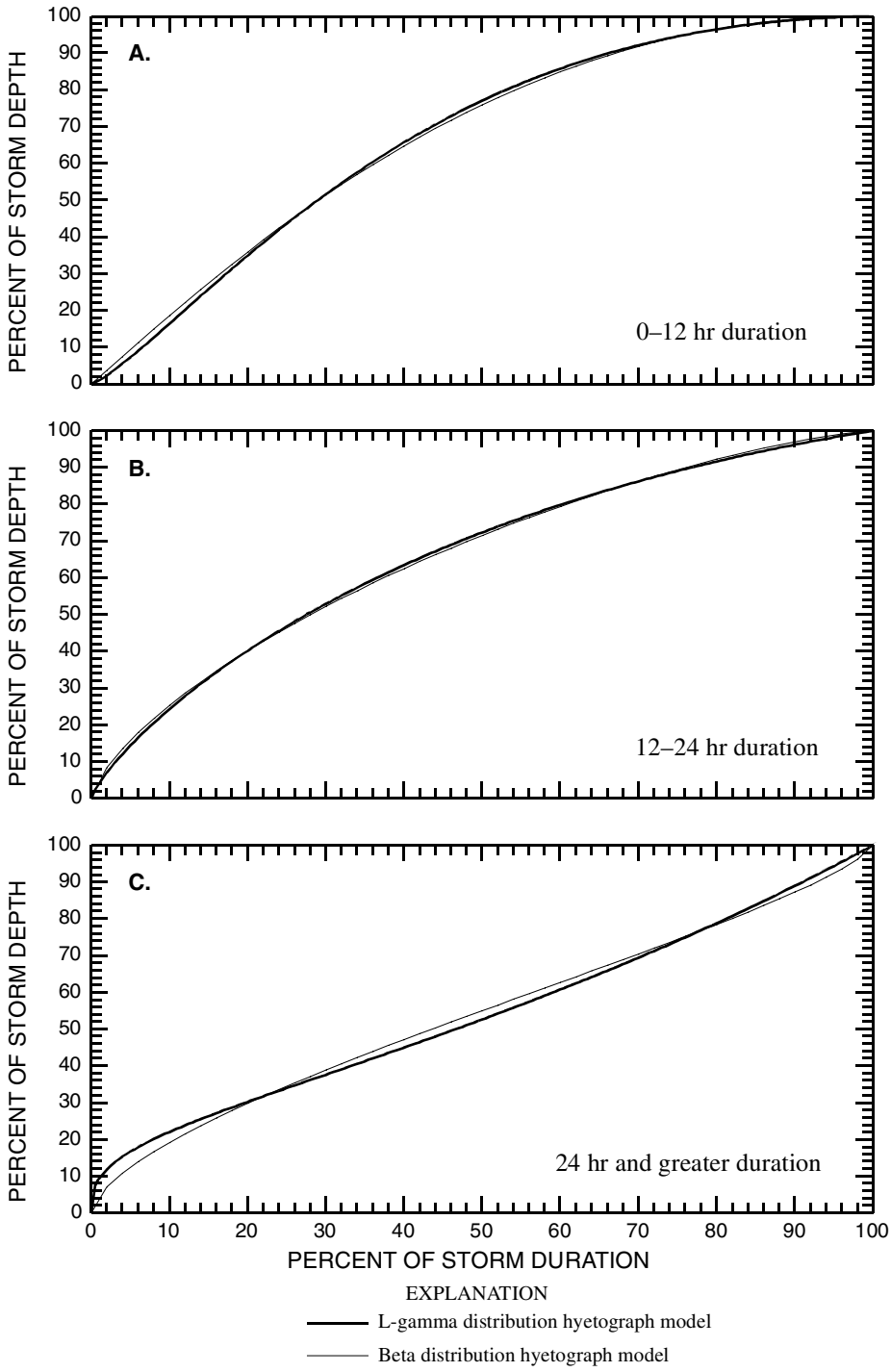

Figure 71. Comparison between L-gamma and Beta distribution hyetograph models for 0–12 hr, 12–24 hr, and 24 hr and greater storm durations and one inch and greater storm depths using the graphical mode statistics for parameter estimation

Model Suitability

The three L-gamma hyetograph models (best illustrated on figure 68) are fit to the most representative values of the dimensionless hyetograph mean and L-scale. The author is concerned that though each model is statistically defensible (acknowledging a weaker defense for the previously discussed heterogeneity for the 24 hr and greater duration) the models might be unsuitable because the models are based on statistics of statistics. It is difficult to visualize how the models are fit to individual hyetographs. The models might be inconsistent with results derived from alternative hyetograph analysis techniques.

To assess suitability of the L-gamma model an alternative analysis of hyetographs that might rely less heavily on complex statistics of statistics, statistical inference, parametric models, and parameter estimation. The analysis is based on duration-interval hyetograph-ordinate statistics and is presented in the following subsection.

Empirical Hyetograph Analysis

The foundation of the alternative hyetograph analysis uses the concept of empirical hyetographs. Empirical hyetographs are produced from statistical analysis of the distribution of dimensionless hyetograph ordinates (percent storm depth) for evenly spaced intervals of storm duration. An *n*-th percentile of each interval defines the *n*-th percentile empirical hyetograph. The construction of empirical hyetographs is performed by decomposing each observed hyetograph (with dimension removed) into 2.5-percent wide intervals of percent storm duration. (A larger and lower resolution

5-percent interval also was investigated.) For the hyetograph ordinates within each interval, percentiles and other statistics are computed. The distribution of hyetograph ordinates is investigated using these interval statistics. Empirical hyetographs provide visualizations of the expected hyetograph without the need for a parametric model such as the triangular model or the Beta and L-gamma distributions. The median of the distribution of hyetograph ordinates within each 2.5-percent interval of percent storm duration defines the 50th percentile empirical hyetograph. Empirical hyetograph analysis also documents the uncertainties in the expected hyetograph—a feature not provided by the parametric models.

It is important to consider that visualization of the influence of individual hyetographs on the model is difficult in the context of previous parametric models because the models are fit to the statistics of other statistics. An excessive degree of smoothing might have occurred. For example, the graphical display of the models on figures such as figure 68 convey little information about the underlying structure of individual hyetographs.

An example of the alternative hyetograph analysis is provided through graphical display on figure 72. The empirical hyetograph (defined by the median statistic) and ancillary statistics for the 0–12 hr duration, and depth greater than 1 in. (25.4 mm) hyetograph is shown in the figure. On graph A of figure 72, each of the 621 events meeting the duration and depth criteria are plotted in a light shade of grey. As

previously done, double one-percent trimming of the leading and trailing tails was performed.

Superimposed on the individual hyetographs is the empirical statistical analysis. On the figure, the median, lower and upper quartiles (25th or 75th percentile), and lower and upper deciles (10th and 90th percentiles) within each 2.5-percent wide interval of percent storm duration are plotted with a star and the line and whisker combinations. A heavy line connecting the medians also has been drawn to help visualize what the expected hyetograph might look like. The mean is plotted as an open circle; early in the storm duration the mean is slightly greater than the median, but generally, the mean is less than the median. Each grouping of statistics are plotted at the mid point or center of the interval.

The means are repeated on graph B of figure 72 with the addition of the sample size within each interval. The sample sizes are reasonably large and therefore the statistics within each interval are expected to be reliable. The reliability is partially evident in that each statistic (median, quartile, decile, and mean) is monotonically or nearly monotonically increasing with percent duration. Some of the sample sizes (801 and 937) for the first and last intervals are each greater than 621 (the total number of hyetographs analyzed). This occurs because of the distribution of data points defining each hyetograph; many hyetographs have multiple points near the 0 percent and 100 percent duration.

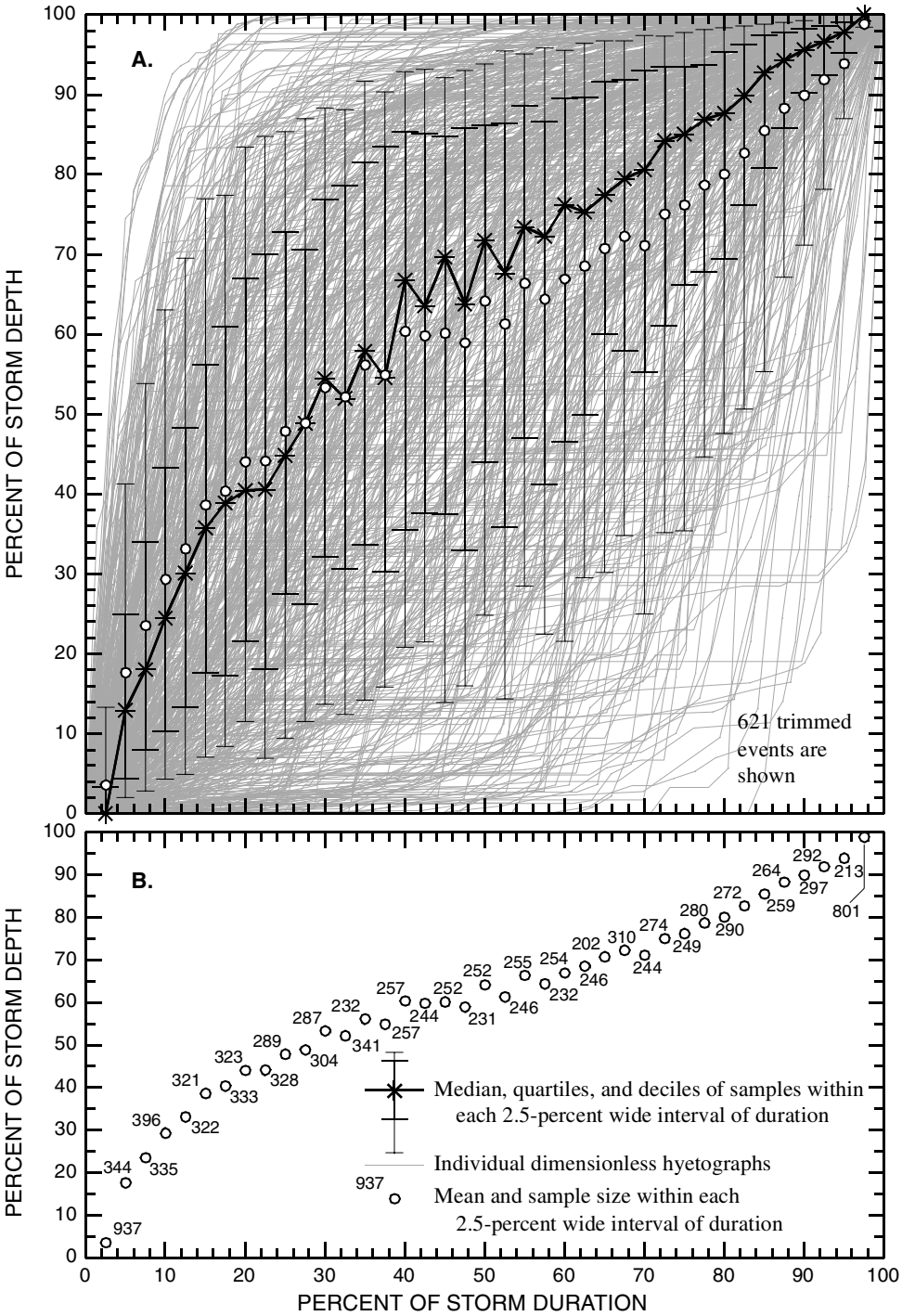

Figure 72. Empirical hyetograph analysis for 0–12 hr storm duration and one inch and greater storm depths

Finally, the empirical hyetographs seem to start after and stop before exactly 0 percent and exactly 100 percent duration. This occurs because of the use of intervals for the analysis and more importantly, the double one-percent tail trimming still leaves repeated 0 and 100 percent values of depth on the tails after the trimmed data was re-expressed in 0–100 percent values. Data fitted hyetographs would necessarily start and stop at 0 and 100 percent.

The empirical hyetographs (10th, 25th, median, 75th, and 90th percentile) for the 0–12 hr duration are repeated on figure 73. Also shown on the figure is the 0–12 hr expected hyetograph estimated by the L-gamma model. It is apparent that both the median empirical hyetograph and the L-gamma expected hyetograph are similar in shape and magnitude for most of the storm duration. It is important to note that because the L-gamma model is estimated in a fundamentally different fashion than the median empirical hyetograph, the L-gamma curve is *not expected* to represent a best fit or even a fit specifically to the median empirical hyetograph. This statement applies for the other two durations (figs. 74 and 75) presented shortly.

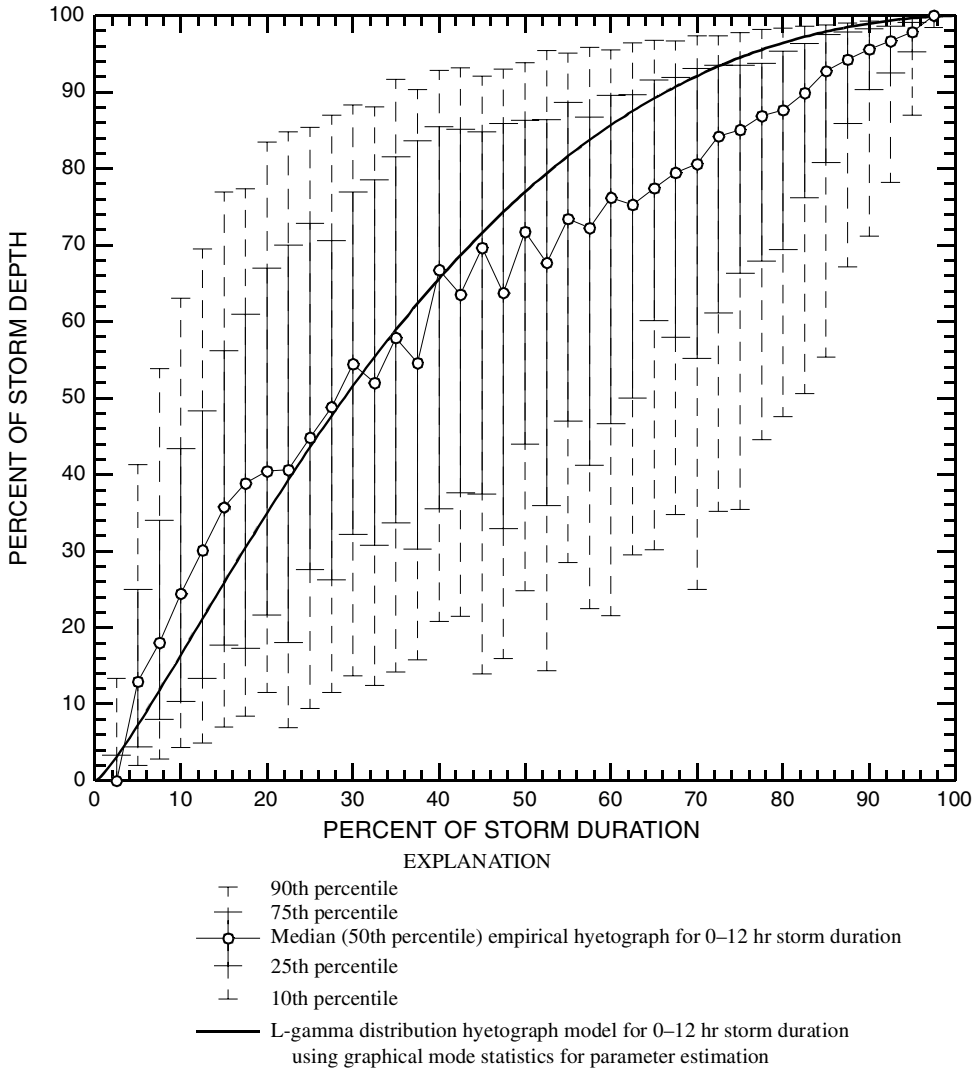

Figure 73. Comparison between empirical hyetographs and the L-gamma distribution hyetograph distribution model for 0–12 hr storm duration and one inch and greater storm depths

The L-gamma hyetograph is necessarily smooth and the empirical hyetograph is not. The general slope of the median empirical hyetograph and the L-gamma hyetograph are similar to about 40 percent of the duration—the two models predict similar rainfall rates. For larger duration percentages the median empirical hyetograph indicates more uniform rainfall rates right to the end of the storm. The L-gamma

model is considered in agreement with the less statistically rigorous empirical hyetographs. Therefore, a conclusion is that the L-gamma model estimates an appropriate runoff-producing the 0–12 hr expected hyetograph for storm depths of one or more inches.

The empirical hyetographs (10th, 25th, median, 75th, and 90th percentile) for the 12–24 hr duration are shown on figure 74. Also shown on the figure is the 12–24 hr expected hyetograph estimated by the L-gamma model. It is apparent that both the median empirical hyetograph and the L-gamma expected hyetograph are similar in shape and magnitude for most of the storm duration. The slopes of the median empirical hyetograph and the L-gamma hyetographs are similar except in the first 15 percent or so of the storm duration. Hence, early in the storm the median empirical hyetograph predicts higher percentage rainfall rates. The higher rates of the median empirical hyetograph are followed by a period of reduced rates between about 30 to 55 percent. Comparable percentage rainfall rates are exhibited from about 55 percent of the storm duration to the end of the storm. The L-gamma model is considered to agree with the less statistically rigorous empirical hyetographs. Therefore, a conclusion is that the L-gamma model estimates an appropriate runoff-producing 12–24 hr expected hyetograph for storm depths of one or more inches.

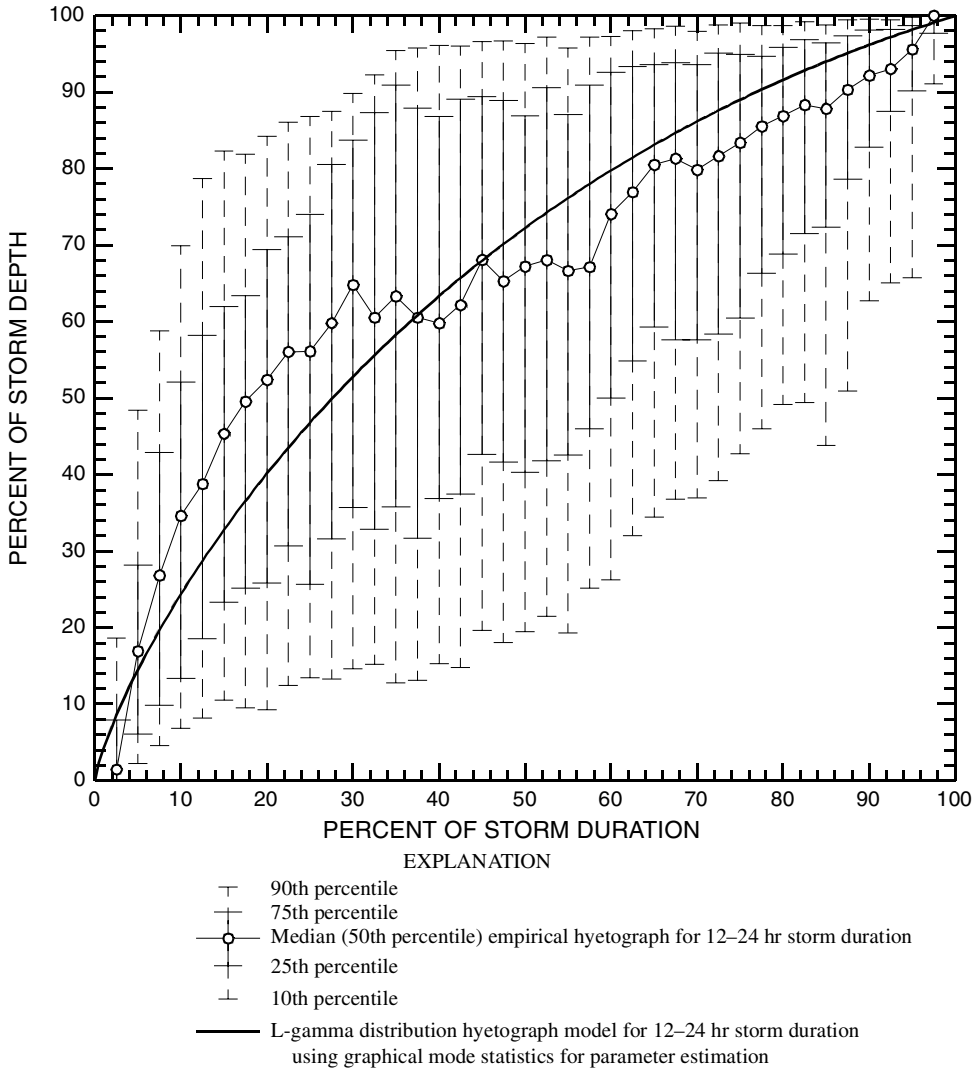

Figure 74. Comparison between empirical hyetographs and the L-gamma distribution hyetograph distribution model for 12–24 hr storm duration and one inch and greater storm depths

The empirical hyetographs (10th, 25th, median, 75th, and 90th percentile) for the 12–24 hr duration are shown on figure 75. Also shown on the figure is the 24 hr and greater expected hyetograph estimated by the L-gamma model. It is apparent that both the median empirical hyetograph and the L-gamma expected hyetograph are similar in shape and magnitude for most of the storm duration. The general slope of the median empirical hyetograph and the L-gamma hyetograph are similar throughout most of the storm duration. The exception being around 10–20 percent; the differences in this duration range are believed to be a vagary of sampling and estimation of the medians within the intervals. The fact that both the median empirical hyetograph and the L-gamma expected hyetograph bend upwards as they approach the end of the storm duration enhances the credibility of the oddly shaped L-gamma model for the 24 hr and greater duration compared to the general shapes of the other two durations. The L-gamma model is considered to agree with the less statistically rigorous empirical hyetographs. Therefore, a conclusion is that the L-gamma model estimates an appropriate runoff-producing 24 hr and greater expected hyetograph for storm depths of one or more inches.

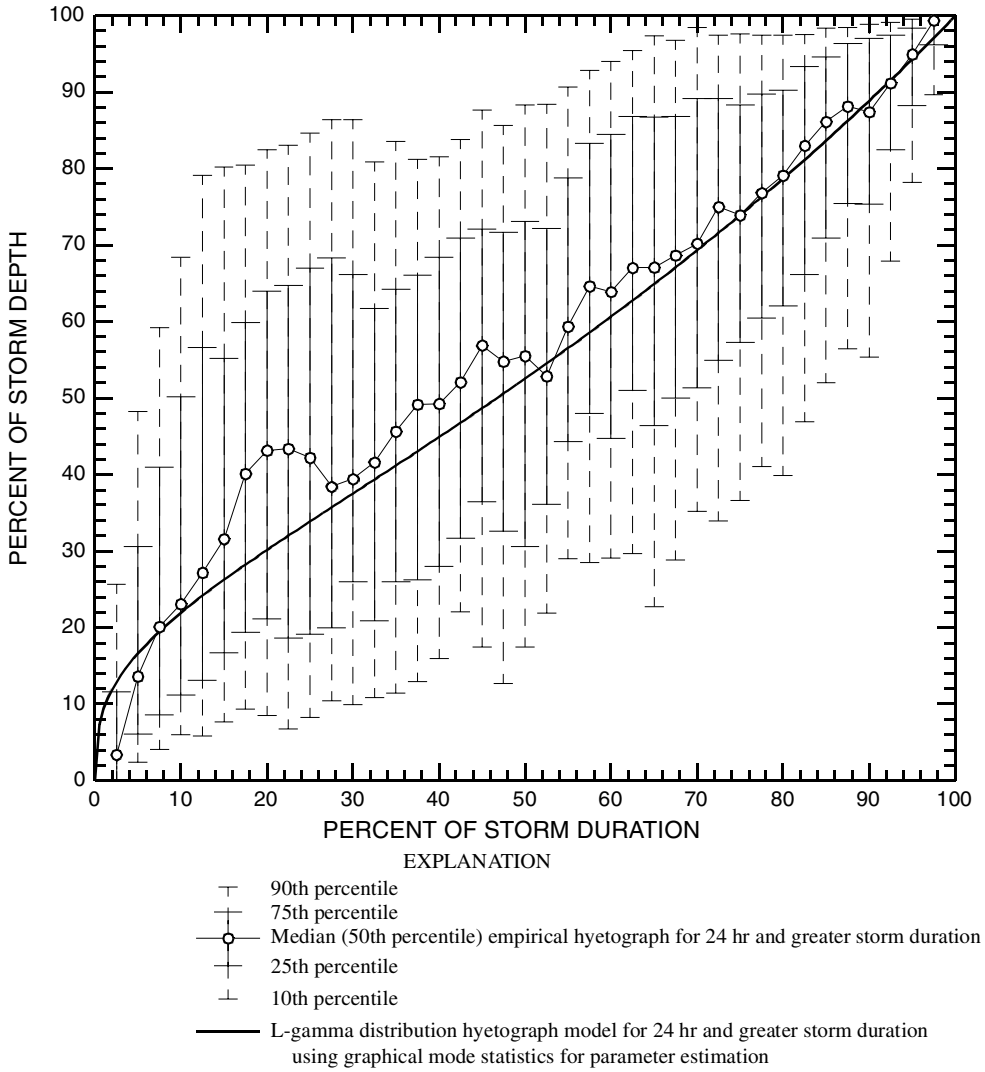

Figure 75. Comparison between empirical hyetographs and the L-gamma distribution hyetograph distribution model for 24 hr and greater storm duration and one inch and greater storm depths

The percentiles used to produce figures 73–75 are listed in tables F1, F3, and F5 of Appendix F for the 0–12 hr, 12–24 hr, and 24 hr and greater durations, respectively. The L-moments of the distribution of ordinates within each interval are listed in tables F2, F4, and F6 of Appendix F for the 0–12 hr, 12–24 hr, and 24 hr and greater durations, respectively. The L-moments in the tables were computed by unbiased

estimators. The tables are provided so that complete and comprehensive documentation of the ordinate distribution within each interval is available for other analysts to research stochastic hyetograph modeling or other research objectives.

For example, Karian and Dudewicz (2000, chap. 4, Appendix D) provide an approach and extensive tables for parameter estimation of the generalized Lambda distribution using the Method of Percentiles. The distribution as a quantile function is

$$Q(F) = \xi + \alpha(F^{\kappa} - (1 - F)^{h}). \tag{95}$$

The percentiles shown in tables F1, F3, and F5 could provide estimates for the ξ, α, κ, and h parameters. The fitted distribution would greatly facilitate simulation of the hyetograph ordinate for a specific 2.5 increment of the percent of storm duration. For example, at the mid point (the median) of the 0–12 hr storm duration (table F1), the median, lower quartile, upper quartile, lower decile, and upper decile of the hyetograph ordinate values are 71.75, 43.99, 86.28, 24.82, and 93.84, respectively. Using the procedures outlines by Karian and Dudewicz (2000, pp. 154–166, 381), an estimate of the parameters is 0.9304, 1.191, 36.91, and 1.98, for ξ, α, κ, and h, respectively. The generalized Lambda modeling (no truncation for $Q < 0$ or $Q > 1$ shown) the distribution of hyetograph ordinates half way through a 0–12 hr storm is

$$Q(F) = 0.9304 + \frac{F^{36.91} - (1 - F)^{1.98}}{1.191}. \tag{96}$$

Additional Empirical Hyetographs

The three durations ranges analyzed thus far in this dissertation are considered large relative to the shorter durations commonly used in hyetograph applications (3–6 hr). Although statistics from chapter 5 of the 0–12 hr and 12–24 hr duration indicate that these durations are combinable, it is informative to consider some additional median empirical hyetographs with other durations. The influence of smaller durations and duration ranges is documented by median empirical hyetograph comparisons such as the curves plotted on figure 76 for storms having one or more inches of rainfall. The very short duration storms (0–3 hr) appear to start proportionally slower (less steep implies slower rainfall rate) or are not consistent than the longer duration storms and then eventually parallel the slightly longer 3–6 hr storms when about 50 percent of the duration has passed. The points defining the 0–3 hr storms are considerably more erratic relative to the other duration ranges; this is likely the result of smaller storm sample sizes of 125 verses 203 for the 0–3 hr and 3–6 hr storms respectively. Another source for the slower starting and erratic behavior of the 0–3 hr storms might be related to the resolution of the time increments in the raw data. The hyetograph generally is less well represented for the short duration events because fewer points were recorded. The most common time intervals defining the data for the short duration (few hours) events was 15 to 30 minutes. Some 5-minute data is present in the hyetograph data base, however. It appears that as the duration increases, the median empirical hyetograph plot lower for percent of storm duration values greater than

about 20 percent. The peak percentage rainfall rates between 0 and 10 percent of the storm duration are equivalent.

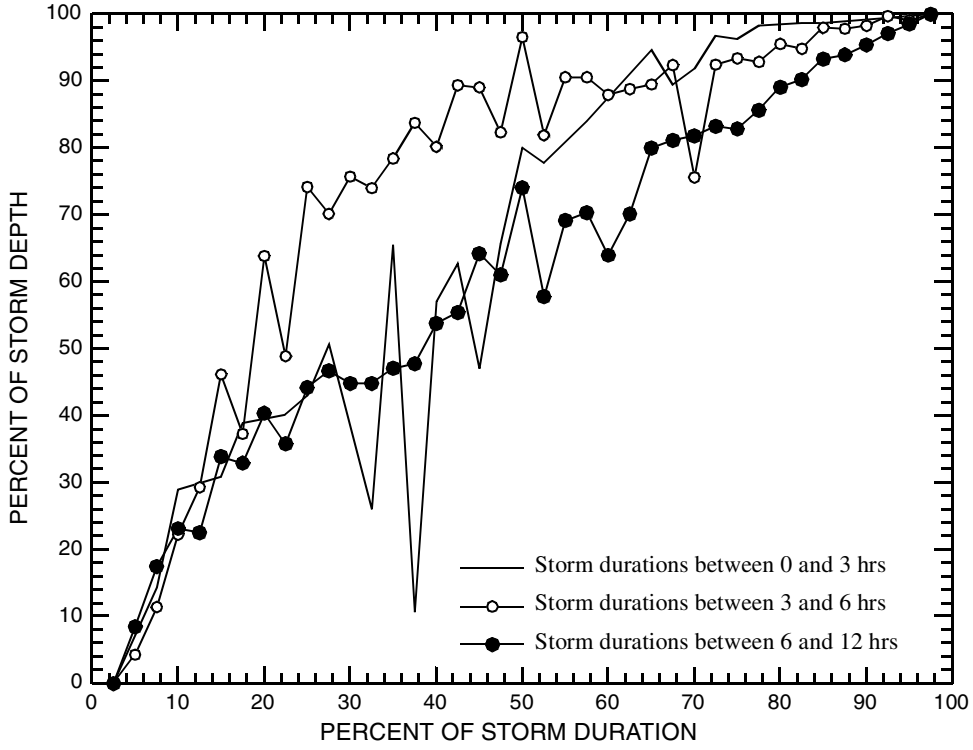

Figure 76. Median empirical hyetographs for storm depths of one inch and greater

The influence of storm magnitude is documented by median empirical hyetograph comparisons on figure 77. Slightly larger storm durations than those considered on figure 76 are used on figure 77 because of smaller numbers of storms meeting the minimum depth criteria for each duration range. In general, the storms all have similar percentage rainfall rates for the first 20 percent of storm duration. As the duration percentage increases separation in the two median empirical hyetographs is exhibited.

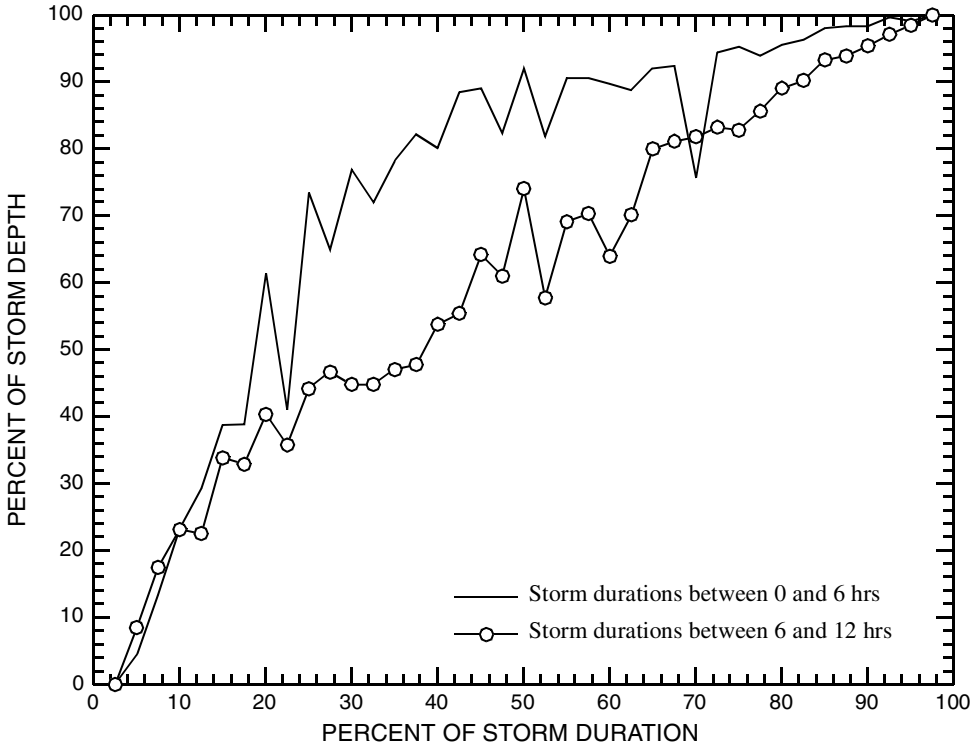

Figure 77. Median empirical hyetographs for storm depths of three inches and greater

Model Criticisms

A major criticism of these expected hyetographs is that the hyetographs might not reflect the typical rainfall rates associated with periods of peak rainfall rates. From an hydrologic design consideration, the peak rainfall rates are important because the peak rainfall rates commonly drive the peak runoff response of a watershed. Specifically, the concern is that a simple few-parameter model, like the L-gamma distribution, is not well suited for reproducing the bursting behavior of many real-world hyetographs. The rainfall bursts are significant contributors to peak streamflow of the runoff hydrograph. Graphical illustration and supporting discussion follows.

For example, consider the dimensionless hyetographs used to produce the third box plot from the left on figures 26–32. For the 3 in. category and the 0–12 hr duration the 108 hyetographs meeting these criteria are illustrated on figure 78. The visual appearance of the hyetographs in the figure are similar for the other categories and durations considered in chapter 5. By inspection of the figure, it is clear that large variations in the hyetograph shape exists. Some hyetographs are remarkably front loaded, whereas, a few are back loaded. Further, it seems unusual for a particular hyetograph to gradually transition from 0 to 100 percent like the L-gamma model implies; more commonly the hyetograph makes relatively distinct jumps. These jumps are indicative of rainfall bursts. Additional observations of the hyetographs are annotated on the figure. Finally, several hyetographs are distinctively un-smooth—the second derivative of the hyetograph is often zero for substantial fractions of the duration.

The occurrence of un-smooth hyetographs is undoubtedly due to factors including: poor data quality or missing values for the original data, poor digitizing of the raw data into tables during the preparation of the data reports, original transcription errors in final production of the data reports, and transcription or other errors on part of the modern research projects. The now-computerized hyetograph data base passes many quality assurance tests, which include test on the monotonic criteria for all cumulating values. A method by which to objectively (algorithmic and not visual inspection) identify and to remove individual undesirably un-smooth hyetographs from analysis is

difficult to envision. So such removal was not performed at all for this dissertation. It has been implicitly assumed for this dissertation that the errors or irregularities in individual hyetographs are "averaged out" when a sufficiently large number of hyetographs are used to compute statistics.

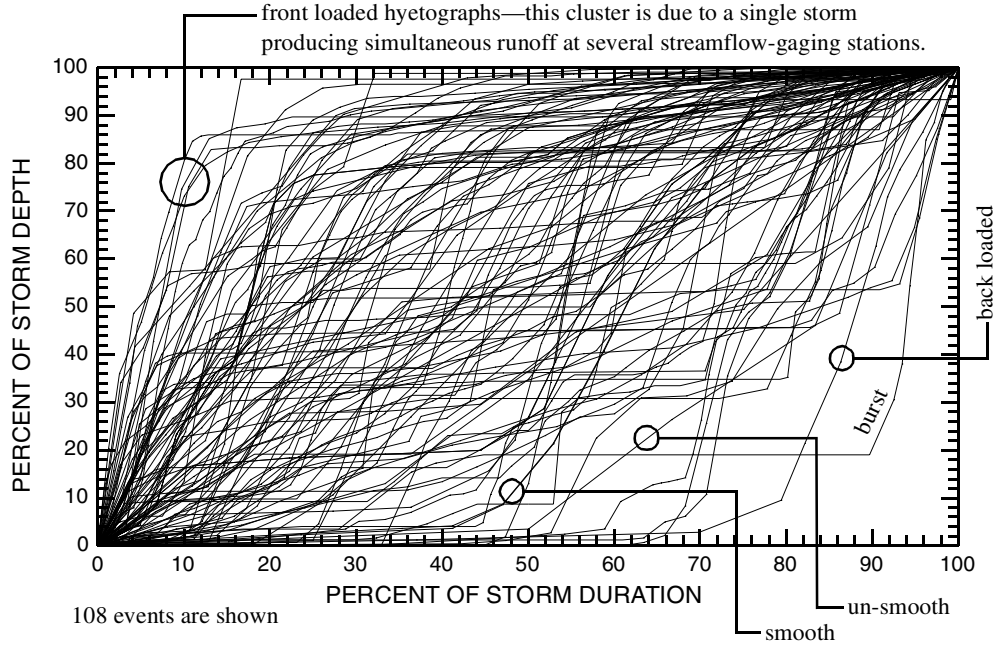

Figure 78. Hyetographs for storms having depths between 2.5 and 3.5 inches and 0–12 hr duration

To continue, there is a concern that the broad rainfall rate uniformity predicted by the L-gamma model is not consistent with the majority of individual hyetographs—that is real storms—as evidenced by visual inspection of figures such as figure 78. (Graphs C on figures 4–8 also provide evidence.) The uniformity of rainfall rate implied by the L-gamma distribution might be attributable to an over degree of smoothing by using "averages" (specifically, means, medians, or graphical modes) of

the mean and L-scale values of observed hyetographs. In a sense a statistic of an ensemble of statistics predicts rainfall rates less than the bursts because rainfall can occur at any time in the duration. To clarify, the rainfall bursts front-loaded storms are approximately balanced in number by the rainfall bursts of back-loaded storms so that on a whole the general rainfall rate of the storm is reduced from the individual bursts.

A bi-variate statistical analysis of the probability of rainfall for a given increment of the storm duration coupled with an analysis of the distribution of the rainfall burst magnitude for the storm duration increment might prove insightful. Such an analysis would be encumbered by the fact that the original hyetograph data is not preserved in constant increments—the motivation for the prior-Probability Weighted Moments.

Example Application of L-gamma Hyetograph

It is informative to show an application of the L-gamma hyetograph for the generation of a streamflow hydrograph. The most common technique is to couple the hyetograph with a unit hydrograph (Chow and others, 1988, pp. 218–221). The unit hydrograph is the hydrograph generated by a unit depth of excess precipitation (runoff) on a watershed. Each pulse of precipitation initiates a separate hydrograph. The total streamflow hydrograph is constructed by adding the hydrograph of each pulse of precipitation for each discrete increment of time. This process is known as convolution and is mathematically expressed in discrete space as

$$Q_n = \sum_{m=1}^{n \le M} P_m U_{n-m+1}, \tag{97}$$

where Q_n is the streamflow for the n-th hydrograph ordinate, P_i is a precipitation pulse, U_i is an ordinate of the unit hydrograph, and M is the number of pulses of precipitation.

For the application example, consider the 3-hr 25-year storm considered in section *Example of the Balanced Storm Hyetograph Method for Austin, Texas* in chapter 2. The total depth of precipitation for the storm is 4.55 in. (116 mm). It is assumed for the example here that all of the precipitation in converted to runoff. No abstraction of precipitation is considered. The dimensionless hyetograph (balanced storm hyetograph) derived in table 9 is used to compute a streamflow hydrograph in table 29. The 30-minute unit hydrograph is from Chow and others (1998, example 7.5.1). The 0–12 hr L-gamma hydrograph model is used to compute the streamflow hydrograph in table 30. Subtle differences between in the totals in tables 29 and 30 are due to rounding errors. The hydrograph corresponding to each precipitation input is placed along the diagonals of the matrix. For example, the 0.219 precipitation in table 30 produces a hydrograph with 30-minute ordinates of 88.5, 236, . . ., 60.0, and 37.9 ft^3/s.

Table 29. Example computation of streamflow hydrograph convolution of a balanced storm hyetograph and a unit hydrograph

[ft^3/s, cubic feet per inch of excess precipitation; hr, hour; in, inches; ft^3/s, cubic feet per second. Total excess precipitation is about 4.55 inches.]

Time	Dimensionless hyetograph	Excess precipitation hyetograph	30-minute unit hydrograph ordinates (ft^3/in)									Streamflow hydrograph
			1	2	3	4	5	6	7	8	9	
(1/2 hr)	( )	(in)	404	1,079	2,343	2,506	1,460	453	381	274	173	(ft^3/s)
1	0.0482	0.219	88.5	--	--	--	--	--	--	--	--	88.5
2	.211	.741	299	236	--	--	--	--	--	--	--	535
3	.737	2.39	966	800	513	--	--	--	--	--	--	2,279
4	.934	.896	362	2,579	1,736	549	--	--	--	--	--	5,226
5	1.00	.300	121	967	5,600	1,857	320	--	--	--	--	8,865
6	1.00	.00	0	324	2,099	5,989	1,082	99.2	--	--	--	9,593
7	Total	4.55	--	0	703	2,245	3,489	336	83.4	--	--	6,856
8			--	--	0	752	1,308	1,083	282	60.0	--	3,485
9			--	--	--	0	438	406	911	203	37.9	1,996
10			--	--	--	--	0	136	341	655	128	1,260
11			--	--	--	--	--	0	114	246	413	773
12			--	--	--	--	--	--	0	82.2	155	237
13			--	--	--	--	--	--	--	0	51.9	51.9
14			--	--	--	--	--	--	--	--	0	0
											Total	41,245

A comparison between the streamflow hydrographs computed using the balanced storm hyetograph (table 29) and the L-gamma hyetograph (table 30) is provided on figure 79. The L-gamma hyetograph produces a peak streamflow that is substantially less than the peak produced by the balanced storm hyetograph. The downward percent change between the hydrographs for the balanced storm and L-gamma hyetograph is about 16 percent. Accordingly, there is a concomitant increase in the spread of the streamflow hydrograph derived from the L-gamma hyetograph for the volumes to remain equivalent.

Table 30. Example computation of streamflow hydrograph convolution of 0–12 hr L-gamma hyetograph and a unit hydrograph

[ft^3/s, cubic feet per inch of excess precipitation; hr, hour; in, inches; ft^3/s, cubic feet per second. Total excess precipitation is about 4.55 inches.]

Time	Dimensionless hyetograph	Excess precipitation hyetograph	30-minute unit hydrograph ordinates (ft^3/in)									Streamflow hydrograph
			1	2	3	4	5	6	7	8	9	
(1/2 hr)	( )	(in)	404	1,079	2,343	2,506	1,460	453	381	274	173	(ft^3/s)
1	0.290	1.32	533	--	--	--	--	--	--	--	--	533
2	.566	1.26	509	1,424	--	--	--	--	--	--	--	1,933
3	.770	.928	375	1,360	3,093	--	--	--	--	--	--	4,828
4	.903	.605	244	1,001	2,952	3,308	--	--	--	--	--	7,505
5	.975	.328	133	653	2,174	3,158	1,927	--	--	--	--	8,045
6	1.00	.114	46.1	354	1,418	2,326	1,840	598	--	--	--	6,581
7	Total	4.56	--	123	769	1,516	1,355	571	503	--	--	4,836
8			--	--	267	822	883	420	480	362	--	3,234
9			--	--	--	286	479	274	355	345	228	1,966
10			--	--	--	--	166	149	231	254	218	1,018
11			--	--	--	--	--	51.6	125	166	161	503
12			--	--	--	--	--	--	43.4	89.9	105	238
13			--	--	--	--	--	--	--	31.2	56.7	87.9
14			--	--	--	--	--	--	--	--	19.7	19.7
											Total	41,322

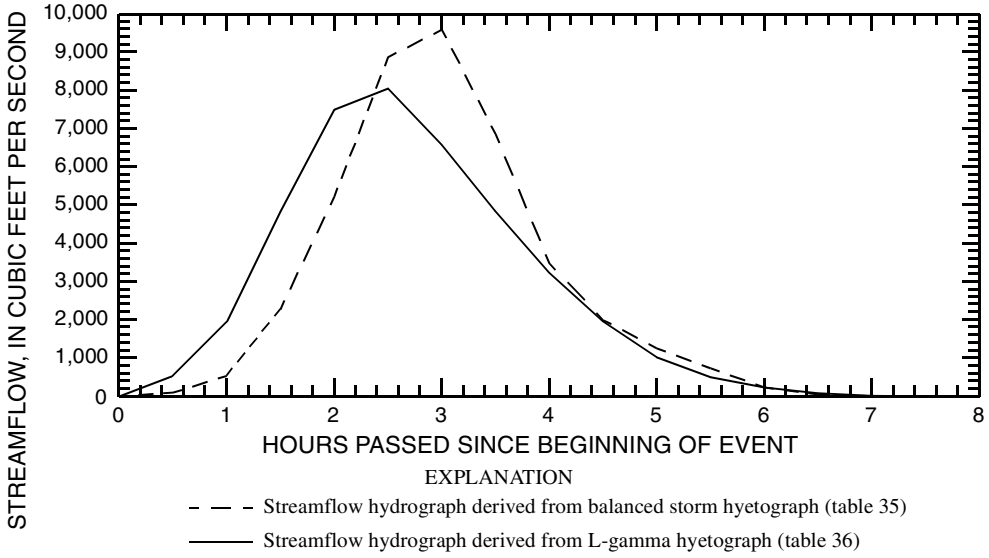

Figure 79. Comparison of streamflow hydrographs derived from L-gamma and balanced storm hyetographs shown in tables 29 and 30

CHAPTER 8
MODIFICATION OF THE CARMAN-KOZENY EQUATION FOR APPLICATION OF L-MOMENT STATISTICS FOR ESTIMATION OF THE INTRINSIC PERMEABILITY OF POROUS MEDIA

Introduction

This chapter is unrelated to all other chapters of this dissertation in that no topics related to rainfall hyetographs are considered. This chapter has several purposes, and these are to provide discussion of a potential application of L-moment statistics for estimation of intrinsic permeability (permeability) of porous media, to suggest future research directions for researchers of L-moment statistics, and to encourage L-moment adoption and research by chemical engineers, geologists, hydrogeologists, petroleum engineers, petrophysicists, water and waste-water engineers, and other specialties that consider fluid flow in porous media. Examples of porous media are sandstone aquifers and water-treatment filtration systems. The estimation of permeability in general is of great socio-economic importance for topics such as chemical processing, energy recovery, subsurface contaminant transport, and water supply.

This chapter does not provide either a specific review of permeability or a general review of the principles of fluid flow in porous media, but instead suggests and demonstrates an application of L-moment statistics following an analytical lead of Panda and Lake (1994). Panda and Lake use the product moments of a grain-size (particle-size) distribution for enhanced permeability estimation using the Carman-Kozeny equation. Panda and Lake provide important background references on

permeability and estimation of permeability. Readers are directed to the cited references of that paper for background information.

From Panda and Lake (1994), intrinsic permeability, k, can be estimated using the Carman-Kozeny (CK) equation. The equation is

$$k = \frac{\phi^3}{2\Upsilon(1+\phi)^2 \times a_v^2}, \tag{98}$$

where ϕ is porosity, Υ is tortuosity, and a_v is the ratio of the internal surface area of the media to the volume of the media solids. The units for k are length^2. Throughout this chapter is it assumed that ϕ and Υ are constant.

If it is assumed that the media is composed of spherical uncemented particles of diameter D then

$$a_v = \frac{\pi D^2 \times \text{no. of spheres}}{\frac{\pi}{6} D^3 \times \text{no. of spheres}} = \frac{6D^2}{D^3} = \frac{6}{D}. \tag{99}$$

(Panda and Lake do not explicitly show the middle terms of eq. 99.) Upon substitution of eq. 99 into the CK equation, the equation becomes

$$k = \frac{D^2 \phi^3}{72\Upsilon(1+\phi)^2}. \tag{100}$$

Panda and Lake then acknowledge that particle diameters have a distribution. The distribution can be defined by the relative number of grains (n_i) for a given diameter. The distribution is characterized by a particle-size distribution (psd) and is

$$f(D_i) = \frac{n_i}{n_{total}}, \text{ and} \tag{101}$$

$$\int_0^\infty f(D_i)dD = 1. \tag{102}$$

The psd is analogous to a probability density function (PDF).

A late note (Jan. 2003) regarding the model for the psd shown in eq. 101 is needed. According to personal communication with Lake (2003), the Log-normal distribution was used for $f(D_i)$. The use of the Log-normal distribution is apparently not referenced in the Panda and Lake (1994) paper.

Using eq. 101, Panda and Lake indicate or assume without showing a proof that the average or expected value for a_v is

$$\bar{a}_v = \frac{6 \times E_2}{E_3}, \tag{103}$$

where

$$E_2 = \text{2nd noncentral product moment} = \int_0^\infty D^2 f(D_i)dD, \text{ and} \tag{104}$$

$$E_3 = \text{3rd noncentral product moment} = \int_0^\infty D^3 f(D_i)dD. \tag{105}$$

In terms of the central product moments the noncentral product moments are

$$E_2 = \overline{D}^2 + \sigma^2, \tag{106}$$

$$E_3 = \overline{D}^3 + 3\sigma^2\overline{D} + \gamma\sigma^3, \tag{107}$$

$$\overline{D} = \int_0^\infty Df(D_i)dD \text{ (mean grain size), and} \tag{108}$$

$$C = \frac{\sigma}{\overline{D}} \text{ (coefficient of variation).} \tag{109}$$

Using standard notation, σ is the standard deviation and γ is the skew of the psd. Panda and Lake then go on to develop the "modified CK equation"

$$k = \frac{\overline{D}^2\phi^3}{72\Upsilon(1+\phi)^2}\left[\frac{(\gamma C^2 + 3C^2 + 1)^2}{(1+C^2)^2}\right], \tag{110}$$

where the quantity in the square brackets is a correction factor to account for the psd. The correction factor is a function of the mean, coefficient of variation, and skewness of the distribution. No other moments are represented. Panda and Lake (1994, p. 1031) conclude that the modified CK equation is *valid for any distribution*.

A late note (Jan. 2003) is needed regarding the Panda and Lake conclusion that the modified CK equation is valid for any distribution. According to Lake (2003), the conclusion seems most appropriate for any "fitted" Log-normal distribution as the Log-normal distribution apparently was used as a basis for the analytical derivations shown in Panda and Lake (1994).

The author is concerned that the distribution independence conclusion is actually an assumption, which might not be supportable. This concern is a partial motivation

for this chapter. Panda and Lake do not indicate that the conclusion of distribution independence is an assumption; neither a proof or further discussion is provided. The remainder of the Panda and Lake paper explores the enhanced predictive capabilities of the modified CK equation.

The author has another concern about the Panda and Lake paper, and this is whether or not an assumption was made for the expected or average value of $\bar{a}_v$ being equal to $6 \times E_2/E_3$. The units (length^{-1}) of E_2/E_3 certainly are consistent for a_v, and squaring or cubing of the diameter is seen in eqs. 104 and 105 as in eq. 99. However, the appropriateness of the equality is not intuitive to the author. For example, any noncentral moment or order n divided by the noncentral moment of order $n + 1$ would yield consistent units for a_v.

The author suggests an alternative analytical track with derivations following the lead established by Panda and Lake. The derivations clarify the distribution independence, the definition of the average a_v, and demonstrate applicability of L-moment statistics to the CK equation.

If D has a distribution, then a quantile function (either algebraically or numerically solved) of the distribution must exist. The particle-size quantile function is

$$D(F) \text{ for } 0 \le F \le 1, \tag{111}$$

where $D(F)$ is the particle size (quantile) for a given nonexceedance probability F.

Because of the ability to perform algebraic manipulations on quantile functions (see Gilchrist, 2000, chapter 3), most surely a_v (for uncemented spherical grains) follows the quantile function

$$a_v(1-F) = \frac{6D^2(F)}{D^3(F)} = \frac{6}{D(F)}. \tag{112}$$

The compliment $(1-F)$ is needed to make a_v an increasing function according to the *reciprocal rule* of quantile function algebra (Gilchrist, 2000, p. 65). By substituting eq. 112 into the CK equation, k also becomes a quantile function

$$k(F) = \frac{\phi^3}{2\Upsilon(1+\phi)^2 \times a^2{}_v(1-F)}. \tag{113}$$

The F is recovered in the left-hand side because of the reciprocal rule. The expected value of $k(F)$ is

$$\bar{k} = \int_0^1 \frac{\phi^3}{2\Upsilon(1+\phi)^2 \times a^2{}_v(1-F)} dF, \tag{114.1}$$

$$\bar{k} = \frac{\phi^3}{72\Upsilon(1+\phi)^2} \int_0^1 D^2(F) dF = \frac{\phi^3}{72\Upsilon(1+\phi)^2} \zeta, \text{ where} \tag{114.2}$$

$$\zeta = \int_0^1 D^2(F) dF. \tag{114.3}$$

Note that the $D(F)$ is recovered in eq. 114.2 from $a_v(1-F)$ because of the reciprocal rule. It is natural to consider various forms of $D(F)$. It is evident from eq. 114.3 that different parametric forms of the quantile function will produce different formulas for the correction factor. Different correction factors imply that the CK equation is influenced by the form (model or type) of the psd and the values of the L-moments and the product moments by generality.

For example, if $D(F) = D$, a constant quantile function, then the usual CK equation results because $\zeta = D^2$; the correction to the CK equation hence is unity. Clearly the particle-size quantile function is not always a constant so this is a degenerate example. Other forms are described in the following sections.

Linear Model of the Particle-Size Distribution

Suppose that the distribution of particle diameter is

$$D(F) = \varepsilon + \alpha F, \tag{115}$$

where ε and α are location and scale parameters, respectively. The first two L-moments of the linear model are

$$\lambda_1 = \int_0^1 D(F)dF = \int_0^1 (\varepsilon + \alpha F)dF = \varepsilon + \alpha/2 \text{ and} \tag{116.1}$$

$$\lambda_2 = \int_0^1 D(F)(2F-1)dF = \int_0^1 (\varepsilon + \alpha F)(2F-1)dF = \alpha/6. \tag{116.2}$$

The parameters in terms of the L-moments are $\varepsilon = \lambda_1 - 3\lambda_2$ and $\alpha = 6\lambda_2$. In terms of the L-moments then

$$\zeta = \int_0^1 (\lambda_1 - 3\lambda_2 + 6\lambda_2 F)^2 dF. \tag{117}$$

However, a more convenient analytical direction is

$$\zeta = \int_0^1 (\varepsilon + \alpha F)^2 dF = \int_0^1 (\varepsilon^2 + 2\varepsilon\alpha F + \alpha^2 F^2) dF, \tag{118.1}$$

$$\zeta = \varepsilon^2 + \varepsilon\alpha + \alpha^2/3, \text{ and} \tag{118.2}$$

$$\zeta = \lambda^2{}_1\left(1 + \frac{3\lambda^2{}_2}{\lambda^2{}_1}\right) = \lambda^2{}_1(1 + 3\tau^2). \tag{118.3}$$

Hence upon substitution into the CK equation and incorporation of the coefficient of L-variation $\tau = \lambda_2/\lambda_1$, the result is

$$\bar{k} = \frac{\lambda^2{}_1\phi^3}{72\Upsilon(1+\phi)^2}(1 + 3\tau^2). \tag{119}$$

Since λ_1 is the expected particle size, $\overline{D}$, a symbolically consistent expression for the CK equation is

$$\bar{k} = \frac{\overline{D}^2\phi^3}{72\Upsilon(1+\phi)^2}(1 + 3\tau^2). \tag{120}$$

The $(1 + 3\tau^2)$ is the correction necessary if the psd is linear. The correction is proportional to the square of the coefficient of L-variation (τ), which is a measure of particle sorting. For example, suppose the mean (λ_1) and L-scale (λ_2) of the psd are 50 mm and 15 mm, respectively. The coefficient of L-variation $\tau = 0.3$ (15/50). Hence the CK equation with this linear model of the psd is

$$\bar{k} = \frac{2500\phi^3}{72\Upsilon(1+\phi)^2}(1.27). \tag{121}$$

Two-Parameter Power Model of the Particle-Size Distribution

As another example, suppose that the distribution of particle diameter is

$$D(F) = \alpha F^{\beta}. \tag{122}$$

This equation is a two-parameter Power distribution similar to the Power distribution shown in eq. 59. Following the lead established for the linear model, the first two L-moments of this model are

$$\lambda_1 = \int_0^1 (\alpha F^{\beta}) dF = \frac{\alpha}{\beta + 1}, \tag{123.1}$$

$$\lambda_2 = \int_0^1 (\alpha F^{\beta})(2F - 1) dF = \frac{\alpha\beta}{(\beta + 2)(\beta + 1)}, \text{ and} \tag{123.2}$$

$$\tau = \frac{\lambda_2}{\lambda_1} = \frac{\beta}{(\beta + 2)}. \tag{123.3}$$

The parameters in terms of the L-moments are

$$\alpha = \lambda_1\left(\frac{-\tau-1}{\tau-1}\right) \text{ and} \tag{124.1}$$

$$\beta = \frac{-2\tau}{\tau-1}. \tag{124.2}$$

Hence, ζ is

$$\zeta = \int_0^1 (\alpha F^{\beta})^2 dF = \frac{\alpha^2}{\beta+1} = \lambda^2{}_1\left(\frac{(\tau+1)^2}{(1-\tau)(3\tau+1)}\right). \tag{125}$$

Therefore the CK equation when the particle size is distributed according to a Power distribution is

$$\bar{k} = \frac{\bar{D}^2\phi^3}{72\Upsilon(1+\phi)^2}\left(\frac{(\tau+1)^2}{(1-\tau)(3\tau+1)}\right). \tag{126}$$

Thus the correction factor on the CK equation for a Power model of the psd is more complicated than that for the linear model. This factor is different than that derived for a linear psd. For example, suppose a psd has a mean of 50 mm and an L-scale (λ_2) of 15 mm; hence, τ is equal to 0.3. Hence the CK equation with this linear model of the psd is

$$\bar{k} = \frac{2500\phi^3}{72\Upsilon(1+\phi)^2}(1.27). \tag{127}$$

The correction of 1.27 for the two-parameter Power model with round off is the same as the correction for the linear model fit to the same L-moments. However, if

$\tau = 0.8$ and the psd a Power distribution, then the correction factor is 4.76—the correction for the linear model is just 2.92. The much larger correction for the Power distributed psd is attributed to the heavier upper tail of the Power distribution. Since k is proportional to the square of the diameter, the larger diameters from the Power model necessarily increase the k. This is exhibited in the larger correction factors as τ increases.

Three-Parameter Power Model of the Particle-Size Distribution

For another example, suppose that the distribution of particle diameter is

$$D(F) = \varepsilon + \alpha F^{\beta}. \tag{128}$$

This model is a three-parameter Power distribution. The L-moments (mean, L-scale, and L-skew) of this distribution are

$$\lambda_1 = \varepsilon + \frac{\alpha}{\beta + 1}, \tag{129.1}$$

$$\lambda_2 = \frac{\alpha\beta}{(\beta + 2)(\beta + 1)}, \text{ and} \tag{129.2}$$

$$\tau_3 = \frac{\beta - 1}{\beta + 1}. \tag{129.3}$$

The parameters in terms of the L-moments are

$$\beta = \frac{3\tau_3 + 1}{1 - \tau_3}, \tag{130.1}$$

$$\alpha = \frac{\lambda_2(\beta + 2)(\beta + 1)}{\beta}, \text{ and} \tag{130.2}$$

$$\varepsilon = \lambda_1 - \frac{\alpha}{\beta + 1}. \tag{130.3}$$

Hence, ζ is

$$\zeta = \int_0^1 (\varepsilon + \alpha F^{\beta})^2 dF = \varepsilon^2 + \frac{2\varepsilon\alpha}{\beta + 1} + \frac{\alpha^2}{2\beta + 1}. \tag{131}$$

Substitution of eqs. 129.1–129.3 into the right-hand side of eq. 130 yields a complicated expression. Therefore, it is more convenient to compute the parameters and substitute their numerical values into eq. 130. For example, suppose that a psd has values for the mean (λ_1), L-scale (λ_2), and L-skew (τ_3) of 50 mm, 15 mm, and 0.1, respectively. The corresponding parameters for ε, α, and β are 21.5 mm, 91.8 mm, and 2.22, respectively. These parameters and provide a ζ = 3237. Dividing this ζ by the square of the mean grain size (50^2 = 2500), yields a correction on the CK equation of 1.29 (3237/2500). Hence the full CK equation for this example is

$$\bar{k} = \frac{2500\phi^3}{72\Upsilon(1 + \phi)^2}(1.29). \tag{132}$$

Four-Parameter Kappa Model of the Particle-Size Distribution

As another example, consider a four-parameter Kappa distribution (Hosking, 1994) model of the psd

$$D(F) = \xi + \frac{\alpha}{\kappa}\left\{1 - \left(\frac{1 - F^h}{h}\right)^{\kappa}\right\}, \tag{133}$$

where ξ, α, κ, and h are location, scale, and shape1 and shape2 parameters of the distribution. The Kappa distribution was considered in chapter 4. The L-moments are shown in eqs. 55.1–55.4. Assuming the parameters of the distribution are known, then ζ becomes

$$\zeta = \int_0^1 \left(\xi + \frac{\alpha}{\kappa} \left\{ 1 - \left(\frac{1 - F^h}{h} \right)^\kappa \right\} \right)^2 dF \text{ and} \tag{134.1}$$

$$\zeta = \xi^2 + \frac{2\xi\alpha}{\kappa}(1 - H_1) + \frac{\alpha^2}{\kappa^2}(1 - 2H_1 + H_2). \tag{134.2}$$

An important identity (Hosking, 1994, eq. 9) is

$$H_r = \int_0^1 [h^{-1}(1 - F^h)]^{r\kappa} dF. \tag{135}$$

where H_1 and H_2 in eq. 134.2 are

$$H_1 = \begin{cases} \dfrac{1}{h^{1+\kappa}} \left(\dfrac{\Gamma(1+\kappa)\Gamma(1/h)}{\Gamma(1+k+1/h)} \right), & h > 0 \\ \dfrac{1}{(-h)^{1+k}} \left(\dfrac{\Gamma(1+\kappa)\Gamma(-\kappa-1/h)}{\Gamma(1-1/h)} \right), & h < 0 \end{cases} \text{ and} \tag{136.1}$$

$$H_2 = \begin{cases} \dfrac{1}{h^{1+2\kappa}} \left(\dfrac{\Gamma(1+2\kappa)\Gamma(1/h)}{\Gamma(1+2\kappa+1/h)} \right), & h > 0 \\ \dfrac{1}{(-h)^{1+2\kappa}} \left(\dfrac{\Gamma(1+2\kappa)\Gamma(-2\kappa-1/h)}{\Gamma(1-1/h)} \right), & h < 0 \end{cases} \tag{136.2}$$

For a computational example, suppose the L-moments of the psd are 50 mm, 15 mm, 0 (zero), and 0.1226, for the mean (λ_1), L-scale (λ_2), L-skew (τ_3), and L-kurtosis (τ_4), respectively. An L-skew of zero and L-kurtosis of 0.1226 corresponds to the Normal distribution. So a Kappa distribution fitted to these L-moments approximates the Normal distribution that has a mean of 50 mm and standard deviation of 26.59 mm ($\sqrt{\pi}\lambda_2$). The parameters corresponding to these L-moments are 42.89, 23.3, 0.2138, and -0.1613 for ξ, α, κ, and h, respectively using algorithms derived from algorithms by Hosking (1996). Substituting these values into eq. 133.2 yields $\zeta = 2620$. Dividing this ζ by the square of the mean grain size ($50^2 = 2500$), yields a correction on the CK equation of 1.29 (3223/2500). Hence the full CK equation this example is

$$\bar{k} = \frac{2500\phi^3}{72\Upsilon(1+\phi)^2}(1.29). \tag{137}$$

The coefficient of variation (C) for this example is 0.5318 (26.59/50), and the skew γ is zero. Upon substitution of C and γ into eq. 110, the Panda and Lake correction is 2.08. So the Panda and Lake correction is about 1.6 times larger than the correction from the Kappa model described here; the expected values for the intrinsic permeability necessarily differ. However, the Kappa or even the Normal distribution fit to the L-moments in this example produce negative quantiles for the particle diameter for very small values of F—a physically impossible situation. Thus, care in

selecting a suitable distribution to model the psd is necessary. Movement of the analysis into log-space of the diameter or a bounded parameter fitting scheme for the Kappa would solve this dilemma.

Four-Parameter Generalized Lambda Model of the Particle-Size Distribution

The four-parameter Generalized Lambda distribution (GLD, eq. 95) is another promising distribution for modeling psd's. It is therefore interesting to consider the ζ multiplier for a psd having a GLD; a slightly more compact form of the distribution is listed at the bottom of table 31. The Method of Percentiles (Karian and Dudewicz, 2000, chapter 4) for parameter estimation is readily used with graphical curves showing the percentiles of the psd—neither complex numerical methods or the manually difficult L-moment computations are required. Karian and Dudewicz (2000) provide a complete discussion and tables for parameter estimation for the GLD using the 10th, 50th, and 90th percentiles. The GLD-based ζ requires the following integral (Abramowitz and Stegun, 1964, p. 258)

$$\int_0^1 F^{\kappa}(1-F)^h dF = \frac{\Gamma(\kappa+1)\Gamma(h+1)}{\Gamma(\kappa+h+2)} \text{ for } \kappa > -1 \text{ and } h > -1 . \quad (138)$$

To conclude the GLD discussion, consider a GLD approximation to the quantile function of the Normal distribution—the Normal distribution has no explicit quantile functional form. The GLD-Normal distribution is

$$D(F) = \overline{D} + \sigma\{5.0633[F^{0.135} - (1-F)^{0.135}]\}, \quad (139)$$

where the quantity within the braces { } is an approximation to the standard normal distribution. Using the ζ derivation for the GLD in table 31 and eq. 139, it can be shown that

$$\zeta = \overline{D}^2 + 25.64\sigma^2(1.575) - 51.27\sigma^2(0.7679) \text{ and}$$

$$\zeta = \overline{D}^2 + \sigma^2 = E_2 \text{ (2nd noncentral product moment, eq. 104).}$$

Finally, using the coefficient of variation C

$$\zeta = \overline{D}^2\left(1 + \frac{\sigma^2}{\overline{D}^2}\right) = \overline{D}^2(1 + C^2). \tag{140}$$

Therefore the correction on the CK equation when the particles are distributed according to a Normal distribution is $1 + C^2$. This correction also indicates that permeability goes up as the degree of sorting goes down.

Additional Remarks on Models of the Particle-Size Distribution

A summary of the ζ for the distributions considered in this chapter is provided in tables 31 and 32. Numerous other distributions could be considered to model the psd, although explicit analytical solutions for the correction factor might not exist. The availability of an explicit analytical solution rapidly diminishes as the number of parameters and hence L-moments are involved. Fortunately, numerical integration of eq. 114.3 is not difficult. Distributions that are bounded below by zero are favorable

because of the physical limitation that particle diameter be greater than zero. Further, four and five parameter distributions are promising as these distributions contain two additional parameters and hence moments—more information concerning the psd is retained.

Panda and Lake (1994) only show that the first three moments influence the CK equation. However, the derivations based on quantile functions indicate that as many moments as present in distribution model are involved in the correction on the CK equation. This is an intuitively satisfactory observation because a distribution is uniquely defined by all of its moments (parameters); hence the correction factor should also be uniquely defined by all of the distribution moments (parameters).

Table 31. Examples of the particle-diameter multiplier on the Carman-Kozeny equation based on quantile function models of the particle-size distribution

[$D(F)$, Quantile function of particle-size distribution; D, diameter; F, nonexceedance probability; ε, α, β, ξ, κ, and h, quantile function parameters; τ, coefficient of L-variation; $\overline{D}$, mean particle diameter; σ, standard deviation; C, coefficient of variation. Note that ζ is multiplied to the CK equation in lieu of the square of the mean particle diameter.]

Quantile model of particle-size distribution	No. of parameters and moments	Equation for the quantile model, $D(F)$	Particle-diameter multiplier ζ for the Carman-Kozeny equation in terms of L-moments or parameters
Constant	1	D	$\overline{D}^2$
Two-parameter linear	2	$\varepsilon + \alpha F$	$\overline{D}^2(1 + 3\tau^2)$
Two-parameter Power	2	αF^{β}	$\overline{D}^2\left(\frac{(\tau+1)^2}{(1-\tau)(3\tau+1)}\right)$
Three-parameter Power	3	$\varepsilon + \alpha F^{\beta}$	$\left(\varepsilon^2 + \frac{2\varepsilon\alpha}{\beta+1} + \frac{\alpha^2}{2\beta+1}\right)$
Generalized Lambda approximation to the Normal distribution	2	$\overline{D} + 5.0633\sigma[F^{0.135} - (1-F)^{0.135}]$	$\overline{D}^2(1 + C^2)$

Emphasis is needed on the fact that when ζ is divided by the square of the mean particle diameter $\overline{D}^2$, the resulting value is the correction on the usual CK equation (eq. 100).

Table 32. Complex examples of the particle-diameter multiplier on the Carman-Kozeny equation based on four-parameter quantile function models of the particle-size distribution

[$D(F)$, Quantile function of particle-size distribution; D, diameter; F, nonexceedance probability; ε, α, ξ, κ, and h, quantile function parameters; $\Gamma(\ )$ is the Gamma function. Note that ζ is multiplied to the CK equation in lieu of the square of the mean particle diameter.]

Quantile model of particle-size distribution	No. of parameters and moments	Equation for the quantile model, $D(F)$	Particle-diameter multiplier ζ for the Carman-Kozeny equation in terms of L-moments or parameters
Four-parameter Kappa	4	$\xi + \frac{\alpha}{\kappa}\left\{1 - \left(\frac{1-F^h}{h}\right)^\kappa\right\}$	see next line
		Multiplier	$\left(\xi^2 + \frac{2\xi\alpha}{\kappa}(1-H_1) + \frac{\alpha^2}{\kappa^2}(1-2H_1+H_2)\right)$
		where $H_1 =$	$\begin{cases} \frac{1}{h^{1+\kappa}}\left(\frac{\Gamma(1+\kappa)\Gamma(1/h)}{\Gamma(1+\kappa+1/h)}\right), & h>0 \\ \frac{1}{(-h)^{1+\kappa}}\left(\frac{\Gamma(1+\kappa)\Gamma(-\kappa-1/h)}{\Gamma(1-1/h)}\right), & h<0 \end{cases}$
		and $H_2 =$	$\begin{cases} \frac{1}{h^{1+2\kappa}}\left(\frac{\Gamma(1+2\kappa)\Gamma(1/h)}{\Gamma(1+2\kappa+1/h)}\right), & h>0 \\ \frac{1}{(-h)^{1+2\kappa}}\left(\frac{\Gamma(1+2\kappa)\Gamma(-2\kappa-1/h)}{\Gamma(1-1/h)}\right), & h<0 \end{cases}$
Four-parameter Generalized Lambda	4	$\xi + \alpha[F^\kappa - (1-F)^h]$	see next line
		$\xi^2 + 2\alpha\xi\left(\frac{1}{\kappa+1} - \frac{1}{h+1}\right) + \alpha^2\left(\frac{1}{2\kappa+1} + \frac{1}{2h+1}\right) - \frac{2\alpha^2\Gamma(\kappa+1)\Gamma(h+1)}{\Gamma(\kappa+h+2)}$	

It is illustrative to compare the correction factors from the equation (eq. 110) suggested by Panda and Lake (1994), the linear distribution (eq. 115), and two-parameter Power distribution models (eqs. 122) described here. A skew of zero was used for the Panda and Lake correction. The comparison is made on figure 80.

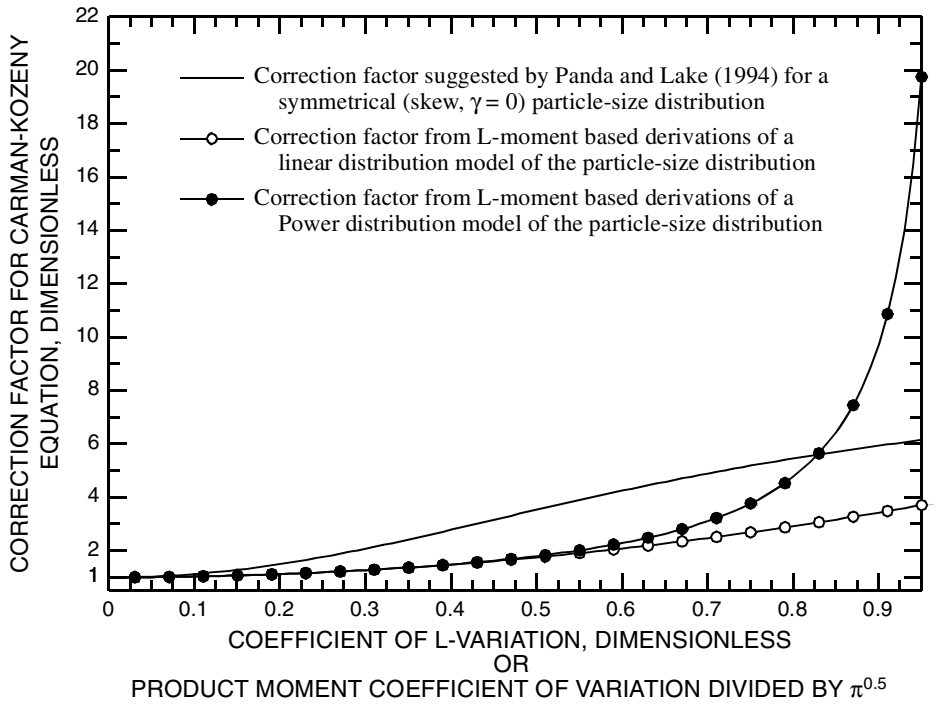

Figure 80. Comparison of correction factors for the Carman-Kozeny equation as a function of the coefficient of L-variation (L-CV) of the particle-size distribution

Chapter Conclusions

The sampling properties described in chapter 4 make L-moments particularly attractive for characterization of particle-size distribution (psd), which are well known to have large ranges, exhibit large variabilities, and are often highly non-Normally distributed. The prior-Probability Weighted Moments for sample L-moment estimation have a natural application to particle or grain size data as suggested in chapter 4. The straightforward derivations and four extended examples in this chapter suggest that L-moment statistics could play a role in estimation of intrinsic permeability using the Carman-Kozeny equation following the product moment-based lead of Panda and Lake (1994). The derivations also indicate that the distribution form

or type influences the intrinsic permeability estimation from the Carman-Kozeny equation; this conclusion is counter to a conclusion reached by Panda and Lake. Naturally, it is unknown whether application of L-moment statistics and particle-size quantile functions would in practice provide a measurable improvement in permeability estimation. A substantial field of research can be envisioned. For example, laboratory research in which porous media of particle diameters following a specific multiple-parameter distribution are constructed would permit direct testing of the hypothesized derivations shown in this chapter. Finally for the derivations shown here, the porosity and tortuosity of the porous media are assumed independent of the psd. A more important application of the derivations provided here could be for estimation of tortuosity (a difficult phenomena to measure) because porosity and intrinsic permeability often can be estimated with simple laboratory experiments.

CHAPTER 9
CONCLUSIONS

The major conclusions of this dissertation are enumerated below. Subordinate conclusions or analysis summaries are provided in *Chapter Conclusions* sections at the end of some chapters.

1. *Primary hypothesis.* Expected hyetographs of runoff-producing storms in Texas were successfully defined using L-moment statistics. This confirms the primary hypothesis of this dissertation. However, there are other model forms could be used as a basis for expected hyetograph definition, or other L-gamma model parameters could be estimated that differ from the preferred models (figure 68 and others). Further, the use of classical product moment statistics could result in subtle analytical differences because of alternative sample statistic estimates. The sole use of product moments in this dissertation are for the computation of coefficient of variation values in tables 11 and 12 of chapter 2.

2. *Secondary hypothesis.* The parameter estimates for the L-gamma model are deemed reliable. The parameters are based on defensible statistical predictions of the mean and L-scale values of observed dimensionless hyetographs. Substantial content of chapters 6 and 8 provides the defense of the statistics. The graphical modes of the mean and L-scale values (figs. 55–57 and table 25) are preferred but values for other statistics are provided to aid the interpretations of other researchers. The empirical hyetograph analysis (figs.

73–75) provides median hyetographs that are consistent with the preferred L-gamma models; the use of the graphical modes is defended.

3. *On the applicability of the L-gamma distribution.* The L-gamma distribution is a viable tool for hyetograph modeling. The Beta distribution and L-gamma distribution when fit to the same hyetograph statistics are similar (see figs. 69–71 in chapter 8). The Beta is a well known distribution so the agreement between the distributions is encouraging. The L-gamma distribution in the context of hyetograph modeling is easier to use, algebraically more compact, and more compatible with L-moments.

4. *On the suitability of the L-gamma model.* The L-gamma model is a suitable tool for modeling the expected hyetograph. Comparison of the three L-gamma models to empirical hyetographs demonstrates a degree of consistency that supports the predicted hyetograph ordinates. The 24 hr and greater (up to about 3 days) expected hyetograph estimated by the L-gamma model likely is not as reliable as the models for 0–12 hr and 12–24 hr durations because of greater perceived heterogeneity of the hyetograph statistics (see chapter 6).

5. *On the double one-percent tail trimming method.* The double one-percent hyetograph tail trimming method was used for almost all analysis and figure construction. The tail trimming is vital. The trimming is symmetrical so substantial distortion of a given hyetograph is avoided. Precise sensitivity analysis of the trimming percentages is difficult to envision. Firm justification

of a need for tail trimming is graphically illustrated by the storm seen on figures 1, 3, and 23 and table 17 of chapters 1 and 4. However, to mitigate against potential interpretive problems by universal use of the trimming method, analyses of untrimmed mean, median, and L-scale values of the observed dimensionless hyetographs are presented in chapter 6 and figures 51–53 and table 25.

6. *On the influence of storm magnitude (frequency) on hyetograph statistics.* Contrary to prior expectation, the storm magnitude or depth of the storm, hence its frequency, appears to have *relatively little influence* on the low-order L-moment statistics (mean and L-scale) and median of the 0–12 hr and 12–24 hr storm durations. This is important because it suggests that all storm recurrence intervals (such as the 25-year storm) have the hyetographs of the same shape even though the depths of the rainfall for the recurrence intervals can be quite different. The higher-order L-moment statistics (L-skew, L-kurtosis, and τ_5) appear influenced, but these statistics are not as critical for hyetograph definition as are the mean, median, and L-scale statistics. The Beta and L-gamma distributions are fit only to the mean and L-scale statistics. For the 24 hr and greater duration storms there is a notable graphical correlation between the storm depth and the hyetograph statistics. A substantial number of figures and concomitant discussion of box plots showing the distribution of each statistic for specific with storm depth categories are provided for each

duration in chapter 6 on figures 26–46. Table 24 of chapter 6 summarizes the conclusions. Further details supporting this conclusion are provided in chapter 3—particularly tables 11 and 12.

7. *On the influence of storm duration on hyetograph statistics.* The storm duration certainly influences the shape of the dimensionless hyetograph. Three storm durations of 0–12 hr, 12–24 hr, and 24 hr and greater principally are considered throughout this dissertation. The shorter durations exhibit more front-loadedness of the rainfall—higher rainfall rates occur early in the storm duration. Contrary to prior expectation, the statistics of the 0–12 hr and 12–24 hr duration dimensionless hyetographs appear comparable. The empirical hyetograph analysis in chapter 8 considers shorter and narrower duration ranges such as 0–3 hr and 3–6 hr. In general, rainfall rates, as expressed in percentage of depth, are equivalent for the first 20 percent or so of the storm duration independent of duration length up to about 12 hr.

8. *On the influence of season or month of storm occurrence on hyetograph statistics.* Very subtle relations between the mean, median, and L-scale statistics of observed dimensionless hyetographs and the month of occurrence were seen, but the relations are difficult to define. It is concluded that any seasonal differences in the hyetograph shape are insignificant compared to other inherent uncertainties in the analysis. The monthly analysis is centered on figure 47 of chapter 6.

9. *On the compatibility of the five data bases.* Five data base modules (`austin`, `dallas`, `fortworth`, `sanantonio`, `smallruralsheds`) of observed rainfall hyetographs are considered. Four of the modules represent the Austin, Dallas, Fort Worth, and San Antonio urban areas and the `smallruralsheds` module represents more disperse rural regions of Texas. The modules are deemed compatible with one exception. The `dallas` module hyetographs having 24 hr and greater durations appear to lack the large mean and median values seen in the other modules for reasons that are not understood. The analysis is graphically illustrated on figures 48–53 of chapter 6. In a few instances the 24 hr and greater hyetographs for the `dallas` module were not considered (see table 25). The text explicitly identifies the exceptions.

10. *On the prior-Probability Weighted Moments.* The use of the prior-Probability Weighted Moments for the computation of the L-moments was required because of the uneven and nonrandom distribution of the data points defining the observed hyetographs. The method requires a simple numerical approximation to a derivative in eq. 46 of chapter 4. The method is useful in the context of the hyetograph analysis but likely has rather limited potential for other applications. The method or similar analogs have not been previously described in the literature. Unbiased estimators of the L-moments were used in all other components of this dissertation outside of the computation of hyetograph L-moments.

11. *On the Modification of the Carman-Kozeny Equation for Application of L-moment Statistics for Estimation of the Intrinsic Permeability of Porous Media.* The Carman-Kozeny equation is important for estimation of the intrinsic permeability of porous media based on physical properties of the media such as grain size (diameter) and porosity. The derivations and supporting discussion in chapter 8 indicate that a promising new application of L-moments for estimation of permeability is possible through

a. Characterizing the distribution of grain size (diameter) data by computing prior-Probability Weighted Moment based L-moment statistics.

b. Selecting a suitable quantile function to model the distribution.

c. Fitting of the suitable quantile function to the L-moments.

d. Solving an integral either analytically or numerically to estimate an correction factor to the Carman-Kozeny equation.

Based on a few simple analytical examples, the correction factor appears dependent on the model of the grain- or particle-size distribution as well as the "moments" of the distribution itself. This conclusion is contrary to a conclusion of distribution independence reached by previous researchers as discussed in chapter 8.

APPENDIX A

Reference list of U.S. Geological Survey reports used for development of the hyetograph data base

AUSTIN URBAN STUDIES

U.S. Geological Survey, 1967, Basic data for urban hydrology study, Austin, Texas, 1967: U.S. Geological Survey, Texas District, 59 p.

U.S. Geological Survey, 1968, Compilation of hydrologic data, Austin, Texas, 1968: U.S. Geological Survey, Texas District, 68 p.

Robbins, W.D., 1969, Annual compilation and analysis of hydrologic data for urban studies in the Austin, Texas metropolitan area, 1969: U.S. Geological Survey, Texas District, 46 p.

VanZandt, J.K., 1972, Annual compilation and analysis of hydrologic data for urban studies in the Austin, Texas metropolitan area, 1970: U.S. Geological Survey Open-File Report, 70 p.

Tovar, F.H., 1973, Annual compilation and analysis of hydrologic data for urban studies in the Austin, Texas metropolitan area, 1971: U.S. Geological Survey Open-File Report, 73 p.

Wehmeyer, E.E., 1974, Hydrologic data for urban studies in the Austin, Texas metropolitan area, 1972: U.S. Geological Survey Open-File Report, 49 p.

Mitchell, R.N., 1975, Hydrologic data for urban studies in the Austin, Texas metropolitan area, 1973: U.S. Geological Survey Open-File Report, 61 p.

Mitchell, R.N., 1976, Hydrologic data for urban studies in the Austin, Texas metropolitan area, 1974: U.S. Geological Survey Open-File Report, 60 p.

Choffel, K.L., Roddy, W.R., and Mitchell, R.N., 1977, Hydrologic data for urban studies in the Austin, Texas metropolitan area, 1975: U.S. Geological Survey Open-File Report 76–885, 126 p.

Maderak, M.L., Gordon, J.D., and Mitchell, R.N., 1978, Hydrologic data for urban studies in the Austin, Texas metropolitan area, 1976: U.S. Geological Survey Open-File Report 78–457, 263 p.

Slade, R.M., Jr., Gordon, J.D., and Mitchell, R.N., 1979, Hydrologic data for urban studies in the Austin, Texas metropolitan area, 1977: U.S. Geological Survey Open-File Report 79–271, 192 p.

Slade, R.M., Jr., Dorsey, M.E., Gordon, J.D., and Mitchell, R.N., 1980, Hydrologic data for urban studies in the Austin, Texas metropolitan area, 1978: U.S. Geological Survey Open-File Report 80–728, 227 p.

Slade, R.M., Jr., Dorsey, M.E., Gordon, J.D., Mitchell, R.N., and Gaylord, J.L., 1981, Hydrologic data for urban studies in the Austin, Texas metropolitan area, 1979: U.S. Geological Survey Open-File Report 81–628, 281 p.

Slade, R.M., Jr., Gaylord, J.L., Dorsey, M.E., Mitchell, R.N., and Gordon, J.D., 1982, Hydrologic data for urban studies in the Austin, Texas metropolitan area, 1980: U.S. Geological Survey Open-File Report 82–506, 264 p.

Massey, B.C., Reeves, W.E., and Lear, W.A., 1982, Flood of May 24-25, 1981, in the Austin, Texas metropolitan area: U.S. Geological Survey Hydrologic Investigations Atlas HA–656, 2 p.

Slade, R.M., Jr., Veenhuis, J.E., Dorsey, M.E., Gardiner, H., and Smith, A.E., 1983, Hydrologic data for urban studies in the Austin, Texas metropolitan area, 1981: U.S. Geological Survey Open-File Report 83–44, 293 p.

Slade, R.M., Jr., Veenhuis, J.E., Dorsey, M.E., Stewart, S.L., and Ruiz, L.M., 1984, Hydrologic data for urban studies in the Austin, Texas metropolitan area, 1982: U.S. Geological Survey Open-File Report 84–061, 196 p.

Gordon, J.D., Pate, D.L., and Dorsey, M.E., 1985, Hydrologic data for urban studies in the Austin, Texas metropolitan area, 1983: U.S. Geological Survey Open-File Report 85–172, 154 p.

Gordon, J.D., Pate, D.L., and Dorsey, M.E., 1986, Hydrologic data for urban studies in the Austin metropolitan area, Texas, 1984: U.S. Geological Survey Open-File Report 85–676, 92 p.

Veenhuis, J.E. and Gannett, D.G., 1986, The effects of urbanization on floods in the Austin metropolitan area, Texas: U.S. Geological Survey Water-Resources Investigations Report 86–4069, 65 p.

Gordon, J.D., Pate, D.L., and Dorsey, M.E., 1987, Hydrologic data for urban studies in the Austin metropolitan area, Texas, 1985: U.S. Geological Survey Open-File Report 87–224, 170 p.

Gordon, J.D., Pate, D.L., and Slagle, D.L., 1988, Hydrologic data for urban studies in the Austin metropolitan area, Texas, 1986: U.S. Geological Survey Open-File Report 87–768, 144 p.

DALLAS URBAN STUDIES

U.S. Geological Survey, 1965, Basic data for urban hydrology study, Dallas, Texas, 1965: U.S. Geological Survey, Texas District, 80 p.

U.S. Geological Survey, 1966, Basic data for urban hydrology study, Dallas, Texas, 1966: U.S. Geological Survey, Texas District, 198 p.

U.S. Geological Survey, 1967, Basic data for urban hydrology study, Dallas, Texas, 1967: U.S. Geological Survey, Texas District, 80 p.

U.S. Geological Survey, 1968, Basic data for urban hydrology study, Dallas, Texas, 1968: U.S. Geological Survey, Texas District, 103 p.

Dempster, G.R., Jr. and Massey, B.C., 1971, Annual compilation and analysis of hydrologic data for urban studies in the Dallas, Texas metropolitan area, 1969: U.S. Geological Survey, Texas District, 136 p.

Dempster, G.R., Jr. and Massey, B.C., 1972, Annual compilation and analysis of hydrologic data for urban studies in the Dallas, Texas metropolitan area, 1970: U.S. Geological Survey, Texas District, 122 p.

Massey, B.C., 1973, Annual compilation and analysis of hydrologic data for urban studies in the Dallas, Texas metropolitan area, 1971: U.S. Geological Survey, Texas District, 84 p.

Massey, B.C. and Wood, C.M., 1974, Hydrologic data for urban studies in the Dallas, Texas metropolitan area, 1972: U.S. Geological Survey Open-File Report, 136 p.

Dempster, G.R., Jr., 1974, Effects of urbanization on floods in the Dallas, Texas metropolitan area: U.S. Geological Survey Water-Resources Investigations Report 60–73, 51 p.

Hampton, B.B., 1975, Hydrologic data for urban studies in the Dallas, Texas metropolitan area, 1973: U.S. Geological Survey Open-File Report, 146 p.

Hampton, B.B., 1976, Hydrologic data for urban studies in the Dallas, Texas metropolitan area, 1974: U.S. Geological Survey Open-File Report, 182 p.

Hampton, B.B. and Wood, C.M.,1977, Hydrologic data for urban studies in the Dallas, Texas metropolitan area, 1975: U.S. Geological Survey Open-File Report 77–381, 209 p.

Hampton, B.B. and Wood, C.M., 1978, Hydrologic data for urban studies in the Dallas, Texas metropolitan area, 1976: U.S. Geological Survey Open-File Report 78–437, 161 p.

Hampton, B.B. and Wood, C.M., 1979, Hydrologic data for urban studies in the Dallas, Texas metropolitan area, 1977: U.S. Geological Survey Open-File Report 79–562, 146 p.

Hampton, B.B. and Wood, C.M., 1980, Hydrologic data for urban studies in the Dallas, Texas metropolitan area, 1978: U.S. Geological Survey Open-File Report 80–1004, 114 p.

Wood, C.M., Butler, H.S., and Benton, J.D., 1981, Hydrologic data for urban studies in the Dallas, Texas metropolitan area, 1979: U.S. Geological Survey Open-File Report 81–491, 147 p.

Land, L.F., Schroeder, E.E., and Hampton, B.B., 1982, Techniques for estimating the magnitude and frequency of floods in the Dallas-Fort Worth metropolitan area, Texas: U.S. Geological Survey Water-Resources Investigations Report 82–18, 55 p.

FORT WORTH URBAN STUDIES

Dempster, G.R., Jr., and Massey, B.C., 1969, Annual compilation and analysis of hydrologic data for urban studies in the Fort Worth, Texas metropolitan area, 1969: U.S. Geological Survey Open-File Report, 50 p.

Dempster, G.R., Jr., and Massey, B.C., 1972, Annual compilation and analysis of hydrologic data for urban studies in the Fort Worth, Texas metropolitan area, 1970: U.S. Geological Survey Open-File Report, 89 p.

Hampton, B.B., 1973, Annual compilation and analysis of hydrologic data for urban studies in the Fort Worth, Texas metropolitan area, 1971: U.S. Geological Survey Open-File Report, 77 p.

Hampton, B.B., 1974, Hydrologic data for urban studies in the Fort Worth, Texas metropolitan area, 1972: U.S. Geological Survey Open-File Report, 123 p.

Hampton, B.B., 1975, Hydrologic data for urban studies in the Fort Worth, Texas metropolitan area, 1973: U.S. Geological Survey Open-File Report, 129 p.

Slade, R.M., Jr., and Taylor, J.M., 1976, Hydrologic data for urban studies in the Fort Worth, Texas metropolitan area, 1974: U.S. Geological Survey Open-File Report, 100 p.

Slade, R.M., Jr., and Taylor, J.M., 1977, Hydrologic data for urban studies in the Fort Worth, Texas metropolitan area, 1975: U.S. Geological Survey Open-File Report 77–266, 96 p.

Slade, R.M., Jr., and Taylor, J.M., 1978, Hydrologic data for urban studies in the Fort Worth, Texas metropolitan area, 1976: U.S. Geological Survey Open-File Report 77–770, 84 p.

Slade, R.M., Jr., Taylor, J.M., and Haynes, D.L., 1979, Hydrologic data for urban studies in the Fort Worth, Texas metropolitan area, 1977: U.S. Geological Survey Open-File Report 79–216, 39 p.

Land, L.F., Schroeder, E.E., and Hampton, B.B., 1982, Techniques for estimating the magnitude and frequency of floods in the Dallas-Fort Worth metropolitan area, Texas: U.S. Geological Survey Water-Resources Investigations Report 82–18, 55 p.
[also listed in DALLAS URBAN STUDIES section]

SAN ANTONIO URBAN STUDIES

Land, L.F., 1971, Annual compilation and analysis of hydrologic data for urban studies in the San Antonio, Texas metropolitan area, 1969: U.S. Geological Survey 109 p.

Land, L.F., 1972, Annual compilation and analysis of hydrologic data for urban studies in the San Antonio, Texas metropolitan area, 1970: U.S. Geological Survey, Texas District, 178 p.

Steger, R.D., 1973, Annual compilation and analysis of hydrologic data for urban studies in the San Antonio, Texas metropolitan area, 1971: U.S. Geological Survey, Texas District, 109 p.

Steger, R.D., 1974, Hydrologic data for urban studies in the San Antonio, Texas metropolitan area, 1972: U.S. Geological Survey Open-File Report, 102 p.

Steger, R.D., 1975, Hydrologic data for urban studies in the San Antonio, Texas metropolitan area, 1973: U.S. Geological Survey Open-File Report, 127 p.

Gonzalez, V., 1976, Hydrologic data for urban studies in the San Antonio, Texas metropolitan area, 1974: U.S. Geological Survey Open-File Report, 109 p.

Harmsen, L., 1977, Hydrologic data for urban studies in the San Antonio, Texas metropolitan area, 1975: U.S. Geological Survey Open-File Report 77–221, 91 p.

Harmsen, L., 1978, Hydrologic data for urban studies in the San Antonio, Texas metropolitan area, 1976: U.S. Geological Survey Open-File Report 78–164, 132 p.

Perez, R., 1980, Hydrologic data for urban studies in the San Antonio, Texas metropolitan area, 1977: U.S. Geological Survey Open-File Report 80–743, 100 p.

Perez, R., 1981, Hydrologic data for urban studies in the San Antonio, Texas metropolitan area, 1978: U.S. Geological Survey Open-File Report 81–922, 91 p.

Perez, R., 1982, Hydrologic data for urban studies in the San Antonio, Texas metropolitan area, 1979–80: U.S. Geological Survey Open-File Report 82–158, 125 p.

Perez, R., 1983, Hydrologic data for urban studies in the San Antonio, Texas metropolitan area, 1981: U.S. Geological Survey Open-File Report 83–35, 58 p.

BRAZOS BASIN: Cow Bayou Watershed Studies

U.S. Geological Survey, 1960, Hydrologic studies of small watersheds, Cow Bayou Basin, Texas: U.S. Geological Survey, Texas District, 52 p.

U.S. Geological Survey, 1961, Hydrologic studies of small watersheds, Cow Bayou Basin, Texas: U.S. Geological Survey, Texas District, 17 p.

U.S. Geological Survey, 1962, Hydrologic data of Cow Bayou, Brazos River Basin, Texas, 1962: U.S. Geological Survey, Texas District, 68 p.

U.S. Geological Survey, 1963, Compilation of hydrologic data, Cow Bayou, Brazos River Basin, Texas, 1963: U.S. Geological Survey, Texas District, 40 p.

U.S. Geological Survey, 1964, Compilation of hydrologic data, Cow Bayou, Brazos River Basin, Texas, 1964: U.S. Geological Survey, Texas District, 55 p.

U.S. Geological Survey, 1965, Compilation of hydrologic data, Cow Bayou, Brazos River Basin, Texas, 1965: U.S. Geological Survey, Texas District, 64 p.

U.S. Geological Survey, 1966, Compilation of hydrologic data, Cow Bayou, Brazos River Basin, Texas, 1966: U.S. Geological Survey, Texas District, 72 p.

U.S. Geological Survey, 1967, Compilation of hydrologic data, Cow Bayou, Brazos River Basin, Texas, 1967: U.S. Geological Survey, Texas District, 62 p.

U.S. Geological Survey, 1968, Compilation of hydrologic data, Cow Bayou, Brazos River Basin, Texas, 1968: U.S. Geological Survey, Texas District, 80 p.

U.S. Geological Survey, 1969, Hydrologic studies of small watersheds, Cow Bayou, Brazos River Basin, Texas, 1955–64: U.S. Geological Survey, Texas District, 66 p.

Sansom, J.N., 1969, Annual compilation and analysis of hydrologic data for Cow Bayou, Brazos River Basin, Texas, 1969: U.S. Geological Survey, Texas District, 76 p.

Watson, J.A., 1970, Annual compilation and analysis of hydrologic data for Cow Bayou, Brazos River Basin, Texas, 1970: U.S. Geological Survey, Texas District, 85 p.

Watson, J.A., 1971, Annual compilation and analysis of hydrologic data for Cow Bayou, Brazos River Basin, Texas, 1971: U.S. Geological Survey, Texas District, 63 p.

VanZandt, J.K., 1972, Hydrologic data for Cow Bayou, Brazos River Basin, Texas, 1972: U.S.Geological Survey Open-File Report, 72 p.

VanZandt, J.K., 1973, Hydrologic data for Cow Bayou, Brazos River Basin, Texas, 1973: U.S.Geological Survey Open-File Report, 74 p.

VanZandt, J.K., 1974, Hydrologic data for Cow Bayou, Brazos River Basin, Texas, 1974: U.S.Geological Survey Open-File Report, 63 p.

Mitchell, R.N. and Wehmeyer, E.E., 1977, Hydrologic data for Cow Bayou, Brazos River Basin, Texas, 1975: U.S.Geological Survey Open-File Report 76–723, 81 p.

BRAZOS RIVER BASIN: Green Creek Watershed Studies

U.S. Geological Survey, 1960, Hydrologic studies of small watersheds, Green Creek Basin, Texas: U.S. Geological Survey, Texas District, 42 p.

U.S. Geological Survey, 1961, Hydrologic studies of small watersheds, Green Creek study area, Texas, 1961: U.S. Geological Survey, Texas District, [variously paged].

U.S. Geological Survey, 1962, Hydrologic data of Green Creek, Brazos River Basin, Texas, 1962: U.S. Geological Survey, Texas District, [variously paged].

U.S. Geological Survey, 1963, Compilation of hydrologic data, Green Creek, Brazos River Basin, Texas, 1963: U.S. Geological Survey, Texas District, 52 p.

U.S. Geological Survey, 1964, Compilation of hydrologic data, Green Creek, Brazos River Basin, Texas, 1964: U.S. Geological Survey, Texas District, 58 p.

U.S. Geological Survey, 1965, Compilation of hydrologic data, Green Creek, Brazos River Basin, Texas, 1965: U.S. Geological Survey, Texas District, 44 p.

U.S. Geological Survey, 1966, Compilation of hydrologic data, Green Creek, Brazos River Basin, Texas, 1966: U.S. Geological Survey, Texas District, 109 p.

U.S. Geological Survey, 1967, Compilation of hydrologic data, Green Creek, Brazos River Basin, Texas, 1967: U.S. Geological Survey, Texas District, 34 p.

U.S. Geological Survey, 1968, Compilation of hydrologic data, Green Creek, Brazos River Basin, Texas, 1968: U.S. Geological Survey, Texas District, 66 p.

Massey, B.C., 1969, Annual compilation and analysis of hydrologic data for Green Creek, Brazos River Basin, Texas, 1969: U.S. Geological Survey, Texas District, 44 p.

U.S. Geological Survey, 1969, Preparation of hydrologic data small watersheds project: U.S. Geological Survey, Texas District, 43 p.

Hampton, B.B., 1970, Annual compilation and analysis of hydrologic data for Green Creek, Brazos River Basin, Texas,1970: U.S. Geological Survey Open-File Report, 42 p.

Hampton, B.B., 1971, Annual compilation and analysis of hydrologic data for Green Creek, Brazos River Basin, Texas, 1971: U.S. Geological Survey Open-File Report, 30 p.

U.S. Geological Survey, 1972, Hydrologic studies of small watersheds, Green Creek, Brazos River Basin, Texas, 1955–66: U.S. Geological Survey, Texas District, 55 p.

BRAZOS RIVER BASIN: Little Pond Creek and North Elm Creek Watershed Studies

Slade, R.M., Jr., 1970, Annual compilation and analysis of hydrologic data for Little Pond Creek and North Elm Creek, Brazos River Basin, Texas, 1970: U.S. Geological Survey Open-File Report, 44 p.

Hawkinson, R.O., 1972, Hydrologic studies of Little Pond Creek and North Elm Creek watersheds, Brazos River Basin, Texas, 1963-69: U.S. Geological Survey, Texas District, 137 p.

VanZandt, J.K., 1973, Annual compilation and analysis of hydrologic data for Little Pond Creek and North Elm Creek, Brazos River Basin, Texas, 1971: U.S. Geological Survey Open-File Report, 52 p.

Mitchell, R.N., 1974, Hydrologic data for Little Pond Creek and North Elm Creek, Brazos River Basin, Texas, 1972: U.S. Geological Survey Open-File Report, 37 p.

COLORADO RIVER BASIN: Deep Creek Watershed Studies

U.S. Geological Survey, 1960, Hydrologic studies of small watersheds, Deep Creek Basin, Texas: U.S. Geological Survey, Texas District, 58 p.

U.S. Geological Survey, 1961, Hydrologic studies of small watersheds, Deep Creek study area, Texas, 1961: U.S. Geological Survey, Texas District, 111 p.

U.S. Geological Survey, 1962, Hydrologic data of Deep Creek, Colorado River Basin, Texas, 1962: U.S. Geological Survey, Texas District, 51 p.

U.S. Geological Survey, 1963, Hydrologic data of Deep Creek, Colorado River Basin, Texas, 1963: U.S. Geological Survey, Texas District, 153 p.

U.S. Geological Survey, 1964, Compilation of hydrologic data, Deep Creek, Colorado River Basin, Texas, 1964: U.S. Geological Survey, Texas District, 78 p.

U.S. Geological Survey, 1965, Hydrologic studies of small watersheds, Deep Creek, Colorado River Basin, Texas, 1951–61: U.S. Geological Survey, Texas District, 123 p.

U.S. Geological Survey, 1965, Compilation of hydrologic data, Deep Creek, Colorado River Basin, Texas, 1965: U.S. Geological Survey, Texas District, 72 p.

U.S. Geological Survey, 1966, Compilation of hydrologic data, Deep Creek, Colorado River Basin, Texas, 1966: U.S. Geological Survey, Texas District, 55 p.

U.S. Geological Survey, 1967, Compilation of hydrologic data, Deep Creek, Colorado River Basin, Texas, 1967: U.S. Geological Survey, Texas District, 87 p.

U.S. Geological Survey, 1968, Compilation of hydrologic data, Deep Creek, Colorado River Basin, Texas, 1968: U.S. Geological Survey, Texas District, 86 p.

Hejl, H.R., 1971, Annual compilation and analysis of hydrologic data for Deep Creek, Colorado River Basin, Texas, 1969: U.S. Geological Survey, Texas District, 73 p.

Hejl, H.R., 1972, Annual compilation and analysis of hydrologic data for Deep Creek, Colorado River Basin, Texas, 1970: U.S. Geological Survey, Texas District, 35 p.

Lee, J.N., 1973, Annual compilation and analysis of hydrologic data for Deep Creek, Colorado River Basin, Texas, 1971: U.S. Geological Survey, Texas District, 76 p.

COLORADO RIVER BASIN: Mukewater Creek Watershed Studies

U.S. Geological Survey, 1960, Hydrologic studies of small watersheds Mukewater Creek Basin, Texas: U.S. Geological Survey, Texas District, 30 p.

U.S. Geological Survey, 1961, Hydrologic studies of small watersheds Mukewater Creek study area, Texas, 1961: U.S. Geological Survey, Texas District, 47 p.

U.S. Geological Survey, 1962, Hydrologic data of Mukewater Creek, Colorado River Basin, Texas, 1962: U.S. Geological Survey, Texas District, 60 p.

U.S. Geological Survey, 1963, Compilation of hydrologic data of small watersheds Mukewater Creek, Colorado River Basin, Texas, 1963: U.S. Geological Survey, Texas District, 80 p.

U.S. Geological Survey, 1964, Compilation of hydrologic data of small watersheds Mukewater Creek, Colorado River Basin, Texas, 1964: U.S. Geological Survey, Texas District, 56 p.

U.S. Geological Survey, 1965, Hydrologic studies of small watersheds Mukewater Creek, Colorado River Basin, Texas, 1952–60: U.S. Geological Survey, Texas District, 70 p.

U.S. Geological Survey, 1965, Compilation of hydrologic data of small watersheds Mukewater Creek, Colorado River Basin, Texas, 1965: U.S. Geological Survey, Texas District, 67 p.

U.S. Geological Survey, 1966, Compilation of hydrologic data of small watersheds Mukewater Creek, Colorado River Basin, Texas, 1966: U.S. Geological Survey, Texas District, 56 p.

U.S. Geological Survey, 1967, Compilation of hydrologic data of small watersheds Mukewater Creek, Colorado River Basin, Texas, 1967: U.S. Geological Survey, Texas District, 87 p.

U.S. Geological Survey, 1968, Compilation of hydrologic data of small watersheds Mukewater Creek, Colorado River Basin, Texas, 1968: U.S. Geological Survey, Texas District, 81 p.

Hejl, H.R., 1969, Annual compilation and analysis of hydrologic data for Mukewater Creek, Colorado River Basin, Texas, 1969: U.S. Geological Survey, Texas District, 84 p.

Hejl, H.R., 1972, Annual compilation and analysis of hydrologic data for Mukewater Creek, Colorado River Basin, Texas, 1970: U.S. Geological Survey Open-File Report, 69 p.

Lee, J.N., 1973, Annual compilation and analysis of hydrologic data for Mukewater Creek, Colorado River Basin, Texas, 1971: U.S. Geological Survey Open-File Report, 89 p.

Lee, J.N., 1974, Hydrologic data for Mukewater Creek, Colorado River Basin, Texas, 1972: U.S. Geological Survey Open-File Report, 67 p.

Lee, J.N., 1975, Hydrologic data for Mukewater Creek, Colorado River Basin, Texas, 1973: U.S. Geological Survey Open-File Report, 65 p.

SAN ANTONIO RIVER BASIN: Calaveras Creek Watershed Studies

U.S. Geological Survey, 1960, Hydrologic studies of small watersheds, Calaveras Creek Basin, Texas, 1960: U.S. Geological Survey, Texas District, 36 p.

U.S. Geological Survey, 1961, Hydrologic studies of small watersheds, Calaveras Creek study area, Texas, 1961: U.S. Geological Survey, Texas District, [variously paged].

U.S. Geological Survey, 1962, Hydrologic data of Calaveras Creek, San Antonio River Basin, Texas, 1962: U.S. Geological Survey, Texas District, 41 p.

U.S. Geological Survey, 1963, Compilation of hydrologic data, Calaveras Creek, San Antonio River Basin, Texas, 1963: U.S. Geological Survey, Texas District, 41 p.

U.S. Geological Survey, 1964, Compilation of hydrologic data, Calaveras Creek, San Antonio River Basin, Texas, 1964: U.S. Geological Survey, Texas District, 50 p.

U.S. Geological Survey, 1965, Compilation of hydrologic data, Calaveras Creek, San Antonio River Basin, Texas, 1965: U.S. Geological Survey, Texas District, 62 p.

U.S. Geological Survey, 1966, Compilation of hydrologic data, Calaveras Creek, San Antonio River Basin, Texas, 1966: U.S. Geological Survey, Texas District, 34 p.

U.S. Geological Survey, 1967, Compilation of hydrologic data, Calaveras Creek, San Antonio River Basin, Texas, 1967: U.S. Geological Survey, Texas District, 47 p.

U.S. Geological Survey, 1968, Compilation of hydrologic data, Calaveras Creek, San Antonio River Basin, Texas, 1968: U.S. Geological Survey, Texas District, 66 p.

Alexander, J.M., 1969, Annual compilation and analysis of hydrologic data for Calaveras Creek, San Antonio River Basin, Texas, 1969: U.S. Geological Survey, Texas District, 56 p.

Reddy, D.R., 1971, Annual compilation and analysis of hydrologic data for Calaveras Creek, San Antonio River Basin, Texas, 1970: U.S. Geological Survey Open-File Report, 63 p.

U.S. Geological Survey, 1972, Hydrologic studies of small watersheds, Calaveras Creek, San Antonio River Basin, Texas, 1955–68: U.S. Geological Survey, Texas District, 109 p.

Steger, R.D., 1973, Annual compilation and analysis of hydrologic data for Calaveras and Escondido Creeks, San Antonio River Basin, Texas, 1971: U.S. Geological Survey Open-File Report, 74 p.

SAN ANTONIO RIVER BASIN: Escondido Creek Watershed Studies

U.S. Geological Survey, 1960, Hydrologic studies of small watersheds, Escondido Creek Basin, Texas, 1960: U.S. Geological Survey, Texas District, 45 p.

U.S. Geological Survey, 1961, Hydrologic studies of small watersheds, Escondido Creek Basin, Texas, 1961: U.S. Geological Survey, Texas District, 70 p.

U.S. Geological Survey, 1962, Hydrologic data of Escondido Creek, San Antonio River Basin, Texas, 1962: U.S. Geological Survey, Texas District, 43 p.

U.S. Geological Survey, 1963, Compilation of hydrologic data, Escondido Creek, San Antonio River Basin, Texas, 1963: U.S. Geological Survey, Texas District, 85 p.

U.S. Geological Survey, 1964, Compilation of hydrologic data, Escondido Creek, San Antonio River Basin, Texas, 1964: U.S. Geological Survey, Texas District, 86 p.

U.S. Geological Survey, 1965, Compilation of hydrologic data, Escondido Creek, San Antonio River Basin, Texas, 1965: U.S. Geological Survey, Texas District, 72 p.

U.S. Geological Survey, 1966, Compilation of hydrologic data, Escondido Creek, San Antonio River Basin, Texas, 1966: U.S. Geological Survey, Texas District, 44 p.

U.S. Geological Survey, 1967, Hydrologic studies of small watersheds, Escondido Creek, San Antonio River Basin, Texas, 1955–63: U.S. Geological Survey, Texas District, 123 p.

U.S. Geological Survey, 1967, Compilation of hydrologic data, Escondido Creek, San Antonio River Basin, Texas, 1967: U.S. Geological Survey, Texas District, 73 p.

U.S. Geological Survey, 1968, Compilation of hydrologic data, Escondido Creek, San Antonio River Basin, Texas, 1968: U.S. Geological Survey, Texas District, 73 p.

Reddy, D.R., 1971, Annual compilation and analysis of hydrologic data for Escondido Creek, San Antonio River Basin Texas, 1969: U.S. Geological Survey, Texas District, 62 p.

Reddy, D.R., 1971, Annual compilation and analysis of hydrologic data for Escondido Creek, San Antonio River Basin, Texas, 1970: U.S. Geological Survey Open-File Report, 65 p.

Steger, R.D., 1973, Annual compilation and analysis of hydrologic data for Calaveras and Escondido Creeks, San Antonio River Basin, Texas, 1971: U.S. Geological Survey Open-File Report, 74 p.
[Also listed in SAN ANTONIO RIVER BASIN Calaveras Creek Watershed Studies Section]

TRINITY RIVER BASIN: Elm Fork Watershed Studies

U.S. Geological Survey, 1961, Hydrologic studies of small watersheds, Elm Fork Trinity River study area, Texas, 1961: U.S. Geological Survey, Texas District, 43 p.

U.S. Geological Survey, 1962, Hydrologic studies of small watersheds, Elm Fork Trinity River Basin, Montague and Cooke Counties, Texas 1956–60: U.S. Geological Survey, Texas District, 77 p.

U.S. Geological Survey, 1962, Hydrologic data of Elm Fork Trinity River, Trinity River Basin, Texas, 1962: U.S. Geological Survey, Texas District, 60 p.

U.S. Geological Survey, 1963, Compilation of hydrologic data, Elm Fork Trinity River, Trinity River Basin, Texas, 1963: U.S. Geological Survey, Texas District, 60 p.

U.S. Geological Survey, 1965, Compilation of hydrologic data, Elm Fork Trinity River, Trinity River Basin, Texas, 1964–65: U.S. Geological Survey, Texas District, 135 p.

U.S. Geological Survey, 1966, Compilation of hydrologic data, Elm Fork Trinity River, Trinity River Basin, Texas, 1966: U.S. Geological Survey, Texas District, 60 p.

U.S. Geological Survey, 1967, Compilation of hydrologic data, Elm Fork Trinity River, Trinity River Basin, Texas, 1967: U.S. Geological Survey, Texas District, 54 p.

U.S. Geological Survey, 1968, Compilation of hydrologic data, Elm Fork Trinity River, Trinity River Basin, Texas, 1968: U.S. Geological Survey, Texas District, 84 p.

Sansom, J.N., 1969, Annual compilation and analysis of hydrologic data for Elm Fork Trinity River, Trinity River Basin, Texas, 1969: U.S. Geological Survey, Texas District, 47 p.

Sansom, J.N., 1972, Annual compilation and analysis of hydrologic data for Elm Fork Trinity River, Trinity River Basin, Texas, 1970: U.S. Geological Survey Open-File Report, 47 p.

Lucero, E.D., 1973, Annual compilation and analysis of hydrologic data for Elm Fork Trinity River, Trinity River Basin, Texas, 1971: U.S. Geological Survey Open-File Report, 27 p.

TRINITY RIVER BASIN: Honey Creek Watershed Studies

U.S. Geological Survey, 1960, Hydrologic studies of small watersheds, Honey Creek Basin, Texas 1960: U.S. Geological Survey, Texas District, 89 p.

U.S. Geological Survey, 1961, Hydrologic studies of small watersheds, Honey Creek Basin, Texas 1961: U.S. Geological Survey, Texas District, 73 p.

U.S. Geological Survey, 1962, Hydrologic studies of small watersheds, Honey Creek Basin, Collin and Grayson Counties, Texas 1953–59: U.S. Geological Survey, Texas District, 102 p.

U.S. Geological Survey, 1962, Hydrologic data of Honey Creek, Trinity River Basin, Texas, 1962: U.S. Geological Survey, Texas District, 148 p.

U.S. Geological Survey, 1963, Compilation of hydrologic data, Honey Creek, Trinity River Basin, Texas, 1963: U.S. Geological Survey, Texas District, 83 p.

U.S. Geological Survey, 1964, Compilation of hydrologic data, Honey Creek, Trinity River Basin, Texas, 1964: U.S. Geological Survey, Texas District, 77 p.

U.S. Geological Survey, 1965, Compilation of hydrologic data, Honey Creek, Trinity River basin Texas, 1965: U.S. Geological Survey, Texas District, 79 p.

U.S. Geological Survey, 1966, Compilation of hydrologic data, Honey Creek, Trinity River Basin, Texas, 1966: U.S. Geological Survey, Texas District, 126 p.

U.S. Geological Survey, 1967, Compilation of hydrologic data, Honey Creek, Trinity River Basin, Texas, 1967: U.S. Geological Survey, Texas District, 68 p.

U.S. Geological Survey, 1968, Compilation of hydrologic data, Honey Creek, Trinity River Basin, Texas, 1968: U.S. Geological Survey, Texas District, 78 p.

Sansom, J.N., 1969, Annual compilation and analysis of hydrologic data, Honey Creek, Trinity River Basin, Texas, 1969: U.S. Geological Survey Open-File Report, 85 p.

Sansom, J.N., 1972, Annual compilation and analysis of hydrologic data, Honey Creek, Trinity River Basin, Texas, 1970: U.S. Geological Survey Open-File Report, 66 p.

Hampton, B.B., 1973, Annual compilation and analysis of hydrologic data for Honey Creek, Trinity River Basin, Texas, 1971: U.S. Geological Survey Open-File Report, 28 p.

TRINITY RIVER BASIN: Little Elm Creek Watershed Studies

U.S. Geological Survey, 1960, Hydrologic studies of small watersheds, Little Elm Creek Basin, Texas, 1960: U.S. Geological Survey, Texas District, 27 p.

U.S. Geological Survey, 1961, Hydrologic studies of small watersheds, Little Elm Creek study area, Trinity River Basin, Texas, 1961: U.S. Geological Survey, Texas District, 23 p.

U.S. Geological Survey, 1962, Hydrologic data of Little Elm Creek, Trinity River Basin, Texas, 1962: U.S. Geological Survey, Texas District, 35 p.

U.S. Geological Survey, 1963, Compilation of hydrologic data, Little Elm Creek, Trinity River Basin, Texas, 1963: U.S. Geological Survey, Texas District, 34 p.

U.S. Geological Survey, 1964, Compilation of hydrologic data, Little Elm Creek, Trinity River Basin, Texas, 1964: U.S. Geological Survey, Texas District, 28 p.

U.S. Geological Survey, 1965, Compilation of hydrologic data, Little Elm Creek, Trinity River Basin, Texas, 1965: U.S. Geological Survey, Texas District, 28 p.

U.S. Geological Survey, 1966, Hydrologic studies of small watersheds, Little Elm Creek, Trinity River Basin, Texas, 1956–62: U.S. Geological Survey, Texas District, 59 p.

U.S. Geological Survey, 1966, Compilation of hydrologic data, Little Elm Creek, Trinity River Basin, Texas, 1966: U.S. Geological Survey, Texas District, 69 p.

U.S. Geological Survey, 1967, Compilation of hydrologic data, Little Elm Creek, Trinity River Basin, Texas, 1967: U.S. Geological Survey, Texas District, 81 p.

U.S. Geological Survey, 1968, Compilation of hydrologic data, Little Elm Creek, Trinity River Basin, Texas, 1968: U.S. Geological Survey, Texas District, 83 p.

Hampton, B.B., 1971, Annual compilation and analysis of hydrologic data for Little Elm Creek, Trinity River Basin, Texas, 1969: U.S. Geological Survey, Texas District, 68 p.

Hampton, B.B., 1972, Annual compilation and analysis of hydrologic data for Little Elm Creek, Trinity River Basin, Texas, 1970: U.S. Geological Survey, Texas District, 100 p.

Hampton, B.B., 1973, Annual compilation and analysis of hydrologic data for Little Elm Creek, Trinity River Basin, Texas, 1971: U.S. Geological Survey, Texas District, 47 p.

Hampton, B.B., 1974, Hydrologic data for Little Elm Creek, Trinity River Basin, Texas, 1972: U.S. Geological Survey Open-File Report, 74 p.

Slade, R.M., Jr., and Taylor, J.M., 1975, Hydrologic data for Little Elm Creek, Trinity River Basin, Texas, 1973: U.S. Geological Survey Open-File Report, 74 p.

Slade, R.M., Jr., and Taylor, J.M., 1976, Hydrologic data for Little Elm Creek, Trinity River Basin, Texas, 1974: U.S. Geological Survey Open-File Report, 73 p.

Slade, R.M., Jr., and Taylor, J.M., 1977, Hydrologic data for Little Elm Creek, Trinity River Basin, Texas, 1975: U.S. Geological Survey Open-File Report 77–83, 108 p.

Slade, R.M., Jr., and Taylor, J.M., 1978, Hydrologic data for Little Elm Creek, Trinity River Basin, Texas, 1976: U.S. Geological Survey Open-File Report 78–100, 78 p.

TRINITY RIVER BASIN: North Creek Watershed Studies

U.S. Geological Survey, 1960, Hydrologic studies of small watersheds, North Creek Basin, Texas: U.S. Geological Survey, Texas District, 19 p.

U.S. Geological Survey, 1961, Hydrologic studies of small watersheds, North Creek study area, Texas: U.S. Geological Survey, Texas District, [variously paged].

U.S. Geological Survey, 1963, Compilation of hydrologic data, North Creek, Trinity River Basin, Texas, 1962–63: U.S. Geological Survey, Texas District, 47 p.

U.S. Geological Survey, 1964, Compilation of hydrologic data, North Creek, Trinity River Basin, Texas, 1964: U.S. Geological Survey, Texas District, 19 p.

U.S. Geological Survey, 1965, Compilation of hydrologic data, North Creek, Trinity River Basin, Texas, 1965: U.S. Geological Survey, Texas District, 30 p.

U.S. Geological Survey, 1966, Compilation of hydrologic data, North Creek, Trinity River Basin, Texas, 1966: U.S. Geological Survey, Texas District, 28 p.

U.S. Geological Survey, 1967, Compilation of hydrologic data, North Creek, Trinity River Basin, Texas, 1967: U.S. Geological Survey, Texas District, 27 p.

U.S. Geological Survey, 1968, Compilation of hydrologic data, North Creek, Trinity River Basin, Texas, 1968: U.S. Geological Survey, Texas District, 36 p.

Kidwell, C.C., 1969, Annual compilation and analysis of hydrologic data for North Creek, Trinity River Basin, Texas, 1969: U.S. Geological Survey, Texas District, 32 p.

Maderak, M.L. and Lucero, E.D., 1971, Annual compilation and analysis of hydrologic data for North Creek, Trinity River Basin, Texas, 1970: U.S. Geological Survey Open-File Report, 32 p.

Lucero, E.D., 1973, Annual compilation and analysis of hydrologic data for North Creek, Trinity River Basin, Texas, 1971: U.S. Geological Survey Open-File Report, 23 p.

Slade, R.M., Jr., 1974, Hydrologic data for North Creek Trinity River Basin, Texas, 1972: U.S. Geological Survey Open-File Report, 31 p.

Slade, R.M., Jr., 1975, Hydrologic data for North Creek Trinity River Basin, Texas, 1973: U.S. Geological Survey Open-File Report, 44 p.

Slade, R.M., Jr., 1976, Hydrologic data for North Creek Trinity River Basin, Texas, 1974: U.S. Geological Survey Open-File Report, 40 p.

Kidwell, C.C., 1977, Hydrologic data for North Creek Trinity River Basin, Texas, 1975: U.S. Geological Survey Open-File Report 76–724, 50 p.

Kidwell, C.C., 1978, Hydrologic data for North Creek Trinity River Basin, Texas, 1976: U.S. Geological Survey Open-File Report 77–732, 42 p.

Kidwell, C.C., 1979, Hydrologic data for North Creek Trinity River Basin, Texas, 1977: U.S. Geological Survey Open-File Report 79–335, 39 p.

Kidwell, C.C., 1980, Hydrologic data for North Creek Trinity River Basin, Texas, 1978: U.S. Geological Survey Open-File Report 80–573, 44 p.

Kidwell, C.C., 1981, Hydrologic data for North Creek Trinity River Basin, Texas, 1979: U.S. Geological Survey Open-File Report 81–823, 38 p.

TRINITY RIVER BASIN: Pin Oak Creek Watershed Studies

U.S. Geological Survey, 1960, Hydrologic studies of small watersheds, Pin Oak Creek, Trinity River Basin, Texas, 1956–62: U.S. Geological Survey, Texas District, 69 p.

U.S. Geological Survey, 1960, Hydrologic studies of small watersheds, Pin Oak Creek Basin, Texas, 1960: U.S. Geological Survey, Texas District, 44 p.

U.S. Geological Survey, 1961, Hydrologic studies of small watersheds, Pin Oak Creek study area, Texas 1961: U.S. Geological Survey, Texas District, 38 p.

U.S. Geological Survey, 1964, Compilation of hydrologic data, Pin Oak Creek, Trinity River Basin, Texas, 1962–64: U.S. Geological Survey, Texas District, 36 p.

U.S. Geological Survey, 1965, Compilation of hydrologic data, Pin Oak Creek, Trinity River Basin, Texas, 1965: U.S. Geological Survey, Texas District, 30 p.

U.S. Geological Survey, 1966, Compilation of hydrologic data, Pin Oak Creek, Trinity River Basin, Texas, 1966: U.S. Geological Survey, Texas District, 27 p.

U.S. Geological Survey, 1967, Compilation of hydrologic data, Pin Oak Creek, Trinity River Basin, Texas, 1967: U.S. Geological Survey, Texas District, 25 p.

U.S. Geological Survey, 1968, Compilation of hydrologic data, Pin Oak Creek, Trinity River Basin Texas, 1968: U.S. Geological Survey, Texas District, 44 p.

Hampton, B.B. and Myers, D.R., 1969, Annual compilation and analysis of hydrologic data, Pin Oak Creek, Trinity River Basin Texas, 1969: U.S. Geological Survey, Texas District, 28 p.

Hampton, B.B. and Myers, D.R., 1972, Annual compilation and analysis of hydrologic data, Pin Oak Creek, Trinity River Basin Texas, 1970: U.S. Geological Survey Open-File Report, 50 p.

Hampton, B.B., 1973, Annual compilation and analysis of hydrologic data for Pin Oak Creek, Trinity River Basin Texas, 1971: U.S. Geological Survey Open-File Report, 18 p.

Hampton, B.B., 1974, Hydrologic data for Pin Oak Creek, Trinity River Basin Texas, 1972: U.S. Geological Survey Open-File Report, 26 p.

APPENDIX B

Background on L-moment Statistical Theory

The L-moments and probability weighted moments are relatively unknown features of univariate statistical theory. Because of the widespread unfamiliarity with these statistics, it is necessary to provide a basic, albeit brief, review in this appendix. References are included in the References section of this dissertation.

MOMENTS OF A DISTRIBUTION

Distribution description is an important component of much statistical analysis and is conducted by the statistical summarization of sample observations of a random variable X. Traditionally, the data are statistically summarized by the product moments of the data (arithmetic mean, standard deviation or variance, skew, and kurtosis). The mathematical definitions and the sampling properties of the product moments are widely known, but are reviewed here.

The theoretical product moments of random variable X are

$$\mu = E[X], \tag{B-1.1}$$

$$\sigma^2 = Var[X] = E[(X-\mu)^2], \tag{B-1.2}$$

$$\mu_3 = E[(X-\mu)^3], \text{ and} \tag{B-1.3}$$

$$\mu_4 = E[(X-\mu)^4] \tag{B-1.4}$$

where μ, σ^2, μ_3, and μ_4 denote the theoretical mean, variance, third moment, and fourth moment, respectively. In general, the higher moments $r \geq 2$ are

$$\mu_r = E[(X-\mu)^r]. \tag{B-2}$$

The $E[\ ]$ is the expectation operator and in terms of the probability density function $f(x)$ is

$$E[X^r] = \int_{-\infty}^{\infty} x^r f(x)dx, \tag{B-3}$$

and in terms of the quantile function $x(F)$ is

$$E[X^r] = \int_0^1 x(F)^r dF. \tag{B-4}$$

Note that the dF term in eq. B-4 is analogous to the incremental probability for each observation in a finite sample. A special treatment of the dF term plays a central role in the p-PWMs described in chapter 4 of this dissertation.

The mean locates the center of the distribution along the real-number line whereas the spread or width of the distribution is measured by the standard deviation, $\sigma = \sqrt{\sigma^2}$. An often used dimensionless representation of the distribution spread is the coefficient of variation, $CV = \sigma/\mu$. The higher moments are almost always expressed as dimensionless quantities $\gamma = \mu_3/\sigma^3$ and $K = \mu_4/\sigma^4$ where γ and K denote the skewness and kurtosis, respectively.

The product moments also are defined for finite samples. The first sample product moment is the mean and is

$$m = \frac{1}{n}\sum_{j=1}^{n} x_j . \tag{B-5}$$

The quantity m is a minimum variance unbiased estimator (MVUE) of the theoretical mean μ. The higher product moments $r \geq 2$ are

$$\overline{m}_r = \frac{1}{n}\sum_{j=1}^{n} (x_j - m)^r . \tag{B-6}$$

$\overline{m}_r$ are not unbiased. Unbiased estimates are obtained by

$$m_2 = s^2 = \frac{n}{(n-1)}\overline{m}_2 , \tag{B-7.1}$$

$$m_3 = \frac{n^2}{(n-1)(n-2)}\overline{m}_3 \text{ , and} \tag{B-7.2}$$

$$m_4 = \frac{n^2}{(n-2)(n-3)}\left\{\left(\frac{n+1}{n-1}\right)\overline{m}_4 - 3m_2^2\right\} . \tag{B-7.3}$$

The sample standard deviation is estimated by the square root of the sample variance, $s = \sqrt{s^2}$. However, though s^2 is unbiased, s is not. The sample CV, skew, and kurtosis are estimated, but are not unbiased, by $cv = s/m$, $g = \overline{m}_3/s^3$, and $k = \bar{k}_4/s^4 + 3$, respectively.

The uniformly minimum variance unbiased estimate (David, 1981, p. 185) of the standard deviation, s_{UMVU}, is

$$s_{UMVU} = \frac{\Gamma[(n-1)/2]}{\Gamma[n/2]\sqrt{2}} \sqrt{\sum_{j=1}^{n} (x_j - m)^2}, \tag{B-8}$$

where the complete Gamma function $\Gamma(k)$ is

$$\Gamma(k) = \int_0^\infty u^{k-1} e^{-u} du \ . \tag{B-9}$$

Finally, it is important to note that sample estimates of cv and g can not exceed certain values. The values depend on the size of the sample regardless of the true values of the statistic (Kirby, 1974). These limits are

$$cv < \sqrt{(n-1)} \text{ and} \tag{B-10.1}$$

$$|g| < \frac{n-2}{\sqrt{(n-1)}} . \tag{B-10.2}$$

For example, if $n = 30$ then $cv < 5.39$ and $|g| < 5.20$ regardless of the true values of CV or γ. These bounds are especially problematic during the analysis of highly variable or highly skewed data. Such data sets in the natural sciences might include annual peak flood time series, grain-size distributions, and permeability measurements.

L-MOMENTS

The majority of this review is derived from Hosking (1990), Hosking and Wallis (1997), and references therein. When the need arises, other references are provided for specifics of L-moment theory development.

Consider a real-valued random variable X with a cumulative distribution function $F(x)$ and a quantile function $x(F)$. As before, F is a cumulative probability or nonexceedance probability and $0 \le F \le 1$. If a random sample of size n is drawn from the distribution of X, and the sample is arranged in ascending order, the values $X_{1:n} \le X_{2:n} \le \ldots \le X_{n:n}$ become the order statistics of X. The mathematical framework of order statistics is well described by David (1981). The expectation of an order statistic can be expressed as

$$E[X_{j:r}] = \frac{r!}{(j-1)!(r-j)!}\int_0^1 x(F)F^{j-1}(1-F)^{r-j}dF \quad . \tag{B-11}$$

The L-moments are the expectations of specific linear combinations of the order statistic expectations. In general, the L-moments are defined by

$$\lambda_r \equiv \frac{1}{r}\sum_{k=0}^{r-1} -1^k \binom{r-1}{k} E[X_{r-k:r}] \quad . \tag{B-12}$$

The formula for the combinations of n distinct items taken r at a time is

$$\binom{a}{b} = {}_aC_b = \frac{a!}{b!(a-b)!} , \tag{B-13}$$

and by definition $\binom{a}{0} = 1$.

The first four L-moments from eq. B-12 are

$$\lambda_1 = E[X_{1:1}] , \tag{B-14.1}$$

$$\lambda_2 = \frac{1}{2}E[X_{2:2} - X_{1:2}] , \tag{B-14.2}$$

$$\lambda_3 = \frac{1}{3}E[X_{3:3} - 2X_{2:3} + X_{1:3}] \text{ , and} \tag{B-14.3}$$

$$\lambda_4 = \frac{1}{4}E[X_{4:4} - 3X_{3:4} + 3X_{2:4} - X_{1:4}] \text{ .} \tag{B-14.4}$$

The first L-moment λ_1 is the mean. The mean is the expected value of a single observation of X. The second L-moment λ_2 is a measure of the dispersion or spread of X much like the usual standard deviation. λ_2 is read as one half the expected difference between the two order statistics of a sample of size $n = 2$, and is referred to as L-scale or L-variation.

The difference in order statistic expectations, $\mathrm{E}[X_{2:2}] - \mathrm{E}[X_{1:2}]$, is known as Gini's Mean Difference (Serfling, 1980, p. 174, 263–264; David, 1981, p. 192; Kaigh and Driscoll, 1987, p. 26; and Hosking, 1990, p. 110 and 114). Gini's Mean Difference can be computed in a variety of ways; David (1981) provides three variations. The algebraically simplest variation is

$$G = \mathrm{E}[X_{2:2}] - \mathrm{E}[X_{1:2}] = \frac{1}{n(n-1)} \sum_{i=1}^{n} \sum_{j=i}^{n} \left| x_i - x_j \right| , \tag{B-15}$$

in which x_i is one of n sample observations. The relation between the G and λ_2 is

$$\lambda_2 = \frac{1}{2}(G) . \tag{B-16}$$

Upon substituting the $E[X_{j:r}]$ expression into the L-moment definition, the L-moments are

$$\lambda_r = \int_0^1 x(F) P^*_{r-1}(F) dF \text{ for } r = 1, 2, \ldots, n \tag{B-17}$$

where $P^*_{r-1}(F)$ is known as the $r-1$ shifted Legendre polynomial with the explicit form

$$P^*_r(F) = \sum_{k=0}^{r} p^*_{r,k} F^k \tag{B-18}$$

in which

$$p^*_{r,k} = -1^{r-k} \binom{r}{k} \binom{r+k}{k} = \frac{-1^{r-k}(r+k)!}{(k!)^2 (r-k)!} \quad . \tag{B-19}$$

It is possible to define an L-moment ratio $\tau \equiv \lambda_2 / \lambda_1$, which is analogous to the usual coefficient of variation. τ is known as L-CV and is referred to as the coefficient of L-variation. τ satisfies $0 < \tau < 1$ (Hosking, 1989).

It is often convenient to standardize the higher L-moments λ_r for $r \geq 3$ so that they are independent of the measurement units of X. This is accomplished through division by the second L-moment λ_2. The L-moment ratios are defined as

$$\tau_r \equiv \frac{\lambda_r}{\lambda_2} \text{ for } r = 3, 4, \ldots \tag{B-20}$$

The L-moment ratios τ_3 and τ_4 can be interpreted as standardized measures of skew and kurtosis, respectively. Hence, τ_3 and τ_4 are known as L-skew and L-kurtosis. The bounds on each are such that $-1 < \tau_3 < 1$ and $\frac{1}{4}(5\tau_3^2 - 1) \leq \tau_4 < 1$. If a distribution can only acquire positive values, then $2\tau - 1 \leq \tau_3 < 1$. The boundedness

on L-skew and L-kurtosis is a very convenient property and is a property that is not shared by the unbounded product moment skew and kurtosis.

PROBABILITY WEIGHTED MOMENTS

The probability weighted moments (PWMs) defined by Greenwood and others (1979) for quantile function $x(F)$ and cumulative probability F are

$$M_{p,\,r,\,s} = E[x(F)^p F^r (1-F)^s] \,. \tag{B-21}$$

The PWM $M_{1,\,0,\,0} = E[x(F)]$ is the mean. The higher PWMs $r > 0$ and $s > 0$ are not easily interpreted. However, the L-moments and PWMs can be expressed as linear combinations of each other. Because of linearity, procedures based on L-moments or the PWMs are equivalent. The PWMs actually predate the L-moments, but the L-moments are far more convenient and directly interpretable as measures of distributions. The PWMs thus are generally considered as a means to compute the L-moments.

Particularly useful PWMs for L-moment theory are $\alpha_r = M_{1,\,0,\,r}$ and $\beta_r = M_{1,\,r,\,0}$. The focus is on β_r here with a note that α_r and β_r can be shown as linear combinations of each other

$$\alpha_r = \int_0^1 x(F)(1-F)^r dF \,, \tag{B-22.1}$$

$$\beta_r = \int_0^1 x(F) F^r dF = \int_{-\infty}^{\infty} x[F(x)]^r f(x) dx \,. \tag{B-22.2}$$

One can contrast β_r with the usual product moment definition (eq. B-4), which is repeated here

$$E[X^r] = \int_0^1 x(F)^r dF \,. \tag{B-23}$$

The L-moments defined in linear terms of the PWMs are the quantities

$$\lambda_{r+1} = \sum_{k=0}^{r} p^*_{r,k}\beta_k \text{ for } r = 0, 1, \ldots, n-1 , \tag{B-24}$$

where $p^*_{r,k}$ was defined earlier. The first four L-moments are

$$\lambda_1 = \beta_0 , \tag{B-25.1}$$

$$\lambda_2 = 2\beta_1 - \beta_0 , \tag{B-25.2}$$

$$\lambda_3 = 6\beta_2 - 6\beta_1 + \beta_0 , \text{ and} \tag{B-25.3}$$

$$\lambda_4 = 20\beta_3 - 30\beta_2 + 12\beta_1 - \beta_0 , \tag{B-25.4}$$

or equivalently in terms of the quantile function as

$$\lambda_1 = \int_0^1 x(F)dF , \tag{B-26.1}$$

$$\lambda_2 = \int_0^1 x(F)(2F-1)dF , \tag{B-26.2}$$

$$\lambda_3 = \int_0^1 x(F)(6F^2 - 6F + 1)dF , \text{ and} \tag{B-26.3}$$

$$\lambda_4 = \int_0^1 x(F)(20F^3 - 30F^2 + 12F - 1)dF . \tag{B-26.4}$$

SAMPLE L-MOMENTS AND PROBABILITY WEIGHTED MOMENTS

L-moments and PWMs are defined for the quantile function $x(F)$, but in general are estimated for finite samples of size n by arranging the sample in ascending order $x_{1:n} \le x_{2:n} \le \ldots \le x_{n:n}$ to acquire the sample order statistics of random variable X. Presently there are two classes of L-moment estimators for finite samples, the unbiased estimators and the plotting-position estimators. An additional class of estimator based on p-PWMs is the subject of chapter 4 of this dissertation.

Unbiased Estimators

Unbiased estimates of β_r, hence λ_r, can be made by

$$b_r = \frac{1}{n}\binom{n-1}{r}^{-1} \sum_{j=r+1}^{n} \binom{j-1}{r} x_{j:n} \quad \text{for } r = 0, 1, \ldots, n-1 \,. \tag{B-27}$$

The "unbiased" weight factor on a specific $x_{j:n}$ is $w_{j,r}$ and is given by

$$w_{j,r} = \frac{\binom{j-1}{r}}{n\binom{n-1}{r}} \,. \tag{B-28}$$

The multiplication to the left of the summation has been included in the unbiased weight factor to facilitate later analysis. The first four unbiased PWM estimators are

$$b_0 = \frac{1}{n} \sum_{j=1}^{n} x_{j:n}, \tag{B-29.1}$$

$$b_1 = \frac{1}{n} \sum_{j=1}^{n} \binom{j-1}{n-1} x_{j:n}, \tag{B-29.2}$$

$$b_2 = \frac{1}{n} \sum_{j=1}^{n} \binom{j-1}{n-1}\binom{j-2}{n-2} x_{j:n} \text{, and} \tag{B-29.3}$$

$$b_3 = \frac{1}{n} \sum_{j=1}^{n} \binom{j-1}{n-1}\binom{j-2}{n-2}\binom{j-3}{n-3} x_{j:n} \,. \tag{B-29.4}$$

Unbiased estimates of the first four L-moments in terms of the unbiased PWM estimates are

$$l_1 = b_0 \,, \tag{B-30.1}$$

$$l_2 = 2b_1 - b_0 \,, \tag{B-30.2}$$

$$l_3 = 6b_2 - 6b_1 + b_0 \text{ , and} \tag{B-30.3}$$

$$l_4 = 20b_3 - 30b_2 + 12b_1 - b_0 \text{ .} \tag{B-30.4}$$

Hence, in general the unbiased L-moment estimator is

$$l_{r+1} = \sum_{k=0}^{r} p^*_{r,k} b_k \text{ for } r = 0, 1, \ldots, n-1 \text{ .} \tag{B-31}$$

Wang (1996b) described an algorithm for unbiased L-moment estimation that does not require the prior computation of b_r. The direct sample L-moment algorithm by Wang is numerically equivalent to eq. B-31.

Natural estimators of τ (L-CV) and the other L-moment ratios are

$$t = l_2/l_1 \text{ , and} \tag{B-32.1}$$

$$t_r = l_r/l_2 \text{ for } r \geq 3 \text{ .} \tag{B-32.2}$$

These t and t_r estimators are not unbiased, but their biases typically are small in moderate and larger samples. The biases are distribution dependent. Fortunately for many distributions, these biases are operationally negligible for sample sizes of $n = 20$ or more.

Plotting-Position Estimators

Estimates of β_r and λ_r also can be made with a second class of estimator called plotting-position estimators. A plotting position is a distribution free or nonparametric estimator of cumulative probability $F(x_{j:n})$. Historically, plotting positions have been commonly used for graphical display of random samples of X. Often recognized reasonable choices include $p_{j:n} = (j + \delta)/(n + \varepsilon)$ for $\delta > \varepsilon > -1$, where $p_{j:n}$ is the plotting position for the jth ascending order observation of a random sample of size n. Hence, the PWMs are estimated as

$$\tilde{\beta}_r = \frac{1}{n}\sum_{i=1}^{n}(p_{j:n})^r x_{j:n}. \tag{B-33}$$

The plotting-position weight factor on a specific $x_{j:n}$ is $\tilde{w}_{j,r}$ and is given by

$$\tilde{w}_{j,r} = \frac{(p_{j:n})^r}{n}. \tag{B-34}$$

The constant n^{-1} is included in the plotting-position weight factor to facilitate later analysis. The plotting-position L-moments and L-moment ratios are estimated as

$$\tilde{\lambda}_{r+1} = \sum_{k=0}^{n} p^*_{r,k}\tilde{\beta}_r, \tag{B-35.1}$$

$$\tilde{\tau} = \tilde{\lambda}_2/\tilde{\lambda}_1, \text{ and} \tag{B-35.2}$$

$$\tilde{\tau}_r = \tilde{\lambda}_r/\tilde{\lambda}_2 \text{ for } r \geq 3. \tag{B-35.3}$$

In general, $\tilde{\lambda}_r$ is not an unbiased estimator of λ_r, but the bias tends to zero in large samples. The biases of $\tilde{\tau}_r$ are generally larger than biases of t_r. The unbiased L-moments and operationally unbiased L-moment ratios generally are preferred over plotting-position estimators (Hosking and Wallis, 1997, pp. 31–34). However, under special circumstances such as when a specific probability distribution is fitted to the data, plotting-position estimators might provide more accurate parameter and quantile estimates. For example, the plotting position $p_{j:n} = (j - 0.35)/n$ performs well for the generalized Pareto (Hosking and Wallis, 1987), generalized extreme value (GEV) (Hosking and others, 1985), and Wakeby (Landwehr and others, 1979b) distributions. These distributions are common in L-moment based magnitude and frequency analysis of environmental data such as flood peak discharge (stream flow) and extreme precipitation. In rare cases, plotting-position estimators can produce L-moments with

theoretically impossible values such as $\lambda_2 < 0$ or $\tau_3 > 1$; such occurrences are not possible with unbiased estimators. This is a very important consideration for algorithm development involving plotting-position PWM estimation. Confirmation that the bounds of the L-moments are satisfied is absolutely required.

EXAMPLE OF MANUAL COMPUTATION OF UNBIASED L-MOMENTS

Compute the unbiased L-moments for the following sample ($n = 10$) that is arranged in ascending order

0, 0.1, 0.2, 0.25, 0.3, 0.3, 1.0, 6.0, 10.0, 25.0

The unbiased PWMs are required

$$b_r = \frac{1}{n}\binom{n-1}{r}^{-1} \sum_{j=r+1}^{n} \binom{j-1}{r} x_{j:n} \quad \text{for } r = 0, 1, \ldots, n-1 . \qquad \text{(B-36)}$$

For the first PWM ($r = 0$)

$$b_0 = \frac{1}{10}\binom{9}{0}^{-1}\left[\binom{0}{0}[0] + \binom{1}{0}[0.1] + \binom{2}{0}[0.2] + \binom{3}{0}[0.25] + \binom{4}{0}[0.3] + \binom{5}{0}[0.3] + \text{more}\right] \qquad \text{(B-37.1)}$$

$$\text{more} = \binom{6}{0}[1.0] + \binom{7}{0}[6.0] + \binom{8}{0}[10.0] + \binom{9}{0}[25.0] , \qquad \text{(B-37.2)}$$

$$b_0 = \frac{1}{10}\frac{1}{1}[1[0] + 1[0.1] + 1[0.2] + 1[0.25] + 1[0.3] + 1[0.3] + \text{more}] \qquad \text{(B-37.3)}$$

$$\text{more} = 1[1.0] + 1[6.0] + 1[10.0] + 1[25.0] , \qquad \text{(B-37.4)}$$

$$b_0 = \frac{1}{10}[43.15] , \text{ and} \qquad \text{(B-37.5)}$$

$$b_0 = 4.315 . \qquad \text{(B-37.6)}$$

The first PWM is equal to the arithmetic mean

$$m = \frac{1}{n}\sum_{j=1}^{n} x_j , \qquad \text{(B-38.1)}$$

$$m = \frac{1}{10}[0 + 0.1 + 0.2 + 0.25 + 0.3 + 0.3 + 1 + 6 + 10 + 25] , \qquad \text{(B-38.2)}$$

$$m = \frac{1}{10}[4.315], \text{ and} \tag{B-38.3}$$

$$m = 4.315 \text{ (a far simpler computation compared to } b_o) \tag{B-38.4}$$

For the second PWM ($r = 1$)

$$b_1 = \frac{1}{10}\binom{9}{1}^{-1}\left[\binom{1}{1}[0.1] + \binom{2}{1}[0.2] + \binom{3}{1}[0.25] + \binom{4}{1}[0.3] + \binom{5}{1}[0.3] + \text{more}\right] \tag{B-39.1}$$

$$\text{more} = \binom{6}{1}[1.0] + \binom{7}{1}[6.0] + \binom{8}{1}[10.0] + \binom{9}{1}[25.0], \tag{B-39.2}$$

$$b_1 = \frac{1}{10}\frac{1}{9}[1[0.1] + 2[0.2] + 3[0.25] + 4[0.3] + 5[0.3] + \text{more}] \tag{B-39.3}$$

$$\text{more} = 6[1.0] + 7[6.0] + 8[10.0] + 9[25.0], \tag{B-39.4}$$

$$b_1 = \frac{1}{90}[356.95], \text{ and} \tag{B-39.5}$$

$$b_1 = 3.966. \tag{B-39.6}$$

For the third PWM ($r = 2$)

$$b_2 = \frac{1}{10}\binom{9}{2}^{-1}\left[\binom{2}{2}[0.2] + \binom{3}{2}[0.25] + \binom{4}{2}[0.3] + \binom{5}{2}[0.3] + \text{more}\right] \tag{B-40.1}$$

$$\text{more} = \binom{6}{2}[1.0] + \binom{7}{2}[6.0] + \binom{8}{2}[10.0] + \binom{9}{2}[25.0], \tag{B-40.2}$$

$$b_2 = \frac{1}{10}\frac{1}{36}[1[0.2] + 3[0.25] + 6[0.3] + 10[0.3] + \text{more}] \tag{B-40.3}$$

$$\text{more} = 15[1.0] + 21[6.0] + 28[10.0] + 36[25.0], \tag{B-40.4}$$

$$b_2 = \frac{1}{360}[1326.75], \text{ and} \tag{B-40.5}$$

$$b_2 = 3.685. \tag{B-40.6}$$

For the fourth PWM ($r = 3$)

$$b_3 = \frac{1}{10}\binom{9}{3}^{-1}\left[\binom{3}{3}[0.25] + \binom{4}{3}[0.3] + \binom{5}{3}[0.3] + \text{more}\right] \tag{B-41.1}$$

$$\text{more} = \binom{6}{3}[1.0] + \binom{7}{3}[6.0] + \binom{8}{3}[10.0] + \binom{9}{3}[25.0], \tag{B-41.2}$$

$$b_3 = \frac{1}{10}\frac{1}{36}[1[0.25] + 4[0.3] + 10[0.3] + \text{more}] \quad \text{(B-41.3)}$$

$$\text{more} = 20[1.0] + 35[6.0] + 56[10.0] + 84[25.0], \quad \text{(B-41.4)}$$

$$b_3 = \frac{1}{840}[2894.25], \text{ and} \quad \text{(B-41.5)}$$

$$b_3 = 3.446. \quad \text{(B-41.6)}$$

For the first L-moment

$$\lambda_1 = b_0 = 4.315. \quad \text{(B-42)}$$

For the second L-moment

$$\lambda_2 = 2b_1 - b_0 = 2(3.966) - 4.315 = 3.617 \text{ and} \quad \text{(B-43.1)}$$

$$\lambda_2 = 3.617. \quad \text{(B-43.2)}$$

For the third L-moment

$$\lambda_3 = 6b_2 - 6b_1 + b_0 = 6(3.685) - 6(3.966) + 4.315 \text{ and} \quad \text{(B-44.1)}$$

$$\lambda_3 = 2.629. \quad \text{(B-45.1)}$$

For the fourth L-moment

$$\lambda_4 = 20b_3 - 30b_2 + 12b_1 - b_0, \quad \text{(B-46.1)}$$

$$\lambda_4 = 20(3.446) - 30(3.685) + 12(3.966) - 4.315, \text{ and} \quad \text{(B-46.2)}$$

$$\lambda_4 = 1.647. \quad \text{(B-46.3)}$$

For the coefficient of L-variation (L-CV)

$$\tau = \frac{\lambda_2}{\lambda_1} = \frac{3.617}{4.315} = 0.8382. \quad \text{(B-47)}$$

For L-skew

$$\tau_3 = \frac{\lambda_3}{\lambda_2} = \frac{2.629}{3.617} = 0.7268, \quad \text{(B-48)}$$

which is a positive or right-tail skewness and is a number $-1 < \tau_3 < 1$.

For L-kurtosis

$$\tau_4 = \frac{\lambda_4}{\lambda_2} = \frac{1.647}{3.617} = 0.4553, \tag{B-49}$$

which is a number $\frac{1}{4}(5\tau_3^2 - 1) \le \tau_4 < 1$ or $0.4103 \le \tau_4 < 1$.

The standard deviation, σ', is related to the second L-moment

$$\sigma' = \sqrt{\pi}\lambda_2 = \sqrt{\pi}(3.617) = 6.411. \tag{B-50}$$

The standard deviation, s_{unbvar}, using an unbiased variance computation through the product moments is

$$s_{unbvar} = \sqrt{\frac{1}{n-1}\sum_{j=1}^{n}(x_j - m)^2} = \sqrt{\frac{1}{9}\sum_{j=1}^{10}(x_j - 4.315)^2} \text{ and} \tag{B-51.1}$$

$$s_{unbvar} = \sqrt{\frac{576.1}{9}} = 8.0. \tag{B-51.2}$$

The standard deviation, s_{bvar}, using an biased variance computation through the product moments is

$$s_{bvar} = \sqrt{\frac{1}{n}\sum_{j=1}^{n}(x_j - m)^2} = \sqrt{\frac{1}{10}\sum_{j=1}^{10}(x_j - 4.315)^2} \text{ and} \tag{B-52.1}$$

$$s_{bvar} = \sqrt{\frac{576.1}{10}} = 7.59. \tag{B-53.1}$$

The uniformly minimum variance unbiased estimate (David, 1981, p. 185) of the standard deviation, s_{UMVU}, is

$$s_{UMVU} = \frac{\Gamma[(n-1)/2]}{\Gamma[n/2]\sqrt{2}}\sqrt{\sum_{j=1}^{n}(x_j - m)^2} \text{ and} \tag{B-54.1}$$

$$s_{UMVU} = \frac{11.6317}{24\sqrt{2}}\sqrt{576.1} = 8.23\,. \qquad \text{(B-55.1)}$$

The computer program, `lmoments.pl`, (Appendix E) can be used to verify the L-moments and PWMs in the above computations. The output from the program is shown below. (B-56.1)

```
[wasquith@linuxhost]$ lmoments.pl -ub
# L-MOMENTS OF A CUMULATIVE PERCENTAGE HYDROGRAPH
# Enter space delimited cumulative probability and data values.
# Working on UB (PP, plotting position; UB, unbiased; PM, product
# moment). If one value is given, then it is used. If two values
# are given, then the second one is used. This feature permits switching
# between the prior-PWM method and the other methods without a change in
# the input stream.
# One value or F   X pair per line
# X  or  F(ignored)   X
0
.1
.2
.25
.3
.3
1
6
10
25

# Probabilities and Data have been entered. . .
# L-moment Computation
# Proability Weighted Moments are:
#   Beta0  = 4.3150
#   Beta1  = 3.9661
#   Beta2  = 3.6854
#   Beta3  = 3.4458
#   Beta4  = 3.2356
# L-moments are:
#   Mean        = 4.3150
#   L-Scale     = 3.6172 (StDev=6.4113)
#   L-CV        = 0.8383
#   L-skew      = 0.7273
#   L-kurtosis  = 0.4510
#   Tau5        = 0.2103
# Samples = 10
# Mean   L-scale   L-CV    L-skew   L-kurtosis   Tau5   Median
4.3150   3.6172   0.8383   0.7273   0.4510   0.2103   0.3
```

APPENDIX C

Supplemental non-uniform simulations showing biases in the unbiased, plotting-position, and prior-Probability Weighted Moment L-moment estimators

Table C1. Comparison of biases for a simulated Kappa distribution using a non-uniform probability distribution by redrawing F if initial F was less than 0.5.

[The Kappa distribution had specified L-moments of 0.114, 0.0378, -0.148, and 0.0476 for the mean, L-scale, L-skew, and L-kurtosis, respectively. These L-moments correspond to estimated Kappa parameters of 0.0669, 0.1439, 1.022, and 0.5045 for the location, scale, shape 1, and shape 2 parameters, respectively. Bias is defined as the simulated mean statistic minus the true value. UB, unbiased; PP, plotting position based probability weighted moments; XF, prior-probability weighted moments.]

Sample size	Estimator type	Mean bias	L-scale bias	L-CV bias	L-skew bias	L-kurtosis bias
n=5	UB	0.0280	-0.0079	-0.0960	-0.0932	0.1047
	PP	.0274	-.0051	-.0779	.0904	.1374
	XF	.0145	.0043	-.0043	-.1307	.1355
n=10	UB	.0275	-.0077	-.1067	-.1296	.1139
	PP	.0276	-.0064	-.0991	.0147	.1226
	XF	.0072	.0002	-.0152	-.1057	.0141
n=20	UB	.0278	-.0076	-.1131	-.1397	.1084
	PP	.0279	-.0072	-.1106	-.0544	.1147
	XF	.0027	-.0005	-.0103	-.0269	-.0260
n=50	UB	.0275	-.0076	-.1153	-.1441	.1064
	PP	.0285	-.0078	-.1183	-.1090	.1109
	XF	.0006	-.0003	-.0043	.0040	-.0176
n=100	UB	.0280	-.0079	-.1191	-.1442	.1074
	PP	.0270	-.0074	-.1142	-.1222	.1027
	XF	.0002	-.0002	-.0022	.0036	-.0100
n=1,000	UB	.0275	-.0076	-.1175	-.1440	.1038
	PP	.0277	-.0078	-.1193	-.1397	.1012
	XF	.0	.0	.0	.0	.0

Table C2. Comparison of biases for a simulated Kappa distribution using a non-uniform probability distribution by redrawing F if initial F was less than 0.2.

[The Kappa distribution had specified L-moments of 0.114, 0.0378, -0.148, and 0.0476 for the mean, L-scale, L-skew, and L-kurtosis, respectively. These L-moments correspond to estimated Kappa parameters of 0.0669, 0.1439, 1.022, and 0.5045 for the location, scale, shape 1, and shape 2 parameters, respectively. Bias is defined as the simulated mean statistic minus the true value. UB, unbiased; PP, plotting position based probability weighted moments; XF, prior-probability weighted moments.]

Sample size	Estimator type	Mean bias	L-scale bias	L-CV bias	L-skew bias	L-kurtosis bias
n=5	UB	0.0214	-0.0095	-0.1093	0.0291	0.0273
	PP	.0210	-.0070	-.0934	.1603	.1272
	XF	.0125	-.0043	-.0701	-.1060	.2236
n=10	UB	.0208	-.0094	-.1141	.0299	.0128
	PP	.0208	-.0083	-.1066	.1265	.0847
	XF	.0090	-.0049	-.0630	-.1045	.1281
n=20	UB	.0211	-.0095	-.1189	.0201	.0126
	PP	.0210	-.0088	-.1134	.0793	.0506
	XF	.0059	-.0037	-.0452	-.0424	.0411
n=50	UB	.0207	-.0094	-.1188	.0200	.0094
	PP	.0209	-.0094	-.1191	.0482	.0256
	XF	.0028	-.0019	-.0233	.0020	.0055
n=100	UB	.0208	-.0095	-.1206	.0202	.0111
	PP	.0207	-.0093	-.1188	.0323	.0193
	XF	.0011	-.0008	-.0095	.0041	-.0028
n=1,000	UB	.0207	-.0094	-.1198	.0173	.0097
	PP	.0213	-.0095	-.1215	.0143	.0149
	XF	.0	.0	-.0003	.0006	-.0007

Table C3. Comparison of biases for a simulated Kappa distribution using a non-uniform probability distribution by redrawing F if initial F was greater than 0.8.

[The Kappa distribution had specified L-moments of 0.114, 0.0378, -0.148, and 0.0476 for the mean, L-scale, L-skew, and L-kurtosis, respectively. These L-moments correspond to estimated Kappa parameters of 0.0669, 0.1439, 1.022, and 0.5045 for the location, scale, shape 1, and shape 2 parameters, respectively. Bias is defined as the simulated mean statistic minus the true value. UB, unbiased; PP, plotting position based probability weighted moments; XF, prior-probability weighted moments.]

Sample size	Estimator type	Mean bias	L-scale bias	L-CV bias	L-skew bias	L-kurtosis bias
n=5	UB	-0.0159	-0.0029	0.07799	0.0284	0.0391
	PP	-.0157	-.0039	.0418	.1880	.0347
	XF	-.0039	-.0138	-.1195	-.2717	.2128
n=10	UB	-.0159	-.0025	.0519	.0168	.0221
	PP	-.0158	-.0031	.0438	.1248	.0348
	XF	-.0026	-.0117	-.0993	-.3113	.1250
n=20	UB	-.0160	-.0028	.0368	.0163	.0159
	PP	-.0155	-.0031	.0313	.0764	.0271
	XF	-.0019	-.0078	-.0649	-.3035	.0412
n=50	UB	-.0158	-.0027	.0307	.0149	.0141
	PP	-.0159	-.0029	.0287	.0429	.0181
	XF	-.0008	-.0031	-.0250	-.1682	.0039
n=100	UB	-.0156	-.0027	.0273	.0143	.0118
	PP	-.0164	-.0025	.0321	.0309	.0142
	XF	-.0003	-.0012	-.0094	-.0676	-.0148
n=1,000	UB	-.0158	-.0026	.0262	.0155	.0125
	PP	-.0156	-.0026	.0260	.0188	.0107
	XF	.0	.0	-.0001	-.0003	-.0017

Table C4. Comparison of biases for a simulated Kappa distribution using a non-uniform probability distribution by redrawing F if initial F was less than 0.1.

[The Kappa distribution had specified L-moments of 0.114, 0.0378, -0.148, and 0.0476 for the mean, L-scale, L-skew, and L-kurtosis, respectively. These L-moments correspond to estimated Kappa parameters of 0.0669, 0.1439, 1.022, and 0.5045 for the location, scale, shape 1, and shape 2 parameters, respectively. Bias is defined as the simulated mean statistic minus the true value. UB, unbiased; PP, plotting position based probability weighted moments; XF, prior-probability weighted moments.]

Sample size	Estimator type	Mean bias	L-scale bias	L-CV bias	L-skew bias	L-kurtosis bias
n=5	UB	0.0135	-.0065	-0.0688	0.0377	0.0042
	PP	.0133	-.0052	-.0622	.1754	.0919
	XF	.0083	-.0051	-.0679	-.0277	.2170
n=10	UB	.0132	-.0065	-.0774	.0324	-.0014
	PP	.0132	-.0059	-.0733	.1345	.0568
	XF	.0058	-.0052	-.0584	-.0470	.0720
n=20	UB	.0128	-.0064	-.0797	.0333	-.0121
	PP	.0129	-.0063	-.0792	.0913	.0259
	XF	.0041	-.0036	-.0412	.0063	-.0128
n=50	UB	.0128	-.0065	-.0827	.0380	-.0174
	PP	.0081	-.0065	-.0831	.0586	.0034
	XF	.0026	-.0023	-.0268	.0293	-.0308
n=100	UB	.0130	-.0064	-.0833	.0320	-.0164
	PP	.0132	-.0065	-.0844	.0470	-.0077
	XF	.0017	-.0015	-.0177	.0222	-.0182
n=1,000	UB	.0132	-.0064	-.0843	.0345	-.0197
	PP	.0132	-.0065	-.0849	.0340	-.0104
	XF	.0001	-.0001	-.0007	.0013	-.0014

Table C5. Comparison of biases for a simulated Kappa distribution using a non-uniform probability distribution by redrawing F if initial F was greater than 0.9.

[The Kappa distribution had specified L-moments of 0.114, 0.0378, -0.148, and 0.0476 for the mean, L-scale, L-skew, and L-kurtosis, respectively. These L-moments correspond to estimated Kappa parameters of 0.0669, 0.1439, 1.022, and 0.5045 for the location, scale, shape 1, and shape 2 parameters, respectively. Bias is defined as the simulated mean statistic minus the true value. UB, unbiased; PP, plotting position based probability weighted moments; XF, prior-probability weighted moments.]

Sample size	Estimator type	Mean bias	L-scale bias	L-CV bias	L-skew bias	L-kurtosis bias
n=5	UB	-0.0092	-0.0015	0.0757	0.0113	0.0254
	PP	-.0089	-.0027	.0457	.1819	.0375
	XF	-.0007	-.0091	-.0822	-.2280	.0564
n=10	UB	-.0088	-.0016	.0353	.0062	.0111
	PP	-.0089	-.0023	.0264	.1185	.0352
	XF	-.0007	-.0076	-.0655	-.2800	-.0082
n=20	UB	-.0084	-.0016	.0217	.0019	.0075
	PP	-.0084	-.0019	.0184	.0636	.0222
	XF	-.0006	-.0048	-.0407	-.2450	-.0472
n=50	UB	-.0085	-.0017	.0145	.0030	.0029
	PP	-.0090	-.0017	.0163	.0313	.0078
	XF	-.0005	-.0026	-.0215	-.1564	-.0569
n=100	UB	-.0087	-.0014	.0155	.0022	.0012
	PP	-.0087	-.0018	.0124	.0171	.0044
	XF	-.0004	-.0016	-.0131	-.0996	-.0474
n=1,000	UB	-.0083	-.0019	.0006	.0033	.0040
	PP	-.0008	-.0017	.0115	.0067	-.0031
	XF	.0	.0	-.0004	-.0028	-.0052

Table C6. Comparison of biases for a simulated Kappa distribution using a non-uniform probability distribution by redrawing F if initial F was greater than 0.25 and less than 0.75.

[The Kappa distribution had specified L-moments of 0.114, 0.0378, -0.148, and 0.0476 for the mean, L-scale, L-skew, and L-kurtosis, respectively. These L-moments correspond to estimated Kappa parameters of 0.0669, 0.1439, 1.022, and 0.5045 for the location, scale, shape 1, and shape 2 parameters, respectively. Bias is defined as the simulated mean statistic minus the true value. UB, unbiased; PP, plotting position based probability weighted moments; XF, prior-probability weighted moments.]

Sample size	Estimator type	Mean bias	L-scale bias	L-CV bias	L-skew bias	L-kurtosis bias
n=5	UB	-0.0047	0.0068	1.6945	0.0039	-0.0457
	PP	-.0038	.0041	.0962	.1919	-.0017
	XF	-.0007	.0062	.0545	.1930	.1344
n=10	UB	-.0048	.0069	.1113	.0068	-.0829
	PP	-.0046	.0055	.0797	.0401	-.0790
	XF	-.0004	.0020	.0192	.1081	.0116
n=20	UB	-.0052	.0068	.0936	.0155	-.0915
	PP	-.0048	.0063	.0866	.0719	-.0585
	XF	-.0001	.0007	.0066	.0489	-.0277
n=50	UB	-.0052	.0068	.0839	.0179	-.0918
	PP	-.0047	.0065	.0797	.0401	-.0790
	XF	.0	.0001	.0009	.0114	-.0095
n=100	UB	-.0046	.0067	.0782	.0152	-.0944
	PP	-.0045	.0066	.0762	.0261	-.0853
	XF	.0	.0	.0	.0044	-.0036
n=1,000	UB	-.0044	.0066	.0739	.0152	-.0948
	PP	-.0050	.0068	.0773	.0203	-.0955
	XF	.0	.0	.0	.0	.0

APPENDIX D

Parameter Space Maps of L-gamma Distribution

Table D1.1 Parameter B of L-gamma distribution as function of the median and values (0.010 to 0.10) of inter-tercile range

Median values	Values for inter-tercile range ------->									
V	0.010	0.020	0.030	0.040	0.050	0.060	0.070	0.080	0.090	0.100
0.000	--	--	--	--	--	--	--	--	--	--
0.010	--	--	--	--	1.855	4.805	7.403	9.700	11.74	13.58
0.020	--	--	--	--	--	--	0.341	2.245	4.051	5.742
0.030	--	--	--	--	--	--	--	--	0.391	1.786
0.040	--	--	--	--	--	--	--	--	--	--
---------- Break ----------										
0.830	--	--	--	--	--	--	--	--	--	--
0.840	--	--	--	--	--	--	--	--	--	0.012
0.850	--	--	--	--	--	--	--	--	--	0.041
0.860	--	--	--	--	--	--	--	--	0.018	0.070
0.870	--	--	--	--	--	--	--	--	0.047	0.098
0.880	--	--	--	--	--	--	--	0.025	0.076	0.126
0.890	--	--	--	--	--	--	0.004	0.054	0.104	0.154
0.900	--	--	--	--	--	--	0.033	0.082	0.132	0.182
0.910	--	--	--	--	--	0.013	0.062	0.111	0.160	0.209
0.920	--	--	--	--	--	0.042	0.090	0.139	0.187	0.236
0.930	--	--	--	--	0.024	0.071	0.119	0.166	0.215	0.263
0.940	--	--	--	0.006	0.052	0.099	0.146	0.194	0.242	0.290
0.950	--	--	--	0.035	0.081	0.127	0.174	0.221	--	--
0.960	--	--	0.018	0.063	0.109	0.155	0.201	--	--	--
0.970	--	0.001	0.046	0.092	0.137	--	--	--	--	--
0.980	--	0.030	0.075	--	--	--	--	--	--	--
0.990	0.015	--	--	--	--	--	--	--	--	--
1.000	--	--	--	--	--	--	--	--	--	--

Table D1.2 Parameter C of L-gamma distribution as function of the median and values (0.010 to 0.10) of inter-tercile range

Median values	Values for inter-tercile range ------->									
V	0.010	0.020	0.030	0.040	0.050	0.060	0.070	0.080	0.090	0.100
0.000	--	--	--	--	--	--	--	--	--	--
0.010	--	--	--	--	-6.638	-2.549	+1.053	+4.237	+7.074	+9.627
0.020	--	--	--	--	--	--	-7.352	-4.712	-2.209	+0.136
0.030	--	--	--	--	--	--	--	--	-6.472	-4.537
0.040	--	--	--	--	--	--	--	--	--	--
---------- Break ----------										
0.830	--	--	--	--	--	--	--	--	--	--
0.840	--	--	--	--	--	--	--	--	--	-0.332
0.850	--	--	--	--	--	--	--	--	--	-0.268
0.860	--	--	--	--	--	--	--	--	-0.277	-0.205
0.870	--	--	--	--	--	--	--	--	-0.213	-0.142
0.880	--	--	--	--	--	--	--	-0.221	-0.151	-0.080
0.890	--	--	--	--	--	--	-0.227	-0.158	-0.089	-0.019
0.900	--	--	--	--	--	--	-0.165	-0.096	-0.028	+0.041
0.910	--	--	--	--	--	-0.170	-0.103	-0.035	+0.033	+0.101
0.920	--	--	--	--	--	-0.108	-0.041	+0.026	+0.093	+0.161
0.930	--	--	--	--	-0.112	-0.047	+0.019	+0.086	+0.152	+0.219
0.940	--	--	--	-0.116	-0.051	+0.014	+0.079	+0.145	+0.211	+0.278
0.950	--	--	--	-0.055	+0.009	+0.074	+0.139	+0.204	--	--
0.960	--	--	-0.057	+0.006	+0.070	+0.133	+0.198	--	--	--
0.970	--	-0.059	+0.003	+0.066	+0.129	--	--	--	--	--
0.980	--	+0.001	+0.063	--	--	--	--	--	--	--
0.990	0.000	--	--	--	--	--	--	--	--	--
1.000	--	--	--	--	--	--	--	--	--	--

Table D1.3 Mean of L-gamma distribution as function of the median
and values (0.010 to 0.10) of inter-tercile range--"s" denotes a simulated value.

Median values	Values for inter-tercile range ------->									
V	0.010	0.020	0.030	0.040	0.050	0.060	0.070	0.080	0.090	0.100
0.000	--	--	--	--	--	--	--	--	--	--
0.010	--	--	--	--	s0.114	s0.124	0.134	0.143	0.153	0.162
0.020	--	--	--	--	--	--	s0.129	s0.136	s0.144	0.151
0.030	--	--	--	--	--	--	--	--	s0.144	s0.150
0.040	--	--	--	--	--	--	--	--	--	--
---------- Break ----------										
0.830	--	--	--	--	--	--	--	--	--	--
0.840	--	--	--	--	--	--	--	--	--	s0.841
0.850	--	--	--	--	--	--	--	--	--	s0.845
0.860	--	--	--	--	--	--	--	--	s0.859	s0.848
0.870	--	--	--	--	--	--	--	--	s0.862	s0.851
0.880	--	--	--	--	--	--	--	s0.876	s0.865	s0.855
0.890	--	--	--	--	--	--	s0.891	s0.879	s0.868	s0.859
0.900	--	--	--	--	--	--	s0.893	s0.882	s0.872	0.862
0.910	--	--	--	--	--	s0.908	s0.896	s0.885	0.875	0.866
0.920	--	--	--	--	--	s0.910	s0.899	0.889	0.879	0.870
0.930	--	--	--	--	s0.924	s0.913	0.902	0.892	0.883	0.874
0.940	--	--	--	s0.939	s0.927	0.916	0.905	0.896	0.886	0.878
0.950	--	--	--	s0.941	0.929	0.919	0.909	0.899	--	--
0.960	--	--	s0.955	0.943	0.932	0.922	0.912	--	--	--
0.970	--	s0.969	0.957	0.946	0.935	--	--	--	--	--
0.980	--	0.971	0.959	--	--	--	--	--	--	--
0.990	0.986	--	--	--	--	--	--	--	--	--
1.000	--	--	--	--	--	--	--	--	--	--

Table D1.4 L-scale of L-gamma distribution as function of the median
and values (0.010 to 0.10) of inter-tercile range--"s" denotes a simulated value.

Median values	Values for inter-tercile range ------->									
V	0.010	0.020	0.030	0.040	0.050	0.060	0.070	0.080	0.090	0.100
0.000	--	--	--	--	--	--	--	--	--	--
0.010	--	--	--	--	s0.089	s0.096	0.103	0.109	0.115	0.121
0.020	--	--	--	--	--	--	s0.096	s0.101	s0.106	0.111
0.030	--	--	--	--	--	--	--	--	s0.103	s0.108
0.040	--	--	--	--	--	--	--	--	--	--
---------- Break ----------										
0.830	--	--	--	--	--	--	--	--	--	--
0.840	--	--	--	--	--	--	--	--	--	s0.052
0.850	--	--	--	--	--	--	--	--	--	s0.054
0.860	--	--	--	--	--	--	--	--	s0.047	s0.057
0.870	--	--	--	--	--	--	--	--	s0.050	s0.060
0.880	--	--	--	--	--	--	--	s0.043	s0.053	s0.062
0.890	--	--	--	--	--	--	s0.036	s0.046	s0.056	s0.064
0.900	--	--	--	--	--	--	s0.039	s0.049	s0.058	0.066
0.910	--	--	--	--	--	s0.032	s0.042	s0.052	0.060	0.068
0.920	--	--	--	--	--	s0.035	s0.045	0.054	0.063	0.070
0.930	--	--	--	--	s0.028	s0.038	0.048	0.057	0.065	0.072
0.940	--	--	--	s0.021	s0.032	0.041	0.050	0.059	0.067	0.074
0.950	--	--	--	s0.025	0.035	0.044	0.053	0.061	--	--
0.960	--	--	s0.018	0.028	0.038	0.047	0.055	--	--	--
0.970	--	s0.011	0.021	0.031	0.041	--	--	--	--	--
0.980	--	0.014	0.025	--	--	--	--	--	--	--
0.990	0.007	--	--	--	--	--	--	--	--	--
1.000	--	--	--	--	--	--	--	--	--	--

Table D2.1 Parameter B of L-gamma distribution as function of the median and values (0.11 to 0.20) of inter-tercile range

Median values	Values for inter-tercile range ------->									
V	0.110	0.120	0.130	0.140	0.150	0.160	0.170	0.180	0.190	0.200
0.000	--	--	--	--	--	--	--	--	--	--
0.010	15.26	16.78	18.19	19.50	20.71	21.85	22.92	--	--	--
0.020	7.318	8.784	10.15	11.42	12.62	13.74	14.80	15.80	16.75	17.65
0.030	3.147	4.459	5.714	6.910	8.047	9.127	10.15	11.13	12.05	12.94
0.040	0.746	1.853	2.945	4.012	5.048	6.051	7.016	7.945	8.837	9.694
0.050	--	0.248	1.170	2.092	3.006	3.906	4.788	5.648	6.484	7.296
0.060	--	--	0.018	0.805	1.598	2.391	3.179	3.959	4.726	5.480
0.070	--	--	--	--	0.618	1.312	2.009	2.707	3.402	4.091
0.080	--	--	--	--	--	0.537	1.153	1.775	2.399	3.024
0.090	--	--	--	--	--	--	0.520	1.075	1.636	2.200
0.100	--	--	--	--	--	--	0.048	0.546	1.050	1.561
0.110	--	--	--	--	--	--	--	0.141	0.598	1.061
0.120	--	--	--	--	--	--	--	--	0.246	0.668
0.130	--	--	--	--	--	--	--	--	--	0.358
0.140	--	--	--	--	--	--	--	--	--	0.110
0.150	--	--	--	--	--	--	--	--	--	--
---------- Break ----------										
0.610	--	--	--	--	--	--	--	--	--	--
0.620	--	--	--	--	--	--	--	--	--	0.012
0.630	--	--	--	--	--	--	--	--	--	0.038
0.640	--	--	--	--	--	--	--	--	--	0.064
0.650	--	--	--	--	--	--	--	--	0.019	0.091
0.660	--	--	--	--	--	--	--	--	0.046	0.117
0.670	--	--	--	--	--	--	--	0.004	0.073	0.142
0.680	--	--	--	--	--	--	--	0.032	0.100	0.168
0.690	--	--	--	--	--	--	--	0.059	0.126	0.194
0.700	--	--	--	--	--	--	0.021	0.086	0.153	0.219
0.710	--	--	--	--	--	--	0.049	0.113	0.179	0.244
0.720	--	--	--	--	--	0.013	0.076	0.140	0.205	0.270
0.730	--	--	--	--	--	0.041	0.104	0.167	0.231	0.295
0.740	--	--	--	--	0.007	0.069	0.131	0.193	0.256	0.319
0.750	--	--	--	--	0.036	0.097	0.158	0.220	0.282	0.344
0.760	--	--	--	0.005	0.064	0.124	0.185	0.246	0.307	0.369
0.770	--	--	--	0.033	0.092	0.152	0.211	0.272	0.332	0.393
0.780	--	--	0.004	0.062	0.120	0.179	0.238	0.297	0.357	0.417
0.790	--	--	0.033	0.090	0.148	0.206	0.264	0.323	0.382	0.441
0.800	--	0.005	0.061	0.118	0.175	0.232	0.290	0.348	0.406	0.465
0.810	--	0.034	0.090	0.146	0.202	0.259	0.316	0.373	0.431	0.489
0.820	0.008	0.063	0.118	0.173	0.229	0.285	0.341	0.398	0.455	0.513
0.830	0.037	0.091	0.145	0.200	0.255	0.311	0.367	0.423	0.479	0.536
0.840	0.065	0.119	0.173	0.227	0.282	0.337	0.392	0.447	0.503	0.559
0.850	0.094	0.147	0.200	0.254	0.308	0.362	0.417	0.472	0.527	0.582
0.860	0.122	0.174	0.227	0.280	0.334	0.387	0.441	0.496	0.550	0.605
0.870	0.150	0.202	0.254	0.307	0.359	0.413	0.466	0.520	0.574	0.628
0.880	0.177	0.229	0.281	0.333	0.385	0.437	0.490	0.544	0.597	0.651
0.890	0.205	0.256	0.307	0.358	0.410	0.462	0.515	0.567	--	--
0.900	0.232	0.282	0.333	0.384	0.435	0.487	0.539	--	--	--
0.910	0.259	0.309	0.359	0.409	0.460	--	--	--	--	--
0.920	0.285	0.335	0.384	--	--	--	--	--	--	--
0.930	0.312	0.361	--	--	--	--	--	--	--	--
0.940	--	--	--	--	--	--	--	--	--	--

Table D2.2 Parameter C of L-gamma distribution as function of the median and values (0.11 to 0.20) of inter-tercile range

Median values	Values for inter-tercile range ------->									
V	0.110	0.120	0.130	0.140	0.150	0.160	0.170	0.180	0.190	0.200
0.000	--	--	--	--	--	--	--	--	--	--
0.010	+11.94	+14.06	+16.01	+17.82	+19.51	+21.09	+22.57	--	--	--
0.020	+2.320	+4.354	+6.248	+8.018	+9.675	+11.23	+12.70	+14.08	+15.40	+16.65
0.030	-2.651	-0.832	+0.908	+2.566	+4.143	+5.640	+7.063	+8.416	+9.704	+10.93
0.040	-5.403	-3.869	-2.356	-0.876	+0.561	+1.950	+3.289	+4.576	+5.813	+7.001
0.050	--	-5.648	-4.369	-3.092	-1.825	-0.577	+0.646	+1.838	+2.998	+4.123
0.060	--	--	-5.602	-4.511	-3.412	-2.313	-1.220	-0.139	+0.925	+1.970
0.070	--	--	--	--	-4.462	-3.500	-2.533	-1.566	-0.602	+0.353
0.080	--	--	--	--	--	-4.308	-3.453	-2.591	-1.726	-0.860
0.090	--	--	--	--	--	--	-4.095	-3.326	-2.548	-1.766
0.100	--	--	--	--	--	--	-4.539	-3.849	-3.149	-2.441
0.110	--	--	--	--	--	--	--	-4.219	-3.586	-2.943
0.120	--	--	--	--	--	--	--	--	-3.899	-3.314
0.130	--	--	--	--	--	--	--	--	--	-3.585
0.140	--	--	--	--	--	--	--	--	--	-3.779
0.150	--	--	--	--	--	--	--	--	--	--
---------- Break ----------										
0.610	--	--	--	--	--	--	--	--	--	--
0.620	--	--	--	--	--	--	--	--	--	-0.940
0.630	--	--	--	--	--	--	--	--	--	-0.871
0.640	--	--	--	--	--	--	--	--	--	-0.803
0.650	--	--	--	--	--	--	--	--	-0.835	-0.736
0.660	--	--	--	--	--	--	--	--	-0.767	-0.669
0.670	--	--	--	--	--	--	--	-0.795	-0.700	-0.603
0.680	--	--	--	--	--	--	--	-0.727	-0.633	-0.538
0.690	--	--	--	--	--	--	--	-0.660	-0.567	-0.474
0.700	--	--	--	--	--	--	-0.685	-0.594	-0.502	-0.409
0.710	--	--	--	--	--	--	-0.618	-0.528	-0.437	-0.346
0.720	--	--	--	--	--	-0.639	-0.551	-0.463	-0.373	-0.283
0.730	--	--	--	--	--	-0.573	-0.486	-0.398	-0.310	-0.221
0.740	--	--	--	--	-0.592	-0.507	-0.421	-0.334	-0.247	-0.159
0.750	--	--	--	--	-0.526	-0.441	-0.356	-0.271	-0.185	-0.098
0.760	--	--	--	-0.543	-0.460	-0.377	-0.293	-0.208	-0.123	-0.038
0.770	--	--	--	-0.477	-0.395	-0.313	-0.230	-0.146	-0.062	+0.022
0.780	--	--	-0.492	-0.411	-0.331	-0.249	-0.167	-0.085	-0.002	+0.081
0.790	--	--	-0.426	-0.347	-0.267	-0.186	-0.106	-0.024	+0.058	+0.140
0.800	--	-0.439	-0.361	-0.283	-0.204	-0.124	-0.044	+0.036	+0.117	+0.199
0.810	--	-0.374	-0.297	-0.220	-0.142	-0.063	+0.016	+0.096	+0.176	+0.256
0.820	-0.386	-0.310	-0.234	-0.157	-0.080	-0.002	+0.076	+0.155	+0.234	+0.314
0.830	-0.322	-0.247	-0.171	-0.095	-0.019	+0.058	+0.135	+0.213	+0.292	+0.370
0.840	-0.258	-0.184	-0.109	-0.034	+0.042	+0.118	+0.194	+0.271	+0.349	+0.427
0.850	-0.195	-0.121	-0.048	+0.027	+0.102	+0.177	+0.253	+0.329	+0.405	+0.482
0.860	-0.132	-0.060	+0.013	+0.087	+0.161	+0.235	+0.310	+0.386	+0.461	+0.538
0.870	-0.071	+0.001	+0.074	+0.146	+0.220	+0.293	+0.367	+0.442	+0.517	+0.592
0.880	-0.010	+0.062	+0.133	+0.205	+0.278	+0.351	+0.424	+0.498	+0.572	+0.647
0.890	+0.051	+0.121	+0.192	+0.264	+0.335	+0.408	+0.480	+0.553	--	--
0.900	+0.111	+0.181	+0.251	+0.322	+0.393	+0.464	+0.536	--	--	--
0.910	+0.170	+0.239	+0.309	+0.379	+0.449	--	--	--	--	--
0.920	+0.229	+0.297	+0.366	--	--	--	--	--	--	--
0.930	+0.287	+0.355	--	--	--	--	--	--	--	--
0.940	--	--	--	--	--	--	--	--	--	--

Table D2.3 Mean of L-gamma distribution as function of the median
and values (0.11 to 0.20) of inter-tercile range--"s" denotes a simulated value.

Median values										
	Values for inter-tercile range ------->									
V	0.110	0.120	0.130	0.140	0.150	0.160	0.170	0.180	0.190	0.200
0.000	--	--	--	--	--	--	--	--	--	--
0.010	0.171	0.180	0.189	0.197	0.206	0.214	0.222	--	--	--
0.020	0.159	0.166	0.174	0.181	0.189	0.196	0.203	0.210	0.218	0.225
0.030	s0.156	s0.162	0.168	0.175	0.182	0.188	0.195	0.202	0.208	0.215
0.040	s0.158	s0.163	s0.168	s0.174	0.179	0.185	0.191	0.197	0.203	0.209
0.050	--	s0.167	s0.171	s0.176	s0.181	s0.186	0.191	0.196	0.201	0.207
0.060	--	--	s0.177	s0.180	s0.184	s0.188	s0.193	s0.197	0.202	0.207
0.070	--	--	--	--	s0.189	s0.192	s0.196	s0.200	s0.204	0.208
0.080	--	--	--	--	--	s0.198	s0.201	s0.204	s0.208	s0.211
0.090	--	--	--	--	--	--	s0.207	s0.210	s0.213	s0.216
0.100	--	--	--	--	--	--	s0.215	s0.216	s0.218	s0.221
0.110	--	--	--	--	--	--	--	s0.224	s0.225	s0.227
0.120	--	--	--	--	--	--	--	--	s0.233	s0.234
0.130	--	--	--	--	--	--	--	--	--	s0.241
0.140	--	--	--	--	--	--	--	--	--	s0.249
0.150	--	--	--	--	--	--	--	--	--	--
---------- Break ----------										
0.610	--	--	--	--	--	--	--	--	--	--
0.620	--	--	--	--	--	--	--	--	--	s0.642
0.630	--	--	--	--	--	--	--	--	--	s0.648
0.640	--	--	--	--	--	--	--	--	--	s0.653
0.650	--	--	--	--	--	--	--	--	s0.668	s0.659
0.660	--	--	--	--	--	--	--	--	s0.673	s0.664
0.670	--	--	--	--	--	--	--	s0.687	s0.678	s0.670
0.680	--	--	--	--	--	--	--	s0.692	s0.683	s0.675
0.690	--	--	--	--	--	--	--	s0.697	s0.689	s0.681
0.700	--	--	--	--	--	--	s0.712	s0.702	s0.694	s0.686
0.710	--	--	--	--	--	--	s0.716	s0.707	s0.699	s0.692
0.720	--	--	--	--	--	s0.731	s0.721	s0.712	s0.704	s0.697
0.730	--	--	--	--	--	s0.735	s0.726	s0.717	s0.710	s0.703
0.740	--	--	--	--	s0.750	s0.740	s0.731	s0.723	s0.715	s0.708
0.750	--	--	--	--	s0.754	s0.744	s0.736	s0.728	s0.720	s0.714
0.760	--	--	--	s0.769	s0.758	s0.749	s0.741	s0.733	s0.726	s0.719
0.770	--	--	--	s0.773	s0.763	s0.754	s0.745	s0.738	s0.731	0.725
0.780	--	--	s0.787	s0.777	s0.767	s0.758	s0.750	s0.743	s0.736	0.730
0.790	--	--	s0.791	s0.781	s0.772	s0.763	s0.755	s0.748	0.742	0.735
0.800	--	s0.805	s0.795	s0.785	s0.776	s0.768	s0.760	0.753	0.747	0.741
0.810	--	s0.809	s0.799	s0.789	s0.781	s0.773	0.765	0.759	0.752	0.746
0.820	s0.824	s0.813	s0.803	s0.794	s0.785	s0.778	0.770	0.764	0.757	0.752
0.830	s0.827	s0.817	s0.807	s0.798	s0.790	0.782	0.775	0.769	0.763	0.757
0.840	s0.830	s0.820	s0.811	s0.803	0.795	0.787	0.780	0.774	0.768	0.762
0.850	s0.834	s0.824	s0.815	0.807	0.799	0.792	0.785	0.779	0.773	0.768
0.860	s0.838	s0.828	0.820	0.812	0.804	0.797	0.790	0.784	0.779	0.773
0.870	s0.842	0.833	0.824	0.816	0.809	0.802	0.796	0.789	0.784	0.778
0.880	s0.845	0.837	0.828	0.821	0.814	0.807	0.801	0.795	0.789	0.784
0.890	0.849	0.841	0.833	0.825	0.818	0.812	0.806	0.800	--	--
0.900	0.853	0.845	0.837	0.830	0.823	0.817	0.811	--	--	--
0.910	0.858	0.849	0.842	0.835	0.828	--	--	--	--	--
0.920	0.862	0.854	0.846	--	--	--	--	--	--	--
0.930	0.866	0.858	--	--	--	--	--	--	--	--
0.940	--	--	--	--	--	--	--	--	--	--

Table D2.4 L-scale of L-gamma distribution as function of the median
and values (0.11 to 0.20) of inter-tercile range--"s" denotes a simulated value.

Median values										
	Values for inter-tercile range ------>									
V	0.110	0.120	0.130	0.140	0.150	0.160	0.170	0.180	0.190	0.200
0.000	--	--	--	--	--	--	--	--	--	--
0.010	0.127	0.133	0.139	0.144	0.150	0.155	0.160	--	--	--
0.020	0.116	0.121	0.126	0.131	0.136	0.141	0.145	0.150	0.154	0.159
0.030	s0.112	s0.116	0.121	0.125	0.129	0.133	0.138	0.142	0.146	0.150
0.040	s0.110	s0.114	s0.118	s0.122	0.125	0.129	0.133	0.137	0.141	0.144
0.050	--	s0.113	s0.117	s0.120	s0.123	s0.127	0.130	0.134	0.137	0.141
0.060	--	--	s0.116	s0.119	s0.122	s0.126	s0.129	s0.132	0.135	0.139
0.070	--	--	--	--	s0.122	s0.125	s0.128	s0.131	s0.134	0.137
0.080	--	--	--	--	--	s0.125	s0.128	s0.131	s0.133	s0.136
0.090	--	--	--	--	--	--	s0.127	s0.130	s0.133	s0.136
0.100	--	--	--	--	--	--	s0.126	s0.130	s0.133	s0.136
0.110	--	--	--	--	--	--	--	s0.129	s0.132	s0.135
0.120	--	--	--	--	--	--	--	--	s0.132	s0.135
0.130	--	--	--	--	--	--	--	--	--	s0.135
0.140	--	--	--	--	--	--	--	--	--	s0.134
0.150	--	--	--	--	--	--	--	--	--	--
---------- Break ----------										
0.610	--	--	--	--	--	--	--	--	--	--
0.620	--	--	--	--	--	--	--	--	--	s0.103
0.630	--	--	--	--	--	--	--	--	--	s0.104
0.640	--	--	--	--	--	--	--	--	--	s0.105
0.650	--	--	--	--	--	--	--	--	s0.098	s0.106
0.660	--	--	--	--	--	--	--	--	s0.099	s0.107
0.670	--	--	--	--	--	--	--	s0.092	s0.100	s0.108
0.680	--	--	--	--	--	--	--	s0.093	s0.101	s0.109
0.690	--	--	--	--	--	--	--	s0.095	s0.102	s0.110
0.700	--	--	--	--	--	--	s0.087	s0.096	s0.104	s0.111
0.710	--	--	--	--	--	--	s0.089	s0.097	s0.105	s0.112
0.720	--	--	--	--	--	s0.082	s0.091	s0.099	s0.106	s0.112
0.730	--	--	--	--	--	s0.084	s0.092	s0.100	s0.107	s0.113
0.740	--	--	--	--	s0.076	s0.085	s0.094	s0.101	s0.108	s0.114
0.750	--	--	--	--	s0.078	s0.087	s0.095	s0.102	s0.109	s0.115
0.760	--	--	--	s0.071	s0.080	s0.089	s0.096	s0.103	s0.110	s0.116
0.770	--	--	--	s0.073	s0.082	s0.090	s0.098	s0.105	s0.111	0.117
0.780	--	--	s0.066	s0.075	s0.084	s0.092	s0.099	s0.106	s0.112	0.118
0.790	--	--	s0.068	s0.077	s0.086	s0.093	s0.100	s0.107	0.113	0.118
0.800	--	s0.061	s0.070	s0.079	s0.087	s0.095	s0.101	0.108	0.114	0.119
0.810	--	s0.063	s0.073	s0.081	s0.089	s0.096	0.103	0.109	0.115	0.120
0.820	s0.056	s0.066	s0.075	s0.083	s0.090	s0.097	0.104	0.110	0.115	0.121
0.830	s0.059	s0.068	s0.077	s0.085	s0.092	0.098	0.105	0.111	0.116	0.122
0.840	s0.061	s0.070	s0.079	s0.086	0.093	0.100	0.106	0.112	0.117	0.122
0.850	s0.064	s0.072	s0.080	0.088	0.095	0.101	0.107	0.113	0.118	0.123
0.860	s0.066	s0.074	0.082	0.089	0.096	0.102	0.108	0.114	0.119	0.124
0.870	s0.068	0.076	0.084	0.091	0.097	0.103	0.109	0.115	0.120	0.125
0.880	s0.070	0.078	0.085	0.092	0.098	0.104	0.110	0.115	0.120	0.125
0.890	0.072	0.080	0.087	0.093	0.100	0.106	0.111	0.116	--	--
0.900	0.074	0.082	0.088	0.095	0.101	0.107	0.112	--	--	--
0.910	0.076	0.083	0.090	0.096	0.102	--	--	--	--	--
0.920	0.078	0.085	0.091	--	--	--	--	--	--	--
0.930	0.080	0.086	--	--	--	--	--	--	--	--
0.940	--	--	--	--	--	--	--	--	--	--

Table D3.1 Parameter B of L-gamma distribution as function of the median and values (0.21 to 0.30) of inter-tercile range

Median values	Values for inter-tercile range ------->									
v	0.210	0.220	0.230	0.240	0.250	0.260	0.270	0.280	0.290	0.300
0.010	--	--	--	--	--	--	--	--	--	--
0.020	18.51	19.33	20.11	--	--	--	--	--	--	--
0.030	13.79	14.60	15.37	16.12	16.83	17.52	--	--	--	--
0.040	10.51	11.30	12.06	12.80	13.50	14.18	14.83	15.47	16.08	--
0.050	8.082	8.843	9.578	10.28	10.97	11.64	12.28	12.90	13.51	14.09
0.060	6.217	6.936	7.637	8.320	8.983	9.628	10.25	10.86	11.45	12.02
0.070	4.772	5.442	6.101	6.747	7.379	7.997	8.600	9.189	9.763	10.32
0.080	3.646	4.265	4.877	5.482	6.078	6.664	7.239	7.803	8.356	8.898
0.090	2.767	3.333	3.898	4.459	5.016	5.568	6.112	6.648	7.177	7.696
0.100	2.076	2.593	3.112	3.631	4.149	4.664	5.176	5.682	6.183	6.679
0.110	1.530	2.004	2.480	2.959	3.439	3.918	4.396	4.872	5.346	5.815
0.120	1.097	1.531	1.969	2.410	2.855	3.300	3.747	4.193	4.638	5.081
0.130	0.751	1.150	1.554	1.962	2.373	2.787	3.203	3.620	4.038	4.455
0.140	0.473	0.841	1.215	1.592	1.974	2.360	2.748	3.138	3.530	3.922
0.150	0.249	0.590	0.937	1.288	1.643	2.002	2.365	2.730	3.097	3.466
0.160	0.067	0.385	0.708	1.035	1.367	1.702	2.041	2.384	2.728	3.076
0.170	--	0.217	0.519	0.825	1.135	1.450	1.768	2.089	2.413	2.740
0.180	--	0.079	0.362	0.650	0.941	1.236	1.535	1.838	2.143	2.451
0.190	--	--	0.233	0.503	0.778	1.056	1.337	1.623	1.911	2.202
0.200	--	--	0.125	0.381	0.640	0.902	1.169	1.438	1.711	1.986
0.210	--	--	0.036	0.278	0.523	0.772	1.024	1.280	1.538	1.799
0.220	--	--	--	0.192	0.425	0.661	0.901	1.143	1.389	1.637
0.230	--	--	--	0.121	0.343	0.567	0.795	1.026	1.259	1.495
0.240	--	--	--	0.062	0.273	0.487	0.704	0.924	1.147	1.372
0.250	--	--	--	0.013	0.215	0.419	0.627	0.837	1.049	1.265
0.260	--	--	--	--	0.166	0.362	0.560	0.761	0.965	1.171
0.270	--	--	--	--	0.126	0.313	0.504	0.696	0.892	1.089
0.280	--	--	--	--	0.093	0.273	0.456	0.641	0.828	1.018
0.290	--	--	--	--	0.066	0.239	0.415	0.593	0.773	0.956
0.300	--	--	--	--	0.045	0.212	0.381	0.552	0.726	0.901
0.310	--	--	--	--	0.028	0.189	0.353	0.518	0.685	0.854
0.320	--	--	--	--	0.016	0.172	0.329	0.489	0.651	0.814
0.330	--	--	--	--	0.008	0.158	0.311	0.465	0.621	0.779
0.340	--	--	--	--	0.002	0.148	0.296	0.445	0.596	0.749
0.350	--	--	--	--	0.000	0.142	0.285	0.429	0.576	0.723
0.360	--	--	--	--	0.001	0.138	0.276	0.417	0.559	0.702
0.370	--	--	--	--	0.003	0.136	0.271	0.407	0.545	0.684
0.380	--	--	--	--	0.008	0.137	0.268	0.401	0.534	0.669
0.390	--	--	--	--	0.014	0.140	0.268	0.396	0.526	0.658
0.400	--	--	--	--	0.022	0.145	0.269	0.394	0.521	0.649
0.410	--	--	--	--	0.032	0.151	0.272	0.394	0.517	0.642
0.420	--	--	--	--	0.043	0.159	0.277	0.396	0.516	0.637
0.430	--	--	--	--	0.055	0.168	0.283	0.399	0.516	0.635
0.440	--	--	--	--	0.068	0.179	0.291	0.404	0.518	0.634
0.450	--	--	--	--	0.082	0.190	0.300	0.410	0.522	0.634
0.460	--	--	--	--	0.097	0.203	0.309	0.418	0.527	0.637
0.470	--	--	--	0.009	0.112	0.216	0.320	0.426	0.533	0.640
0.480	--	--	--	0.028	0.128	0.230	0.332	0.435	0.540	0.645
0.490	--	--	--	0.047	0.145	0.244	0.344	0.446	0.548	0.651
0.500	--	--	--	0.066	0.162	0.260	0.358	0.457	0.557	0.657
0.510	--	--	--	0.086	0.180	0.275	0.371	0.469	0.566	0.665
0.520	--	--	0.014	0.106	0.198	0.292	0.386	0.481	0.577	0.674
0.530	--	--	0.036	0.126	0.217	0.308	0.401	0.494	0.588	0.683
0.540	--	--	0.058	0.146	0.236	0.326	0.416	0.508	0.600	0.693
0.550	--	--	0.080	0.167	0.255	0.343	0.432	0.522	0.612	0.704
0.560	--	0.018	0.103	0.188	0.274	0.361	0.448	0.536	0.625	0.715
0.570	--	0.042	0.126	0.209	0.294	0.379	0.465	0.551	0.639	0.727
0.580	--	0.067	0.148	0.231	0.314	0.397	0.482	0.567	0.653	0.739
0.590	0.011	0.091	0.171	0.252	0.334	0.416	0.499	0.582	0.667	0.752
0.600	0.036	0.115	0.194	0.274	0.354	0.435	0.516	0.598	0.681	0.765
0.610	0.062	0.139	0.217	0.295	0.374	0.454	0.534	0.615	0.696	0.778
0.620	0.087	0.163	0.240	0.317	0.394	0.473	0.552	0.631	0.711	0.792
0.630	0.112	0.187	0.263	0.338	0.415	0.492	0.570	0.648	0.727	0.806
0.640	0.138	0.211	0.285	0.360	0.435	0.511	0.588	0.665	0.742	0.821
0.650	0.163	0.235	0.308	0.382	0.456	0.531	0.606	0.682	0.758	0.835
0.660	0.188	0.259	0.331	0.404	0.477	0.550	0.624	0.699	0.774	0.850
0.670	0.212	0.283	0.354	0.425	0.497	0.570	0.643	0.717	0.791	0.865

Table D3.1 continued

Median values										
	values for inter-tercile range ------->									
V	0.210	0.220	0.230	0.240	0.250	0.260	0.270	0.280	0.290	0.300
0.680	0.237	0.307	0.377	0.447	0.518	0.590	0.662	0.734	0.807	0.881
0.690	0.262	0.330	0.399	0.469	0.539	0.609	0.680	0.752	0.824	0.896
0.700	0.286	0.354	0.422	0.490	0.559	0.629	0.699	0.769	0.840	0.912
0.710	0.311	0.377	0.444	0.512	0.580	0.649	0.718	0.787	0.857	0.928
0.720	0.335	0.401	0.467	0.534	0.601	0.668	0.736	0.805	0.874	0.943
0.730	0.359	0.424	0.489	0.555	0.621	0.688	0.755	0.823	0.891	0.959
0.740	0.383	0.447	0.512	0.577	0.642	0.708	0.774	0.841	0.908	0.976
0.750	0.407	0.470	0.534	0.598	0.663	0.728	0.793	0.859	0.925	0.992
0.760	0.431	0.493	0.556	0.619	0.683	0.747	0.812	0.877	0.942	1.008
0.770	0.454	0.516	0.578	0.641	0.704	0.767	0.831	0.895	0.959	1.024
0.780	0.478	0.539	0.600	0.662	0.724	0.787	0.850	0.913	0.977	1.041
0.790	0.501	0.561	0.622	0.683	0.744	0.806	0.868	0.931	0.994	1.057
0.800	0.524	0.584	0.644	0.704	0.765	0.826	0.887	0.949	1.011	1.074
0.810	0.547	0.606	0.665	0.725	0.785	0.845	0.906	0.967	1.029	1.090
0.820	0.570	0.629	0.687	0.746	0.805	0.865	0.925	0.985	--	--
0.830	0.593	0.651	0.709	0.767	0.825	0.884	0.944	--	--	--
0.840	0.616	0.673	0.730	0.787	0.845	--	--	--	--	--
0.850	0.638	0.695	0.751	0.808	--	--	--	--	--	--
0.860	0.661	0.716	0.772	--	--	--	--	--	--	--
0.870	0.683	--	--	--	--	--	--	--	--	--
0.880	--	--	--	--	--	--	--	--	--	--

Table D3.2 Parameter C of L-gamma distribution as function of the median and values (0.21 to 0.30) of inter-tercile range

Median values	Values for inter-tercile range ------->									
v	0.210	0.220	0.230	0.240	0.250	0.260	0.270	0.280	0.290	0.300
0.010	--	--	--	--	--	--	--	--	--	--
0.020	+17.83	+18.97	+20.05	--	--	--	--	--	--	--
0.030	+12.10	+13.22	+14.30	+15.33	+16.32	+17.27	--	--	--	--
0.040	+8.142	+9.238	+10.29	+11.30	+12.28	+13.22	+14.13	+15.01	+15.86	--
0.050	+5.212	+6.267	+7.287	+8.273	+9.226	+10.14	+11.04	+11.90	+12.74	+13.55
0.060	+2.992	+3.989	+4.961	+5.907	+6.826	+7.720	+8.588	+9.432	+10.25	+11.04
0.070	+1.297	+2.226	+3.140	+4.035	+4.911	+5.768	+6.604	+7.420	+8.216	+8.992
0.080	+0.003	+0.861	+1.709	+2.548	+3.374	+4.186	+4.984	+5.766	+6.533	+7.283
0.090	-0.981	-0.195	+0.588	+1.366	+2.138	+2.902	+3.657	+4.401	+5.133	+5.853
0.100	-1.728	-1.010	-0.290	+0.429	+1.147	+1.861	+2.570	+3.272	+3.967	+4.653
0.110	-2.293	-1.637	-0.976	-0.313	+0.352	+1.017	+1.680	+2.340	+2.996	+3.647
0.120	-2.720	-2.118	-1.511	-0.899	-0.283	+0.335	+0.953	+1.572	+2.188	+2.803
0.130	-3.039	-2.487	-1.927	-1.361	-0.791	-0.217	+0.360	+0.939	+1.518	+2.096
0.140	-3.277	-2.766	-2.249	-1.725	-1.195	-0.661	-0.123	+0.418	+0.961	+1.505
0.150	-3.449	-2.976	-2.496	-2.009	-1.517	-1.019	-0.516	-0.010	+0.499	+1.011
0.160	-3.572	-3.131	-2.684	-2.230	-1.771	-1.305	-0.835	-0.361	+0.117	+0.599
0.170	--	-3.243	-2.825	-2.400	-1.970	-1.534	-1.093	-0.648	-0.198	+0.255
0.180	--	-3.320	-2.927	-2.529	-2.125	-1.716	-1.301	-0.882	-0.459	-0.031
0.190	--	--	-2.999	-2.624	-2.244	-1.858	-1.467	-1.072	-0.672	-0.269
0.200	--	--	-3.045	-2.691	-2.332	-1.968	-1.599	-1.225	-0.847	-0.465
0.210	--	--	-3.071	-2.736	-2.396	-2.051	-1.701	-1.347	-0.989	-0.627
0.220	--	--	--	-2.761	-2.439	-2.111	-1.780	-1.444	-1.103	-0.759
0.230	--	--	--	-2.772	-2.464	-2.153	-1.837	-1.518	-1.194	-0.866
0.240	--	--	--	-2.769	-2.476	-2.179	-1.878	-1.573	-1.264	-0.952
0.250	--	--	--	-2.755	-2.475	-2.191	-1.904	-1.613	-1.318	-1.019
0.260	--	--	--	--	-2.464	-2.193	-1.917	-1.639	-1.357	-1.071
0.270	--	--	--	--	-2.444	-2.184	-1.920	-1.653	-1.383	-1.109
0.280	--	--	--	--	-2.418	-2.168	-1.914	-1.658	-1.398	-1.135
0.290	--	--	--	--	-2.384	-2.144	-1.900	-1.654	-1.404	-1.151
0.300	--	--	--	--	-2.346	-2.114	-1.880	-1.642	-1.402	-1.158
0.310	--	--	--	--	-2.303	-2.080	-1.853	-1.624	-1.392	-1.158
0.320	--	--	--	--	-2.257	-2.041	-1.822	-1.601	-1.377	-1.151
0.330	--	--	--	--	-2.207	-1.998	-1.787	-1.573	-1.356	-1.138
0.340	--	--	--	--	-2.154	-1.952	-1.747	-1.540	-1.331	-1.119
0.350	--	--	--	--	-2.099	-1.903	-1.705	-1.505	-1.302	-1.097
0.360	--	--	--	--	-2.043	-1.852	-1.660	-1.466	-1.269	-1.070
0.370	--	--	--	--	-1.984	-1.799	-1.613	-1.424	-1.233	-1.040
0.380	--	--	--	--	-1.924	-1.745	-1.563	-1.380	-1.195	-1.007
0.390	--	--	--	--	-1.863	-1.689	-1.512	-1.334	-1.154	-0.971
0.400	--	--	--	--	-1.802	-1.632	-1.460	-1.286	-1.111	-0.933
0.410	--	--	--	--	-1.739	-1.573	-1.406	-1.237	-1.066	-0.893
0.420	--	--	--	--	-1.676	-1.514	-1.351	-1.186	-1.020	-0.852
0.430	--	--	--	--	-1.612	-1.454	-1.295	-1.134	-0.972	-0.808
0.440	--	--	--	--	-1.548	-1.394	-1.239	-1.082	-0.923	-0.763
0.450	--	--	--	--	-1.484	-1.333	-1.182	-1.028	-0.874	-0.717
0.460	--	--	--	--	-1.419	-1.272	-1.124	-0.974	-0.823	-0.670
0.470	--	--	--	-1.497	-1.355	-1.211	-1.066	-0.920	-0.772	-0.623
0.480	--	--	--	-1.429	-1.290	-1.150	-1.008	-0.864	-0.720	-0.574
0.490	--	--	--	-1.362	-1.226	-1.088	-0.949	-0.809	-0.668	-0.525
0.500	--	--	--	-1.295	-1.161	-1.027	-0.890	-0.753	-0.615	-0.475
0.510	--	--	--	-1.228	-1.097	-0.965	-0.832	-0.697	-0.562	-0.425
0.520	--	--	-1.289	-1.162	-1.033	-0.904	-0.773	-0.641	-0.508	-0.374
0.530	--	--	-1.220	-1.095	-0.969	-0.842	-0.714	-0.585	-0.454	-0.323
0.540	--	--	-1.152	-1.029	-0.906	-0.781	-0.655	-0.529	-0.401	-0.272
0.550	--	--	-1.084	-0.964	-0.843	-0.720	-0.597	-0.472	-0.347	-0.220
0.560	--	-1.134	-1.017	-0.899	-0.780	-0.659	-0.538	-0.416	-0.293	-0.169
0.570	--	-1.065	-0.950	-0.834	-0.717	-0.599	-0.480	-0.360	-0.239	-0.117
0.580	--	-0.997	-0.884	-0.770	-0.655	-0.539	-0.422	-0.304	-0.185	-0.065
0.590	-1.040	-0.929	-0.818	-0.706	-0.593	-0.479	-0.364	-0.248	-0.131	-0.013
0.600	-0.971	-0.862	-0.753	-0.642	-0.531	-0.419	-0.306	-0.192	-0.077	+0.039
0.610	-0.903	-0.796	-0.688	-0.579	-0.470	-0.360	-0.248	-0.136	-0.024	+0.090
0.620	-0.835	-0.730	-0.624	-0.517	-0.409	-0.301	-0.191	-0.081	+0.030	+0.142
0.630	-0.768	-0.665	-0.560	-0.455	-0.349	-0.242	-0.134	-0.026	+0.083	+0.194
0.640	-0.702	-0.600	-0.497	-0.393	-0.289	-0.184	-0.078	+0.029	+0.137	+0.245
0.650	-0.636	-0.536	-0.434	-0.332	-0.229	-0.126	-0.021	+0.084	+0.190	+0.296
0.660	-0.571	-0.472	-0.372	-0.272	-0.170	-0.068	+0.035	+0.138	+0.243	+0.348
0.670	-0.506	-0.409	-0.310	-0.211	-0.111	-0.011	+0.090	+0.192	+0.295	+0.399

Table D3.2 continued

Median values										
	values for inter-tercile range ------->									
v	0.210	0.220	0.230	0.240	0.250	0.260	0.270	0.280	0.290	0.300
0.680	-0.443	-0.346	-0.249	-0.152	-0.053	+0.046	+0.146	+0.246	+0.348	+0.449
0.690	-0.379	-0.284	-0.189	-0.092	+0.005	+0.102	+0.201	+0.300	+0.400	+0.500
0.700	-0.316	-0.223	-0.128	-0.033	+0.062	+0.159	+0.256	+0.353	+0.452	+0.551
0.710	-0.254	-0.162	-0.069	+0.025	+0.119	+0.214	+0.310	+0.406	+0.503	+0.601
0.720	-0.193	-0.101	-0.010	+0.083	+0.176	+0.270	+0.364	+0.459	+0.555	+0.651
0.730	-0.132	-0.042	+0.049	+0.140	+0.232	+0.325	+0.418	+0.511	+0.606	+0.701
0.740	-0.071	+0.018	+0.107	+0.197	+0.288	+0.379	+0.471	+0.563	+0.657	+0.750
0.750	-0.011	+0.077	+0.165	+0.254	+0.343	+0.433	+0.524	+0.615	+0.707	+0.800
0.760	+0.048	+0.135	+0.222	+0.310	+0.398	+0.487	+0.577	+0.667	+0.757	+0.849
0.770	+0.107	+0.193	+0.279	+0.365	+0.453	+0.541	+0.629	+0.718	+0.807	+0.897
0.780	+0.165	+0.250	+0.335	+0.421	+0.507	+0.594	+0.681	+0.769	+0.857	+0.946
0.790	+0.223	+0.307	+0.391	+0.475	+0.561	+0.646	+0.732	+0.819	+0.906	+0.994
0.800	+0.281	+0.363	+0.446	+0.530	+0.614	+0.699	+0.784	+0.869	+0.956	+1.042
0.810	+0.337	+0.419	+0.501	+0.584	+0.667	+0.750	+0.835	+0.919	+1.004	+1.090
0.820	+0.394	+0.474	+0.556	+0.637	+0.719	+0.802	+0.885	+0.969	--	--
0.830	+0.450	+0.529	+0.610	+0.690	+0.771	+0.853	+0.935	--	--	--
0.840	+0.505	+0.584	+0.663	+0.743	+0.823	--	--	--	--	--
0.850	+0.560	+0.638	+0.716	+0.795	--	--	--	--	--	--
0.860	+0.614	+0.691	+0.769	--	--	--	--	--	--	--
0.870	+0.668	--	--	--	--	--	--	--	--	--
0.880	--	--	--	--	--	--	--	--	--	--

Table D3.3 Mean of L-gamma distribution as function of the median
and values (0.21 to 0.30) of inter-tercile range--"s" denotes a simulated value.

Median values	Values for inter-tercile range ------->									
v	0.210	0.220	0.230	0.240	0.250	0.260	0.270	0.280	0.290	0.300
0.010	--	--	--	--	--	--	--	--	--	--
0.020	0.232	0.239	0.246	--	--	--	--	--	--	--
0.030	0.221	0.228	0.234	0.240	0.247	0.253	--	--	--	--
0.040	0.215	0.221	0.227	0.233	0.239	0.245	0.251	0.257	0.263	--
0.050	0.213	0.218	0.224	0.229	0.235	0.241	0.246	0.252	0.257	0.263
0.060	0.212	0.217	0.222	0.227	0.233	0.238	0.243	0.249	0.254	0.259
0.070	0.213	0.218	0.222	0.227	0.232	0.237	0.242	0.247	0.252	0.257
0.080	0.215	0.219	0.224	0.228	0.233	0.237	0.242	0.247	0.251	0.256
0.090	s0.219	s0.223	0.226	0.230	0.234	0.239	0.243	0.247	0.252	0.256
0.100	s0.224	s0.227	s0.230	0.233	0.237	0.241	0.245	0.249	0.253	0.257
0.110	s0.229	s0.232	s0.234	s0.238	0.241	0.244	0.248	0.251	0.255	0.259
0.120	s0.235	s0.237	s0.240	s0.242	s0.245	0.248	0.251	0.255	0.258	0.262
0.130	s0.242	s0.243	s0.245	s0.247	s0.250	s0.253	0.255	0.258	0.262	0.265
0.140	s0.249	s0.250	s0.252	s0.253	s0.255	s0.258	s0.260	0.263	0.266	0.269
0.150	s0.257	s0.257	s0.258	s0.260	s0.261	s0.263	s0.265	s0.268	0.270	0.273
0.160	s0.266	s0.265	s0.265	s0.266	s0.267	s0.269	s0.271	s0.273	0.275	0.277
0.170	--	s0.273	s0.273	s0.273	s0.274	s0.275	s0.277	s0.278	s0.280	0.282
0.180	--	s0.282	s0.281	s0.280	s0.281	s0.282	s0.283	s0.284	s0.286	s0.288
0.190	--	--	s0.289	s0.288	s0.288	s0.288	s0.289	s0.290	s0.292	s0.293
0.200	--	--	s0.297	s0.296	s0.295	s0.295	s0.296	s0.297	s0.298	s0.299
0.210	--	--	s0.306	s0.304	s0.303	s0.303	s0.303	s0.303	s0.304	s0.305
0.220	--	--	--	s0.312	s0.311	s0.310	s0.310	s0.310	s0.311	s0.312
0.230	--	--	--	s0.321	s0.319	s0.318	s0.317	s0.317	s0.317	s0.318
0.240	--	--	--	s0.329	s0.327	s0.325	s0.325	s0.324	s0.324	s0.325
0.250	--	--	--	s0.338	s0.335	s0.333	s0.332	s0.331	s0.331	s0.331
0.260	--	--	--	--	s0.343	s0.341	s0.340	s0.339	s0.338	s0.338
0.270	--	--	--	--	s0.352	s0.349	s0.347	s0.346	s0.345	s0.345
0.280	--	--	--	--	s0.360	s0.357	s0.355	s0.353	s0.352	s0.352
0.290	--	--	--	--	s0.368	s0.365	s0.363	s0.361	s0.360	s0.359
0.300	--	--	--	--	s0.377	s0.373	s0.370	s0.368	s0.367	s0.366
0.310	--	--	--	--	s0.385	s0.381	s0.378	s0.376	s0.374	s0.373
0.320	--	--	--	--	s0.393	s0.389	s0.386	s0.384	s0.382	s0.380
0.330	--	--	--	--	s0.402	s0.397	s0.394	s0.391	s0.389	s0.388
0.340	--	--	--	--	s0.410	s0.405	s0.402	s0.399	s0.397	s0.395
0.350	--	--	--	--	s0.418	s0.413	s0.409	s0.406	s0.404	s0.402
0.360	--	--	--	--	s0.426	s0.421	s0.417	s0.414	s0.411	s0.409
0.370	--	--	--	--	s0.434	s0.429	s0.425	s0.421	s0.419	s0.417
0.380	--	--	--	--	s0.442	s0.437	s0.432	s0.429	s0.426	s0.424
0.390	--	--	--	--	s0.450	s0.444	s0.440	s0.436	s0.433	s0.431
0.400	--	--	--	--	s0.457	s0.452	s0.447	s0.444	s0.441	s0.438
0.410	--	--	--	--	s0.465	s0.459	s0.455	s0.451	s0.448	s0.445
0.420	--	--	--	--	s0.472	s0.467	s0.462	s0.458	s0.455	s0.452
0.430	--	--	--	--	s0.480	s0.474	s0.470	s0.466	s0.462	s0.459
0.440	--	--	--	--	s0.487	s0.482	s0.477	s0.473	s0.469	s0.467
0.450	--	--	--	--	s0.494	s0.489	s0.484	s0.480	s0.477	s0.474
0.460	--	--	--	--	s0.502	s0.496	s0.491	s0.487	s0.484	s0.481
0.470	--	--	--	s0.515	s0.509	s0.503	s0.498	s0.494	s0.491	s0.488
0.480	--	--	--	s0.522	s0.516	s0.510	s0.505	s0.501	s0.498	s0.494
0.490	--	--	--	s0.529	s0.523	s0.517	s0.512	s0.508	s0.505	s0.501
0.500	--	--	--	s0.536	s0.530	s0.524	s0.519	s0.515	s0.511	s0.508
0.510	--	--	--	s0.543	s0.536	s0.531	s0.526	s0.522	s0.518	s0.515
0.520	--	--	s0.557	s0.549	s0.543	s0.538	s0.533	s0.529	s0.525	s0.522
0.530	--	--	s0.563	s0.556	s0.550	s0.544	s0.540	s0.536	s0.532	s0.529
0.540	--	--	s0.570	s0.563	s0.557	s0.551	s0.546	s0.542	s0.539	s0.535
0.550	--	--	s0.576	s0.569	s0.563	s0.558	s0.553	s0.549	s0.545	s0.542
0.560	--	s0.590	s0.582	s0.576	s0.570	s0.564	s0.560	s0.556	s0.552	s0.548
0.570	--	s0.596	s0.589	s0.582	s0.576	s0.571	s0.566	s0.562	s0.558	s0.555
0.580	--	s0.602	s0.595	s0.588	s0.583	s0.577	s0.573	s0.569	s0.565	s0.562
0.590	s0.616	s0.608	s0.601	s0.595	s0.589	s0.584	s0.579	s0.575	s0.572	s0.568
0.600	s0.622	s0.614	s0.607	s0.601	s0.595	s0.590	s0.586	s0.582	s0.578	0.575
0.610	s0.628	s0.620	s0.613	s0.607	s0.602	s0.597	s0.592	s0.588	s0.584	0.581
0.620	s0.634	s0.626	s0.620	s0.613	s0.608	s0.603	s0.599	s0.595	0.591	0.587
0.630	s0.640	s0.632	s0.626	s0.620	s0.614	s0.609	s0.605	s0.601	0.597	0.594
0.640	s0.645	s0.638	s0.632	s0.626	s0.620	s0.616	s0.611	0.607	0.604	0.600
0.650	s0.651	s0.644	s0.638	s0.632	s0.627	s0.622	s0.618	0.614	0.610	0.607
0.660	s0.657	s0.650	s0.644	s0.638	s0.633	s0.628	0.624	0.620	0.616	0.613
0.670	s0.662	s0.656	s0.650	s0.644	s0.639	s0.634	0.630	0.626	0.622	0.619

Table D3.3 continued

Median values										
	values for inter-tercile range ------->									
V	0.210	0.220	0.230	0.240	0.250	0.260	0.270	0.280	0.290	0.300
0.680	s0.668	s0.662	s0.656	s0.650	s0.645	0.640	0.636	0.632	0.629	0.625
0.690	s0.674	s0.667	s0.661	s0.656	0.651	0.647	0.642	0.638	0.635	0.631
0.700	s0.679	s0.673	s0.667	s0.662	0.657	0.653	0.648	0.645	0.641	0.638
0.710	s0.685	s0.679	s0.673	0.668	0.663	0.659	0.654	0.651	0.647	0.644
0.720	s0.691	s0.685	s0.679	0.674	0.669	0.665	0.661	0.657	0.653	0.650
0.730	s0.696	s0.690	0.685	0.680	0.675	0.671	0.667	0.663	0.659	0.656
0.740	s0.702	0.696	0.691	0.686	0.681	0.677	0.673	0.669	0.665	0.662
0.750	s0.707	0.702	0.696	0.691	0.687	0.683	0.679	0.675	0.671	0.668
0.760	0.713	0.707	0.702	0.697	0.693	0.688	0.684	0.681	0.677	0.674
0.770	0.719	0.713	0.708	0.703	0.699	0.694	0.690	0.687	0.683	0.680
0.780	0.724	0.719	0.714	0.709	0.704	0.700	0.696	0.693	0.689	0.686
0.790	0.730	0.724	0.719	0.715	0.710	0.706	0.702	0.699	0.695	0.692
0.800	0.735	0.730	0.725	0.720	0.716	0.712	0.708	0.704	0.701	0.698
0.810	0.741	0.735	0.731	0.726	0.722	0.718	0.714	0.710	0.707	0.704
0.820	0.746	0.741	0.736	0.732	0.727	0.723	0.720	0.716	--	--
0.830	0.752	0.747	0.742	0.737	0.733	0.729	0.725	--	--	--
0.840	0.757	0.752	0.747	0.743	0.739	--	--	--	--	--
0.850	0.763	0.758	0.753	0.749	--	--	--	--	--	--
0.860	0.768	0.763	0.759	--	--	--	--	--	--	--
0.870	0.773	--	--	--	--	--	--	--	--	--
0.880	--	--	--	--	--	--	--	--	--	--

Table D3.4 L-scale of L-gamma distribution as function of the median
and values (0.21 to 0.30) of inter-tercile range--"s" denotes a simulated value.

Median values	Values for inter-tercile range ------->									
v	0.210	0.220	0.230	0.240	0.250	0.260	0.270	0.280	0.290	0.300
0.010	--	--	--	--	--	--	--	--	--	--
0.020	0.163	0.167	0.172	--	--	--	--	--	--	--
0.030	0.154	0.158	0.162	0.166	0.170	0.174	--	--	--	--
0.040	0.148	0.152	0.156	0.159	0.163	0.167	0.170	0.174	0.177	--
0.050	0.144	0.148	0.151	0.155	0.158	0.162	0.165	0.169	0.172	0.175
0.060	0.142	0.145	0.148	0.152	0.155	0.158	0.161	0.165	0.168	0.171
0.070	0.140	0.143	0.146	0.149	0.152	0.156	0.159	0.162	0.165	0.168
0.080	0.139	0.142	0.145	0.148	0.151	0.154	0.157	0.160	0.162	0.165
0.090	s0.139	s0.141	0.144	0.147	0.149	0.152	0.155	0.158	0.161	0.163
0.100	s0.138	s0.141	s0.143	0.146	0.149	0.151	0.154	0.157	0.159	0.162
0.110	s0.138	s0.141	s0.143	s0.146	0.148	0.151	0.153	0.156	0.158	0.161
0.120	s0.138	s0.141	s0.143	s0.146	s0.148	0.150	0.153	0.155	0.158	0.160
0.130	s0.138	s0.140	s0.143	s0.145	s0.148	s0.150	0.152	0.155	0.157	0.160
0.140	s0.137	s0.140	s0.143	s0.145	s0.148	s0.150	s0.152	0.155	0.157	0.159
0.150	s0.137	s0.140	s0.143	s0.145	s0.148	s0.150	s0.152	s0.155	0.157	0.159
0.160	s0.136	s0.139	s0.142	s0.145	s0.148	s0.150	s0.152	s0.155	0.157	0.159
0.170	--	s0.139	s0.142	s0.145	s0.148	s0.150	s0.152	s0.155	s0.157	0.159
0.180	--	s0.138	s0.142	s0.145	s0.148	s0.150	s0.152	s0.155	s0.157	s0.159
0.190	--	--	s0.141	s0.144	s0.147	s0.150	s0.152	s0.155	s0.157	s0.159
0.200	--	--	s0.140	s0.144	s0.147	s0.150	s0.152	s0.155	s0.157	s0.159
0.210	--	--	s0.139	s0.143	s0.147	s0.150	s0.152	s0.155	s0.157	s0.159
0.220	--	--	--	s0.143	s0.146	s0.149	s0.152	s0.155	s0.157	s0.159
0.230	--	--	--	s0.142	s0.146	s0.149	s0.152	s0.155	s0.157	s0.159
0.240	--	--	--	s0.141	s0.145	s0.149	s0.152	s0.155	s0.157	s0.159
0.250	--	--	--	s0.140	s0.144	s0.148	s0.151	s0.154	s0.157	s0.159
0.260	--	--	--	--	s0.144	s0.148	s0.151	s0.154	s0.157	s0.159
0.270	--	--	--	--	s0.143	s0.147	s0.151	s0.154	s0.157	s0.159
0.280	--	--	--	--	s0.142	s0.147	s0.150	s0.154	s0.157	s0.159
0.290	--	--	--	--	s0.141	s0.146	s0.150	s0.153	s0.156	s0.159
0.300	--	--	--	--	s0.140	s0.145	s0.149	s0.153	s0.156	s0.159
0.310	--	--	--	--	s0.140	s0.145	s0.149	s0.153	s0.156	s0.159
0.320	--	--	--	--	s0.139	s0.144	s0.148	s0.152	s0.156	s0.159
0.330	--	--	--	--	s0.138	s0.143	s0.148	s0.152	s0.155	s0.158
0.340	--	--	--	--	s0.137	s0.143	s0.148	s0.152	s0.155	s0.158
0.350	--	--	--	--	s0.137	s0.142	s0.147	s0.151	s0.155	s0.158
0.360	--	--	--	--	s0.136	s0.142	s0.147	s0.151	s0.155	s0.158
0.370	--	--	--	--	s0.135	s0.141	s0.146	s0.151	s0.154	s0.158
0.380	--	--	--	--	s0.135	s0.141	s0.146	s0.150	s0.154	s0.158
0.390	--	--	--	--	s0.135	s0.140	s0.145	s0.150	s0.154	s0.157
0.400	--	--	--	--	s0.134	s0.140	s0.145	s0.150	s0.154	s0.157
0.410	--	--	--	--	s0.134	s0.140	s0.145	s0.149	s0.153	s0.157
0.420	--	--	--	--	s0.133	s0.139	s0.145	s0.149	s0.153	s0.157
0.430	--	--	--	--	s0.133	s0.139	s0.144	s0.149	s0.153	s0.157
0.440	--	--	--	--	s0.133	s0.139	s0.144	s0.149	s0.153	s0.156
0.450	--	--	--	--	s0.133	s0.139	s0.144	s0.149	s0.153	s0.156
0.460	--	--	--	--	s0.133	s0.139	s0.144	s0.148	s0.153	s0.156
0.470	--	--	--	s0.126	s0.133	s0.139	s0.144	s0.148	s0.152	s0.156
0.480	--	--	--	s0.126	s0.133	s0.138	s0.144	s0.148	s0.152	s0.156
0.490	--	--	--	s0.126	s0.133	s0.138	s0.144	s0.148	s0.152	s0.156
0.500	--	--	--	s0.126	s0.133	s0.138	s0.143	s0.148	s0.152	s0.156
0.510	--	--	--	s0.126	s0.133	s0.138	s0.143	s0.148	s0.152	s0.156
0.520	--	--	s0.120	s0.127	s0.133	s0.138	s0.143	s0.148	s0.152	s0.156
0.530	--	--	s0.120	s0.127	s0.133	s0.139	s0.144	s0.148	s0.152	s0.156
0.540	--	--	s0.120	s0.127	s0.133	s0.139	s0.144	s0.148	s0.152	s0.156
0.550	--	--	s0.121	s0.127	s0.133	s0.139	s0.144	s0.148	s0.152	s0.156
0.560	--	s0.114	s0.121	s0.128	s0.134	s0.139	s0.144	s0.148	s0.152	s0.156
0.570	--	s0.114	s0.122	s0.128	s0.134	s0.139	s0.144	s0.148	s0.152	s0.156
0.580	--	s0.115	s0.122	s0.128	s0.134	s0.139	s0.144	s0.148	s0.152	s0.156
0.590	s0.108	s0.116	s0.123	s0.129	s0.134	s0.140	s0.144	s0.149	s0.153	s0.156
0.600	s0.109	s0.116	s0.123	s0.129	s0.135	s0.140	s0.144	s0.149	s0.153	0.156
0.610	s0.110	s0.117	s0.124	s0.130	s0.135	s0.140	s0.145	s0.149	s0.153	0.156
0.620	s0.111	s0.118	s0.124	s0.130	s0.135	s0.140	s0.145	s0.149	0.153	0.156
0.630	s0.111	s0.118	s0.125	s0.130	s0.136	s0.141	s0.145	s0.149	0.153	0.157
0.640	s0.112	s0.119	s0.125	s0.131	s0.136	s0.141	s0.145	0.149	0.153	0.157
0.650	s0.113	s0.120	s0.126	s0.131	s0.136	s0.141	s0.145	0.149	0.153	0.157
0.660	s0.114	s0.120	s0.126	s0.132	s0.137	s0.141	0.146	0.150	0.153	0.157
0.670	s0.115	s0.121	s0.127	s0.132	s0.137	s0.142	0.146	0.150	0.154	0.157

Table D3.4 continued

Median values										
	values for inter-tercile range ------->									
V	0.210	0.220	0.230	0.240	0.250	0.260	0.270	0.280	0.290	0.300
0.680	s0.116	s0.122	s0.127	s0.133	s0.137	0.142	0.146	0.150	0.154	0.157
0.690	s0.116	s0.122	s0.128	s0.133	0.138	0.142	0.146	0.150	0.154	0.158
0.700	s0.117	s0.123	s0.128	s0.134	0.138	0.143	0.147	0.151	0.154	0.158
0.710	s0.118	s0.124	s0.129	0.134	0.139	0.143	0.147	0.151	0.155	0.158
0.720	s0.119	s0.124	s0.130	0.134	0.139	0.143	0.147	0.151	0.155	0.158
0.730	s0.119	s0.125	0.130	0.135	0.139	0.144	0.148	0.151	0.155	0.159
0.740	s0.120	0.125	0.131	0.135	0.140	0.144	0.148	0.152	0.155	0.159
0.750	s0.121	0.126	0.131	0.136	0.140	0.144	0.148	0.152	0.156	0.159
0.760	0.121	0.127	0.132	0.136	0.141	0.145	0.149	0.152	0.156	0.159
0.770	0.122	0.127	0.132	0.137	0.141	0.145	0.149	0.153	0.156	0.160
0.780	0.123	0.128	0.133	0.137	0.142	0.146	0.149	0.153	0.156	0.160
0.790	0.124	0.129	0.133	0.138	0.142	0.146	0.150	0.153	0.157	0.160
0.800	0.124	0.129	0.134	0.138	0.142	0.146	0.150	0.154	0.157	0.160
0.810	0.125	0.130	0.134	0.139	0.143	0.147	0.150	0.154	0.157	0.161
0.820	0.126	0.130	0.135	0.139	0.143	0.147	0.151	0.154	--	--
0.830	0.126	0.131	0.136	0.140	0.144	0.148	0.151	--	--	--
0.840	0.127	0.132	0.136	0.140	0.144	--	--	--	--	--
0.850	0.128	0.132	0.137	0.141	--	--	--	--	--	--
0.860	0.128	0.133	0.137	--	--	--	--	--	--	--
0.870	0.129	--	--	--	--	--	--	--	--	--
0.880	--	--	--	--	--	--	--	--	--	--

Table D4.1 Parameter B of L-gamma distribution as function of the median and values (0.31 to 0.40) of inter-tercile range

Median values	Values for inter-tercile range ------->									
v	0.310	0.320	0.330	0.340	0.350	0.360	0.370	0.380	0.390	0.400
0.040	--	--	--	--	--	--	--	--	--	--
0.050	14.66	15.21	--	--	--	--	--	--	--	--
0.060	12.58	13.13	13.65	14.17	--	--	--	--	--	--
0.070	10.86	11.40	11.92	12.42	12.91	13.40	--	--	--	--
0.080	9.427	9.945	10.45	10.94	11.43	11.90	12.36	12.81	--	--
0.090	8.206	8.707	9.198	9.679	10.15	10.61	11.06	11.51	11.94	12.37
0.100	7.167	7.648	8.121	8.587	9.045	9.495	9.936	10.37	10.79	11.21
0.110	6.280	6.739	7.194	7.642	8.084	8.519	8.948	9.370	9.785	10.19
0.120	5.521	5.959	6.392	6.821	7.246	7.666	8.080	8.489	8.892	9.289
0.130	4.872	5.286	5.699	6.109	6.515	6.918	7.317	7.712	8.102	8.487
0.140	4.315	4.707	5.098	5.488	5.876	6.262	6.645	7.025	7.401	7.773
0.150	3.836	4.207	4.578	4.948	5.318	5.686	6.053	6.417	6.779	7.138
0.160	3.425	3.775	4.126	4.477	4.829	5.180	5.530	5.879	6.226	6.572
0.170	3.069	3.400	3.733	4.066	4.400	4.734	5.068	5.402	5.735	6.067
0.180	2.762	3.075	3.390	3.706	4.023	4.342	4.660	4.979	5.298	5.616
0.190	2.496	2.792	3.091	3.391	3.692	3.995	4.299	4.603	4.908	5.213
0.200	2.265	2.546	2.829	3.114	3.401	3.689	3.979	4.270	4.561	4.853
0.210	2.063	2.330	2.599	2.870	3.143	3.418	3.695	3.972	4.251	4.530
0.220	1.888	2.141	2.397	2.656	2.916	3.178	3.442	3.707	3.974	4.241
0.230	1.734	1.976	2.220	2.466	2.714	2.965	3.217	3.471	3.726	3.982
0.240	1.600	1.831	2.063	2.299	2.536	2.775	3.016	3.259	3.503	3.749
0.250	1.482	1.703	1.925	2.150	2.377	2.606	2.837	3.070	3.304	3.540
0.260	1.379	1.590	1.803	2.019	2.236	2.455	2.677	2.900	3.125	3.351
0.270	1.289	1.491	1.695	1.902	2.110	2.321	2.533	2.747	2.963	3.181
0.280	1.210	1.404	1.600	1.798	1.998	2.200	2.405	2.610	2.818	3.027
0.290	1.140	1.326	1.515	1.706	1.898	2.093	2.289	2.487	2.687	2.888
0.300	1.079	1.259	1.440	1.624	1.809	1.996	2.185	2.376	2.569	2.763
0.310	1.026	1.199	1.374	1.551	1.729	1.910	2.092	2.276	2.462	2.649
0.320	0.979	1.146	1.315	1.486	1.658	1.832	2.008	2.186	2.365	2.546
0.330	0.939	1.100	1.263	1.428	1.595	1.763	1.933	2.104	2.278	2.452
0.340	0.903	1.060	1.217	1.377	1.538	1.701	1.865	2.031	2.198	2.367
0.350	0.873	1.024	1.177	1.331	1.487	1.645	1.804	1.965	2.127	2.290
0.360	0.847	0.994	1.142	1.291	1.442	1.595	1.749	1.905	2.062	2.220
0.370	0.825	0.967	1.111	1.256	1.402	1.550	1.700	1.851	2.003	2.157
0.380	0.806	0.944	1.084	1.225	1.367	1.511	1.656	1.802	1.950	2.099
0.390	0.791	0.925	1.060	1.197	1.335	1.475	1.616	1.758	1.902	2.047
0.400	0.778	0.908	1.040	1.173	1.308	1.443	1.580	1.719	1.858	1.999
0.410	0.768	0.895	1.023	1.153	1.283	1.415	1.549	1.683	1.819	1.956
0.420	0.760	0.884	1.009	1.135	1.262	1.391	1.520	1.651	1.784	1.917
0.430	0.754	0.875	0.997	1.119	1.244	1.369	1.495	1.623	1.752	1.882
0.440	0.750	0.868	0.987	1.107	1.228	1.350	1.473	1.598	1.723	1.850
0.450	0.748	0.863	0.979	1.096	1.214	1.333	1.454	1.575	1.697	1.821
0.460	0.748	0.860	0.973	1.087	1.203	1.319	1.436	1.555	1.674	1.795
0.470	0.749	0.858	0.969	1.081	1.193	1.307	1.422	1.537	1.654	1.771
0.480	0.751	0.858	0.966	1.075	1.186	1.297	1.409	1.522	1.636	1.751
0.490	0.755	0.859	0.965	1.072	1.180	1.288	1.398	1.508	1.620	1.732
0.500	0.759	0.862	0.965	1.070	1.175	1.281	1.388	1.497	1.606	1.715
0.510	0.765	0.865	0.967	1.069	1.172	1.276	1.381	1.487	1.593	1.701
0.520	0.771	0.870	0.969	1.069	1.170	1.272	1.375	1.478	1.583	1.688
0.530	0.779	0.875	0.973	1.071	1.170	1.269	1.370	1.471	1.574	1.677
0.540	0.787	0.881	0.977	1.073	1.170	1.268	1.367	1.466	1.566	1.667
0.550	0.796	0.889	0.982	1.077	1.172	1.268	1.364	1.462	1.560	1.659
0.560	0.805	0.896	0.988	1.081	1.174	1.268	1.363	1.459	1.555	1.652
0.570	0.815	0.905	0.995	1.086	1.177	1.270	1.363	1.457	1.551	1.646
0.580	0.826	0.914	1.002	1.092	1.182	1.272	1.364	1.456	1.548	1.642
0.590	0.837	0.924	1.010	1.098	1.186	1.275	1.365	1.456	1.547	1.638
0.600	0.849	0.934	1.019	1.105	1.192	1.279	1.368	1.456	1.546	1.636
0.610	0.861	0.944	1.028	1.113	1.198	1.284	1.371	1.458	1.546	1.634
0.620	0.873	0.955	1.038	1.121	1.205	1.290	1.375	1.460	1.547	1.634
0.630	0.886	0.967	1.048	1.130	1.212	1.296	1.379	1.464	1.548	1.634
0.640	0.899	0.979	1.059	1.139	1.220	1.302	1.384	1.467	1.551	1.635
0.650	0.913	0.991	1.070	1.149	1.229	1.309	1.390	1.472	1.554	1.637
0.660	0.927	1.003	1.081	1.159	1.237	1.317	1.396	1.477	1.557	1.639
0.670	0.941	1.016	1.093	1.169	1.247	1.325	1.403	1.482	1.562	1.642
0.680	0.955	1.029	1.104	1.180	1.256	1.333	1.410	1.488	1.566	1.645
0.690	0.969	1.043	1.117	1.191	1.266	1.342	1.418	1.495	1.572	1.649
0.700	0.984	1.056	1.129	1.203	1.276	1.351	1.426	1.501	1.577	1.654

Table D4.1 continued

Median values										
	values for inter-tercile range ------->									
v	0.310	0.320	0.330	0.340	0.350	0.360	0.370	0.380	0.390	0.400
0.710	0.998	1.070	1.142	1.214	1.287	1.360	1.434	1.509	1.584	1.659
0.720	1.013	1.084	1.155	1.226	1.298	1.370	1.443	1.516	1.590	1.664
0.730	1.028	1.098	1.168	1.238	1.309	1.380	1.452	1.524	1.597	--
0.740	1.044	1.112	1.181	1.251	1.320	1.391	1.461	1.533	--	--
0.750	1.059	1.127	1.195	1.263	1.332	1.401	1.471	--	--	--
0.760	1.074	1.141	1.208	1.276	1.344	1.412	--	--	--	--
0.770	1.090	1.156	1.222	1.289	--	--	--	--	--	--
0.780	1.105	1.170	1.236	--	--	--	--	--	--	--
0.790	1.121	1.185	--	--	--	--	--	--	--	--
0.800	1.137	--	--	--	--	--	--	--	--	--
0.810	--	--	--	--	--	--	--	--	--	--

Table D4.2 Parameter C of L-gamma distribution as function of the median and values (0.31 to 0.40) of inter-tercile range

Median values	Values for inter-tercile range ------->									
v	0.310	0.320	0.330	0.340	0.350	0.360	0.370	0.380	0.390	0.400
0.040	--	--	--	--	--	--	--	--	--	--
0.050	+14.34	+15.10	--	--	--	--	--	--	--	--
0.060	+11.82	+12.57	+13.30	+14.02	--	--	--	--	--	--
0.070	+9.749	+10.48	+11.20	+11.90	+12.59	+13.25	--	--	--	--
0.080	+8.017	+8.735	+9.437	+10.12	+10.79	+11.45	+12.09	+12.71	--	--
0.090	+6.560	+7.254	+7.935	+8.603	+9.257	+9.898	+10.52	+11.14	+11.74	+12.33
0.100	+5.330	+5.997	+6.654	+7.299	+7.934	+8.557	+9.170	+9.771	+10.36	+10.94
0.110	+4.291	+4.928	+5.558	+6.179	+6.792	+7.395	+7.990	+8.575	+9.150	+9.716
0.120	+3.413	+4.020	+4.621	+5.216	+5.805	+6.386	+6.961	+7.527	+8.086	+8.637
0.130	+2.673	+3.248	+3.820	+4.388	+4.951	+5.510	+6.063	+6.610	+7.151	+7.685
0.140	+2.049	+2.593	+3.136	+3.676	+4.214	+4.749	+5.280	+5.806	+6.327	+6.844
0.150	+1.524	+2.038	+2.552	+3.066	+3.578	+4.088	+4.596	+5.101	+5.603	+6.101
0.160	+1.082	+1.568	+2.054	+2.542	+3.029	+3.515	+4.001	+4.485	+4.966	+5.445
0.170	+0.711	+1.170	+1.630	+2.093	+2.556	+3.019	+3.482	+3.945	+4.406	+4.866
0.180	+0.399	+0.833	+1.270	+1.708	+2.148	+2.589	+3.031	+3.473	+3.914	+4.355
0.190	+0.139	+0.549	+0.963	+1.379	+1.797	+2.217	+2.638	+3.060	+3.483	+3.905
0.200	-0.079	+0.310	+0.702	+1.098	+1.496	+1.895	+2.297	+2.700	+3.104	+3.509
0.210	-0.261	+0.109	+0.482	+0.858	+1.236	+1.617	+2.001	+2.385	+2.772	+3.159
0.220	-0.411	-0.060	+0.295	+0.653	+1.014	+1.377	+1.743	+2.111	+2.481	+2.852
0.230	-0.535	-0.200	+0.138	+0.479	+0.824	+1.171	+1.520	+1.872	+2.226	+2.581
0.240	-0.636	-0.317	+0.006	+0.332	+0.661	+0.993	+1.327	+1.664	+2.003	+2.343
0.250	-0.717	-0.412	-0.104	+0.208	+0.523	+0.840	+1.160	+1.483	+1.808	+2.135
0.260	-0.782	-0.490	-0.194	+0.104	+0.406	+0.710	+1.017	+1.326	+1.638	+1.951
0.270	-0.832	-0.552	-0.269	+0.018	+0.307	+0.599	+0.893	+1.190	+1.489	+1.791
0.280	-0.869	-0.600	-0.328	-0.053	+0.224	+0.504	+0.787	+1.073	+1.361	+1.651
0.290	-0.895	-0.637	-0.375	-0.111	+0.156	+0.425	+0.698	+0.972	+1.249	+1.528
0.300	-0.912	-0.663	-0.412	-0.157	+0.100	+0.359	+0.622	+0.886	+1.153	+1.422
0.310	-0.921	-0.681	-0.438	-0.193	+0.055	+0.305	+0.558	+0.813	+1.070	+1.330
0.320	-0.922	-0.690	-0.456	-0.219	+0.020	+0.261	+0.505	+0.751	+1.000	+1.250
0.330	-0.916	-0.692	-0.466	-0.238	-0.007	+0.227	+0.462	+0.700	+0.940	+1.182
0.340	-0.905	-0.689	-0.470	-0.249	-0.026	+0.200	+0.428	+0.658	+0.890	+1.124
0.350	-0.889	-0.680	-0.468	-0.254	-0.038	+0.181	+0.401	+0.624	+0.849	+1.075
0.360	-0.869	-0.666	-0.461	-0.253	-0.044	+0.168	+0.382	+0.597	+0.815	+1.035
0.370	-0.845	-0.648	-0.449	-0.248	-0.044	+0.161	+0.368	+0.577	+0.788	+1.001
0.380	-0.818	-0.626	-0.433	-0.238	-0.040	+0.159	+0.360	+0.563	+0.768	+0.975
0.390	-0.787	-0.601	-0.413	-0.224	-0.032	+0.162	+0.357	+0.554	+0.753	+0.954
0.400	-0.754	-0.573	-0.391	-0.206	-0.020	+0.168	+0.358	+0.550	+0.744	+0.939
0.410	-0.719	-0.543	-0.365	-0.185	-0.004	+0.179	+0.364	+0.550	+0.739	+0.928
0.420	-0.682	-0.510	-0.337	-0.162	+0.015	+0.193	+0.373	+0.554	+0.738	+0.922
0.430	-0.643	-0.475	-0.306	-0.136	+0.036	+0.210	+0.385	+0.562	+0.740	+0.920
0.440	-0.602	-0.439	-0.274	-0.108	+0.060	+0.229	+0.400	+0.573	+0.747	+0.922
0.450	-0.560	-0.401	-0.240	-0.078	+0.086	+0.251	+0.418	+0.586	+0.756	+0.927
0.460	-0.516	-0.361	-0.204	-0.046	+0.114	+0.276	+0.438	+0.602	+0.768	+0.935
0.470	-0.472	-0.320	-0.167	-0.012	+0.144	+0.302	+0.461	+0.621	+0.783	+0.946
0.480	-0.427	-0.278	-0.128	+0.023	+0.176	+0.330	+0.485	+0.642	+0.800	+0.959
0.490	-0.381	-0.235	-0.089	+0.059	+0.209	+0.359	+0.511	+0.664	+0.819	+0.974
0.500	-0.334	-0.192	-0.048	+0.097	+0.243	+0.390	+0.539	+0.688	+0.839	+0.992
0.510	-0.287	-0.147	-0.007	+0.135	+0.278	+0.422	+0.568	+0.714	+0.862	+1.011
0.520	-0.239	-0.102	+0.036	+0.174	+0.314	+0.456	+0.598	+0.741	+0.886	+1.032
0.530	-0.190	-0.056	+0.078	+0.214	+0.352	+0.490	+0.629	+0.770	+0.912	+1.055
0.540	-0.142	-0.010	+0.122	+0.255	+0.390	+0.525	+0.662	+0.800	+0.939	+1.079
0.550	-0.093	+0.036	+0.166	+0.297	+0.429	+0.561	+0.696	+0.831	+0.967	+1.104
0.560	-0.043	+0.083	+0.210	+0.339	+0.468	+0.598	+0.730	+0.862	+0.996	+1.131
0.570	+0.006	+0.130	+0.255	+0.381	+0.508	+0.636	+0.765	+0.895	+1.026	+1.158
0.580	+0.056	+0.177	+0.300	+0.424	+0.549	+0.674	+0.801	+0.928	+1.057	+1.187
0.590	+0.105	+0.225	+0.346	+0.467	+0.590	+0.713	+0.837	+0.963	+1.089	+1.216
0.600	+0.155	+0.273	+0.391	+0.511	+0.631	+0.752	+0.874	+0.997	+1.121	+1.246
0.610	+0.205	+0.321	+0.437	+0.554	+0.673	+0.792	+0.912	+1.033	+1.154	+1.277
0.620	+0.255	+0.368	+0.483	+0.598	+0.715	+0.832	+0.950	+1.068	+1.188	+1.309
0.630	+0.305	+0.416	+0.529	+0.642	+0.757	+0.872	+0.988	+1.105	+1.223	+1.341
0.640	+0.354	+0.464	+0.575	+0.687	+0.799	+0.912	+1.027	+1.141	+1.257	+1.374
0.650	+0.404	+0.512	+0.621	+0.731	+0.842	+0.953	+1.065	+1.179	+1.292	+1.407
0.660	+0.453	+0.560	+0.667	+0.776	+0.884	+0.994	+1.105	+1.216	+1.328	+1.441
0.670	+0.503	+0.608	+0.714	+0.820	+0.927	+1.035	+1.144	+1.254	+1.364	+1.475
0.680	+0.552	+0.656	+0.760	+0.865	+0.970	+1.077	+1.184	+1.292	+1.400	+1.510
0.690	+0.601	+0.703	+0.806	+0.909	+1.013	+1.118	+1.223	+1.330	+1.437	+1.544
0.700	+0.650	+0.751	+0.852	+0.954	+1.056	+1.159	+1.263	+1.368	+1.473	+1.579

Table D4.2 continued

Median values										
	values for inter-tercile range ------->									
v	0.310	0.320	0.330	0.340	0.350	0.360	0.370	0.380	0.390	0.400
0.710	+0.699	+0.798	+0.898	+0.998	+1.099	+1.201	+1.303	+1.406	+1.510	+1.615
0.720	+0.748	+0.845	+0.944	+1.043	+1.142	+1.243	+1.343	+1.445	+1.547	+1.650
0.730	+0.796	+0.893	+0.990	+1.087	+1.185	+1.284	+1.384	+1.484	+1.585	--
0.740	+0.845	+0.940	+1.035	+1.131	+1.228	+1.326	+1.424	+1.523	--	--
0.750	+0.893	+0.986	+1.081	+1.176	+1.271	+1.367	+1.464	--	--	--
0.760	+0.941	+1.033	+1.126	+1.220	+1.314	+1.409	--	--	--	--
0.770	+0.988	+1.079	+1.171	+1.264	--	--	--	--	--	--
0.780	+1.036	+1.126	+1.216	--	--	--	--	--	--	--
0.790	+1.083	+1.172	--	--	--	--	--	--	--	--
0.800	+1.130	--	--	--	--	--	--	--	--	--
0.810	--	--	--	--	--	--	--	--	--	--

Table D4.3 Mean of L-gamma distribution as function of the median
and values (0.31 to 0.40) of inter-tercile range--"s" denotes a simulated value.

Median values	Values for inter-tercile range ------->									
v	0.310	0.320	0.330	0.340	0.350	0.360	0.370	0.380	0.390	0.400
0.040	--	--	--	--	--	--	--	--	--	--
0.050	0.269	0.274	--	--	--	--	--	--	--	--
0.060	0.265	0.270	0.275	0.280	--	--	--	--	--	--
0.070	0.262	0.267	0.272	0.277	0.283	0.288	--	--	--	--
0.080	0.261	0.266	0.271	0.276	0.280	0.285	0.290	0.295	--	--
0.090	0.261	0.265	0.270	0.275	0.279	0.284	0.289	0.294	0.298	0.303
0.100	0.262	0.266	0.270	0.275	0.279	0.284	0.288	0.293	0.297	0.302
0.110	0.263	0.267	0.271	0.275	0.280	0.284	0.288	0.293	0.297	0.301
0.120	0.265	0.269	0.273	0.277	0.281	0.285	0.289	0.293	0.297	0.302
0.130	0.268	0.272	0.275	0.279	0.283	0.287	0.291	0.294	0.298	0.303
0.140	0.272	0.275	0.278	0.282	0.285	0.289	0.292	0.296	0.300	0.304
0.150	0.276	0.279	0.282	0.285	0.288	0.291	0.295	0.298	0.302	0.306
0.160	0.280	0.283	0.285	0.288	0.291	0.295	0.298	0.301	0.305	0.308
0.170	0.285	0.287	0.290	0.292	0.295	0.298	0.301	0.304	0.307	0.311
0.180	0.290	0.292	0.294	0.297	0.299	0.302	0.305	0.308	0.311	0.314
0.190	0.295	0.297	0.299	0.301	0.304	0.306	0.309	0.312	0.314	0.317
0.200	s0.301	0.302	0.304	0.306	0.308	0.311	0.313	0.316	0.318	0.321
0.210	s0.307	0.308	0.310	0.311	0.313	0.315	0.318	0.320	0.322	0.325
0.220	s0.313	s0.314	0.315	0.317	0.319	0.320	0.322	0.325	0.327	0.329
0.230	s0.319	s0.320	0.321	0.322	0.324	0.326	0.327	0.329	0.331	0.334
0.240	s0.325	s0.326	0.327	0.328	0.330	0.331	0.333	0.334	0.336	0.338
0.250	s0.332	s0.332	s0.333	0.334	0.335	0.337	0.338	0.340	0.341	0.343
0.260	s0.338	s0.339	s0.339	0.340	0.341	0.342	0.344	0.345	0.347	0.348
0.270	s0.345	s0.345	s0.346	0.346	0.347	0.348	0.349	0.350	0.352	0.353
0.280	s0.352	s0.352	s0.352	s0.352	0.353	0.354	0.355	0.356	0.357	0.359
0.290	s0.359	s0.358	s0.358	s0.359	0.359	0.360	0.361	0.362	0.363	0.364
0.300	s0.365	s0.365	s0.365	s0.365	0.366	0.366	0.367	0.368	0.369	0.370
0.310	s0.372	s0.372	s0.372	s0.372	0.372	0.372	0.373	0.374	0.374	0.375
0.320	s0.379	s0.379	s0.378	s0.378	0.378	0.378	0.379	0.380	0.380	0.381
0.330	s0.386	s0.386	s0.385	s0.385	s0.385	0.385	0.385	0.386	0.386	0.387
0.340	s0.394	s0.393	s0.392	s0.391	s0.391	0.391	0.391	0.392	0.392	0.393
0.350	s0.401	s0.399	s0.399	s0.398	s0.398	0.398	0.398	0.398	0.398	0.399
0.360	s0.408	s0.406	s0.405	s0.405	s0.404	0.404	0.404	0.404	0.404	0.405
0.370	s0.415	s0.413	s0.412	s0.411	s0.411	0.411	0.410	0.410	0.410	0.411
0.380	s0.422	s0.420	s0.419	s0.418	s0.418	0.417	0.417	0.417	0.417	0.417
0.390	s0.429	s0.427	s0.426	s0.425	s0.424	0.424	0.423	0.423	0.423	0.423
0.400	s0.436	s0.434	s0.433	s0.432	s0.431	0.430	0.430	0.429	0.429	0.429
0.410	s0.443	s0.441	s0.440	s0.438	s0.437	0.437	0.436	0.436	0.435	0.435
0.420	s0.450	s0.448	s0.447	s0.445	0.444	0.443	0.442	0.442	0.442	0.441
0.430	s0.457	s0.455	s0.453	s0.452	0.451	0.450	0.449	0.448	0.448	0.448
0.440	s0.464	s0.462	s0.460	s0.459	0.457	0.456	0.455	0.455	0.454	0.454
0.450	s0.471	s0.469	s0.467	s0.465	0.464	0.463	0.462	0.461	0.461	0.460
0.460	s0.478	s0.476	s0.474	s0.472	0.471	0.469	0.468	0.468	0.467	0.466
0.470	s0.485	s0.483	s0.481	s0.479	0.477	0.476	0.475	0.474	0.473	0.473
0.480	s0.492	s0.489	s0.487	0.485	0.484	0.483	0.481	0.480	0.480	0.479
0.490	s0.499	s0.496	s0.494	0.492	0.490	0.489	0.488	0.487	0.486	0.485
0.500	s0.505	s0.503	s0.501	0.499	0.497	0.496	0.494	0.493	0.492	0.491
0.510	s0.512	s0.510	s0.507	0.505	0.504	0.502	0.501	0.500	0.499	0.498
0.520	s0.519	s0.516	0.514	0.512	0.510	0.509	0.507	0.506	0.505	0.504
0.530	s0.526	s0.523	0.521	0.519	0.517	0.515	0.514	0.512	0.511	0.510
0.540	s0.532	s0.530	0.527	0.525	0.523	0.521	0.520	0.519	0.518	0.516
0.550	s0.539	0.536	0.534	0.532	0.530	0.528	0.526	0.525	0.524	0.523
0.560	s0.545	0.543	0.540	0.538	0.536	0.534	0.533	0.531	0.530	0.529
0.570	0.552	0.549	0.547	0.545	0.543	0.541	0.539	0.538	0.536	0.535
0.580	0.559	0.556	0.553	0.551	0.549	0.547	0.545	0.544	0.543	0.541
0.590	0.565	0.562	0.560	0.557	0.555	0.553	0.552	0.550	0.549	0.548
0.600	0.572	0.569	0.566	0.564	0.562	0.560	0.558	0.557	0.555	0.554
0.610	0.578	0.575	0.573	0.570	0.568	0.566	0.564	0.563	0.561	0.560
0.620	0.584	0.582	0.579	0.577	0.574	0.572	0.571	0.569	0.568	0.566
0.630	0.591	0.588	0.585	0.583	0.581	0.579	0.577	0.575	0.574	0.572
0.640	0.597	0.594	0.592	0.589	0.587	0.585	0.583	0.581	0.580	0.578
0.650	0.603	0.601	0.598	0.596	0.593	0.591	0.589	0.588	0.586	0.585
0.660	0.610	0.607	0.604	0.602	0.600	0.597	0.596	0.594	0.592	0.591
0.670	0.616	0.613	0.610	0.608	0.606	0.604	0.602	0.600	0.598	0.597
0.680	0.622	0.619	0.617	0.614	0.612	0.610	0.608	0.606	0.604	0.603
0.690	0.628	0.626	0.623	0.620	0.618	0.616	0.614	0.612	0.610	0.609
0.700	0.635	0.632	0.629	0.627	0.624	0.622	0.620	0.618	0.617	0.615

Table D4.3 continued

Median values										
	values for inter-tercile range ------->									
v	0.310	0.320	0.330	0.340	0.350	0.360	0.370	0.380	0.390	0.400
0.710	0.641	0.638	0.635	0.633	0.630	0.628	0.626	0.624	0.623	0.621
0.720	0.647	0.644	0.641	0.639	0.636	0.634	0.632	0.630	0.629	0.627
0.730	0.653	0.650	0.647	0.645	0.643	0.640	0.638	0.636	0.635	--
0.740	0.659	0.656	0.653	0.651	0.649	0.646	0.644	0.642	--	--
0.750	0.665	0.662	0.659	0.657	0.655	0.652	0.650	--	--	--
0.760	0.671	0.668	0.666	0.663	0.661	0.658	--	--	--	--
0.770	0.677	0.674	0.672	0.669	--	--	--	--	--	--
0.780	0.683	0.680	0.677	--	--	--	--	--	--	--
0.790	0.689	0.686	--	--	--	--	--	--	--	--
0.800	0.695	--	--	--	--	--	--	--	--	--
0.810	--	--	--	--	--	--	--	--	--	--

Table D4.4 L-scale of L-gamma distribution as function of the median
and values (0.31 to 0.40) of inter-tercile range--"s" denotes a simulated value.

Median values | v	Values for inter-tercile range -------> 0.310	0.320	0.330	0.340	0.350	0.360	0.370	0.380	0.390	0.400
0.040	--	--	--	--	--	--	--	--	--	--
0.050	0.179	0.182	--	--	--	--	--	--	--	--
0.060	0.174	0.178	0.181	0.184	--	--	--	--	--	--
0.070	0.171	0.174	0.177	0.180	0.183	0.186	--	--	--	--
0.080	0.168	0.171	0.174	0.177	0.180	0.183	0.186	0.189	--	--
0.090	0.166	0.169	0.172	0.175	0.178	0.180	0.183	0.186	0.189	0.192
0.100	0.165	0.167	0.170	0.173	0.176	0.178	0.181	0.184	0.187	0.189
0.110	0.164	0.166	0.169	0.171	0.174	0.177	0.179	0.182	0.185	0.187
0.120	0.163	0.165	0.168	0.170	0.173	0.175	0.178	0.180	0.183	0.186
0.130	0.162	0.164	0.167	0.169	0.172	0.174	0.177	0.179	0.182	0.184
0.140	0.162	0.164	0.166	0.169	0.171	0.173	0.176	0.178	0.181	0.183
0.150	0.161	0.164	0.166	0.168	0.170	0.173	0.175	0.177	0.180	0.182
0.160	0.161	0.163	0.166	0.168	0.170	0.172	0.175	0.177	0.179	0.181
0.170	0.161	0.163	0.165	0.168	0.170	0.172	0.174	0.176	0.179	0.181
0.180	0.161	0.163	0.165	0.168	0.170	0.172	0.174	0.176	0.178	0.180
0.190	0.161	0.163	0.165	0.167	0.170	0.172	0.174	0.176	0.178	0.180
0.200	s0.161	0.163	0.165	0.168	0.170	0.172	0.174	0.176	0.178	0.180
0.210	s0.161	0.163	0.166	0.168	0.170	0.172	0.174	0.176	0.178	0.180
0.220	s0.162	s0.164	0.166	0.168	0.170	0.172	0.174	0.176	0.178	0.180
0.230	s0.162	s0.164	0.166	0.168	0.170	0.172	0.174	0.176	0.178	0.180
0.240	s0.162	s0.164	0.166	0.168	0.170	0.172	0.174	0.176	0.178	0.180
0.250	s0.162	s0.164	s0.166	0.168	0.170	0.172	0.174	0.176	0.178	0.180
0.260	s0.162	s0.164	s0.166	0.168	0.170	0.172	0.174	0.176	0.178	0.180
0.270	s0.162	s0.164	s0.166	0.168	0.170	0.172	0.174	0.176	0.178	0.180
0.280	s0.162	s0.164	s0.166	s0.168	0.170	0.172	0.174	0.176	0.178	0.180
0.290	s0.162	s0.164	s0.166	s0.169	0.171	0.173	0.175	0.176	0.178	0.180
0.300	s0.162	s0.164	s0.166	s0.169	0.171	0.173	0.175	0.177	0.179	0.180
0.310	s0.162	s0.164	s0.166	s0.169	0.171	0.173	0.175	0.177	0.179	0.181
0.320	s0.161	s0.164	s0.166	s0.169	0.171	0.173	0.175	0.177	0.179	0.181
0.330	s0.161	s0.164	s0.166	s0.169	s0.171	0.173	0.175	0.177	0.179	0.181
0.340	s0.161	s0.164	s0.166	s0.169	s0.171	0.173	0.175	0.177	0.179	0.181
0.350	s0.161	s0.164	s0.166	s0.169	s0.171	0.173	0.175	0.177	0.179	0.181
0.360	s0.161	s0.164	s0.166	s0.169	s0.171	0.173	0.175	0.177	0.179	0.181
0.370	s0.161	s0.164	s0.166	s0.169	s0.171	0.173	0.175	0.178	0.180	0.181
0.380	s0.161	s0.164	s0.166	s0.169	s0.171	0.173	0.176	0.178	0.180	0.182
0.390	s0.161	s0.163	s0.166	s0.169	s0.171	0.173	0.176	0.178	0.180	0.182
0.400	s0.160	s0.163	s0.166	s0.169	s0.171	0.173	0.176	0.178	0.180	0.182
0.410	s0.160	s0.163	s0.166	s0.169	s0.171	0.174	0.176	0.178	0.180	0.182
0.420	s0.160	s0.163	s0.166	s0.169	0.171	0.174	0.176	0.178	0.180	0.182
0.430	s0.160	s0.163	s0.166	s0.169	0.171	0.174	0.176	0.178	0.180	0.182
0.440	s0.160	s0.163	s0.166	s0.169	0.171	0.174	0.176	0.178	0.180	0.182
0.450	s0.160	s0.163	s0.166	s0.169	0.171	0.174	0.176	0.178	0.180	0.183
0.460	s0.160	s0.163	s0.166	s0.169	0.171	0.174	0.176	0.178	0.181	0.183
0.470	s0.160	s0.163	s0.166	s0.169	0.171	0.174	0.176	0.178	0.181	0.183
0.480	s0.160	s0.163	s0.166	0.169	0.171	0.174	0.176	0.178	0.181	0.183
0.490	s0.160	s0.163	s0.166	0.169	0.171	0.174	0.176	0.179	0.181	0.183
0.500	s0.159	s0.163	s0.166	0.169	0.171	0.174	0.176	0.179	0.181	0.183
0.510	s0.159	s0.163	s0.166	0.169	0.171	0.174	0.176	0.179	0.181	0.183
0.520	s0.159	s0.163	0.166	0.169	0.171	0.174	0.176	0.179	0.181	0.183
0.530	s0.159	s0.163	0.166	0.169	0.171	0.174	0.176	0.179	0.181	0.183
0.540	s0.159	s0.163	0.166	0.169	0.171	0.174	0.177	0.179	0.181	0.183
0.550	s0.159	0.163	0.166	0.169	0.171	0.174	0.177	0.179	0.181	0.184
0.560	s0.160	0.163	0.166	0.169	0.172	0.174	0.177	0.179	0.181	0.184
0.570	0.159	0.163	0.166	0.169	0.172	0.174	0.177	0.179	0.182	0.184
0.580	0.160	0.163	0.166	0.169	0.172	0.174	0.177	0.179	0.182	0.184
0.590	0.160	0.163	0.166	0.169	0.172	0.174	0.177	0.179	0.182	0.184
0.600	0.160	0.163	0.166	0.169	0.172	0.174	0.177	0.179	0.182	0.184
0.610	0.160	0.163	0.166	0.169	0.172	0.175	0.177	0.180	0.182	0.184
0.620	0.160	0.163	0.166	0.169	0.172	0.175	0.177	0.180	0.182	0.184
0.630	0.160	0.163	0.166	0.169	0.172	0.175	0.177	0.180	0.182	0.184
0.640	0.160	0.163	0.167	0.169	0.172	0.175	0.177	0.180	0.182	0.185
0.650	0.160	0.164	0.167	0.170	0.172	0.175	0.178	0.180	0.182	0.185
0.660	0.160	0.164	0.167	0.170	0.172	0.175	0.178	0.180	0.183	0.185
0.670	0.161	0.164	0.167	0.170	0.173	0.175	0.178	0.180	0.183	0.185
0.680	0.161	0.164	0.167	0.170	0.173	0.175	0.178	0.180	0.183	0.185
0.690	0.161	0.164	0.167	0.170	0.173	0.176	0.178	0.181	0.183	0.185
0.700	0.161	0.164	0.167	0.170	0.173	0.176	0.178	0.181	0.183	0.185

Table D4.4 continued

Median values										
	values for inter-tercile range ------->									
V	0.310	0.320	0.330	0.340	0.350	0.360	0.370	0.380	0.390	0.400
0.710	0.161	0.165	0.168	0.170	0.173	0.176	0.178	0.181	0.183	0.186
0.720	0.162	0.165	0.168	0.171	0.173	0.176	0.179	0.181	0.183	0.186
0.730	0.162	0.165	0.168	0.171	0.174	0.176	0.179	0.181	0.184	--
0.740	0.162	0.165	0.168	0.171	0.174	0.176	0.179	0.181	--	--
0.750	0.162	0.165	0.168	0.171	0.174	0.177	0.179	--	--	--
0.760	0.162	0.166	0.169	0.171	0.174	0.177	--	--	--	--
0.770	0.163	0.166	0.169	0.172	--	--	--	--	--	--
0.780	0.163	0.166	0.169	--	--	--	--	--	--	--
0.790	0.163	0.166	--	--	--	--	--	--	--	--
0.800	0.163	--	--	--	--	--	--	--	--	--
0.810	--	--	--	--	--	--	--	--	--	--

Table D5.1 Parameter B of L-gamma distribution as function of the median and values (0.41 to 0.50) of inter-tercile range

Median values	Values for inter-tercile range ------->									
v	0.410	0.420	0.430	0.440	0.450	0.460	0.470	0.480	0.490	0.500
0.090	--	--	--	--	--	--	--	--	--	--
0.100	11.62	--	--	--	--	--	--	--	--	--
0.110	10.59	10.98	11.37	--	--	--	--	--	--	--
0.120	9.681	10.06	10.44	10.81	--	--	--	--	--	--
0.130	8.867	9.243	9.613	9.978	10.33	--	--	--	--	--
0.140	8.142	8.506	8.867	9.223	9.574	9.921	--	--	--	--
0.150	7.494	7.847	8.197	8.542	8.884	9.223	9.557	--	--	--
0.160	6.915	7.256	7.594	7.929	8.262	8.591	8.917	9.239	--	--
0.170	6.397	6.725	7.052	7.377	7.699	8.018	8.335	8.649	8.960	--
0.180	5.933	6.249	6.564	6.878	7.189	7.499	7.807	8.112	8.415	8.715
0.190	5.518	5.822	6.125	6.427	6.728	7.028	7.326	7.622	7.916	8.209
0.200	5.145	5.437	5.729	6.020	6.310	6.600	6.888	7.176	7.461	7.745
0.210	4.810	5.091	5.371	5.652	5.932	6.211	6.490	6.768	7.045	7.321
0.220	4.510	4.779	5.049	5.319	5.588	5.858	6.128	6.396	6.665	6.932
0.230	4.240	4.498	4.757	5.017	5.277	5.537	5.797	6.057	6.316	6.575
0.240	3.996	4.245	4.494	4.743	4.994	5.244	5.495	5.747	5.997	6.248
0.250	3.777	4.015	4.255	4.495	4.736	4.978	5.220	5.463	5.705	5.948
0.260	3.579	3.808	4.038	4.270	4.502	4.735	4.969	5.203	5.438	5.673
0.270	3.400	3.620	3.842	4.065	4.289	4.514	4.739	4.966	5.192	5.420
0.280	3.238	3.450	3.664	3.879	4.094	4.311	4.529	4.748	4.967	5.187
0.290	3.091	3.296	3.502	3.709	3.917	4.126	4.337	4.548	4.760	4.973
0.300	2.958	3.155	3.354	3.554	3.755	3.957	4.160	4.365	4.570	4.776
0.310	2.838	3.028	3.220	3.412	3.607	3.802	3.999	4.196	4.395	4.594
0.320	2.728	2.912	3.097	3.283	3.471	3.660	3.850	4.041	4.233	4.427
0.330	2.628	2.806	2.985	3.165	3.347	3.530	3.714	3.899	4.085	4.272
0.340	2.538	2.710	2.883	3.057	3.233	3.410	3.588	3.768	3.948	4.129
0.350	2.455	2.622	2.789	2.958	3.129	3.300	3.473	3.647	3.822	3.998
0.360	2.380	2.541	2.704	2.868	3.033	3.199	3.367	3.535	3.705	3.876
0.370	2.312	2.468	2.626	2.785	2.945	3.106	3.269	3.432	3.597	3.763
0.380	2.250	2.401	2.554	2.709	2.864	3.021	3.179	3.337	3.497	3.658
0.390	2.193	2.340	2.489	2.639	2.790	2.942	3.095	3.250	3.405	3.562
0.400	2.141	2.284	2.429	2.575	2.721	2.869	3.018	3.169	3.320	3.472
0.410	2.094	2.234	2.374	2.516	2.659	2.803	2.948	3.094	3.241	3.389
0.420	2.051	2.187	2.324	2.462	2.601	2.741	2.882	3.024	3.167	3.312
0.430	2.013	2.145	2.278	2.412	2.548	2.684	2.822	2.960	3.100	3.240
0.440	1.977	2.106	2.236	2.367	2.499	2.632	2.766	2.901	3.037	3.174
0.450	1.945	2.071	2.197	2.325	2.454	2.583	2.714	2.846	2.978	3.112
0.460	1.916	2.039	2.162	2.287	2.412	2.539	2.666	2.795	2.924	3.055
0.470	1.890	2.010	2.130	2.252	2.374	2.498	2.622	2.748	2.874	3.001
0.480	1.866	1.983	2.101	2.220	2.340	2.460	2.582	2.704	2.828	2.952
0.490	1.845	1.959	2.075	2.191	2.308	2.425	2.544	2.664	2.784	2.906
0.500	1.826	1.938	2.050	2.164	2.278	2.394	2.510	2.627	2.744	2.863
0.510	1.809	1.918	2.029	2.140	2.251	2.364	2.478	2.592	2.707	2.823
0.520	1.794	1.901	2.009	2.117	2.227	2.337	2.448	2.560	2.673	2.787
0.530	1.781	1.885	1.991	2.097	2.204	2.312	2.421	2.531	2.641	2.752
0.540	1.769	1.872	1.975	2.079	2.184	2.290	2.396	2.504	2.612	2.721
0.550	1.759	1.859	1.961	2.063	2.166	2.269	2.374	2.479	2.585	2.691
0.560	1.750	1.848	1.948	2.048	2.149	2.250	2.353	2.456	2.559	2.664
0.570	1.742	1.839	1.936	2.035	2.134	2.233	2.333	2.435	2.536	2.639
0.580	1.736	1.831	1.926	2.023	2.120	2.218	2.316	2.415	2.515	2.615
0.590	1.731	1.824	1.918	2.012	2.108	2.203	2.300	2.397	2.495	2.594
0.600	1.727	1.818	1.910	2.003	2.097	2.191	2.286	2.381	2.477	2.574
0.610	1.724	1.813	1.904	1.995	2.087	2.179	2.272	2.366	2.461	2.556
0.620	1.721	1.810	1.899	1.988	2.078	2.169	2.261	2.353	2.445	--
0.630	1.720	1.807	1.894	1.982	2.071	2.160	2.250	2.341	--	--
0.640	1.720	1.805	1.891	1.977	2.064	2.152	2.241	--	--	--
0.650	1.720	1.804	1.888	1.973	2.059	2.145	--	--	--	--
0.660	1.721	1.803	1.886	1.970	2.054	2.139	--	--	--	--
0.670	1.722	1.804	1.885	1.968	2.051	--	--	--	--	--
0.680	1.725	1.805	1.885	1.966	--	--	--	--	--	--
0.690	1.728	1.806	1.886	--	--	--	--	--	--	--
0.700	1.731	1.808	--	--	--	--	--	--	--	--
0.710	1.735	--	--	--	--	--	--	--	--	--
0.720	--	--	--	--	--	--	--	--	--	--

Table D5.2 Parameter C of L-gamma distribution as function of the median and values (0.41 to 0.50) of inter-tercile range

Median values	Values for inter-tercile range ------->									
v	0.410	0.420	0.430	0.440	0.450	0.460	0.470	0.480	0.490	0.500
0.090	--	--	--	--	--	--	--	--	--	--
0.100	+11.50	--	--	--	--	--	--	--	--	--
0.110	+10.27	+10.81	+11.35	--	--	--	--	--	--	--
0.120	+9.180	+9.714	+10.24	+10.75	--	--	--	--	--	--
0.130	+8.212	+8.733	+9.246	+9.752	+10.25	--	--	--	--	--
0.140	+7.355	+7.860	+8.360	+8.853	+9.340	+9.821	--	--	--	--
0.150	+6.595	+7.084	+7.569	+8.048	+8.522	+8.991	+9.455	--	--	--
0.160	+5.921	+6.394	+6.862	+7.327	+7.788	+8.244	+8.696	+9.143	--	--
0.170	+5.324	+5.780	+6.232	+6.682	+7.129	+7.572	+8.011	+8.446	+8.877	--
0.180	+4.795	+5.234	+5.670	+6.105	+6.537	+6.966	+7.393	+7.816	+8.236	+8.652
0.190	+4.327	+4.749	+5.169	+5.588	+6.006	+6.421	+6.834	+7.245	+7.653	+8.058
0.200	+3.913	+4.318	+4.723	+5.126	+5.529	+5.931	+6.330	+6.729	+7.125	+7.518
0.210	+3.547	+3.936	+4.325	+4.714	+5.102	+5.489	+5.876	+6.261	+6.645	+7.027
0.220	+3.224	+3.597	+3.971	+4.345	+4.719	+5.093	+5.466	+5.839	+6.211	+6.581
0.230	+2.938	+3.296	+3.656	+4.015	+4.376	+4.736	+5.097	+5.457	+5.817	+6.176
0.240	+2.686	+3.030	+3.375	+3.721	+4.069	+4.416	+4.764	+5.112	+5.460	+5.808
0.250	+2.463	+2.794	+3.126	+3.459	+3.793	+4.129	+4.464	+4.800	+5.137	+5.473
0.260	+2.267	+2.585	+2.904	+3.225	+3.547	+3.870	+4.194	+4.519	+4.844	+5.170
0.270	+2.095	+2.400	+2.708	+3.017	+3.327	+3.639	+3.951	+4.265	+4.579	+4.894
0.280	+1.943	+2.237	+2.533	+2.831	+3.130	+3.431	+3.733	+4.036	+4.340	+4.644
0.290	+1.810	+2.093	+2.378	+2.666	+2.954	+3.245	+3.536	+3.829	+4.123	+4.418
0.300	+1.693	+1.966	+2.242	+2.519	+2.797	+3.078	+3.360	+3.643	+3.927	+4.212
0.310	+1.591	+1.855	+2.121	+2.388	+2.658	+2.928	+3.201	+3.475	+3.750	+4.026
0.320	+1.503	+1.758	+2.014	+2.273	+2.533	+2.795	+3.059	+3.324	+3.590	+3.858
0.330	+1.426	+1.673	+1.921	+2.171	+2.422	+2.676	+2.931	+3.188	+3.446	+3.705
0.340	+1.360	+1.599	+1.839	+2.081	+2.324	+2.570	+2.817	+3.065	+3.315	+3.567
0.350	+1.304	+1.535	+1.767	+2.002	+2.238	+2.475	+2.715	+2.956	+3.198	+3.442
0.360	+1.256	+1.480	+1.705	+1.932	+2.161	+2.392	+2.624	+2.858	+3.093	+3.329
0.370	+1.216	+1.433	+1.652	+1.872	+2.094	+2.318	+2.543	+2.770	+2.998	+3.228
0.380	+1.183	+1.394	+1.606	+1.820	+2.035	+2.252	+2.471	+2.691	+2.913	+3.136
0.390	+1.157	+1.361	+1.567	+1.775	+1.984	+2.195	+2.408	+2.622	+2.837	+3.054
0.400	+1.136	+1.334	+1.535	+1.737	+1.940	+2.145	+2.352	+2.560	+2.770	+2.981
0.410	+1.120	+1.313	+1.508	+1.704	+1.902	+2.102	+2.303	+2.505	+2.709	+2.915
0.420	+1.109	+1.297	+1.487	+1.678	+1.870	+2.065	+2.260	+2.457	+2.656	+2.856
0.430	+1.102	+1.285	+1.470	+1.656	+1.844	+2.033	+2.224	+2.416	+2.609	+2.804
0.440	+1.099	+1.278	+1.458	+1.639	+1.822	+2.006	+2.192	+2.379	+2.568	+2.758
0.450	+1.100	+1.274	+1.449	+1.626	+1.805	+1.984	+2.166	+2.348	+2.532	+2.717
0.460	+1.103	+1.273	+1.445	+1.617	+1.791	+1.967	+2.143	+2.321	+2.501	+2.681
0.470	+1.110	+1.276	+1.443	+1.612	+1.782	+1.953	+2.125	+2.299	+2.474	+2.651
0.480	+1.120	+1.282	+1.445	+1.609	+1.775	+1.943	+2.111	+2.281	+2.452	+2.624
0.490	+1.131	+1.290	+1.449	+1.610	+1.772	+1.936	+2.100	+2.266	+2.433	+2.602
0.500	+1.145	+1.300	+1.456	+1.614	+1.772	+1.932	+2.093	+2.255	+2.418	+2.583
0.510	+1.161	+1.313	+1.465	+1.619	+1.774	+1.931	+2.088	+2.247	+2.407	+2.567
0.520	+1.179	+1.327	+1.477	+1.628	+1.779	+1.932	+2.086	+2.241	+2.398	+2.555
0.530	+1.199	+1.344	+1.490	+1.638	+1.786	+1.936	+2.087	+2.239	+2.392	+2.546
0.540	+1.220	+1.362	+1.505	+1.650	+1.795	+1.942	+2.090	+2.239	+2.388	+2.539
0.550	+1.242	+1.382	+1.522	+1.664	+1.806	+1.950	+2.095	+2.241	+2.387	+2.535
0.560	+1.266	+1.403	+1.541	+1.679	+1.819	+1.960	+2.102	+2.245	+2.389	+2.533
0.570	+1.291	+1.425	+1.560	+1.696	+1.833	+1.972	+2.111	+2.251	+2.392	+2.534
0.580	+1.317	+1.449	+1.581	+1.715	+1.849	+1.985	+2.121	+2.259	+2.397	+2.536
0.590	+1.344	+1.473	+1.603	+1.734	+1.866	+1.999	+2.133	+2.268	+2.404	+2.541
0.600	+1.372	+1.499	+1.627	+1.755	+1.885	+2.015	+2.147	+2.279	+2.412	+2.547
0.610	+1.401	+1.525	+1.651	+1.777	+1.904	+2.033	+2.162	+2.292	+2.423	+2.554
0.620	+1.430	+1.553	+1.676	+1.800	+1.925	+2.051	+2.178	+2.305	+2.434	--
0.630	+1.461	+1.581	+1.702	+1.824	+1.947	+2.071	+2.195	+2.321	--	--
0.640	+1.491	+1.610	+1.729	+1.849	+1.969	+2.091	+2.213	--	--	--
0.650	+1.523	+1.639	+1.756	+1.874	+1.993	+2.112	--	--	--	--
0.660	+1.555	+1.669	+1.784	+1.900	+2.017	+2.135	--	--	--	--
0.670	+1.587	+1.699	+1.813	+1.927	+2.042	--	--	--	--	--
0.680	+1.620	+1.730	+1.842	+1.954	--	--	--	--	--	--
0.690	+1.653	+1.762	+1.872	--	--	--	--	--	--	--
0.700	+1.686	+1.794	--	--	--	--	--	--	--	--
0.710	+1.720	--	--	--	--	--	--	--	--	--
0.720	--	--	--	--	--	--	--	--	--	--

Table D5.3 Mean of L-gamma distribution as function of the median
and values (0.41 to 0.50) of inter-tercile range--"s" denotes a simulated value.

Median values	Values for inter-tercile range ------->									
v	0.410	0.420	0.430	0.440	0.450	0.460	0.470	0.480	0.490	0.500
0.090	--	--	--	--	--	--	--	--	--	--
0.100	0.306	--	--	--	--	--	--	--	--	--
0.110	0.306	0.310	0.315	--	--	--	--	--	--	--
0.120	0.306	0.310	0.314	0.319	--	--	--	--	--	--
0.130	0.307	0.311	0.315	0.319	0.323	--	--	--	--	--
0.140	0.308	0.312	0.316	0.320	0.324	0.328	--	--	--	--
0.150	0.309	0.313	0.317	0.321	0.325	0.329	0.333	--	--	--
0.160	0.312	0.315	0.319	0.322	0.326	0.330	0.334	0.338	--	--
0.170	0.314	0.317	0.321	0.324	0.328	0.332	0.335	0.339	0.343	--
0.180	0.317	0.320	0.323	0.327	0.330	0.334	0.337	0.341	0.344	0.348
0.190	0.320	0.323	0.326	0.329	0.333	0.336	0.339	0.343	0.346	0.350
0.200	0.324	0.327	0.330	0.333	0.336	0.339	0.342	0.345	0.348	0.352
0.210	0.328	0.330	0.333	0.336	0.339	0.342	0.345	0.348	0.351	0.354
0.220	0.332	0.334	0.337	0.339	0.342	0.345	0.348	0.351	0.354	0.357
0.230	0.336	0.338	0.341	0.343	0.346	0.349	0.351	0.354	0.357	0.360
0.240	0.340	0.343	0.345	0.347	0.350	0.352	0.355	0.358	0.360	0.363
0.250	0.345	0.347	0.349	0.352	0.354	0.356	0.359	0.361	0.364	0.367
0.260	0.350	0.352	0.354	0.356	0.358	0.360	0.363	0.365	0.368	0.370
0.270	0.355	0.357	0.359	0.361	0.363	0.365	0.367	0.369	0.372	0.374
0.280	0.360	0.362	0.364	0.365	0.367	0.369	0.371	0.373	0.376	0.378
0.290	0.366	0.367	0.369	0.370	0.372	0.374	0.376	0.378	0.380	0.382
0.300	0.371	0.372	0.374	0.375	0.377	0.379	0.380	0.382	0.384	0.386
0.310	0.376	0.378	0.379	0.380	0.382	0.384	0.385	0.387	0.389	0.391
0.320	0.382	0.383	0.384	0.386	0.387	0.389	0.390	0.392	0.394	0.395
0.330	0.388	0.389	0.390	0.391	0.392	0.394	0.395	0.397	0.398	0.400
0.340	0.393	0.394	0.395	0.396	0.398	0.399	0.400	0.402	0.403	0.405
0.350	0.399	0.400	0.401	0.402	0.403	0.404	0.405	0.407	0.408	0.410
0.360	0.405	0.406	0.407	0.407	0.408	0.409	0.411	0.412	0.413	0.415
0.370	0.411	0.412	0.412	0.413	0.414	0.415	0.416	0.417	0.418	0.420
0.380	0.417	0.418	0.418	0.419	0.420	0.420	0.421	0.422	0.424	0.425
0.390	0.423	0.423	0.424	0.424	0.425	0.426	0.427	0.428	0.429	0.430
0.400	0.429	0.429	0.430	0.430	0.431	0.432	0.432	0.433	0.434	0.435
0.410	0.435	0.435	0.436	0.436	0.437	0.437	0.438	0.439	0.440	0.440
0.420	0.441	0.441	0.442	0.442	0.442	0.443	0.443	0.444	0.445	0.446
0.430	0.447	0.447	0.448	0.448	0.448	0.449	0.449	0.450	0.450	0.451
0.440	0.454	0.454	0.454	0.454	0.454	0.454	0.455	0.455	0.456	0.457
0.450	0.460	0.460	0.460	0.460	0.460	0.460	0.461	0.461	0.462	0.462
0.460	0.466	0.466	0.466	0.466	0.466	0.466	0.466	0.467	0.467	0.468
0.470	0.472	0.472	0.472	0.472	0.472	0.472	0.472	0.472	0.473	0.473
0.480	0.478	0.478	0.478	0.478	0.478	0.478	0.478	0.478	0.478	0.479
0.490	0.485	0.484	0.484	0.484	0.484	0.484	0.484	0.484	0.484	0.484
0.500	0.491	0.490	0.490	0.490	0.489	0.489	0.489	0.490	0.490	0.490
0.510	0.497	0.496	0.496	0.496	0.495	0.495	0.495	0.495	0.496	0.496
0.520	0.503	0.503	0.502	0.502	0.501	0.501	0.501	0.501	0.501	0.501
0.530	0.509	0.509	0.508	0.508	0.507	0.507	0.507	0.507	0.507	0.507
0.540	0.516	0.515	0.514	0.514	0.513	0.513	0.513	0.513	0.513	0.513
0.550	0.522	0.521	0.520	0.520	0.519	0.519	0.519	0.519	0.519	0.519
0.560	0.528	0.527	0.526	0.526	0.525	0.525	0.525	0.524	0.524	0.524
0.570	0.534	0.533	0.533	0.532	0.531	0.531	0.531	0.530	0.530	0.530
0.580	0.540	0.539	0.539	0.538	0.537	0.537	0.536	0.536	0.536	0.536
0.590	0.547	0.546	0.545	0.544	0.543	0.543	0.542	0.542	0.542	0.542
0.600	0.553	0.552	0.551	0.550	0.549	0.549	0.548	0.548	0.548	0.547
0.610	0.559	0.558	0.557	0.556	0.555	0.555	0.554	0.554	0.553	0.553
0.620	0.565	0.564	0.563	0.562	0.561	0.561	0.560	0.560	0.559	--
0.630	0.571	0.570	0.569	0.568	0.567	0.567	0.566	0.565	--	--
0.640	0.577	0.576	0.575	0.574	0.573	0.572	0.572	--	--	--
0.650	0.583	0.582	0.581	0.580	0.579	0.578	--	--	--	--
0.660	0.589	0.588	0.587	0.586	0.585	0.584	--	--	--	--
0.670	0.595	0.594	0.593	0.592	0.591	--	--	--	--	--
0.680	0.601	0.600	0.599	0.598	--	--	--	--	--	--
0.690	0.608	0.606	0.605	--	--	--	--	--	--	--
0.700	0.614	0.612	--	--	--	--	--	--	--	--
0.710	0.620	--	--	--	--	--	--	--	--	--
0.720	--	--	--	--	--	--	--	--	--	--

Table D5.4 L-scale of L-gamma distribution as function of the median and values (0.41 to 0.50) of inter-tercile range--"s" denotes a simulated value.

Median values	Values for inter-tercile range ------->									
v	0.410	0.420	0.430	0.440	0.450	0.460	0.470	0.480	0.490	0.500
0.090	--	--	--	--	--	--	--	--	--	--
0.100	0.192	--	--	--	--	--	--	--	--	--
0.110	0.190	0.193	0.195	--	--	--	--	--	--	--
0.120	0.188	0.191	0.193	0.196	--	--	--	--	--	--
0.130	0.187	0.189	0.192	0.194	0.197	--	--	--	--	--
0.140	0.185	0.188	0.190	0.193	0.195	0.198	--	--	--	--
0.150	0.184	0.187	0.189	0.191	0.194	0.196	0.199	--	--	--
0.160	0.184	0.186	0.188	0.190	0.193	0.195	0.197	0.200	--	--
0.170	0.183	0.185	0.187	0.190	0.192	0.194	0.196	0.199	0.201	--
0.180	0.182	0.185	0.187	0.189	0.191	0.193	0.196	0.198	0.200	0.202
0.190	0.182	0.184	0.186	0.188	0.191	0.193	0.195	0.197	0.199	0.201
0.200	0.182	0.184	0.186	0.188	0.190	0.192	0.194	0.196	0.199	0.201
0.210	0.182	0.184	0.186	0.188	0.190	0.192	0.194	0.196	0.198	0.200
0.220	0.182	0.184	0.185	0.187	0.189	0.191	0.193	0.195	0.198	0.200
0.230	0.182	0.183	0.185	0.187	0.189	0.191	0.193	0.195	0.197	0.199
0.240	0.182	0.183	0.185	0.187	0.189	0.191	0.193	0.195	0.197	0.199
0.250	0.182	0.183	0.185	0.187	0.189	0.191	0.193	0.195	0.197	0.199
0.260	0.182	0.184	0.185	0.187	0.189	0.191	0.193	0.195	0.197	0.198
0.270	0.182	0.184	0.185	0.187	0.189	0.191	0.193	0.195	0.197	0.198
0.280	0.182	0.184	0.186	0.187	0.189	0.191	0.193	0.195	0.196	0.198
0.290	0.182	0.184	0.186	0.188	0.189	0.191	0.193	0.195	0.196	0.198
0.300	0.182	0.184	0.186	0.188	0.189	0.191	0.193	0.195	0.197	0.198
0.310	0.182	0.184	0.186	0.188	0.190	0.191	0.193	0.195	0.197	0.198
0.320	0.183	0.184	0.186	0.188	0.190	0.191	0.193	0.195	0.197	0.198
0.330	0.183	0.185	0.186	0.188	0.190	0.192	0.193	0.195	0.197	0.199
0.340	0.183	0.185	0.187	0.188	0.190	0.192	0.194	0.195	0.197	0.199
0.350	0.183	0.185	0.187	0.188	0.190	0.192	0.194	0.195	0.197	0.199
0.360	0.183	0.185	0.187	0.189	0.190	0.192	0.194	0.196	0.197	0.199
0.370	0.183	0.185	0.187	0.189	0.191	0.192	0.194	0.196	0.197	0.199
0.380	0.184	0.185	0.187	0.189	0.191	0.193	0.194	0.196	0.198	0.199
0.390	0.184	0.186	0.187	0.189	0.191	0.193	0.194	0.196	0.198	0.199
0.400	0.184	0.186	0.188	0.189	0.191	0.193	0.195	0.196	0.198	0.200
0.410	0.184	0.186	0.188	0.190	0.191	0.193	0.195	0.197	0.198	0.200
0.420	0.184	0.186	0.188	0.190	0.192	0.193	0.195	0.197	0.198	0.200
0.430	0.184	0.186	0.188	0.190	0.192	0.193	0.195	0.197	0.199	0.200
0.440	0.184	0.186	0.188	0.190	0.192	0.194	0.195	0.197	0.199	0.200
0.450	0.185	0.186	0.188	0.190	0.192	0.194	0.196	0.197	0.199	0.201
0.460	0.185	0.187	0.189	0.190	0.192	0.194	0.196	0.197	0.199	0.201
0.470	0.185	0.187	0.189	0.191	0.192	0.194	0.196	0.198	0.199	0.201
0.480	0.185	0.187	0.189	0.191	0.193	0.194	0.196	0.198	0.200	0.201
0.490	0.185	0.187	0.189	0.191	0.193	0.195	0.196	0.198	0.200	0.201
0.500	0.185	0.187	0.189	0.191	0.193	0.195	0.196	0.198	0.200	0.202
0.510	0.185	0.187	0.189	0.191	0.193	0.195	0.197	0.198	0.200	0.202
0.520	0.185	0.187	0.189	0.191	0.193	0.195	0.197	0.199	0.200	0.202
0.530	0.185	0.188	0.190	0.191	0.193	0.195	0.197	0.199	0.201	0.202
0.540	0.186	0.188	0.190	0.192	0.194	0.195	0.197	0.199	0.201	0.202
0.550	0.186	0.188	0.190	0.192	0.194	0.196	0.197	0.199	0.201	0.203
0.560	0.186	0.188	0.190	0.192	0.194	0.196	0.198	0.199	0.201	0.203
0.570	0.186	0.188	0.190	0.192	0.194	0.196	0.198	0.199	0.201	0.203
0.580	0.186	0.188	0.190	0.192	0.194	0.196	0.198	0.200	0.201	0.203
0.590	0.186	0.188	0.190	0.192	0.194	0.196	0.198	0.200	0.202	0.203
0.600	0.186	0.188	0.191	0.193	0.194	0.196	0.198	0.200	0.202	0.204
0.610	0.186	0.189	0.191	0.193	0.195	0.197	0.198	0.200	0.202	0.204
0.620	0.187	0.189	0.191	0.193	0.195	0.197	0.199	0.200	0.202	--
0.630	0.187	0.189	0.191	0.193	0.195	0.197	0.199	0.201	--	--
0.640	0.187	0.189	0.191	0.193	0.195	0.197	0.199	--	--	--
0.650	0.187	0.189	0.191	0.193	0.195	0.197	--	--	--	--
0.660	0.187	0.189	0.191	0.193	0.195	0.197	--	--	--	--
0.670	0.187	0.189	0.192	0.194	0.196	--	--	--	--	--
0.680	0.187	0.190	0.192	0.194	--	--	--	--	--	--
0.690	0.188	0.190	0.192	--	--	--	--	--	--	--
0.700	0.188	0.190	--	--	--	--	--	--	--	--
0.710	0.188	--	--	--	--	--	--	--	--	--
0.720	--	--	--	--	--	--	--	--	--	--

Table D6.1 Parameter B of L-gamma distribution as function of the median and values (0.51 to 0.60) of inter-tercile range

Median values		values for inter-tercile range ------->									
	v	0.510	0.520	0.530	0.540	0.550	0.560	0.570	0.580	0.590	0.600
0.180		--	--	--	--	--	--	--	--	--	--
0.190		8.499	--	--	--	--	--	--	--	--	--
0.200		8.027	8.308	--	--	--	--	--	--	--	--
0.210		7.595	7.868	--	--	--	--	--	--	--	--
0.220		7.198	7.463	7.727	--	--	--	--	--	--	--
0.230		6.834	7.091	7.348	7.603	--	--	--	--	--	--
0.240		6.499	6.749	6.998	7.246	--	--	--	--	--	--
0.250		6.191	6.433	6.675	6.916	7.157	--	--	--	--	--
0.260		5.908	6.142	6.377	6.612	6.846	--	--	--	--	--
0.270		5.647	5.875	6.102	6.330	6.557	--	--	--	--	--
0.280		5.407	5.628	5.848	6.069	6.290	6.511	--	--	--	--
0.290		5.186	5.400	5.614	5.828	6.043	6.257	--	--	--	--
0.300		4.982	5.189	5.397	5.605	5.813	6.022	6.230	--	--	--
0.310		4.794	4.995	5.196	5.398	5.600	5.803	6.006	--	--	--
0.320		4.620	4.815	5.010	5.206	5.403	5.599	5.797	--	--	--
0.330		4.460	4.649	4.838	5.028	5.219	5.410	5.602	--	--	--
0.340		4.312	4.495	4.679	4.863	5.049	5.235	5.421	--	--	--
0.350		4.174	4.352	4.531	4.710	4.890	5.071	5.252	5.434	--	--
0.360		4.047	4.220	4.393	4.568	4.743	4.918	5.095	5.272	--	--
0.370		3.930	4.097	4.266	4.435	4.605	4.776	4.948	5.120	--	--
0.380		3.820	3.983	4.147	4.312	4.477	4.644	4.811	4.978	--	--
0.390		3.719	3.878	4.037	4.197	4.358	4.520	4.683	4.846	--	--
0.400		3.625	3.779	3.934	4.090	4.247	4.405	4.563	4.722	--	--
0.410		3.538	3.688	3.839	3.991	4.144	4.297	4.451	4.606	--	--
0.420		3.457	3.603	3.750	3.898	4.047	4.196	4.347	--	--	--
0.430		3.382	3.524	3.667	3.811	3.956	4.102	4.249	--	--	--
0.440		3.311	3.450	3.590	3.731	3.872	4.014	4.157	--	--	--
0.450		3.246	3.382	3.518	3.655	3.793	3.932	4.071	--	--	--
0.460		3.186	3.318	3.451	3.585	3.719	3.855	3.991	--	--	--
0.470		3.129	3.258	3.388	3.519	3.650	3.783	--	--	--	--
0.480		3.077	3.203	3.330	3.457	3.586	3.715	--	--	--	--
0.490		3.028	3.151	3.275	3.400	3.525	3.652	--	--	--	--
0.500		2.983	3.103	3.224	3.346	3.469	--	--	--	--	--
0.510		2.940	3.058	3.177	3.296	3.416	--	--	--	--	--
0.520		2.901	3.016	3.132	3.249	3.366	--	--	--	--	--
0.530		2.864	2.977	3.091	3.205	--	--	--	--	--	--
0.540		2.830	2.941	3.052	3.164	--	--	--	--	--	--
0.550		2.799	2.907	3.016	--	--	--	--	--	--	--
0.560		2.769	2.875	2.982	--	--	--	--	--	--	--
0.570		2.742	2.846	--	--	--	--	--	--	--	--
0.580		2.717	2.819	--	--	--	--	--	--	--	--
0.590		2.693	--	--	--	--	--	--	--	--	--
0.600		--	--	--	--	--	--	--	--	--	--

Table D6.2 Parameter C of L-gamma distribution as function of the median and values (0.51 to 0.60) of inter-tercile range

Median values		Values for inter-tercile range ------->									
	v	0.510	0.520	0.530	0.540	0.550	0.560	0.570	0.580	0.590	0.600
0.180	--	--	--	--	--	--	--	--	--	--	--
0.190	+8.460	--	--	--	--	--	--	--	--	--	--
0.200	+7.910	+8.298	--	--	--	--	--	--	--	--	--
0.210	+7.408	+7.786	--	--	--	--	--	--	--	--	--
0.220	+6.950	+7.318	+7.684	--	--	--	--	--	--	--	--
0.230	+6.534	+6.891	+7.247	+7.601	--	--	--	--	--	--	--
0.240	+6.155	+6.501	+6.847	+7.191	--	--	--	--	--	--	--
0.250	+5.810	+6.146	+6.481	+6.816	+7.149	--	--	--	--	--	--
0.260	+5.495	+5.821	+6.147	+6.472	+6.796	--	--	--	--	--	--
0.270	+5.210	+5.525	+5.841	+6.156	+6.472	--	--	--	--	--	--
0.280	+4.950	+5.256	+5.562	+5.868	+6.174	+6.480	--	--	--	--	--
0.290	+4.714	+5.010	+5.307	+5.604	+5.901	+6.199	--	--	--	--	--
0.300	+4.499	+4.786	+5.074	+5.362	+5.651	+5.940	+6.229	--	--	--	--
0.310	+4.304	+4.582	+4.861	+5.141	+5.421	+5.702	+5.983	--	--	--	--
0.320	+4.126	+4.396	+4.667	+4.939	+5.211	+5.484	+5.757	--	--	--	--
0.330	+3.965	+4.227	+4.490	+4.754	+5.018	+5.283	+5.549	--	--	--	--
0.340	+3.820	+4.073	+4.328	+4.584	+4.841	+5.099	+5.357	--	--	--	--
0.350	+3.687	+3.934	+4.181	+4.430	+4.679	+4.930	+5.181	+5.433	--	--	--
0.360	+3.567	+3.807	+4.047	+4.289	+4.531	+4.775	+5.019	+5.265	--	--	--
0.370	+3.459	+3.691	+3.925	+4.160	+4.396	+4.633	+4.871	+5.109	--	--	--
0.380	+3.361	+3.587	+3.814	+4.042	+4.272	+4.502	+4.734	+4.966	--	--	--
0.390	+3.273	+3.492	+3.713	+3.935	+4.159	+4.383	+4.608	+4.835	--	--	--
0.400	+3.193	+3.407	+3.622	+3.838	+4.055	+4.274	+4.493	+4.714	--	--	--
0.410	+3.121	+3.329	+3.539	+3.749	+3.961	+4.174	+4.388	+4.603	--	--	--
0.420	+3.057	+3.260	+3.464	+3.669	+3.875	+4.082	+4.291	--	--	--	--
0.430	+3.000	+3.197	+3.396	+3.596	+3.797	+3.999	+4.202	--	--	--	--
0.440	+2.949	+3.141	+3.335	+3.530	+3.726	+3.923	+4.121	--	--	--	--
0.450	+2.903	+3.091	+3.280	+3.470	+3.661	+3.854	+4.047	--	--	--	--
0.460	+2.863	+3.046	+3.231	+3.416	+3.603	+3.791	+3.980	--	--	--	--
0.470	+2.828	+3.007	+3.187	+3.368	+3.550	+3.734	--	--	--	--	--
0.480	+2.798	+2.972	+3.148	+3.325	+3.503	+3.682	--	--	--	--	--
0.490	+2.771	+2.942	+3.114	+3.286	+3.460	+3.636	--	--	--	--	--
0.500	+2.748	+2.915	+3.083	+3.252	+3.422	--	--	--	--	--	--
0.510	+2.729	+2.893	+3.057	+3.222	+3.389	--	--	--	--	--	--
0.520	+2.714	+2.873	+3.034	+3.196	+3.359	--	--	--	--	--	--
0.530	+2.701	+2.857	+3.015	+3.173	--	--	--	--	--	--	--
0.540	+2.691	+2.844	+2.998	+3.153	--	--	--	--	--	--	--
0.550	+2.684	+2.834	+2.985	--	--	--	--	--	--	--	--
0.560	+2.679	+2.826	+2.974	--	--	--	--	--	--	--	--
0.570	+2.677	+2.821	--	--	--	--	--	--	--	--	--
0.580	+2.677	+2.818	--	--	--	--	--	--	--	--	--
0.590	+2.678	--	--	--	--	--	--	--	--	--	--
0.600	--	--	--	--	--	--	--	--	--	--	--

Table D6.3 Mean of L-gamma distribution as function of the median
and values (0.51 to 0.60) of inter-tercile range--"s" denotes a simulated value.

Median values										
	values for inter-tercile range ------->									
v	0.510	0.520	0.530	0.540	0.550	0.560	0.570	0.580	0.590	0.600
0.180	--	--	--	--	--	--	--	--	--	--
0.190	0.353	--	--	--	--	--	--	--	--	--
0.200	0.355	0.359	--	--	--	--	--	--	--	--
0.210	0.358	0.361	--	--	--	--	--	--	--	--
0.220	0.360	0.363	0.366	--	--	--	--	--	--	--
0.230	0.363	0.366	0.369	0.372	--	--	--	--	--	--
0.240	0.366	0.369	0.372	0.375	--	--	--	--	--	--
0.250	0.369	0.372	0.375	0.378	0.381	--	--	--	--	--
0.260	0.373	0.375	0.378	0.381	0.384	--	--	--	--	--
0.270	0.376	0.379	0.382	0.384	0.387	--	--	--	--	--
0.280	0.380	0.383	0.385	0.388	0.390	0.393	--	--	--	--
0.290	0.384	0.387	0.389	0.391	0.394	0.396	--	--	--	--
0.300	0.388	0.391	0.393	0.395	0.398	0.400	0.403	--	--	--
0.310	0.393	0.395	0.397	0.399	0.401	0.404	0.406	--	--	--
0.320	0.397	0.399	0.401	0.403	0.405	0.408	0.410	--	--	--
0.330	0.402	0.404	0.406	0.408	0.410	0.412	0.414	--	--	--
0.340	0.406	0.408	0.410	0.412	0.414	0.416	0.418	--	--	--
0.350	0.411	0.413	0.415	0.416	0.418	0.420	0.422	0.424	--	--
0.360	0.416	0.418	0.419	0.421	0.423	0.425	0.426	0.428	--	--
0.370	0.421	0.422	0.424	0.426	0.427	0.429	0.431	0.433	--	--
0.380	0.426	0.427	0.429	0.430	0.432	0.434	0.435	0.437	--	--
0.390	0.431	0.432	0.434	0.435	0.437	0.438	0.440	0.442	--	--
0.400	0.436	0.438	0.439	0.440	0.442	0.443	0.445	0.446	--	--
0.410	0.442	0.443	0.444	0.445	0.446	0.448	0.449	0.451	--	--
0.420	0.447	0.448	0.449	0.450	0.451	0.453	0.454	--	--	--
0.430	0.452	0.453	0.454	0.455	0.456	0.458	0.459	--	--	--
0.440	0.458	0.458	0.459	0.460	0.461	0.463	0.464	--	--	--
0.450	0.463	0.464	0.465	0.466	0.467	0.468	0.469	--	--	--
0.460	0.468	0.469	0.470	0.471	0.472	0.473	0.474	--	--	--
0.470	0.474	0.475	0.475	0.476	0.477	0.478	--	--	--	--
0.480	0.479	0.480	0.481	0.481	0.482	0.483	--	--	--	--
0.490	0.485	0.485	0.486	0.487	0.487	0.488	--	--	--	--
0.500	0.490	0.491	0.492	0.492	0.493	--	--	--	--	--
0.510	0.496	0.497	0.497	0.498	0.498	--	--	--	--	--
0.520	0.502	0.502	0.502	0.503	0.504	--	--	--	--	--
0.530	0.507	0.508	0.508	0.508	--	--	--	--	--	--
0.540	0.513	0.513	0.514	0.514	--	--	--	--	--	--
0.550	0.519	0.519	0.519	--	--	--	--	--	--	--
0.560	0.524	0.524	0.525	--	--	--	--	--	--	--
0.570	0.530	0.530	--	--	--	--	--	--	--	--
0.580	0.536	0.536	--	--	--	--	--	--	--	--
0.590	0.541	--	--	--	--	--	--	--	--	--
0.600	--	--	--	--	--	--	--	--	--	--

Table D6.4 L-scale of L-gamma distribution as function of the median
and values (0.51 to 0.60) of inter-tercile range--"s" denotes a simulated value.

Median values										
	values for inter-tercile range ------->									
v	0.510	0.520	0.530	0.540	0.550	0.560	0.570	0.580	0.590	0.600
0.180	--	--	--	--	--	--	--	--	--	--
0.190	0.204	--	--	--	--	--	--	--	--	--
0.200	0.203	0.205	--	--	--	--	--	--	--	--
0.210	0.202	0.204	--	--	--	--	--	--	--	--
0.220	0.202	0.204	0.206	--	--	--	--	--	--	--
0.230	0.201	0.203	0.205	0.207	--	--	--	--	--	--
0.240	0.201	0.203	0.205	0.207	--	--	--	--	--	--
0.250	0.201	0.202	0.204	0.206	0.208	--	--	--	--	--
0.260	0.200	0.202	0.204	0.206	0.208	--	--	--	--	--
0.270	0.200	0.202	0.204	0.206	0.208	--	--	--	--	--
0.280	0.200	0.202	0.204	0.206	0.207	0.209	--	--	--	--
0.290	0.200	0.202	0.204	0.206	0.207	0.209	--	--	--	--
0.300	0.200	0.202	0.204	0.205	0.207	0.209	0.211	--	--	--
0.310	0.200	0.202	0.204	0.205	0.207	0.209	0.211	--	--	--
0.320	0.200	0.202	0.204	0.205	0.207	0.209	0.211	--	--	--
0.330	0.200	0.202	0.204	0.205	0.207	0.209	0.211	--	--	--
0.340	0.200	0.202	0.204	0.205	0.207	0.209	0.211	--	--	--
0.350	0.201	0.202	0.204	0.206	0.207	0.209	0.211	0.212	--	--
0.360	0.201	0.202	0.204	0.206	0.207	0.209	0.211	0.212	--	--
0.370	0.201	0.202	0.204	0.206	0.207	0.209	0.211	0.212	--	--
0.380	0.201	0.203	0.204	0.206	0.208	0.209	0.211	0.213	--	--
0.390	0.201	0.203	0.204	0.206	0.208	0.209	0.211	0.213	--	--
0.400	0.201	0.203	0.205	0.206	0.208	0.210	0.211	0.213	--	--
0.410	0.202	0.203	0.205	0.206	0.208	0.210	0.211	0.213	--	--
0.420	0.202	0.203	0.205	0.207	0.208	0.210	0.211	--	--	--
0.430	0.202	0.204	0.205	0.207	0.208	0.210	0.212	--	--	--
0.440	0.202	0.204	0.205	0.207	0.209	0.210	0.212	--	--	--
0.450	0.202	0.204	0.206	0.207	0.209	0.210	0.212	--	--	--
0.460	0.203	0.204	0.206	0.207	0.209	0.211	0.212	--	--	--
0.470	0.203	0.204	0.206	0.208	0.209	0.211	--	--	--	--
0.480	0.203	0.205	0.206	0.208	0.209	0.211	--	--	--	--
0.490	0.203	0.205	0.206	0.208	0.210	0.211	--	--	--	--
0.500	0.203	0.205	0.207	0.208	0.210	--	--	--	--	--
0.510	0.204	0.205	0.207	0.208	0.210	--	--	--	--	--
0.520	0.204	0.205	0.207	0.209	0.210	--	--	--	--	--
0.530	0.204	0.206	0.207	0.209	--	--	--	--	--	--
0.540	0.204	0.206	0.207	0.209	--	--	--	--	--	--
0.550	0.204	0.206	0.208	--	--	--	--	--	--	--
0.560	0.204	0.206	0.208	--	--	--	--	--	--	--
0.570	0.205	0.206	--	--	--	--	--	--	--	--
0.580	0.205	0.207	--	--	--	--	--	--	--	--
0.590	0.205	--	--	--	--	--	--	--	--	--
0.600	--	--	--	--	--	--	--	--	--	--

APPENDIX E

Computer Programs

The Perl programming language was used universally for this dissertation. Ports of several FORTRAN algorithms were made, and references are provided where necessary. The executable programs end in `.pl` extensions, and the modules end in `.pm` extensions.

lmoments.pl

```
#!/usr/bin/perl -w
use strict;

# Perl program to compute L-moments using unbiased, plotting-position,
# and prior-Probability Weighted Moments.  The product moments can also
# be computed.  Algorithms derived from numerous sources by J.R.M Hosking
# and Q.J. Wang.  Citations provided in dissertation by W.H. Asquith.

# AUTHOR: William H. Asquith, August 2002
# $Author: wasquith $
# $Date: 2002/11/06 14:30:33 $
# $Revision: 1.13 $

use constant sqrtPI => scalar sqrt(3.1415926);

my $DATA;  # hash reference to the probabilities and data
my $NODATA = '--';

# Work on what type of probability weighted moment
# computations are going to be performed and process other
# command line options.
use Getopt::Long;
my %OPTS = (); # command line options
my @options = qw ( pp xf ub pm data datalimits Fdiv100 help );
# these are the valid command line options
&GetOptions(\%OPTS, @options); # parse the command line options

&Help(), exit if($OPTS{help});

my $type = ($OPTS{pp}) ? "PP" :
           ($OPTS{xf}) ? "XF" :
           ($OPTS{ub}) ? "UB" :
           ($OPTS{pm}) ? "PM" : undef;
die "Moment computation type is not defined by ".
    "-ub, -pp, -xf, or -pm on the command line\n" unless($type);
# End of command line option handling.


print "# L-MOMENTS OF A CUMULATIVE PERCENTAGE HYDROGRAPH\n";

print STDERR "# Enter space delimited cumulative probability and data
values.\n";
if($type eq 'XF') {
   print STDERR "# Working on $type (prior-PWM).\n";
   print STDERR "# One pair per line.\n",
                "# F    X\n";
}
else {
   print STDERR "# Working on $type (PP, plotting position; UB, unbiased; PM,
product moment).\n";
   print STDERR "# If one value is given, then it is used.  If two values are
given, then the\n",
```

```
              "# second one is used.  This feature permits switching between
the prior-PWM\n",
               "# method and the other methods without a change in the input
stream.\n";
   print STDERR "# One value or F   X pair per line\n",
                "# X  or  F(ignored)   X\n";
}

my $i = 0;
my $F_count_below_05;
while(1) {
  $_ = <STDIN>;
  last if(not defined $_);
  next if(/[a-zA-Z]|^#/); # quietly skip any nonnumeric lines or leading #
  chomp;
  last if($_ eq "");
  my ($F, $x) = split(/\s+/o, $_, 2);

  # insert dummy F if type UB or PP and only one value entered.
  # a priori F is not needed for non-pPWM computations
  ($x, $F) = ($F, $i) if(not defined $x and $type ne "XF");
  $F_count_below_05++ if($F < 0.5);
  next if(not &isNumber($F) or not &isNumber($x));
  $F /= 100 if($OPTS{'Fdiv100'}); # the probabilities can in as percentages
  die "Bad data entered, F is not defined.\n" if(not defined $F);
  die "Bad data entered, X if not defined.\n" if(not defined $x);

  $DATA->{$F} = $x;
  $i++;
}

print STDERR "# Probabilities and Data have been entered. . .\n";

if($type ne 'PM') {
  my ($PWM, $LMOM);
  my $median = undef;
  if($type eq 'UB') {
     my @data;
     foreach my $F (keys %$DATA) {
       push(@data, $DATA->{$F});
     }
     $LMOM = &LinearMoments([@data], 1);
     $PWM  = &LMOM2PWM($LMOM);
     foreach my $key (keys %$LMOM) {
        $LMOM->{$key} = &_decimals($LMOM->{$key});
     }
     foreach my $p (@$PWM) {
        $p = &_decimals($p);
     }
     $median = &Median(@data);
     $median = int(10000*$median)/10000 if(defined $median);
  }
  else {
    if($type eq 'XF') {
```

```
      $median = &Median_with_PriorProbabilities($DATA);
      $median = int(10000*$median)/10000 if(defined $median);
    }
    else {
      my @data;
      foreach my $F (keys %$DATA) {
        push(@data, $DATA->{$F});
      }
      $median = &Median(@data);
      $median = int(10000*$median)/10000 if(defined $median);
    }
    $PWM  = &computePWM($type,$DATA);
    $LMOM = &PWM2LMOM($PWM);
  }
  $median = "--" if(not defined $median);
  print "# L-moment Computation\n";
  print &PWMasString($PWM),"\n";
  print &LMOMasString($LMOM),"\n";
  print "# Samples = $i\n";
  print "# Mean   L-scale   L-CV    L-skew   L-kurtosis   Tau5   Median\n";
  print &LMOMasRow($LMOM),"   $median\n";
}
else {
   my @data;
   foreach my $F (keys %$DATA) {
      push(@data, $DATA->{$F});
   }
   my $samples = scalar(@data);
   my $min     = $data[0];
   my $max     = $data[$#data];
   my $median  = &Median(@data);
      $median  = int(10000*$median)/10000 if(defined $median);
   my $harmean = &HarmonicMean(@data);
   my $geomean = &GeometricMean(@data);
   my ($mean,$stdev,$skew,$kurt) = &ProductMoments(@data);
   my $cv = $stdev / $mean;
   $median  = (defined $median ) ? sprintf("%0.6f",$median ) : 'undef';
   $harmean = (defined $harmean) ? sprintf("%0.6f",$harmean) : 'undef';
   $geomean = (defined $geomean) ? sprintf("%0.6f",$geomean) : 'undef';
   $mean    = (defined $mean   ) ? sprintf("%0.6f",$mean   ) : 'undef';
   $stdev   = (defined $stdev  ) ? sprintf("%0.6f",$stdev  ) : 'undef';
   $skew    = (defined $skew   ) ? sprintf("%0.6f",$skew   ) : 'undef';
   $kurt    = (defined $kurt   ) ? sprintf("%0.6f",$kurt   ) : 'undef';
   $cv      = (defined $cv     ) ? sprintf("%0.6f",$cv     ) : 'undef';
   print "# Product Moment Computation\n";
   print "# Samples = $samples\n";
   print "Mean   Stdev  CV  Skew   Kurtosis  Median  ",
         "GeometricMean  HarmonicMean\n";
   print join("   ",($mean,$stdev,$cv,$skew,$kurt,
                     $geomean,$harmean)),"\n";
}
print &dumpData($DATA) if($OPTS{'data'});
print &dumpDataLimits($DATA) if($OPTS{'datalimits'});
print "\n";
```

```
##########################################
# SUBROUTINES
##########################################
sub computePWM {
   my ($type, $data) = @_;
   my $pwm;
   print "# PWMs of type $type are started ";
   map { $pwm->[$_] = &getPWM($type,$_,$data) } (0..4);
   print "and completed.\n";
   return $pwm;
}

sub getPWM {
   my ($which) = shift;
   return &getPWMbyPP(@_) if($which eq 'PP');
   return &getPWMbyXF(@_) if($which eq 'XF');
   die "getPWM should not be here logically\n";
}

sub getPWMbyPP {
   my ($order, $data) = @_;
   my $beta = 0;
   my @Fs   = sort { $a <=> $b } keys %$data;
   my $nF   = scalar(@Fs);
   my $i    = 1;

   return $NODATA if($nF == 0 or $order+1 > $nF);

   foreach my $F (@Fs) {
      $beta += $data->{$F} * (($i-0.35)/$nF)**$order;
      $i++;
   }

   return &_decimals($beta/$nF);
}



sub getPWMbyXF {
   my ($order, $data) = @_;
   my $beta = 0;
   my @Fs   = sort { $a <=> $b } keys %$data;
   my $nF   = scalar(@Fs);
   my ($X, $dF) = 0;
   my $F;
   return $NODATA if($nF == 0 or $order+1 > $nF);

   # Work on first data point
   $F     =   $Fs[0];
   $dF    = ( $Fs[1] + $Fs[0] ) / 2;
   #$dF    = ( $Fs[1] ) / 2;
   $X     = $data->{$F};
   $beta += $X * $F**$order * $dF;
```

```
   # Work on middle data points
   for(my $i=1;$i<=$#Fs-1;$i++) {
      $F     =   $Fs[$i];
      $dF    = ( $Fs[$i+1] - $Fs[$i-1] ) / 2;
      $X     = $data->{$F};
      $beta += $X * $F**$order * $dF;
   }

   # Work on last data point
   $F  = $Fs[$#Fs];
   $dF = 1 - ($Fs[$#Fs] + $Fs[$#Fs-1]) / 2;
   #$dF = (1 - $Fs[$#Fs-1])/2;
   $X  = $data->{$F};
   $beta += $X * $F**$order * $dF;

   return &_decimals($beta);
}

sub PWM2LMOM {
   my ($pwm) = @_;
   my @p = @$pwm;
   my %lmom;

   $lmom{L1} = $lmom{L2} =
   $lmom{T2} = $lmom{T3} =
   $lmom{T4} = $lmom{T5} = $NODATA;

   return \%lmom if($p[0] eq $NODATA);
   $lmom{L1} = &_decimals($p[0]);

   return \%lmom if($p[1] eq $NODATA);
   $lmom{L2} =  2*$p[1] -     $p[0];
   $lmom{T2} = ($lmom{L1}) ? $lmom{L2}/$lmom{L1} : “mean=zero”;
   $lmom{L2} = $NODATA, return \%lmom if(not $lmom{L2});

   # If L-scale is less than zero, we have poorly choosen
   # F and X pairs.  More data is likely needed to define
   # the distribution.
   $lmom{T2} = $lmom{L2} = $NODATA,
               return \%lmom if($lmom{L2} < 0);
   $lmom{L2} = &_decimals($lmom{L2});
   $lmom{T2} = &_decimals($lmom{T2});

   return \%lmom if($p[2] eq $NODATA);
   $lmom{L3} =  6*$p[2] -   6*$p[1] +    $p[0];
   $lmom{T3} = $lmom{L3}/$lmom{L2};

   # If L-skew is less than -1 or greater than 1, we have poorly choosen
   # F and X pairs.  More data is likely needed to define
   # the distribution.
   $lmom{T3} = $lmom{L3} = $NODATA,
               return \%lmom if($lmom{T3} < -1 or $lmom{T3} > 1);
   $lmom{T3} = &_decimals($lmom{L3}/$lmom{L2});
```

```
   return \%lmom if($p[3] eq $NODATA);
   $lmom{L4} = 20*$p[3] -  30*$p[2] + 12*$p[1] -    $p[0];
   $lmom{T4} = $lmom{L4}/$lmom{L2};

   # If L-kurtosis is less than 0.25*(5*Tau3**2 - 1) or greater than 1,
   # we have poorly choosen F and X pairs.  More data is likely needed to
   # define the distribution.
   $lmom{T4} = $lmom{L4} = $NODATA,
               return \%lmom if($lmom{T4} < (0.25*(5*$lmom{T3}**2 -1 ) ) or
                                $lmom{T4} > 1);
   $lmom{T4} = &_decimals($lmom{T4});

   return \%lmom if($p[4] eq $NODATA);
   $lmom{L5} = 70*$p[4] - 140*$p[3] + 90*$p[2] - 20*$p[1] + $p[0];

   # Tau5 can not be greater than 1, it has a lower limit, but Hosking
   # did not derive in the 1990 paper.
   $lmom{T5} = $lmom{L5}/$lmom{L2};
   $lmom{T5} = $lmom{L5} = $NODATA,
               return \%lmom if($lmom{T5} > 1);
   $lmom{T5} = &_decimals($lmom{T5});

   return \%lmom;
}

sub LMOM2PWM {
   my ($lmom) = @_;
   my @p = ($NODATA, $NODATA, $NODATA, $NODATA, $NODATA,);
   if($lmom->{L1} ne $NODATA) {
      $p[0] =        $lmom->{L1};
   }
   if($lmom->{L2} ne $NODATA) {
      $p[1] =   0.5*($lmom->{L2}+$p[0]);
   }
   if($lmom->{T3} ne $NODATA) {
      $p[2] = (1/6)*($lmom->{L2}*$lmom->{T3}+6*$p[1]-$p[0]);
   }
   if($lmom->{T4} ne $NODATA) {
      $p[3] = (1/20)*($lmom->{L2}*$lmom->{T4}+30*$p[2]-12*$p[1]+$p[0]);
   }
   if($lmom->{T5} ne $NODATA) {
      $p[4] = (1/70)*($lmom->{L2}*$lmom->{T5}+140*$p[3] -
                                90*$p[2]+20*$p[1]-$p[0]);
   }
   return \@p;
}

sub LinearMoments {
# DIRECT L-MOMENT CALCULATION
# adopted from Q.J. Wang, Direct sample estimators of
# L-moments, Water Resour. Res., 32(12), 3617-3619
# and modified for T5 via email from Dr. Wang
# 07/06/1998.  Routine ported from FORTRAN to Perl 10/04/1998
```

```
# Pass data array into routine and routine returns the L-moment array
#   @L_moment contains the mean, L-scale, Tau3, Tau4, and Tau5
  my ( $dataref, $needsort) = @_;
  $needsort = ($needsort and $needsort eq 'nosort') ? 0 : 1;

  my %lmom;
     $lmom{L1} = $lmom{L2} =
     $lmom{T2} = $lmom{T3} =
     $lmom{T4} = $lmom{T5} = $NODATA;

  my ( @L_moments) = ();
  my ( $n, $i, $iold );
  my ( $L1,$L2,$L3,$L4,$L5 );
  my ( $CL1,$CL2,$CL3,$CL4 );
  my ( $CR1,$CR2,$CR3,$CR4 );
  my ( $C1,$C2,$C3,$C4,$C5 );
  my(@X) = @$dataref;    # dereference the passed scalar
  ($L1,$L2,$L3,$L4,$L5) = (0,0,0,0,0);  # initialized values which will show
  ($C1,$C2,$C3,$C4,$C5) = (0,0,0,0,0);  # an uninitialized value warning
  ($CL1,$CL2,$CL3,$CL4) = (0,0,0,0);
  ($CR1,$CR2,$CR3,$CR4) = (0,0,0,0);
  $n = @X;# determine length of array

  if(not $n) {
     print STDERR "CalcStatistics::LinearMoments--Yipes undefined data\n";
     return \%lmom;
  }

  # First need to detemine whether all the data values are identical
  my $firstval = $X[0];  # initialize the first value in array
  my $all_equal = 1;     # flag set to yes as an initial guess
  foreach my $val (@X) {
     next if($val == $firstval); # if equal, go to next one
     $all_equal = 0;             # at least one is different, ok to continue
     last;
  }
  if($all_equal) {  # always compute the mean
       return { -mean => &Mean($dataref), -l_scale => 0,
                -tau3 => undef, -tau4 => undef, -tau5 => undef };
  }

  # go ahead and sort the array
  @X = sort { $a <=> $b } (@X) if($needsort);

  # Use the O-statistics subroutine to calculated whatever L-moments
  # that are possible with the given sample size.
  # This section needs further development--1/29/1999
  if($n < 5) {
     my $mean = &Mean($dataref);
     my ($lscale, $tau3, $tau4, $tau5);
     my $ostats = &generateOrderStatistics( \@X, 'nosort');
     CHECK: {
       my $o;
       my @o;
```

```
      last CHECK if($n == 1);
       $o = &getOrderStatistics($ostats,2);   @o = @$o;
       $lscale = 0.5*($o[1] - $o[0]);

      last CHECK if($n == 2);
       $o = &getOrderStatistics($ostats,3);   @o = @$o;
       $tau3 = (1/3)*($o[2] - 2*$o[1] + $o[0]);
       $tau3 /= $lscale;

      last CHECK if($n == 3);
       $o = &getOrderStatistics($ostats,4);   @o = @$o;
       $tau4 = (1/4)*($o[3] - 3*$o[2] + 3*$o[1] - $o[0]);
       $tau4 /= $lscale;

      last CHECK if($n == 4);
       $o = &getOrderStatistics($ostats,5);   @o = @$o;
       $tau5 = (1/5)*($o[4] - 4*$o[3] + 6*$o[2]
                            - 4*$o[1] +   $o[0] );
       $tau5 /= $lscale;
    }
    $lmom{L1} = $mean         if(defined $mean);
    $lmom{L2} = $lscale       if(defined $lscale);
    $lmom{T2} = $lscale/$mean if(defined $lscale);
    $lmom{T3} = $tau3         if(defined $tau3);
    $lmom{T4} = $tau4         if(defined $tau4);
    $lmom{T5} = $tau5         if(defined $tau5);
    return \%lmom;
  }

  # Sample size is greater than 5 so proceed with first 5 L-moment
calculation
  foreach my $i (1..$n) {
    $CL1 = $i-1;
    $CL2 = $CL1 * ($i-1-1) / 2;
    $CL3 = $CL2 * ($i-1-2) / 3;
    $CL4 = $CL3 * ($i-1-3) / 4;
    $CR1 = $n-$i;
    $CR2 = $CR1 * ($n-$i-1) / 2;
    $CR3 = $CR2 * ($n-$i-2) / 3;
    $CR4 = $CR3 * ($n-$i-3) / 4;
    $L1 += $X[$i-1];
    $L2 += $X[$i-1] * ($CL1 - $CR1);
    $L3 += $X[$i-1] * ($CL2 - 2*$CL1*$CR1 + $CR2);
    $L4 += $X[$i-1] * ($CL3 - 3*$CL2*$CR1 + 3*$CL1*$CR2 - $CR3);
    $L5 += $X[$i-1] * ($CL4 - 4*$CL3*$CR1 + 6*$CL2*$CR2
                            - 4*$CL1*$CR3 + $CR4);
  }

  $C1 = $n;
  $C2 = $C1 * ($n-1) / 2;
  $C3 = $C2 * ($n-2) / 3;
  $C4 = $C3 * ($n-3) / 4;
  $C5 = $C4 * ($n-4) / 5;
  $L1 = $L1 / $C1;
```

```
  $L2 = $L2 / $C2 / 2;
  $L3 = $L3 / $C3 / 3;
  $L4 = $L4 / $C4 / 4;
  $L5 = $L5 / $C5 / 5;

  $lmom{L1} = $L1;
  $lmom{L2} = $L2;
  $lmom{T2} = $L2/$L1;
  $lmom{T3} = $L3/$L2;
  $lmom{T4} = $L4/$L2;
  $lmom{T5} = $L5/$L2;
  return \%lmom;
}


# Compute mean of an array reference.
sub Mean {
   my ($arrayref) = @_;
   my $result;
   map { $result += $_ } ( @$arrayref );
   return $result / @$arrayref;
}


sub _decimals { return ($_[0] eq '--') ? $_[0] : sprintf("%0.4f", $_[0]); }

sub LMOMasRow {
   my ($lmom) = @_;
   my %l = %$lmom;
   return join("   ", @l{qw(L1 L2 T2 T3 T4 T5)});
}


sub LMOMasString {
   my ($lmom) = @_;
   my %l = %$lmom;
   my $stdev = ($l{L2} eq $NODATA) ? $l{L2} : &_decimals($l{L2}*sqrtPI);
   return "# L-moments are:\n".
          "#   Mean        = $l{L1}\n".
          "#   L-Scale     = $l{L2} (StDev=$stdev)\n".
          "#   L-CV        = $l{T2}\n#   L-skew      = $l{T3}\n".
          "#   L-kurtosis  = $l{T4}\n#   Tau5        = $l{T5}";
}

sub PWMasString {
   my ($pwm) = @_;
   my @p = @$pwm;
   return "# Proability Weighted Moments are:\n".
          "#   Beta0  = $p[0]\n#   Beta1  = $p[1]\n".
          "#   Beta2  = $p[2]\n#   Beta3  = $p[3]\n".
          "#   Beta4  = $p[4]";
}

sub dumpData {
```

```
   my ($data) = @_;
   print "# DATA: Cumulative_prob.(F)       Data\n",
         "# DATA: Nonexceedance_prob.       value\n";
   foreach my $F (sort { $a <=> $b } keys %$data) {
       print "# DATA:        $F             $data->{$F}\n";
   }
}


sub dumpDataLimits {
   my ($data) = @_;
   my ($fmin, $fmax, $xmin, $xmax);
   foreach my $F (sort { $a <=> $b } keys %$data) {
       my $val = $data->{$F};
       $fmin = (not defined $fmin or   $F < $fmin) ?   $F : $fmin;
       $fmax = (not defined $fmax or   $F > $fmax) ?   $F : $fmax;
       $xmin = (not defined $xmin or $val < $xmin) ? $val : $xmin;
       $xmax = (not defined $xmax or $val > $xmax) ? $val : $xmax;
   }
   $fmin = "--" if(not defined $fmin);
   $fmax = "--" if(not defined $fmax);
   $xmin = "--" if(not defined $xmin);
   $xmax = "--" if(not defined $xmax);

   print "# F_MIN    F_MAX    X_MIN    X_MAX\n";
   print "# $fmin    $fmax    $xmin    $xmax\n";
   return;
}

sub isNumber {
  if(not defined $_[0] ) {
     my @call = caller(1);
     map { $call[$_] = "" if(not defined $call[$_]) } (0..$#call);
     print STDERR "isNumber(undef) as @call\n";
     return 0;
  }
  $_[0] =~ /^\s*[+-]?\d+\.?\d*\s*$/o                 ||
    $_[0] =~ /^\s*[+-]?\.\d+\s*$/o                   ||
      $_[0] =~ /^\s*[+-]?\d+\.?\d*[eE][+-]?\d+\s*$/o ||
        $_[0] =~ /^\s*[+-]?\.\d+[eE][+-]?\d+\s*$/o;
}


# ORDER STATISTICS
# generateOrderStatistics
# Calculate the O-statistics.  Given a data array that can be
# presorted, call sub with false second parameter, or an unsorted
# array, call sub with true second parameter, this subroutine
# returns the O-statistic matrix.  The individual O-stat arrays
# are retrieved from the O-statistic matrix using retrieveOrderStatistics
# $ref = retrieveOrderStatistics(generateOrderStatistics(\@data),1);
# print "THE MEAN OF THE DATA = $ref->[0]\n";
#    The O-statistics are the expectations of the usual order statistics
sub generateOrderStatistics {
```

```
   my ($dataref, $needsort) = ( shift, shift);
   $needsort = ($needsort and $needsort eq 'nosort') ? 0 : 1;
   my @X = @$dataref;
   my @OX;

   # User is responsible for calling with the proper
   # sorting switch.  The data array must be sorted
   # in ascending order.
   @X = sort { $a <=> $b } @X if($needsort);

   my $n = scalar(@X); # size of data
   # Fill O-statistics array at order $n with the data
   $OX[$n] = [ @X ];  # create new anonymous array

   #  r        d
   #  _ |_3____2_____1__  TEST EXAMPLE
   #  0 | 1   5/3    3
   #  1 | 3  13/3
   #  2 | 5

   # COMPUTE THE O-STATISTICS OF ORDER (n-1) TO 0
   # (see equation 2.3 in Kaigh, W.D., and Driscoll, M.F., 1987,
   # The American Statistician, vol. 41, no. 1, pp. 25-32)
   foreach my $d (reverse (1..($n - 1)) ) {
      foreach my $r (0..($d - 1)) {
         my $d1 = $d + 1;
         my $X1 = $OX[$d1][$r];
         my $X2 = $OX[$d1][$r + 1];
         $OX[$d][$r] = ( (($d-$r) * $X1) + (($r+1) * $X2) ) / ($d+1);
      }
   }
   return \@OX;
}

sub getOrderStatistics {
   my ( $OXref, $order, $lowup) = @_;
   if($order < 1 or $order >= @$OXref) {
      #print STDERR "getOrderStatistics: Retrieval order '$order' ".
      #             "can not be less than 1 or greater than length of ".
      #             "the O-statistics ".
      #             "array which is ",scalar(@$OXref),".\n";
      return undef;
   }
   elsif($lowup) {  # values should be either 'lower' or 'upper'
      return ( $lowup eq 'lower') ? $OXref->[$order]->[0] :
                                    $OXref->[$order]->[ $#{$OXref->[$order]} ];
   }
   else {
      return $OXref->[$order];
   }
}


sub ProductMoments {
```

```
  my (@X) = @_;
  my $sumM;
  my $n = @X;
  if(not $n) {
     print STDERR "ProductMoments--Yipes undefined data\n";
     return (undef,undef,undef,undef);
  }
  foreach my $v (@X) { $sumM += $v }
  my $mean = $sumM/$n;

  my ($sumSTD, $sumSKW, $sumKUR) = (0, 0, 0);
  foreach my $v (@X) {
    $sumSTD += ($v-$mean)**2;
    $sumSKW += ($v-$mean)**3;
    $sumKUR += ($v-$mean)**4;
  }

  my ($stdev,$skew,$kurt);
  CHECK: {
    last CHECK if($n == 1);
     $stdev = ($sumSTD/($n-1))**0.5;
    last CHECK if($n == 2 or $stdev == 0); # division by zero protection
     $skew = $n*($sumSKW)/(($n-1)*($n-2)*$stdev**3);
    last CHECK if($n == 3);
     $kurt = (($n*($n+1))/(($n-1)*($n-2)*($n-3)))*($sumKUR/($stdev**4));
     # $kurt = $kurt-(3*($n-1)**2)/(($n-2)*($n-3));  # for excesses kurt
  }
  return ($mean,$stdev,$skew,$kurt);
}

sub HarmonicMean {
   my @data = @_;
   my $sum;
   my $count = scalar(@data);
   return undef if($count == 0); # trap a no data condition

   foreach my $val (@data) {
      my $tmp;
      eval { $tmp = 1/$val };
      return undef if($@); # must have been a division by zero solution
      $sum += $tmp;
   }
   $sum /= $count;
   return 1/$sum;
}


sub GeometricMean {
   my @data = @_;
   my $tmp = 1;
   map { $tmp *= $_ } @data;
   my $count = scalar(@data);
   # trap for roots of negative numbers and for no data at all
   return ($count == 0 or $tmp < 0) ? undef : ($tmp)**( 1 / $count);
```

```
}

# Compute median of an array
sub Median {
   my @d = @_;
      @d = sort { $a <=> $b } @d;
   return undef unless(@d > 2); # trap undef variable warning
   return (@d % 2) ? $d[@d/2] : ($d[@d/2 - 1]+$d[@d/2])/2;
}


# Compute median of an array with prior probabilities
sub Median_with_PriorProbabilities {
   my $data = shift;
   my @probs = sort { $a <=> $b } keys %$data;
   return undef unless(@probs);
   if(@probs == 1 and $probs[0] == 0.50) {
      return $data->{$probs[0]};
   }

   my ($plo, $phi) = (undef,undef);
   foreach my $prob (@probs) {
      return $data->{$prob} if($prob == 0.50);
      $plo = $prob if($prob < 0.50);
      $phi = $prob, last if($prob > 0.50);
   }
   warn "############ $plo and $phi\n";
   if(defined $plo and defined $phi) {
      my ($lo, $hi) = ($data->{$plo}, $data->{$phi});
      return ((0.50-$plo)/($phi-$plo))*($hi-$lo) + $lo;
   }
   return undef;
}


sub Help {
  my ($AUTHOR, $BUILDDATE, $VERSION) = &getCVSstamps();
  print <<HERE

NAME
 lmoments.pl version $VERSION by $AUTHOR on $BUILDDATE

DESCRIPTION
 L-moment and Product Moment computation program
 (see notes below)
 by William H. Asquith, USGS, June 2002

DEPENDENCIES


USAGE
 lmoments.pl [options]

     -data         Show the data.
```

```
     -datalimits   Show the limits of the data.
     -help         This help.
     -ub           L-moments by unbiased estimators.
     -xf           L-moments by prior-Probability Weighted Moments.
     -pp           L-moments by plotting position.
     -pm           Perform Product Moment computation.
     -Fdiv100      The nonexceedance probability stream is in percent
                   not fractional precent (probability) so divide
                   the values by 100.


NOTES


EXAMPLES



WARNINGS



HERE
}

sub getCVSstamps {
   my $df = “not known”;
   my ($auth, $date, $ver) = ($df, $df, $df);
   while(<DATA>) {
      last if(/cvs(\s+)?end/io);
      $auth = $1, next if(/Author:\s+(.+)\s+\$/);
      $date = $1, next if(/Date:\s+(.+)\s+\$/);
      $ver  = $1, next if(/Revision:\s+(.+)\s+\$/);
      last if($auth ne $df and
              $date ne $df and
              $ver  ne $df);
   }
   return ($auth, $date, $ver);
}


__DATA__
# $Author: wasquith $
# $Date: 2002/11/06 14:30:33 $
# $Revision: 1.13 $
# CVSEND


1;
```

useGammaFunctions.pl

```
#!/usr/bin/perl -w

# Perl program to interface with Perl module to compute the
# Gamma and Incomplete Gamma funcations.  The algorithms in the
# GammaFunctions module were derived from:
#
# Press, W.H., Teukolsky, S.A., Vetterling, W.T., and
#      Flannery, B.P., 1992, Numerical Recipes in FORTRAN: Cambridge
#      University Press, pp. 206-213.
#

# AUTHOR: William H. Asquith, August 2002
# $Author: wasquith $
# $Date: 2002/08/28 12:42:31 $
# $Revision: 1.3 $

# Library path pointing to directory for the Modules/GammaFunctions Perl
# module that is 'used' in the next statement.
use lib qw(/home/wasquith/txdot_databases/programs/perl);
# import two functions from the module
use Modules::GammaFunctions qw(IncompleteGamma NatLogGamma);

# Remind the user on how the program works.
die "a and x for Gamma function, G(a) and Incomplete Gamma function, ",
    "P(a,x) are reguired on command line\n" unless(@ARGV == 2);

($a, $x) = @ARGV; # get the two command line arguments
print "# Arguments are: a=$a and x=$x\n"; # echo the arguments
my $G = exp(&NatLogGamma($a));            # compute the Gamma function

# Trap cascading errors if the argument to the Gamma function is invalid.
die "DIED: Gamma($a) is not defined\n" if(not defined $G);

print "#   G(a):G(",$a,")=$G\n";   # output the results

my $P = &IncompleteGamma($a,$x);   # compute the Incomplete Gamma function

# Trap cascading errors if the arguments are invalid.
die "DIED: IncompleteGamma($a,$x) is not defined\n" if(not defined $P);

print "# P(a,x):P(",$a,",",$x,")=$P\n";  # output the results

# The following product is to aid in manual compuations of L-gamma L-moments
print "# G(a)*P(a,x) = ",$P*$G,"\n";
exit;
```

Modules::GammaFunctions.pm

```
package Modules::GammaFunctions;

# Perl module implementing algorithms for the Gamma and Incomplete
# Gamma functions derived from:

# Press, W.H., Teukolsky, S.A., Vetterling, W.T., and Flannery, B.P., 1992,
#    Numerical Recipes in FORTRAN: Cambridge University Press, pp. 206-213.
#

# AUTHOR: William H. Asquith, August 2002
# $Author: wasquith $
# $Date: 2002/08/28 12:42:31 $
# $Revision: 1.3 $

use strict;

use Exporter;
use vars qw(@COF @ISA @EXPORT_OK);

@ISA = qw(Exporter);
@EXPORT_OK = qw(IncompleteGamma NatLogGamma);

use constant EPS   => scalar 3e-7;
use constant ITMAX => scalar 100;
use constant FPMIN => scalar 1e-30;
use constant STP   => scalar 2.5066282746310005;
use constant SER   => scalar 1.000000000190015;

@COF = ( 76.18009172947146      ,
        -86.50532032941677      ,
         24.01409824083091      ,
         -1.231739572450155     ,
          0.001208650973866179  ,
         -0.00000539523984953 );

sub IncompleteGamma {
  my ($a, $x) = @_;

  # Uses IncompleteGamma_bySeries and IncompleteGamma_byContinuedFraction

  my ($gammp,$gln);

  if($x < 0) {
     warn "Bad second argument in IncompleteGamma: x($x) < 0\n";
     return undef;
  }
  if($a <= 0) {
     warn "Bad first argument in IncompleteGamma: a($a) <= 0\n";
     return undef;
  }
  if($x < $a+1) {
     ($gammp, $gln) = &IncompleteGamma_bySeries($a,$x);
```

```
      # warn "IncompleteGamma returned by P_bySeries $gammp\n";
      return (wantarray) ? ($gammp,$gln) : ($gammp);
   }
   else {
      ($gammp, $gln) = &IncompleteGamma_byContinuedFraction($a,$x);
      $gammp = 1 - $gammp; # take compliment
      return (wantarray) ? ($gammp, $gln) : ($gammp);
   }
}

sub IncompleteGamma_bySeries {
   # Uses NatLogGamma
   # Returns the incomplete gamma function P(a,x) evaluated by its series
   # representation as gamser.  Also returns ln(gamma(a)) as gln.

   my ($a, $x) = @_;

   my $gln = &NatLogGamma($a);

   if($x <= 0 ) {
      warn "x <= 0 in IncompleteGamma_bySeries\n";
      return (0,$gln);
   }

   my $ap  = $a;
   my $sum = 1/$a;
   my $del = $sum;

   my $clean_exit = 0;
   for(my $i=1; $i<=ITMAX; $i++) {
      $ap++;
      $del *= $x/$ap;
      $sum += $del;
      $clean_exit = 1, last if(abs($del) < abs($sum)*EPS);
   }

   warn "a too large, ITMAX too small in ",
        "IncompleteGamma_bySeries\n" if(not $clean_exit);

   my $gamser = $sum * exp(-$x + $a * log($x) - $gln);
   return ($gamser, $gln);
}

sub IncompleteGamma_byContinuedFraction {
   # Uses NatLogGamma
   # Returns the incomplete gamma function Q(a,x) evaluated by its
   # continued fraction representation.  Returns ln[gamma(a)] too.

   my ($a, $x) = @_;

   my $gln = &NatLogGamma($a);
   my $b = $x + 1 - $a;
   my $c = 1/FPMIN;
   my $d = 1/$b;
```

```
   my $h = $d;
   my ($an, $del);

   my $clean_exit = 0;
   for(my $i=1;$i<=ITMAX;$i++) {
      $an  = -$i*($i-$a);
      $b  += 2;
      $d   = $an*$d + $b;
      $d   = FPMIN if(abs($d) < FPMIN);
      $c   = $b + $an/$c;
      $c   = FPMIN if(abs($c) < FPMIN);
      $d   = 1/$d;
      $del = $d*$c;
      $h  *= $del;
      $clean_exit = 1, last if(abs($del - 1) < EPS);
   }
   warn "a too large, ITMAX too small in ",
        "IncompleteGamma_byContinuedFraction\n" if(not $clean_exit);

   my $gamcf = exp(-$x+$a*log($x) - $gln)*$h;
   return ($gamcf, $gln);
}

sub NatLogGamma {
   # Returns the value ln[gamma($xx)] for $xx > 0

   my ($xx) = @_;
   return undef if($xx <= 0); # division by zero protection

   my $x   = $xx;
   my $y   = $x;
   my $tmp = $x + 5.5;
      $tmp = ($x + 0.5)*log($tmp)-$tmp;
   my $ser = SER;
   for(my $j=0;$j<=5;$j++) {
      $y++;
      $ser += $COF[$j]/$y;
   }
   return $tmp + log(STP*$ser / $x);
}

1;
```

APPENDIX F

Supplemental Tables for Chapter 7.

The tables contained in this appendix document the empirical hyetographs for the 0–12 hr, 12–24hr, and 24 hr and greater storm durations. These hyetographs are described in chapter 7. Tables F1, F3, and F5 document the actual percentiles of the empirical hyetographs; whereas tables F2, F4, and F6 document the L-moments of the empirical hyetographs. Tables F7, F8, and F9 document graphically smoothed values of the percentiles listed in tables F1, F3, and F5; the smoothed values are provided to increase the applicability of the percentiles in hydrologic design applications at the request of staff from the Texas Department of Transportation (Stolpa, personal commun., 2002) and consensus of the Texas Tech University, University of Houston, and Lamar University hyetograph research team.

Table F1. Percentile statistics for empirical hyetograph analysis for the 0–12 hr storm duration and one or more inches of depth

Center of percent of storm duration interval (percent)	No. of samples ( )	Median 50th percentile (percent)	Lower quartile 25th percentile (percent)	Upper quartile 75th percentile (percent)	Lower decile 10th percentile (percent)	Upper decile 90th percentile (percent)
2.5	937	0.00	0.00	3.333	0.00	13.34
5.0	344	12.95	4.416	25.00	1.999	41.30
7.5	335	18.04	8.046	34.00	2.798	53.83
10.0	396	24.45	10.36	43.37	4.332	63.02
12.5	322	30.13	13.40	48.36	4.943	69.53
15.0	321	35.75	17.73	56.21	7.038	76.93
17.5	333	38.87	17.34	61.00	8.422	77.38
20.0	323	40.46	21.67	66.97	11.53	83.45
22.5	328	40.62	18.06	70.04	6.91	84.78
25.0	289	44.84	27.56	72.82	9.47	85.37
27.5	304	48.86	26.23	70.62	11.56	87.02
30.0	287	54.47	32.17	76.95	13.69	88.31
32.5	341	52.00	30.75	78.56	12.41	88.10
35.0	232	57.89	33.70	81.57	14.21	91.66
37.5	257	54.58	30.23	83.61	15.82	90.31
40.0	257	66.77	35.58	85.47	20.83	92.83
42.5	244	63.54	37.65	85.11	21.47	93.14
45.0	252	69.66	37.44	84.80	13.92	92.12
47.5	231	63.77	32.95	85.91	15.96	93.03
50.0	252	71.75	43.99	86.28	24.82	93.84
52.5	246	67.70	35.95	86.38	14.39	95.44
55.0	255	73.43	47.02	88.62	28.52	95.13
57.5	232	72.25	41.19	86.70	22.47	95.82
60.0	254	76.23	46.65	89.59	21.59	95.55
62.5	246	75.30	50.00	89.70	29.54	96.44
65.0	202	77.45	60.11	91.57	30.16	96.76
67.5	310	79.49	57.95	91.90	34.82	96.71
70.0	244	80.61	55.22	93.06	24.99	97.38
72.5	274	84.22	61.14	93.50	35.21	97.32
75.0	249	85.07	66.29	93.47	35.43	97.80
77.5	280	86.88	67.89	93.77	44.60	98.17
80.0	290	87.66	69.44	95.32	47.56	98.38
82.5	272	89.90	76.21	96.32	50.63	98.62
85.0	259	92.76	80.81	97.50	55.34	98.80
87.5	264	94.27	85.91	97.82	67.17	99.00
90.0	297	95.60	90.30	98.30	71.15	99.26
92.5	292	96.67	92.48	98.65	78.16	100.0
95.0	213	97.86	95.22	99.14	86.99	100.0
97.5	801	100.0	100.0	100.0	98.42	100.0

Table F2. L-moment statistics for empirical hyetograph analysis for the 0–12 hr storm duration and one or more inches of depth

Center of percent of storm duration interval (percent)	No. of samples ( )	Mean (percent)	L-scale (percent)	L-CV ( )	L-skew ( )	L-kurtosis ( )	τ_5 ( )
2.5	937	3.617	2.999	0.8292	0.6818	0.3782	0.1744
5.0	344	17.69	8.698	.4917	.2933	.1075	.07006
7.5	335	23.58	10.69	.4534	.2288	.08766	.04637
10.0	396	29.35	12.68	.4321	.2008	.07642	.03628
12.5	322	33.18	13.79	.4157	.1809	.07749	.02645
15.0	321	38.67	14.16	.3662	.1159	.07483	.02441
17.5	333	40.41	14.84	.3673	.08651	.01826	.01751
20.0	323	44.08	15.48	.3512	.07921	.01584	-.002722
22.5	328	44.18	16.59	.3755	.06167	-.009633	-.002197
25.0	289	47.88	15.68	.3274	.008481	.02000	-.006014
27.5	304	48.91	15.74	.3219	.007976	.01414	.004665
30.0	287	53.37	15.85	.2971	-.04174	.004482	-.008986
32.5	341	52.20	16.23	.3109	-.03955	.002352	-.01036
35.0	232	56.19	16.13	.2871	-.0634	.006389	-.007393
37.5	257	54.95	16.47	.2998	-.0423	-.01971	-.01620
40.0	257	60.40	15.95	.2640	-.1235	-.003574	-.006250
42.5	244	59.84	15.68	.2620	-.1003	.009002	-.01487
45.0	252	60.17	16.74	.2781	-.1670	-.004018	.02968
47.5	231	58.97	16.91	.2868	-.1200	-.02203	.009590
50.0	252	64.19	14.95	.2329	-.1799	.02796	.007438
52.5	246	61.33	16.69	.2721	-.1517	.004242	.01297
55.0	255	66.41	14.65	.2205	-.1758	.02404	-.008292
57.5	232	64.43	15.50	.2405	-.1847	.02611	.009597
60.0	254	66.96	15.27	.2280	-.2262	.03243	.009398
62.5	246	68.58	14.47	.2110	-.2233	.04760	-.006480
65.0	202	70.77	13.84	.1955	-.2711	.1110	-.03178
67.5	310	72.29	13.09	.1811	-.2591	.07725	-.02420
70.0	244	71.14	14.37	.2020	-.2840	.07629	-.009121
72.5	274	75.07	12.73	.1696	-.3194	.09683	-.01019
75.0	249	76.22	12.33	.1618	-.3283	.1173	-.02282
77.5	280	78.71	11.14	.1415	-.3394	.1165	-.01964
80.0	290	80.09	10.53	.1314	-.3382	.1182	-.03085
82.5	272	82.72	9.665	.1168	-.3939	.1718	-.06469
85.0	259	85.52	8.577	.1003	-.4495	.2176	-.1082
87.5	264	88.31	7.006	.07933	-.4827	.2770	-.1583
90.0	297	89.95	6.486	.07210	-.5550	.3471	-.2082
92.5	292	91.93	5.419	.05894	-.5692	.3614	-.2214
95.0	213	93.91	4.286	.04564	-.6395	.4548	-.3112
97.5	801	98.87	1.070	.01082	-.8943	.7668	-.6391

Table F3. Percentile statistics for empirical hyetograph analysis for the 12–24 hr storm duration and one or more inches of depth

Center of percent of storm duration interval (percent)	No. of samples ( )	Median 50th percentile (percent)	Lower quartile 25th percentile (percent)	Upper quartile 75th percentile (percent)	Lower decile 10th percentile (percent)	Upper decile 90th percentile (percent)
2.5	1251	1.505	0.000	7.965	0.000	18.61
5.0	632	16.94	6.065	28.21	2.274	48.43
7.5	624	26.87	9.896	42.88	4.612	58.75
10.0	599	34.64	13.41	52.06	6.849	69.96
12.5	556	38.81	18.53	58.18	8.219	78.73
15.0	529	45.37	23.36	61.99	10.54	82.27
17.5	517	49.58	25.19	63.42	9.546	81.84
20.0	464	52.42	25.82	69.45	9.247	84.20
22.5	449	56.07	30.70	71.06	12.44	86.03
25.0	440	56.14	25.67	74.01	13.44	86.85
27.5	430	59.84	31.60	80.50	13.26	87.49
30.0	374	64.81	35.70	83.74	14.66	89.79
32.5	388	60.55	32.87	87.36	15.20	92.29
35.0	343	63.34	35.76	90.91	12.76	95.42
37.5	350	60.56	31.71	87.87	13.15	95.75
40.0	349	59.81	36.87	86.78	15.26	96.10
42.5	320	62.18	37.43	89.07	14.76	95.98
45.0	307	68.11	42.68	89.43	19.64	96.59
47.5	337	65.30	41.65	88.89	18.04	96.70
50.0	329	67.22	40.27	86.87	19.47	96.39
52.5	352	68.06	41.78	90.58	21.49	97.19
55.0	311	66.67	42.58	87.10	19.29	95.73
57.5	313	67.17	46.01	90.87	25.14	97.22
60.0	301	74.07	49.98	92.61	26.26	97.28
62.5	294	76.94	54.90	93.30	32.00	98.04
65.0	297	80.52	59.27	93.59	34.42	98.26
67.5	306	81.33	57.63	93.82	36.80	98.62
70.0	278	79.85	57.62	93.59	36.97	97.93
72.5	301	81.65	58.37	95.07	39.248	98.74
75.0	286	83.41	60.43	94.94	42.75	99.02
77.5	326	85.53	66.34	94.68	46.01	98.71
80.0	316	86.88	68.84	95.88	49.18	98.67
82.5	308	88.35	71.49	96.82	49.44	99.20
85.0	337	87.84	72.34	96.46	43.85	98.77
87.5	373	90.34	78.62	97.35	50.92	99.47
90.0	388	92.19	82.80	98.11	62.71	99.53
92.5	350	93.04	87.48	98.17	65.05	99.45
95.0	378	95.59	90.20	98.70	65.70	99.77
97.5	897	100.0	97.67	100.0	91.05	100.0

Table F4. L-moment statistics for empirical hyetograph analysis for the 12–24 hr storm duration and one or more inches of depth

Center of percent of storm duration interval (percent)	No. of samples ( )	Mean (percent)	L-scale (percent)	L-CV ( )	L-skew ( )	L-kurtosis ( )	τ_5 ( )
2.5	1251	6.251	4.558	0.7291	0.5396	0.245367	0.136111
5.0	632	20.76	9.868	.4754	.2755	.138637	.088947
7.5	624	28.83	11.81	.4095	.1628	.071053	.059363
10.0	599	35.51	13.67	.3850	.1220	.043538	.037284
12.5	556	40.34	14.66	.3635	.09853	.056111	.016525
15.0	529	44.83	14.89	.3321	.04748	.05421	.01283
17.5	517	46.66	14.95	.3205	-.005984	.06574	.02673
20.0	464	49.70	15.12	.3041	-.05062	.06304	.03288
22.5	449	52.49	14.92	.2843	-.09168	.06198	.03205
25.0	440	51.97	15.87	.3054	-.07457	.003331	.03420
27.5	430	55.63	16.08	.2891	-.1311	-.002824	.01784
30.0	374	58.51	16.21	.2771	-.1583	-.007448	.01756
32.5	388	58.90	16.81	.2854	-.1247	-.02987	-.002221
35.0	343	60.62	17.19	.2836	-.1339	-.01799	-.01281
37.5	350	58.59	17.22	.2938	-.1000	-.01844	-.00867
40.0	349	59.08	16.68	.2823	-.08732	.002014	-.02434
42.5	320	60.31	16.71	.2771	-.1043	-.005200	-.01775
45.0	307	63.14	16.08	.2546	-.1411	.01482	-.02070
47.5	337	61.84	16.47	.2663	-.1233	.002887	-.01068
50.0	329	61.89	15.93	.2574	-.1161	.01174	-.01160
52.5	352	63.76	16.15	.2533	-.1318	-.01044	-.009891
55.0	311	62.11	15.79	.2542	-.1198	.006295	-.008991
57.5	313	65.54	14.88	.2271	-.1239	.009506	-.03097
60.0	301	69.02	14.64	.2122	-.2022	.02528	-.01438
62.5	294	70.96	13.66	.1925	-.1972	.03959	-.03362
65.0	297	72.85	13.31	.1827	-.2433	.06553	-.02381
67.5	306	73.75	13.08	.1773	-.2496	.06067	-.02114
70.0	278	72.95	13.12	.1799	-.2293	.05122	-.01645
72.5	301	74.15	12.99	.1751	-.2382	.05100	-.02954
75.0	286	76.26	12.18	.1597	-.2606	.07025	-.03829
77.5	326	78.44	11.04	.1407	-.2795	.08845	-.03992
80.0	316	79.58	10.92	.1373	-.3260	.1211	-.06497
82.5	308	80.83	10.73	.1328	-.3569	.1411	-.07603
85.0	337	79.97	11.14	.1393	-.3509	.1258	-.05265
87.5	373	83.42	9.765	.1171	-.4039	.1749	-.07394
90.0	388	86.47	8.260	.09553	-.4526	.2394	-.1554
92.5	350	87.69	7.686	.08765	-.5202	.3387	-.2197
95.0	378	89.42	7.173	.08021	-.5603	.3304	-.1753
97.5	897	96.58	2.929	.03033	-.7478	.5145	-.3540

Table F5. Percentile statistics for empirical hyetograph analysis for the 24 hr and greater storm duration and one or more inches of depth

Center of percent of storm duration interval (percent)	No. of samples ( )	Median 50th percentile (percent)	Lower quartile 25th percentile (percent)	Upper quartile 75th percentile (percent)	Lower decile 10th percentile (percent)	Upper decile 90th percentile (percent)
2.5	1526	3.390	0.000	11.63	0.000	25.68
5.0	719	13.64	6.061	30.58	2.439	48.26
7.5	662	20.11	8.587	41.01	4.062	59.20
10.0	647	23.11	11.120	50.164	5.994	68.39
12.5	594	27.20	13.14	56.58	5.861	79.13
15.0	589	31.58	16.74	55.18	7.645	80.18
17.5	546	40.12	19.44	59.85	9.328	80.45
20.0	480	43.18	21.19	63.97	8.5433	82.51
22.5	446	43.37	18.68	64.71	6.757	83.03
25.0	412	42.20	19.12	67.01	8.271	84.62
27.5	408	38.43	20.02	68.36	10.49	86.42
30.0	379	39.43	26.00	66.13	9.962	86.40
32.5	358	41.61	20.89	61.70	10.83	80.90
35.0	393	45.64	26.04	64.25	11.48	83.57
37.5	383	49.17	26.25	66.05	12.91	81.24
40.0	416	49.27	28.02	68.39	15.93	81.55
42.5	410	52.07	31.72	70.89	22.05	83.79
45.0	400	56.91	36.49	72.08	17.49	87.67
47.5	405	54.80	32.57	71.64	12.70	85.67
50.0	412	55.52	30.61	73.11	17.48	88.29
52.5	392	52.89	36.09	72.16	21.91	88.37
55.0	379	59.35	44.31	78.76	29.02	90.62
57.5	393	64.62	48.02	83.30	28.54	92.88
60.0	370	63.90	44.71	84.44	29.14	93.99
62.5	404	67.04	50.99	86.85	29.65	95.44
65.0	387	67.10	46.42	86.73	22.72	97.35
67.5	375	68.66	50.00	86.79	28.83	96.73
70.0	383	70.21	51.32	89.19	35.20	98.47
72.5	421	75.00	54.95	89.19	33.97	97.47
75.0	471	73.90	57.27	88.32	36.60	97.58
77.5	459	76.82	60.45	89.78	41.05	97.47
80.0	463	79.11	62.07	90.28	39.85	97.47
82.5	486	83.01	66.16	93.37	46.92	97.49
85.0	501	86.11	70.94	94.57	52.04	98.32
87.5	523	88.14	75.40	96.34	56.46	98.41
90.0	537	87.40	75.35	97.04	55.37	98.86
92.5	553	91.16	82.46	97.40	67.88	99.15
95.0	550	94.96	88.20	98.32	78.19	99.55
97.5	1238	99.38	96.22	100.0	89.63	100.0

Table F6. L-moment statistics for empirical hyetograph analysis for the 24 hr and greater storm duration and one or more inches of depth

Center of percent of storm duration interval (percent)	No. of samples ( )	Mean (percent)	L-scale (percent)	L-CV ( )	L-skew ( )	L-kurtosis ( )	τ_5 ( )
2.5	1526	8.790	6.028	0.6858	0.4929	0.2245	0.1339
5.0	719	21.03	10.50	.4994	.3178	.1242	.05618
7.5	662	26.73	12.11	.4529	.2445	.07722	.03255
10.0	647	31.27	13.81	.4417	.2345	.05807	.005247
12.5	594	35.51	15.25	.4294	.2033	.03884	-.01834
15.0	589	37.89	14.97	.3951	.1741	.06258	.003964
17.5	546	41.74	15.12	.3622	.09784	.05468	.01842
20.0	480	44.79	15.73	.3513	.05137	.03029	.01798
22.5	446	43.59	16.14	.3701	.06245	.02712	.02149
25.0	412	44.05	16.38	.3718	.06935	.008111	.01472
27.5	408	44.44	16.21	.3647	.08889	.01636	-.003169
30.0	379	45.47	15.36	.3378	.09027	.04793	-.009051
32.5	358	43.71	14.86	.3399	.08673	.05646	.03103
35.0	393	47.35	14.97	.3162	.04121	.05414	.02339
37.5	383	48.04	14.65	.3049	.009838	.04422	.04283
40.0	416	49.15	14.33	.2916	.008136	.03859	.02183
42.5	410	52.21	13.76	.2636	.02263	.03866	.004998
45.0	400	54.02	14.74	.2729	-.02930	.06430	.004514
47.5	405	52.32	15.35	.2933	-.04043	.05126	.02626
50.0	412	53.06	15.14	.2853	-.01078	.03271	.01334
52.5	392	53.83	14.01	.2603	.02288	.06559	-.01847
55.0	379	60.15	13.18	.2191	-.02562	.07155	-.04466
57.5	393	63.24	13.77	.2178	-.1220	.08023	-.03065
60.0	370	63.20	13.89	.2198	-.07004	.03157	-.04287
62.5	404	65.74	13.67	.2079	-.1138	.05475	-.04862
65.0	387	64.26	14.89	.2317	-.1205	.04477	-.02989
67.5	375	66.03	13.93	.2109	-.1321	.05598	-.03400
70.0	383	68.25	13.64	.1998	-.1233	.03936	-.05435
72.5	421	70.65	12.75	.1805	-.1597	.05603	-.03155
75.0	471	70.74	12.17	.1720	-.1452	.07805	-.04709
77.5	459	72.91	11.69	.1604	-.1863	.1014	-.06483
80.0	463	73.23	12.05	.1645	-.2278	.1099	-.05578
82.5	486	76.86	10.88	.1416	-.2556	.1058	-.05552
85.0	501	79.85	10.15	.1272	-.3067	.1296	-.06453
87.5	523	82.61	9.310	.1127	-.3432	.1411	-.08276
90.0	537	82.56	9.223	.1117	-.3073	.1090	-.06038
92.5	553	87.30	6.794	.07782	-.3380	.1523	-.09454
95.0	550	91.33	5.005	.05480	-.4113	.2077	-.1244
97.5	1238	96.60	2.580	.02671	-.5947	.3164	-.1937

Table F7. Graphically smoothed percentile statistics for empirical hyetograph analysis for the 0–12 hr storm duration and one or more inches of depth

Center of percent of storm duration interval (percent)	Median 50th percentile (percent)	Lower quartile 25th percentile (percent)	Upper quartile 75th percentile (percent)	Lower decile 10th percentile (percent)	Upper decile 90th percentile (percent)
2.5	3.00	2.00	6.00	1.00	9.00
5.0	11.00	4.416	25.00	1.999	41.30
7.5	18.04	8.046	34.00	2.798	53.83
10.0	24.45	10.36	43.37	4.332	63.02
12.5	30.13	13.40	48.36	4.943	69.53
15.0	35.75	15.00	56.21	7.038	76.93
17.5	38.87	17.34	61.00	8.00	80.00
20.0	40.46	20.00	67.50	8.00	83.45
22.5	42.00	22.00	70.04	8.50	84.78
25.0	44.84	24.00	72.82	9.47	85.37
27.5	48.86	26.50	74.00	11.56	87.02
30.0	51.50	30.00	76.95	13.00	88.31
32.5	54.00	30.75	78.56	14.00	88.10
35.0	56.50	32.00	81.57	14.21	89.00
37.5	59.50	33.00	83.61	15.82	90.31
40.0	62.00	34.00	84.50	16.50	91.00
42.5	63.54	36.00	85.11	17.50	91.50
45.0	66.00	36.50	85.00	18.00	92.12
47.5	68.00	37.50	85.91	19.50	93.03
50.0	70.00	39.50	86.28	20.00	93.84
52.5	71.00	40.50	86.38	21.00	95.00
55.0	72.50	42.00	87.00	22.00	95.13
57.5	73.50	44.00	88.00	22.47	95.82
60.0	75.00	46.65	89.59	25.00	95.55
62.5	76.50	50.00	89.70	27.50	96.44
65.0	77.45	53.00	91.57	30.16	96.76
67.5	79.49	56.00	91.90	32.00	96.71
70.0	81.50	58.00	93.06	33.50	97.38
72.5	83.50	61.14	93.50	35.21	97.32
75.0	85.07	65.00	93.47	38.50	97.80
77.5	86.88	67.89	93.77	43.50	98.17
80.0	87.66	72.00	95.32	47.56	98.38
82.5	89.90	76.21	96.32	50.63	98.62
85.0	92.76	80.81	97.50	55.34	98.80
87.5	94.27	85.91	97.82	64.00	99.00
90.0	95.60	90.30	98.30	71.15	99.26
92.5	96.67	92.48	98.65	78.16	100.0
95.0	97.86	95.22	99.14	86.99	100.0
97.5	99.40	98.90	99.90	98.42	100.0

Table F8. Graphically smoothed percentile statistics for empirical hyetograph analysis for the 12–24 hr storm duration and one or more inches of depth

Center of percent of storm duration interval (percent)	Median 50th percentile (percent)	Lower quartile 25th percentile (percent)	Upper quartile 75th percentile (percent)	Lower decile 10th percentile (percent)	Upper decile 90th percentile (percent)
2.5	3.00	1.50	7.965	1.00	18.61
5.0	16.94	6.065	28.21	2.274	48.43
7.5	26.87	9.896	42.88	4.612	58.75
10.0	34.64	13.41	52.06	6.849	69.96
12.5	38.81	18.53	58.18	8.219	78.73
15.0	45.37	23.00	61.99	9.00	81.50
17.5	49.58	25.19	63.42	9.546	83.50
20.0	52.42	25.82	68.50	10.50	84.20
22.5	55.50	27.50	71.06	12.00	86.03
25.0	57.50	29.50	74.01	13.00	86.85
27.5	59.84	31.00	80.50	13.26	87.49
30.0	60.50	32.00	83.74	14.00	89.79
32.5	61.50	32.87	86.50	14.50	92.29
35.0	62.00	34.50	87.50	15.00	94.50
37.5	63.00	35.50	87.87	15.00	95.75
40.0	63.50	36.87	88.50	15.50	96.10
42.5	64.00	37.43	89.07	14.76	95.98
45.0	65.50	39.00	89.43	17.00	96.59
47.5	65.30	39.50	88.89	18.04	96.70
50.0	67.22	40.27	89.50	19.47	96.39
52.5	68.06	41.78	90.58	21.49	97.00
55.0	70.00	42.58	91.00	22.50	97.00
57.5	71.00	46.01	90.87	24.00	97.22
60.0	73.00	49.50	92.61	27.50	97.28
62.5	76.00	54.90	93.30	32.00	98.04
65.0	77.50	57.00	93.59	34.42	98.26
67.5	80.00	57.63	93.82	36.80	98.62
70.0	81.00	57.62	94.00	38.00	98.50
72.5	81.65	58.37	94.50	39.248	98.74
75.0	83.41	60.43	94.94	42.75	99.02
77.5	85.53	66.34	95.50	45.50	98.71
80.0	86.88	68.84	95.88	48.00	98.67
82.5	88.35	71.49	96.82	49.44	99.20
85.0	90.00	72.34	96.46	50.50	98.77
87.5	90.50	78.62	97.35	53.00	99.47
90.0	92.19	82.80	98.11	60.50	99.53
92.5	93.04	87.48	98.17	65.05	99.45
95.0	95.59	90.20	98.70	67.00	99.77
97.5	98.00	97.00	99.50	91.05	100.0

Table F9. Graphically smoothed percentile statistics for empirical hyetograph analysis for the 24 hr and greater storm duration and one or more inches of depth

Center of percent of storm duration interval (percent)	Median 50th percentile (percent)	Lower quartile 25th percentile (percent)	Upper quartile 75th percentile (percent)	Lower decile 10th percentile (percent)	Upper decile 90th percentile (percent)
2.5	5.00	2.50	11.63	0.50	25.68
5.0	13.64	6.061	30.58	2.439	48.26
7.5	20.11	8.587	41.01	4.062	59.20
10.0	24.00	11.120	50.164	5.994	68.39
12.5	27.20	13.14	54.00	7.00	78.00
15.0	31.58	16.74	57.00	7.645	80.18
17.5	35.50	18.00	59.85	8.50	81.50
20.0	37.50	19.00	63.97	8.5433	82.51
22.5	39.50	19.50	64.71	9.00	83.03
25.0	40.00	20.00	66.00	9.50	84.00
27.5	41.00	20.02	67.00	10.00	84.50
30.0	42.00	21.00	66.13	9.962	84.50
32.5	43.00	21.50	66.50	10.83	84.00
35.0	45.64	23.00	67.00	11.48	84.50
37.5	47.50	25.00	67.50	12.91	84.50
40.0	49.27	28.02	68.39	15.50	85.00
42.5	52.07	30.00	70.00	17.00	85.00
45.0	54.00	31.00	72.08	17.49	85.50
47.5	56.00	31.50	72.50	18.00	87.00
50.0	57.00	33.00	73.11	19.50	88.29
52.5	58.00	36.09	74.00	21.91	88.37
55.0	59.35	41.00	77.50	26.00	90.62
57.5	61.00	44.00	81.00	28.54	92.00
60.0	63.50	44.71	84.44	29.14	93.99
62.5	66.00	45.50	85.50	29.65	95.44
65.0	67.10	46.42	86.73	30.00	96.00
67.5	68.66	49.00	86.79	31.00	96.73
70.0	70.21	51.32	88.00	32.50	97.00
72.5	72.50	54.95	89.00	33.97	97.47
75.0	73.90	57.27	89.00	36.60	97.58
77.5	76.82	60.45	89.78	40.00	97.47
80.0	79.11	62.07	90.28	43.00	97.47
82.5	83.01	66.16	92.50	46.92	98.00
85.0	85.00	70.94	94.57	52.04	98.32
87.5	88.00	74.00	96.34	55.50	98.41
90.0	89.00	75.35	97.04	60.00	98.86
92.5	91.16	82.46	97.40	67.88	99.15
95.0	94.96	88.20	98.32	78.19	99.55
97.5	98.50	96.22	99.50	89.63	100.0

REFERENCES

Abramowitz, M., and Stegun, I.A., 1964, Handbook of mathematical functions: National Bureau of Standards Applied Mathematics Series, vol. 55, reprinted in 1972, 1046 p.

Aron, G., and Adl, I., 1992, Effects of storm patterns on runoff hydrographs: Water Resources Bulletin, American Water Resources Association, vol. 28, no. 3, pp. 569–575.

Asquith, W.H., 1998, Depth-duration frequency of precipitation for Texas: U.S. Geological Survey Water-Resources Investigations Report 98–4044, 107 p.

Asquith, W.H., 1999, Areal-reduction factors for the precipitation of the 1-day design storm in Texas: U.S. Geological Survey Water-Resources Investigations Report 99–4267, 81 p.

Asquith, W.H., 2002, Effects of regulation on L-moments of annual peak streamflow in Texas: U.S. Geological Survey Water-Resources Investigations Report 01–4243, 66 p.

Asquith, W.H., and Slade, R.M., 1997, Regional equations for estimation of peak-streamflow frequency for natural basins in Texas: U.S. Geological Survey Water-Resources Investigations Report 96–4307, 68 p.

Balakrishnan, N., and Chan, P.S., 1995a, Maximum likelihood estimation for the log-gamma distribution under type-II censored samples and associated inference, in Recent Advances in Life-Testing and Reliability, edited by N. Balakrishnan, chapter 22, CRC Press, Boca Raton, Fla., pp. 409–437.

Balakrishnan, N., and Chan, P.S., 1995b, Maximum likelihood estimation for the three-parameter log-gamma distribution under type-II censored samples and associated inference, in Recent Advances in Life-Testing and Reliability, edited by N. Balakrishnan, chapter 23, CRC Press, Boca Raton, Fla., pp. 439–453.

Barnett, V., and Lewis, T., 1995, Outliers in statistical data, third edition: John Wiley and Sons Inc., New York, 584 p.

Benjamin, J.R., and Cornell, C.A., 1970, Probability, statistics, and decision for civil engineers: McGraw-Hill, New York, 684 p.

Bonta, J.V., and Rao, A.R., 1988a, Comparison of four design-storm hyetographs: Transactions American Society of Agricultural Engineers, vol. 31, no. 1, pp. 102–106.

Bonta, J.V., and Rao, A.R., 1988b, Fitting equations to families of dimensionless cumulative hyetographs: Transactions American Society of Agricultural Engineers, vol. 31, no. 3, pp. 756–760.

Bonta, J.V., and Rao, A.R., 1989, Regionalization of storm hyetographs: Water Resources Bulletin, vol. 25, no. 1, pp. 211–217.

Cheng, K.S., Hueter, I., Hsu, E.C., and Yeh, H.C., 2001, A scale-invariant Gauss-Markov model for design storm hyetographs: Journal of the American Water Resources Association, American Water Resources Association, vol. 28, no. 3, pp. 723–735.

Chow, V.T., Maidment, D.R., Mays, L.W., 1988, Applied hydrology: McGraw-Hill Publishing Company, New York, 572 p.

Chukwuma, G.O., and Schwab, G.O., 1983, Procedure for developing design hyetographs for small watersheds: Transactions American Society of Agricultural Engineers, vol. 26, no. 5, pp. 1386–1389.

Croley II, T.E., 1980, Gamma synthetic hydrographs: Journal of Hydrology, vol. 47, pp. 41–52.

Cunnane, C., 1989, Statistical distributions for flood frequency analysis: World Meteorological Organization Operational Hydrology Report No. 33, variously paged.

David, H.A., 1981, Order statistics: John Wiley and Sons Inc., New York, 360 p.

Davis, J.C., 1986, Statistics and data analysis in Geology: John Wiley and Sons Inc., New York, 646 p.

Dingman, S.L., 2002, Physical Hydrology: Prentice Hall, New Jersey, 2nd edition, 646 p.

Drufuca, G., and Rogers, R.R., 1978, Statistics of rainfall over paths from 1 to 50 kilometers: Atmospheric Environment, vol. 12, pp. 2333–2342.

Edson, C.G., 1951, Parameters for relating unit hydrographs to watershed characteristics: American Geophysical Union Transactions, vol. 32, 591–596.

Evans M., Hastings, N.A.J., and Peacock, J. B., 2000, Statistical distributions, 3rd ed.: John Wiley and Sons Inc., 221 p.

Fill, H.D., and Stedinger, J.R., 1995, L-moment and probability plot correlation coefficient goodness-of-fit tests for the Gumbel distribution and impact of autocorrelation: Water Resources Research, vol. 31, no. 1, pp. 225–229.

Frederick, R.H., Meyers, V.A., and Auciello, E.P., 1977, Five- to 60-minute precipitation frequency for the eastern and central United States: National Oceanic and Atmospheric Administration Technical Memorandum NWS HYDRO–35, 36 p.

French, R.H., 1983, Development of design hyetographs for southern Nevada: Water Resources Center, Desert Research Institute, University of Nevada, variously paged.

Gilchrist, W.G., 2000, Statistical modeling with quantile functions: Chapman and Hall CRC Press, Boca Raton, Fla., 320 p.

Gilchrist, W.G., 2002, E-mail written communication: W.G.Gilchrist@shu.ac.uk, Sheffield Hallam University, Sheffield, United Kingdom.

Greenwood, J.A., Landwehr, J.M., Matalas, N.C., and Wallis, J.R., 1979, Probability weighted moments—definition and relation to parameters of several distributions expressible in inverse form: Water Resources Research, vol. 15, pp. 1029–1054.

Haan, C.T., Barfield, B.J., and Hayes, J.C., 1994, Design hydrology and sedimentology for small catchments: Academic Press, San Diego, 558 p.

Haktanir, T., and Bozduman, A., 1995, A study on sensitivity of the probability-weighted moments method on the choice of the plotting position formula: Journal of Hydrology, vol. 168, pp. 265–281.

Hansen, W.R, 1991, Suggestions to authors of the reports of the United States Geological Survey, 7th edition: U.S. Government Printing Office, 289 p.

Hald, A., 1998, A history of mathematical statistics from 1750 to 1930: John Wiley and Sons Inc., 795 p.

Helsel, D.R., 1989, written communication, Statistics—New series of technical briefing papers: U.S. Geological Survey, Branch of Systems Analysis Technical Memorandum 89–01, June 19, 13 p.

Helsel, D.R., and Hirsch, R.M., 1992, Statistical methods in water resources—Studies in Environmental Science 49: Elsevier, Amsterdam, 529 p.

Herrmann, G., 2002, E-mail written communication: Texas Department of Transportation, San Angelo, Texas.

Hershfield, D.M., 1962, Rainfall frequency atlas of the United States for durations from 30 minutes to 24 hours and return periods from 1 to 100 years: Washington, D.C., U.S. Weather Bureau Technical Paper 40, 61 p.

Hollander, M., and Wolfe, D.A., 1973, Nonparametric statistical methods: John Wiley and Sons Inc., 503 p.

Hosking, J.R.M., 1986, The theory of probability weighted moments, Research Report RC12210, IBM Research Division, T.J. Watson Research Center, Yorktown Heights, New York.

Hosking, J.R.M., 1989, Some theoretical results concerning L-moments, Research Report RC14492, IBM Research Division, T.J. Watson Research Center, Yorktown Heights, New York.

Hosking, J.R.M., 1990, L-moments: Analysis and estimation of distributions using linear combination of order statistics: Journal Royal Statistical Society, B, vol. 52, no. 1, pp. 105–124.

Hosking, J.R.M., 1992, Moments or L moments? An example comparing two measures of distributional shape: The American Statistician., vol 46, no. 3, pp. 186–189.

Hosking, J.R.M., 1994, The four-parameter Kappa distribution: IBM Journal of Research and Development, vol. 38, no. 3, pp. 251–258.

Hosking, J.R.M., 1995, The use of L-moments in the analysis of censored data, in Recent Advances in Life-Testing and Reliability, edited by N. Balakrishnan, chapter 29, CRC Press, Boca Raton, Fla., pp. 546–560.

Hosking, J.R.M., 1996, FORTRAN routines for use with the method of L-moments, version 3: Research Report RC20525, IBM Research Division, T.J. Watson Research Center, Yorktown Heights, New York.

Hosking, J.R.M., 2002, E-mail written communication: hosking@watson.ibm.com, IBM Research Division, T.J. Watson Research Center, Yorktown Heights, New York.

Hosking, J.R.M., and Wallis, J.R., 1987, Parameter and quantile estimation for the generalized Pareto distribution: Technometrics, vol. 29, pp. 339–349.

Hosking, J.R.M., and Wallis, J.R., 1993a, Some statistics useful in regional frequency analysis: Water Resources Research, vol. 29, no. 2, pp. 271–281.

Hosking, J.R.M., and Wallis, J.R., 1993b, Some statistics useful in regional frequency analysis, Research Report RC-17096, IBM Research Division, T.J. Watson Research Center, Yorktown Heights, New York, 23 p.

Hosking, J.R.M., and Wallis, J.R., 1995, A comparison of unbiased and plotting-position estimators of L moments: Water Resources Research, vol. 31, no. 8, pp. 2019–2025.

Hosking, J.R.M., and Wallis, J.R., 1997, Regional frequency analysis—An approach based on L-moments: Cambridge University Press, 224 p.

Hosking, J.R.M., Wallis, J.R., and Wood, E.F., 1985, Estimation of the generalized extreme-value distribution by the method of probability-weighted moments: Technometrics, vol. 27, pp. 251–261.

Huff, F.A., 1967, Time distributions in heavy storms: Water Resources Research, no. 4, pp. 1007–1019.

Huff, F.A., 1990, Time distributions of heavy rainstorms in Illinois: Illinois State Water Survey Circular 173, Champaign, 18 p.

Jin, C.X., 1992, A deterministic gamma-type geomorphologic instantaneous unit hydrograph based on path types: Water Resources Research, vol. 28, no. 2, pp. 479–486.

Jones, D.A., 1985, Applied Hydrology Informal Note 103: Institute of Hydrology, Wallingford, United Kingdom.

Kaigh, W.D., and Driscoll, M.F., 1987, Numerical and graphical data summary using O-statistics: The American Statistician, vol. 41, no. 1, pp. 25–32.

Karian, Z.A., Dudewicz, E.J., 2000, Fitting statistical distribution—the generalized Lambda distribution and generalized bootstrap methods: CRC Press, Boca Raton, Fla., 438 p.

Keifer, C.J., and Chu, H.H., 1957, Synthetic storm pattern for drainage design: Journal Hydraulics Division, American Society of Civil Engineers, vol. 83, HY4, pp. 1–25.

Kirby, W., 1974, Algebraic boundedness of sample statistics: Water Resources Research, vol. 10, pp. 220–222.

Kite, G.W., 1988, Frequency and risk analyses in hydrology: Water Resources Publications, Littleton, Colorado, 257 p.

Kroll, C.N., 2002, E-mail written communication: cnkroll@esf.edu, SUNY College of Environmental Science and Forestry, Syracuse, New York.

Landwehr, J.M., Matalas, N.C., and Wallis, J.R., 1979a, Probability weighted moments compared with some traditional techniques in estimating Gumbel parameters and quantiles: Water Resources Research, vol. 15, no. 5, pp. 1055–1064.

Landwehr, J.M., Matalas, N.C., and Wallis, J.R., 1979b, Estimation of parameters and quantiles of Wakeby distributions: Water Resources Research, vol. 15, no. 5, pp. 1362–1379.

Lawless, J.F., 1980, Inference in the generalized gamma and log-gamma distribution: Technometrics, vol. 22, pp. 67–82.

Mahler, B.J., 2002, personal communication, U.S. Geological Survey, Austin, Texas.

Nash, J. E.,1959, Systematic determination of unit hydrograph parameters: Journal Geophysical Research 64, pp. 111–115.

Norbury, J.R., and White, J.K., 1975, Intensity-time profiles of high-intensity rainfall: The Meteorological Magazine, vol. 104, no. 1237, pp. 221–227.

Panda, M.N., and Lake, L.W., 1994, Estimation of single-phase permeability from parameters of particle-size distribution: American Association of Petroleum Geologists Bulletin, vol. 78, no. 7, pp. 1028–1039.

Pani, E.A., and Haragan, D.R., 1981, A comparison of Texas and Illinois temporal rainfall distributions: Fourth Conference on Hydrometeorology, American Meteorological Society, pp. 76–80.

Parrett, C.P., 1998, Characteristics of extreme storms in Montana and methods for constructing synthetic storm hyetographs: U.S. Geological Survey Water-Resources Investigations Report 98–4100, 55 p.

Pilgrim, D.H., and Cordery, I., 1975, Rainfall temporal patterns for design floods: Journal of the Hydraulics Division, American Society of Civil Engineers, vol. 101, HY1, pp. 81–95.

Pilgrim, D.H., and Cordery, I., 1993, Flood runoff, in Handbook of Applied Hydrology, chapter 9, editor-in-chief D. A. Maidment: McGraw-Hill, New York.

Pinkham, R.S., 1961, On the distribution of first significant digits: Annals of Mathematical Statistics, vol. 32, pp. 1223–1230.

Prentice, R.L., 1974, A log-gamma model and its maximum likelihood estimation: Biometrika, vol. 61, pp. 539–544.

Press, W.H., Teukolsky, S.A., Vetterling, W.T., Flannery, B.P., 1992, Numerical recipes in FORTRAN: Cambridge University Press, 963 p.

Preul, H.C., and Papadakis, C.N., 1973, Development of design storm hyetographs for Cincinnati, Ohio: Water Resources Bulletin, vol. 9, no. 2, pp. 291–300.

Ross, S., 1994, A first course in probability, 4th ed.: MacMillan College Publishing Company, New York, 473 p.

Schaefer, M.G., 1989, Characteristics of extreme precipitation events in Washington State: Washington State Department of Ecology Report 89-51, variously paged.

Schaefer, M.G., 1993, Dam safety guidelines technical note 3—Design storm construction: Washington State Department of Ecology Report 92-55G, variously paged.

Serfling, R.J., 1980, Approximation theorems of mathematical statistics: John Wiley and Sons Inc., New York.

Serfling, R.J., 2002, E-mail written communication: serfling@utdallas.edu, University of Texas at Dallas.

Shen, H.W., and Julien, P.Y., 1993, Erosion and sediment transport, in Handbook of Applied Hydrology, chapter 12, editor-in-chief D.A. Maidment: McGraw-Hill, New York.

Soil Conservation Service, 1973, A method for estimating volume and rate of runoff in small watersheds: SCS-TP-149, U.S. Department of Agriculture, Soil Conservation Service, Washington, D.C.

Stedinger, J.R., Vogel, R.M., and Foufoula-Georgiou, E., 1992, Frequency analysis of extreme events, in Handbook of Hydrology, chapter 18, editor-in-chief D. A. Maidment: McGraw-Hill, New York.

Stolpa, D., 2002, E-mail written communication: Texas Department of Transportation, Austin, Texas.

Texas Department of Water Resources, 1980, HIPLEX 1980 operations plan, Big Spring, Texas, LP-125: Austin, Texas, 47 pp.

Thompson, D.B., 2001, personal communication: Department of Civil Engineering, Texas Tech University, Lubbock, Texas.

Thompson, D.B., 2002, personal communication: Department of Civil Engineering, Texas Tech University, Lubbock, Texas.

Tocher, K.D., 1954, The application of automatic computers to sampling experiments: Journal Royal Statistical Society, B, vol. 16, pp. 39–61.

Troutman, B., 2002, E-mail written communication: troutman@usgs.gov, U.S. Geological Survey, Denver, Colorado.

Veneziano, D., and Villani, P., 1999, Best linear unbiased design hyetograph: Water Resources Research, vol. 35, no. 9, pp. 2725–2738.

Vogel, R.M., and Fennessey, N.M., 1993, L moment diagrams should replace product moment diagrams: Water Resources Research, vol. 29, no. 6, pp. 1745–1752.

Vogel, R.M., 2002, E-mail written communication: rvogel@emerald.tufts.edu, Tufts University, Medford, Massachusetts.

Wallis, J.R., 2002, E-mail written communication: james.wallis@yale.edu, Yale University, New Haven, Connecticut.

Wallis, J.R., Matalas, N.C., and Slack, J.R., 1974, Just a moment!: Water Resources Research, vol. 10, pp. 211–219.

Wang, Q.J., 1996a, Using partial probability weighted moments to fit the extreme value distributions to censored samples: Water Resources Research, vol. 32, no. 6, pp. 1767–1771.

Wang, Q.J., 1996b, Direct sample estimators of L-moments: Water Resources Research, vol. 32, no. 12., pp. 3617–3619.

Wilks, D.S., 1995, Statistical methods in the atmospheric sciences: Academic Press, San Diego, 467 p.

Yen, B.C., and Chow, V.T., 1980, Design hyetographs for small drainage structures: Journal of the Hydraulics Division, American Society of Civil Engineers, vol. 106, HY6, pp. 1055–1076.

Yue, S., Ouarda, T.B.M.J., Bobée, B., Legendre, P., and Bruneau, P., 2002, Approach for describing statistical properties of flood hydrograph: Journal of Hydrologic Engineering, vol. 7, no. 2, pp. 147–153.

Zafirakou-Koulouris, A., Vogel, R.M., Craig, S.M., and Habermeier, J., 1998, L-moment diagrams for censored observations: Water Resources Research, vol. 34, no. 5, pp. 1241–1249.

VITA

William Harold Asquith was born in Dallas, Texas on October 4, 1969, the son of Anne Louise Asquith and Dr. George Benjamin Asquith. After completing his work at Canyon High School, Canyon, Texas, in 1988, he entered the University of Texas at Austin. During the summers of 1988 and 1989, he attended West Texas State University in Canyon. He received the degree of Bachelor of Science in Civil Engineering from University of Texas at Austin in December 1992, and after entering the Graduate School of the University of Texas at Austin in January 1993 he received the degree of Master of Science in Civil Engineering in December 1994. During the years between 1992 and the present he has been employed as a hydrologist at the United States Geological Survey in Austin. He has over 20 publications on surface water and precipitation hydrology in Texas. In January 1998 he again entered the Graduate School of the University of Texas at Austin in pursuit of a Ph.D. in Geosciences.

Permanent Address: 8708 Little Laura Drive, Austin, Texas 78757

This dissertation was typed by the author using Adobe™ Framemaker™ 7.0.